Alma Mater Studiorum - Università di Bologna

DOTTORATO DI RICERCA IN

MONITORAGGIO E GESTIONE DELLE STRUTTURE E DELL'AMBIENTE - SEHM2

Ciclo 35

Settore Concorsuale: 08/B3 - TECNICA DELLE COSTRUZIONI

Settore Scientifico Disciplinare: ICAR/09 - TECNICA DELLE COSTRUZIONI

STRENGTH AND DUCTILITY OF CORRODED STRANDS WITHIN THE FRAMEWORK OF SAFETY ASSESSMENT OF EXISTING BRIDGES

Presentata da: Matteo Marra

Coordinatore Dottorato
Prof. Luca De Marchi

Supervisore
Prof. Stefano Silvestri

Co-supervisori
Prof. Michele Palermo

Prof. Tomaso Trombetti

Esame finale anno 2023

Alla mia famiglia.
Ai miei nonni, per i loro insegnamenti.

Abstract

Existing bridges built in the last 50 years face challenges due to states far different than those envisaged when they were designed, due to increased loads, ageing of materials, and poor maintenance. For post-tensioned bridges, the need emerged for reliable engineering tools for the evaluation of their capacity in case of steel corrosion due to lack of mortar injection. This can lead to sudden brittle collapses, highlighting the need for proper maintenance and monitoring.

This thesis proposes a peak strength model for corroded strands, introducing a "group coefficient" that aims at considering corrosion variability in the wires constituting the strands. The application of the introduced model in a deterministic approach leads to the proposal of strength curves for corroded strands, which represent useful engineering tools for estimating their maximum strength considering both geometry of the corrosion and steel material parameters. Together with the proposed ultimate displacement curves, constitutive laws of the steel material reduced by the effects of corrosion can be obtained. The effects of corroded strands on post-tensioned beams can be evaluated through the reduced bending moment-curvature diagram accounting for these reduced stress-strain relationships. The application of the introduced model in a probabilistic approach allows to estimate peak strength probability functions and consecutive design-oriented safety factors to consider corrosion effects in safety assessment verifications. Both approaches consider two procedures that are based on the knowledge level of the corrosion in the strands.

On the sidelines of this main research line, this thesis also presents a study of a seismic upgrading intervention of a case-study bridge through HDRB isolators providing a simplified procedure for the identification of the correct device. The study also investigates the effects due to the variability of the shear modulus of the rubber material of the HDRB isolators on the structural response of the isolated bridge.

Contents

List of Figures

List of Tables

1

Introduction

Sommario

Questo lavoro di ricerca affronta principalmente il problema della corrosione nei trefoli, usualmente utilizzati negli elementi in cemento armato precompresso. I risultati ottenuti si pongono come strumenti ingegneristici utili ai fini delle valutazioni di sicurezza di tali elementi, la cui necessità è emersa dai recenti eventi riguardanti i ponti post-tesi esistenti.

Questo capitolo riporta: (i) un'introduzione relativa al suddettetto contesto, (ii) gli obiettivi del lavoro di ricerca e (iii) l'organizzazione del testo.

Summary

This research work mainly addresses the problem of corrosion in strands, usually used in prestressed concrete elements. The results obtained are useful engineering tools for the purposes of safety assessments of these elements. Their need has emerged from recent events concerning existing post-tensioned bridges.

This chapter presents: (i) an introduction relating to the aforementioned context, (ii) the objectives of the research work and (iii) the organization of the text.

1.1 Background

Most of the existing bridges have been built during the last 50 years. The increasing of static and dynamic loads, like the volume of traffic, has led to the condition in which they are subjected to loads far higher than those envisaged when they have been designed. The effects of chlorides, either in a marine environment or from de-icing salts, alkali-silica reactions, carbonation and inadequate corrosion protection are causing progressive deterioration of the bridge structural elements. An example of a damaged Gerber saddle due to corrosion phenomena is reported in Figure 1.1.

During their service life bridges may be subjected to a loss of strength as a result of structural damage or material degradation reaching, at some point, a minimum acceptable level of performance. This condition is not easily defined and a sound decision making

process needs to take into account a number of factors including the consequences of failure in terms of both costs and potential loss of life. Therefore, bridges need effective maintenance strategies to increase their service life at the minimum cost.

(a) Damaged Gerber saddle

(b) Viaduct collapse in Lecco, Italy

Pictures taken from a) www.cte-it.org and b) www.edilportale.com

Figure 1.1: Examples of the current condition of existing bridges

In recent years, especially after on disastrous collapses (see Figure 1.2) [1], [2], most of these aspects, like the ageing of the constitutive material, and the lack of maintenance over the years, came to light, showing several problems regarding the precarious conditions of the existing bridges.

(a) Rest of the collapsed pier number 9

(b) Corroded strands

Pictures taken from a) www.tg24.sky.it and b) www.espresso.repubblica.it

Figure 1.2: Details of the Polcevera bridge after its collapse, Genoa, Italy.

In Italy, due to the particular and probably unique geographical conformation, the infrastructure system is constituted by a large number of bridges whose correct management is often difficult to implement. In fact, there are about one and a half million kilometres of roads whose competence is divided between the State, Regions, Provinces, Municipalities and other numerous public and private companies. This makes it difficult to implement a national register of the infrastructures, in fact, a Bridge Management System (BMS), which accounts for inspections, retrofitting, etc., is currently still missing. A BMS can be

used as a tool for communicating with governments and bridge managers about the conditions of the infrastructural network, traffic safety and structural vulnerability of bridges to hazard events, such as earthquakes, scour, etc.

Moreover, maintaining bridges in safe and serviceable conditions is complicated also by the wide variety of structural types. Each type of structure behaves differently, suffers from different types of deterioration and has different maintenance needs.

With particular reference to prestressed concrete bridges, especially the post-tensioned ones, in the last years emerged the need for reliable engineering tools for the evaluation of their capacity in corrosion conditions. In fact, particular environments, like the one following lack of injections in the mortar filling the duct in which are located prestressing steel strands, led to corrosion phenomena that can strongly reduce their strength and ductility capacities, whit consequently possible brittle sudden collapses. As a matter of fact, corrosion phenomena in strands represent nowadays a complex problem that structural engineers have to face.

1.2 Objectives

The main objectives of this thesis are to provide engineering tools to easily estimate the effects of corrosion in steel strands by means of simplified and analytical models. Consequently, the specific research objectives are therefore:

- to represent the variability of the strength of corroded strands that emerged from experimental campaigns;
- to develop of strength reduction curves for corroded strands;
- to provide design-oriented safety factors and combinations coefficients useful for taking into account corrosion phenomena in safety and assessment phases;
- to develop of ultimate displacement reduction curves for corroded strands;
- to estimate the effects of the corrosion in strands on the structural behaviour of the elements in which they are essential, like post-tensioned beams.

The results obtained in this thesis represent an original proposal to face the complex problem of corrosion in prestressing strands that has become tragically popular nowadays.

1.3 Outline of the thesis

The thesis has been written in three parts and is focused on aspects regarding the existing bridges, from a general overview to the specific problem concerning corrosion

in prestressing steel strands, also including a small part regarding the seismic upgrading of bridges through deck isolation. This organization is schematized in Figure 1.3 with reference to the current framework regarding existing bridges.

- Part I General overview, from chapter 2 to chapter 6;
- Part II: Corrosion in wires and strands, from chapter 7 to chapter 13;
- Part III: Seismic upgrading through deck isolation, from chapter 14 to chapter 19.

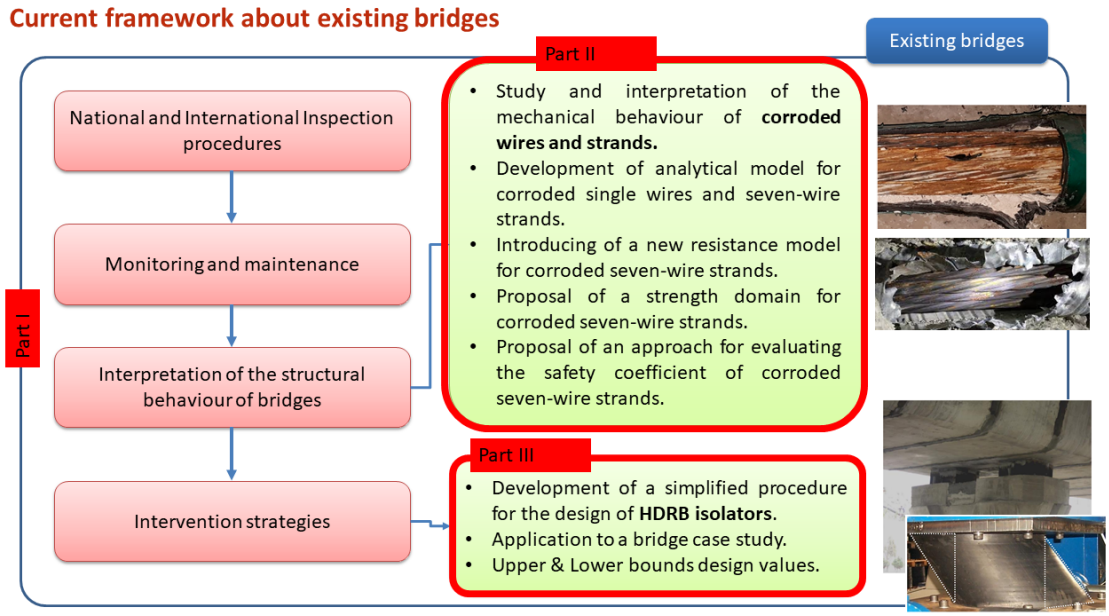

a

Figure 1.3: Current framework about existing bridges.

[a]Pictures taken from: [3], [4], [5]

Part I provides a general overview of safety assessment of existing bridges. It encompasses chapter 2 through chapter 6. Chapter 2 describes the historical-cultural framework that has led to the current situation, trying to underline the importance of inspections and safety assessment, interpretation of the structural behaviour, monitoring and maintenance.

In this regard, chapter 3 summarizes the procedures adopted for bridge management at National and International levels; chapter 4 describes typical damages that could affect existing bridges categorizing most of them with respect to their structural typology; chapter 5 describes the Structural Health Monitoring from the different phases of its implementation to specific mathematical techniques useful for the extraction of the significant parameters of monitored bridges and to the management of long-term data. Finally,

chapter 6 reports some examples of interventions applicable to existing bridges.

Part II represents the core of the thesis, providing the main original results. It encompasses chapter 7 through chapter 13.

Chapter 7 constitutes the introduction to the current issues of corroded steel strands in post-tensioned elements and describes the approaches followed to manage their structural behaviour and their effects on the structural behaviour of post-tensioned elements.

Chapter 8 describes the analytical model for corroded wires and a parametric study to highlight the effects of the geometry of the corrosion and the steel material parameters on its structural behaviour.

Chapter 9 describes the analytical models for corroded seven-wire strands and a parametric study to highlight the effects of the geometry of the corrosion and the steel material parameters on their structural behaviour. This highlighted the effects of the variability of the corrosion in the wires on the strength of corroded seven-wire strand.

Chapter 10 presents the peak strength resistance model for corroded strands. The model introduces a new coefficient, which is defined as the "group coefficient" that aims at describing the dispersion of the response that emerged from the parametric study conducted in chapter 9, which also emerged from experimental campaigns available in the literature. The application of the peak strength resistance model in deterministic and probabilist approaches allowed to define resistance curves and design-oriented results for corroded seven-wire strands. These approaches have been applied with reference to two procedures based on the knowledge level of corrosion for the specific cases at hand. The parameters that define the resistance model have been estimated through several Monte Carlo simulations of corroded seven-wire strands.

Chapter 11 describes ultimate displacements reduction curves for corroded wire strands estimated thanks to the Monte Carlo simulations of corroded seven-wire strands.

Chapter 12 combines the results achieved in the previous chapter. From the combination of the strength and the ultimate displacement reduction curves, it is estimated a reduced sigma-epsilon relationship for the steel material that allows to take into account the effects of corroded strands into the structural behaviour of post-tensioned beams, for instance, through a reduced bending moment-curvature diagram.

Chapter 13 reports a summary of the results obtained in part II.

Part III reports an application of seismic upgrading of an existing bridge through deck isolation.

The case-study bridge is presented in chapter 15 with its modelling through finite element model and minimal systems.

Chapter 16 presents a simplified procedure for the identification of the horizontal stiffness of the isolator.

Chapter 17 reports the results of a series of time-history analyses conducted through the finite element model of the case-study bridge to study the effects of different modelling of the behaviour of the isolators.

Chapter 18 reports the results of a series of time-history and response spectrum analyses conducted through the finite element model of the case-study bridge to study the effects due to the vertical component of the seismic actions and the effectiveness of considering these effects by combining the two types of analyses or through complete dynamic analyses.

Chapter 19 reports the results of a series of time-history conducted through the minimal systems of the case-study bridge to study the effects of the variability of the shear modulus of the rubber material of the HDRB isolators on the structural behaviour of the isolated bridge. The analyses of the different variability in the response parameters that emerged (displacement of the isolators, at the top of the piles and abutments) allowed to define the values of Upper & lower bounds useful for design purposes.

Chapter 20 reports the conclusions of this thesis.

Appendix A reports all the results obtained in part II of this thesis.

Appendix B and Appendix D provide analytical demonstrations of partial results used in chapter 10.

Appendix C provides analytical demonstrations of partial results used in chapter 8.

Part I

General overview

2

Historical-cultural framework

Sommario

Questo capitolo descrive brevemente il contesto storico riguardante i ponti esistenti. I principali aspetti legati all'aumento dei carichi da traffico, all'invecchiamento dei materiali e alla mancanza di manutenzione necessitano di un corretto piano di gestione delle ispezioni e degli interventi. Da qui l'origine del concetto di Bridge Management System (BMS). Vengono ripercorse le principali tappe che hanno visto la nascita di diverse società gestori del patrimonio infrastrutturale italiano per poi, infine, sottolineare l'importanza delle ispezioni e delle valuzioni di sicurezza, dell'interpretazione del comportamento strutturale dei ponti e delle attività di manutenzione e monitoraggio.

Summary

This chapter briefly describes the historical context regarding the existing bridges. The main aspects related to the increase in traffic loads, the ageing of materials and the lack of maintenance require a correct management plan for inspections and interventions. Hence the origin of the concept of Bridge Management System (BMS). The main stages that have seen the birth of various companies managing the Italian infrastructure heritage are described. Finally, the importance of inspections and safety assessments, of the correct interpretation of the structural behaviour of bridges and of maintenance and monitoring activities is underlined.

2.1 The issue: degradation and ageing of bridges

A bridge is a structure that allows the overcoming of natural or artificial obstacles [6]. Bridges are key components of the nation's infrastructure net that provide transportation connectivity to waterways, railways, highways and roadways. During the service life, a bridge has to support the entire set of loads that can occur on the viable surface (deck), such as traffic loads and pedestrian loads, and below the viable surface, for instance, due to the effects of the flow of a river. In addition, the structure of a bridge has to deal with

the ageing of the material whose elements are made up. This is a relatively new problem that engineers have to become familiar with. In fact, the problems associated with the ageing and the decay of materials, like concrete and steel, were unknown when most of the bridges that constitute the infrastructure net were built. Furthermore, the traffic loads are increased in the last decades, if compared with those ones supposed during the design phase and often the ordinary maintenance procedure has not been applied. If neglected, all these aspects can lead either to the replacement of the bridge (or to its parts) or to the collapse of the bridge itself, leading to an increase in the costs for the society. In fact, a correct maintenance plan, which has to be applied during the service life of bridges, allows the correct management of the infrastructure also from an economic point of view. The service life is a period of time in which only ordinary maintenance has supposed to be applied to the structures. On the contrary, extraordinary maintenances have to be fielded after the service life is nominally passed.

The factors that influence the management of a bridge are generally of social and economic nature and affect both the single bridge and the entire infrastructural net in which they are inserted. A correct management should take into account the following aspects: (i) conditions of the structure, (ii) capacity of the structure, (iii) deterioration rate of the materials, (iv) available maintenance treatments, their effectiveness and their duration over time, (v) costs related to maintenance treatments, (vi) traffic management costs, and (vii) evolution of traffic flow and associated daily costs. As a matter of fact, the management of the entire infrastructural net, which is constituted of thousands of bridges, that takes into account all of these points requires a system that should be able to follow the health of the net and help the owners towards the correct interventions, both from an economic and temporal point of views. The direct cost of the engineering work necessary to maintain a satisfactory road network is high, however, indirect costs due to the resulting traffic congestion and disruption can be much higher and cause a severe economic penalty, particularly on the increasing number of roads where traffic flows are reaching saturation.

Nowadays, automated systems for managing bridge maintenance are catching up with modern Bridge Management Systems (BMS). In addition, to collect all the description data of the bridge, i.e. age, owner, size, etc., they allow the storing of the data deriving from inspections and successively the management and the scheduling of the interventions and future inspections. In fact, they consent to establish the priorities of intervention through particular procedures that also consider economic aspects. The economic aspects can be evaluated from cost-benefit analysis taking into account different maintenance strategies and different cost factors, such as those ones related to the delay due to traffic, the deterioration rate of the bridges, the effective duration of the repair systems, the value over time of the money and the benefits related to the improvements. Then, a BMS is constituted by the following parts: (i) inventory of the bridges, (ii) assessment of the conditions, (iii) assessment of the structural safety, (iii) comparison between the

maintenance options, (iv) program of optimal maintenances, and (v) program of proprietary maintenances. Clearly, all these parts require valid techniques for the estimation of the material decay effects, for the strategies of intervention and for the priority of the inspections and/or interventions.

2.2 Origins of the modern conception of Bridge Management

The collapse of the Silver Bridge in 1698, Ohio, USA, led to the creation of a nationwide, standardized bridge inspection program. In fact, the Federal Highway Administration (FHWA) published the National Bridge Inspection Standard (NBIS) [7], which are standards established for the safety inspections of highway bridges on public roads throughout the United States. In addition, they also developed the so-called National Bridge Inventory (NBI) which is a database with information of all bridges and tunnels in the United States that have roads passing above or below them. The bridge information includes the design of the bridge and the dimensions of the usable portion. The data are often used to analyse bridges and to judge their condition. The inventory is developed for the purpose of having a unified database for bridges to ensure the safety of the travelling public, as required by the Federal Aid Highway Act of 1968 [8]. National Bridge Inventory includes identification information, bridge types and specifications, operational conditions, geometric and functional descriptions, and inspection data.

In 1991, the FHWA developed a bridge management system (BMS) called “Pontis”. The system is owned by the American Association of State Highway and Transportation Officials (AASHTO). Many states began using Pontis when the Intermodal Surface Transportation Efficiency Act [9] required each state to implement a BMS. As of 2008, it was licensed by AASHTO to over 45 United State transportation departments and other organizations in the U.S. and other countries. In the same years, the National Cooperative Highway Research Program (NCHRP) developed the BRIDGIT software, which is a micro-computer-based bridge management system (BMS), with the purpose to implement the requirements proposed by the Federal Highway Administration (FHWA). Other states, like New York, Pennsylvania, North Carolina, Alabama e Indiana started to develop software for the bridge management system (BMS).

Some years later, in Europe the BRIME project [10] was born, whose objectives are to develop a framework for the management of bridges on the European road network and identify the inputs required to implement such a system. This project will look at the various modules required to enable the bridges to be managed, review the current state-of-the-art and produce an outline framework for the management of the bridges. As a result of the project, the sources of bridge deterioration could be divided into three groups: (i)

deterioration or defects arising from faults in design and construction, (ii) defects arising during construction, and (iii) deterioration from external influences.

A simple model has been developed for categorising damaged locations in concrete structures. The model is based on a visual assessment of the damaged area as well as on test results, both on-site and in the laboratory. It uses the neural network hybrid model and can assess the type of repair work required on structures with a large number of deteriorated areas. The structural assessment module, developed for the BRIME project, has given information on the load-carrying capacity of bridges. It has consequently reconstructed the load-carrying capacity history of a specific bridge and of the overall bridge network. The project has developed a method that considers all costs involved in the designing, constructing, inspecting, maintaining, repairing, strengthening and demolishing of a bridge together with the associated road user costs, in order to choose between bridge repair alternatives. It has also shown how is it possible to combine results from the main bridge management activities, such as inspections, assessment, testing, maintenance, prioritisation and replacement, to produce a framework for a computerised bridge management system.

2.3 Italian historical framework

The management context of the Italian infrastructure comes from a complex process of agreements between the Italian government and the private companies identified as managers of the infrastructure network. In 1950, on the initiative of the Institute for Industrial Reconstruction (IRI), it was founded the society Società Autostrade Concessioni e Costruzioni s.p.a.. Its main objective was to take part, together with the other industrial groups, in the reconstruction of the Italian infrastructural system after the second world war. In 1950, was also established the first agreement between the Società Autostrade Concessioni e Costruzioni s.p.a (today known as Autostrade s.p.a) and the society "Azienda Nazionale Autonoma delle Strade (ANAS)", which was founded in 1954, with the purposes of building the so-called Autostrada del Sole, the longer Italian highway (it links Milan to Naples). Thereafter, a series of other agreements followed to delineate the country's infrastructural network.

In 1999, the IRI decided to privatize a series of companies like "Società Autostrade Concessioni e Costruzioni s.p.a.", transferring the management and maintenance of the infrastructure to private companies. In 2003, after the definition of a new asset for these activities, it was founded the "Autostrade Per l'Italia s.p.a. (ASPI)" fully controlled by Autostrade s.p.a. (today known as Atlantia company). Nowadays, the Italian infrastructural network is managed by ANAS, ASPI and other private companies that have the task of maintenance of the infrastructure itself.

In this context, after some bridge collapses, like the Ariccia bridge, in Ariccia, Italy, it was highlighted the need for a survey procedure for existing bridges (which had a different meaning with respect to maintenance). The collapses led to the definition of technical codes for the surveillance of the exiting bridges that required the development of specific procedures by the companies in charge of the management of the infrastructure network. Therefore, in the following years was created a complex scientific system that was able to define where, when and how to make interventions also with cost evaluations: the bridge terotechnology was born. The surveillance of bridges was basically based on visual inspections with non-destructive tests.

In 1961 it was founded the "SPEA s.p.a." that developed a complex manual surveillance based on visual inspections that have been extensively adopted until nowadays.

In Italy, most of the bridges were built around the middle of the last century. Nowadays, they have passed the service life supposed during their design phase, which was typically equal to 50 years

2.4 Evolution of the capacity and demand over time

As briefly introduced, the state of bridges tends to change over time, both from a capacity and demand point of view. The capacity is mainly related to the state of the constitutive materials and to the geometry of the structural elements. Although the geometry can be considered constant over the years, this is not the case for the state of the materials. They are subjected to ageing that together with lack of maintenance leads to an increase in their decay that in turn provoke decreasing in the structural elements capacity, both from strength and ductility point of view. In parallel, the demand increases over time.

For instance, the dead load can change configuration due to the addition of structural and/or not-structural elements, such as New Jersey, asphalt layers, etc. In addition, also the traffic loads tend to change according to the development of society. This is the case of bridges built in the 70s, which are the majority of the existing ones, in which the design phases have been conducted referring to a completely different traffic load scenario.

Figure 2.1 reports a graphical representation of these aspects. As a matter of fact, if there happens to be a common point between the curves that describe the trend of the capacity (green) and the demand over time (orange), a collapse would occur. Thus, a possible way to avoid sudden local and/or global collapses is to perform maintenance and monitoring activities. These two activities should be carried out in symbiosis in such a way as to "follow" the structure state over time and make interventions when they are considered more appropriate, from both the structural and the economic point of view. This allows to increase the residual lifetime of the structure and enhance the management of the maintenance plans for future activities, leading to a better allocation of funds. In

fact, Structural Health Monitoring can guide in the performing of intervention strategies aimed at improving the deficiencies associated to anomalies of features implemented as health-descriptors in the monitoring system itself.

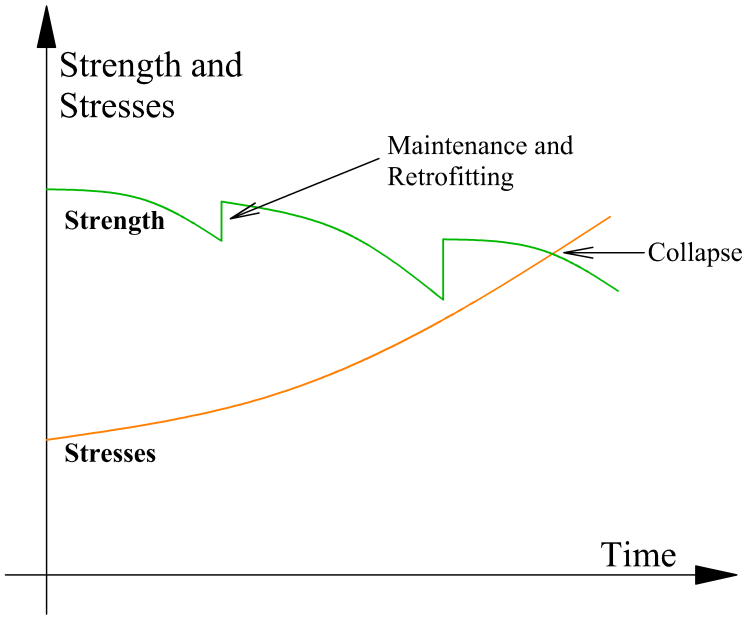

Figure 2.1: Evolution of the capacity and demand overt time

2.5 The importance of inspection and safety assessment, interpretation of the structural behaviour, monitoring and maintenance

Quite similar to what is required by the Italian technical code [11], which identifies, as fundamental principles for new structures: (i) the correct design, (ii) the correct construction, and (iii) the testing, and (iv) the maintenance, the present thesis aims at identifying for the existing structures and bridges: (i) the principles of inspection and safety assessment, (ii) general indication for a sound interpretation of the structural behaviour, (iii) monitoring, and (iv) maintenance. In fact, inspection and safety assessment procedures (chapter 3) are carried out on existing bridges in order to check the current condition (design+construction) and to identify issues that can compromise both their structural and functional behaviour. The interpretation of the structural behaviour plays a central role in understanding the effects related to the different scenarios of damages that can occur on the bridges, especially with reference to their structural scheme and constitutive material (chapter 4). Moreover, monitoring (chapter 5) and maintenance (chapter 6) are two important tools that should help the manager of bridges in order to follow their conditions

and guide in performing interventions and retrofitting operations to prevent limit states. As a matter of fact, for the proper management of existing bridges, main activities should be conducted properly.

3

National and International bridge inspection and safety assessment procedures

Sommario

Questo capitolo descrive i principali aspetti delle varie procedure di valutazione delle condizioni strutturali di ponti esistenti adottate a livello nazionale ed internazionale. A livello nazionale, oltre che i più diffusi approcci, quali quelli proposti da SPEA s.p.a. e CIAS, è descritto anche il recente approccio multilivello previsto dalle attuali Linee guida per la classificazione del rischio, la valutazione della sicurezza ed il monitoraggio dei ponti esistenti, datate 2022.

Summary

This chapter describes the main aspects of the various procedures for evaluating the structural condition of existing bridges adopted at national and international levels. At the national level, in addition to the most used approaches, such as those proposed by SPEA s.p.a. and CIAS, the recent multilevel approach envisaged by the current Guidelines for risk classification, safety assessment and monitoring of existing bridges is also described, dated 2022.

To determine which structures require maintenance, it is necessary to undertake a systematic programme of inspections. One of the main purposes of these inspections is to provide data on those structures that are in poor or critical condition and to decide whether they need interventions, strengthening or retrofitting. The results of these periodic inspections are used to provide an assessment of the condition of both the structural elements and the structure itself. Most of the methods of condition assessment use two different approaches for both the assessment of individual elements and the assessment of the structure as a whole. The first uses a cumulative condition rating which is derived from the condition of individual elements and the second uses the condition rating of the bridge element in the worst condition as the condition rating of the structure itself. The condition assessment is based on bridge inspection.

The main purpose of bridge management, which is the most important use of information on the conditions of a large number of bridges in a bridge dataset, is to identify those that are most deteriorated and need priority interventions. Different methods have been developed for evaluating bridge inspection data to give the bridge a condition rating. A short description of some methods that have been developed in the USA and in Europe is here presented.

3.1 Bridge management according to United States approaches

The National Bridge Inspection Standard (NBIS)[7] in the USA, establishes the national standards for the management of existing bridges. In addition, other manuals supporting this purpose are the Bridge Inspector's Training Manual [12], the Manual for Maintenance and Inspection of Bridges [13], the Recording and Coding Guide for the Structure Inventory and the Appraisal of the Nation's Bridge [14]. Following collapses that occurred over the years, the Federal Highway Administration published: the Culvert Inspection Manual [15], the Inspection of Fracture Critical Bridge Members [16], after the collapse of the Mianus River Bridge (Connecticut, 1983), Evaluating Scour at Bridges [17] (after the collapse of Schoharie Creek Bridge, New York, 1987).

In the 80s the technical manuals available in the USA allowed the company in charge of the maintenance of the existing bridges to correctly implement the standards established by the National Bridge Inspection Standard. This led to two important innovations in the next years: (i) the bridge management system implementations by most of the departments in infrastructural network management and (ii) the publishing of the Manual for Bridge Evaluation [18], which represents a reference document in the United States. Generally, the following performance measures and indexes can be defined:

- the Bridge Health Index (BHI);
- the National Bridge Inventory (NBI) condition rating;
- the Sufficiency Rating (SR);
- Structural Deficiency (SD) and Functional Obsolescence (FO);
- Geometric Rating;
- Load Rating;
- Vulnerability Rating (VR).

However, some of these performance indexes and conditions can be also recognized in other bridge management approaches.

The Bridge Health Index (BHI) is calculated from an element-level inspection as a ratio between the current and the initial value of all elements of the bridge and is used with the purpose of preserving the existing bridges by means of the establishment of a scheduled plan of maintenance and interventions. BHI may range from 0%, corresponding to the worst possible health, to 100% for the best possible health. The hypothesis of the BHI is that the new condition of each bridge element represents the best condition state. During the service life, the elements might deteriorate to a lower condition state due to increasing of traffic loads, lack of maintenance, and design or construction flaws. This situation requires interventions in order to improve the condition of the elements until the best condition state. Thus, the bridge element-level inspections are needed for calculating the BHI that should reflect the bridge condition. The element-level inspection aims at the evaluation of the condition of all the bridge elements according to the following states:

- good: state 1;
- fair: state 2;
- poor: state 3;
- severe: state 4.

For each element, a description of the condition that allows identifying the states is provided. To aggregate the element-level condition to the whole bridge-level condition, weights are assigned to the elements according to the economic consequences of element failure. The choice of failure cost is a function of models for optimal actions. The introduction of the failure costs allows scaling of the importance of each element with respect to the other (i.e. girders have more weight than bearings). Consequently, elements whose failures have relatively reduced economic effects are characterized by a small weight than elements whose failure could lead to closing the bridge.

The NBI condition rating takes into account the main bridge structural elements such as superstructure (deck), substructure (pears, abutments) and foundations. The definition of the rating is based on condition states on a scale from 0 to 9, according to Table 3.1. It is worth noting that NBI is transitioning to a new data standard, guidance, procedures, and web application: the National Bridge Inventory Based on the SNBI (Specific for National Standard Inventory) [19] which provides a complete guide to inventory the bridges, with reference to:

- bridge identification: through the location part (in terms of state, country, coordinates, etc.) and the classification part (in terms of owner, historical significance, etc.);

- bridge material and type;
- bridge geometry;
- features in terms of the road type;
- inspections conducted;
- bridge conditions in terms of: structural parts, such as the deck, the superstructure and the substructure, and in terms of global condition classification.

As a matter of fact, the NBI condition rating does not represent the overall condition of an entire bridge but shows the localized condition of the main bridge elements. This leads to the difficult management of the bridge in a complete BMS approach. In addition, like all the rating systems, the NBI index depends on the interpretations of the inspectors who have to decide which defect most represents the bridge condition when multiple defects may influence negatively the ratings. This is not the case of the BHI that for each element of the bridge allows to calculate the parts of the element itself that are represented by the different states.

Table 3.1: Definition of the bridge rating based on condition states according to NBI

Code	**Condition**	**Physical Description**
N	Not applicable	New bridge
9	Excellent	Isolated inherent defects.
8	Very good	Some inherent defects.
7	Good	Some minor defects.
6	Satisfactory	Widespread minor or isolated moderate defects.
5	Fair	Some moderate defects; strength and performance of the component are not affected.
4	Poor	Widespread moderate or isolated major defects; strength and/or performance of the component is affected.
3	Serious	Major defects; strength and/or performance of the component is seriously affected. Condition typically necessitates more frequent monitoring, load restrictions, and/or corrective actions.
2	Critical	Major defects, component is severely compromised. Condition typically necessitates frequent monitoring, significant load restrictions, and/or corrective actions in order to keep the bridge open.
1	Imminent failure	Bridge is closed to traffic due to component condition. Repair or rehabilitation may return the bridge to service

0	Failed	Bridge is closed due to component condition, and is beyond corrective action. Replacement is required to restore service.

The Sufficient Rating (SR) is an index that combines the functional and condition data in the NBI into a single number from 0 to 100. SR aims at representing the bridge suitability to remain in service. It is also used to allocate funds for retrofitting operations. Typically, if the SR is less than 50 and the bridge results are classified with low condition states, replacement possibility is evaluated. If SR is within 50 and 80 and the bridge results are classified with medium-high condition states, retrofitting operations are considered. However, the goal of the SR index is not the determination of the bridge condition or for implementing maintenance decisions, it emphasizes large-scale functional and geometric characteristics.

The Structural Deficiency (SD) is a classification for bridges that have an NBI rating for the deck, superstructure and substructure equal to 4 or less (according to Table 3.1). Structurally deficient does not imply that they are unsafe but that they need maintenance, retrofitting or element replacement. In many cases, structurally deficient bridges are subjected to restrictions of the traffic loads maintaining the operational functionality. On the other hand, Functional Obsolescence (FO) is a classification for bridges that were built with reference to standards that don't satisfy the actual ones for new bridges. The functionally obsolete classification is also used for prioritizing the interventions of retrofitting and element replacements.

The Geometric Rating is an overall rating for deck geometry based on two NBI items: bridge roadway width and vertical over-clearance. The geometric rating varies from 0 to 9 as the NBI rating scale according to Table 3.1.

The Load Rating is a procedure to evaluate the adequacy of various structural components to carry predetermined live loads. This may lead to load restrictions on the bridge or identification of components that require maintenance or retrofitting to avoid the closing of the bridge. However, the load rating does not indicate the overall condition of the bridge, it can reflect problems with the load-carrying structural member such as the beams and girders.

The Vulnerability Rating (VR) is associated with a certain likelihood of a hazard event. The consequence score is based on the type of bridge failure (catastrophic, partial collapse or structural damage) and the exposure to the public from that failure. It is used to measure the vulnerability of the bridge to structural or operational hazard events such as earthquakes, and over-load traffic loads.

Clearly, the manager of the infrastructural network could use different types of performance measurements and indexes for bridge management decision-making. For instance,

Table 3.2 reports some examples of performance measurements that may be adopted in the United State of America, whit reference to different goals.

Table 3.2: Examples of performance measurements

Goal	**Performance measurement**
Preservation of Bridge Condition	NBI Rating
	Bridge Health Index
	Sufficiency Rating
Traffic Safety Enhancement	Geometric Rating/Functional Obsolescence
	Inventory Rating or Operating Rating
	Scour Vulnerability Rating
Protection from Extreme Events	Fatigue/Fracture Criticality Rating
	Earthquake Vulnerability Rating
	Other Disaster Vulnerability Rating (collision, overload, man-made)

A good bridge management operation is then based on: (i) the development of an inventory of the infrastructural network and (ii) the identification of the structural elements that need maintenance and retrofitting interventions. The latter point can be conducted by using different indexes related to the final golf of the bridge manager. Nowadays, most of bridge management systems (BMS) are based on element-level information for performing bridge performance measurements. Basically, the following approaches for their calculation can be identified:

- Ratio-based approaches in which the bridge performance measurement is performed with reference to the condition of the structural element in new condition. In other words, the index provides an estimation of the remaining value of the bridge. The health index introduced by AASTHO bridge management software, i.e. Pontis is an example of a ratio-based method.
- Weighted averaging approaches in which it is estimated the condition of the whole bridge taking into account the condition ratings of all structural elements of the bridge weighted by their significance or contribution to the structural integrity of the bridge.
- Worst-conditioned approaches in which the condition of the bridge is approximated by the ratings of the component in the worst condition. In fact, the evaluations are carried out on key bridge components neglecting the minor bridge elements.

- Qualitative approaches in which the condition of the bridge is not expressed on a numerical scale. They describe the bridge structure with qualitative levels, like "Poor," "Fair," or "Good," based on the condition state and importance of the elements under investigation.

Furthermore, there are other bridge condition indexes that have been developed by combining some of the above-listed methods. One example is the sufficiency ratings (SR), which combine the weighted averaging and the worst condition component approaches.

In order to evaluate the bridge performance measures according to the national bridge inspections standards, the manual for bridge evaluation [18] developed by AASTHO, identifies inspections as initial, routine, in-depth, fracture-critical member, underwater, special and damage. Briefly descriptions of these inspections are reported as follows:

1. **Initial Inspection**. It is the first inspection that is performed for a new or an existing bridge. The main objective of the inspection is to acquire the bridge inventory data and establish a timeline for future inspections. These inspections require qualified technicians since they may require some analytical determination of the load capacity of the bridge. At this level two are the aims of the inspections: (i) to provide all the information required by the national bridge inventor (NBI) and (ii) to acquire the conditions of the bridge, including all the existing defects and their extensions and positions. Typically, this kind of inspection is conducted 90 days after the construction/retrofitting of the bridge.

2. **Routine Inspection**. It is a regularly scheduled inspection regarding all the structural elements that need the determination of the physical and functional conditions, basically those identified in previous inspections. This inspection aims at identifying any changes from the initial conditions or previous recorded conditions and to ensure that the safety of the structure is still present. The inspections are conducted starting from the deck until the foundation including, if it is necessary, limited inspections of underwater positions. If some part requires a more detailed inspection in order to determine its impact on the safety conditions of the structure, in-depth inspections have to be carried out. Usually. routine inspections are conducted every 24 months.

3. **In-Depth Inspection**. It is a detailed inspection regarding one or more parts of the bridge above or below the water level in order to identify any capacity loss that emerged during the routine inspection. The in-depth inspection is conducted using visual or non-destructive techniques requiring traffic control and special equipment, such as under-bridge inspection equipment and workboats.

4. **Fracture-Critical Member Inspection**. It is an inspection regarding steel members in tension, or with tension elements, whose failure might cause a partial or complete collapse of the bridge. Examples of these elements are: two-girder systems and suspension systems. Typically, it is performed every 24 months.

5. **Underwater Inspection**. It is an inspection that is conducted on the parts of the bridge that are under the water level. Typically, it is conducted every 60 months.

6. **Special Inspection**. It is an inspection that is scheduled by the owner of the bridge. It is used to monitor a particular known or suspected deficiency, such as crack, settlements, or scour.

7. **Damage Inspection**. It is an inspection that is not scheduled and that aims at assess the structural damage resulting from environmental events, such as earthquakes, flooding, or human actions, like impacts. The amount of effort of this kind of inspection depends on the events and the extent of the damage.

The manual identifies the qualified personnel in charge of the different inspections: (i) the program manager who is responsible for all bridge inspections activities, including reporting and maintaining an inventory, (ii) the inspection team leader who is in charge of an inspection team responsible for planning, preparing, and performing the on-site inspection of the bridge, (iii) load rating manager who is responsible for the load ratings, establishing consistent methods to be used during the inspections, and (iv) underwater bridge inspection driver who is in charge of performing the underwater inspection.

When the condition of existing bridges requires attention, based on the aforementioned results, like structural conditions, material properties, loads etc., a safety assessment has to be performed.

The bridge evaluation according to AASHTO requires safety assessments. The results are generally expressed in terms of a rating factor for a particular live load model. Rating factors greater than one indicate that the bridge is safe for the loads tested. There are two methods available for load rating bridges:

- load factor rating: it can be performed with reference to inventory and operating conditions. The inventory rating level corresponds to usual design-type loads while the operating rating level corresponds to the maximum permissible live load the structure can withstand safely. Further, the inventory load rating accommodates live loads that a bridge can carry for an indefinite period, while the operating load

rating refers to live loads that could potentially shorten the bridge life if applied in a continuous way. The load rating is given by the following formula:

$$RF = \frac{C - A_1 D}{A_2 L(1 + I)} \tag{3.1}$$

where *C* is the capacity of the structural element, *D* is the demand due to the load loads on the element, *L* is the demand due to the traffic loads on the element, *I* is the impact factor, A_1 is the factor for dead loads, and A_2 is the factor for traffic loads.

The impact factor takes into account all live loads to consider their speed, vibration, etc.. It can be evaluated according to the following formula:

$$I = \frac{50}{L + 125} \leq 0.3 \tag{3.2}$$

Then the rating factor is multiplied for the weight of the live load truck to yield the bridge member rating for that structural element. The overall rating of the bridge is controlled by the structural element with the lowest rating.

- Load and Resistance Factor Rating (LRFR): it can be performed with reference to inventory and operating conditions. LRFR uses limit states for strength, service, and fatigue to ensure safety and serviceability in the load rating. These limit states are provided by AASHTO specifications.

  The strength limit state accounts for the strength capacity of the structure under permanent and live loading while the service limit state accounts for stress, deformation, and crack width.

  The rating is given by the following formula:

$$RF = \frac{C - \gamma_{DC} DC - \gamma_{DW} DW \pm \gamma_P P}{\gamma_L LL(1 + IM)} \tag{3.3}$$

  where $C = \Phi \Phi_c \Phi_s R_n$ and $\Phi_c \Phi_s \geq 0.85$.

  DC is the effect on the structural components due to dead loads, *DW* is the effect on wearing surfaces and utilities due to dead loads, *P* is the permanent load in addition to the dead ones, *LL* is the effect on the structural components due to live loads, *IM* is the dynamic load allowance. The different γ indicate the load factors associated to the corresponding effect. Φ_c, which takes into account the increasing of uncertainties due to the deteriorated conditions, and Φ_s, which accounts for the level of redundancy in the structure, are the condition and system factors, respectively. Φ is the same factor valid for new structures accounting for general uncertainties.

  The result of the load rating depends on the bridge material, the present condition of the structural elements, etc.. Therefore, after determining the nominal resistance,

the capacity of the bridge can be obtained by applying the three safety factors Φ,Φ_c and Φ_s.

The aforementioned load and resistance factors are provided by AASHTO and can be calibrated using the selected safety index targets to achieve uniform safety for all material types, spans, and load effects, according to the procedures reported in [20].

3.2 Bridge management according to Swiss approach

The responsibility for the maintenance of the Swiss national road network was transferred in 2008 from the cantons (member states of the Swiss Confederation) to the federal administration. Bridges are preferably repaired in large so-called maintenance sections, involving repair and upgrade of all elements of the highway, allowing reduction of the traffic disturbances. In this regard, the large maintenance sections are maximum of 15 km in length. Therefore, construction sites shall not be longer than 3–5 km.

The main objective of the federal administration is to ensure a period of 15 years without the need for additional construction interventions.

Bridges and overpasses within the highway perimeter are assessed by means of various programs ranging from operational maintenance to long-term inspection plans. The first one is provided once a year and might require maintenance work to ensure proper serviceability of the bridges and to minimize the deterioration processes.

The main inspections are carried out by engineers every 5 years. The aim of the main inspection is to update the bridge management system with comprehensive information on the structural elements, the deterioration mechanisms and the current conditions. The possible conditions are reported in the following table and allow to derive the conditions of the whole structure from the conditions of the single elements.

Table 3.3: Condition levels according to the Swiss approach

Level	**Condition**	**Damages**
1	Good condition	No or insignificant damages
2	Acceptable condition	Insignificant damages
3	Damaged condition	Significant damages
4	Bad condition	Large damages
5	Alarming condition	Urgent countermeasures
9	Condition not evaluated	Condition can not be inspected

Based on the identified condition, the residual service life can be estimated and interventions and measurements planned to improve durability.

In addition to visual inspections, laboratory testing programs also provide the basis for condition assessment and estimation of the further deterioration process. Thus, the activities to be performed for the correct condition assessment are: (i) knowledge of the bridge (thanks to all the available documentation of the bridge), (ii) visual inspections, and (iii) laboratory testing.

In the structural assessments loads and resistances need to be verified according to the Swiss codes for new structures(SIA 260 to 267). The material properties can be assumed as defined in the documentation of the bridge under examination. If verification is not possible, material properties shall be updated. In case the geometrical dimensions of the structural element are verified by appropriate measurements, the partial safety factor for permanent loads can be reduced. If the verifications fail, traffic loads can be reduced according to the provisions in the code SIA 269/1 for actions on existing structures.

In Italy, the activities regarding the management and the safety assessment of an existing bridge have been conducted by referring to the manuals of inspections provided by SPEA Engineering S.p.A. and CIAS. However, the collapse of the Polcevera Bridge in Genoa has highlighted the complex management of the Italian existing infrastructure system, which is constituted of a large number of bridges. The point is that, due to the now well-known increased traffic load over time, lack of maintenance and material decay over time, the infrastructure network managers have to deal with a framework that needs priorities of interventions. Thus, the Italian Ministry of Infrastructure and Sustainable Mobility enactment of the so-called guidelines for risk classification and management, safety assessment and monitoring of existing bridges that aims at providing a procedure for the safety management of the existing bridges.

3.3 Bridge management according to SPEA approach

SPEA Engineering S.p.A. (“Società Progettazioni Edili Autostradali”) is a company of the Atlantia group with over 50 years of experience in integrated engineering services in the transport infrastructure sector, such as roads, motorways, airports, railways and vehicle parking systems. The consulting services offered by the specialists of SPEA Engineering include feasibility studies, design, construction management, monitoring and maintenance, both for the construction of new infrastructures and for the rehabilitation and expansion of existing ones, including adjustments to safety standards. The SPEA company has for a long time managed the maintenance of the highways on behalf of Autostrade per l’Italia, in Italy. The achievement of the goals dictated by the correct main-

tenance of the existing highways was obtained through the application of the surveillance manual. The main objective of this manual, which can also be seen as a possible procedure to follow for the correct management of the existing infrastructures, is to guide the owner in the maintenance of a proper safety level and a high-quality level of service provided by the infrastructure itself.

The points introduced by the manual are the following:

- the surveillance;
- the evaluations of the conditions of the structure elements;
- the definition of the strategies for maintenance through the identification of the interventions and the costs.

The first point is the most important and is described in the manual by visual inspections only. They consent to estimate the decay of the structure and the assignment of scores that allow the calculation of a quality global index. The index allows to evaluate the decay evolutions and the priority of interventions, to establish their costs and to plan future activities in terms of interventions. These activities are supported through the software STONE and SAMOA (Sorveglianza Auscultazione Manutenzione Opere d'Arte).

The manual introduces four types of inspections:

- ordinary inspections: they are performed by qualified technicians every 3 months and do not require special equipment. The inspections provide not-destructive tests, for instance in order to evaluate the elastic modulus of the concrete (through the sclerometric test), and the survey of the steel bars (examination by radiography, radioscopy and reflectometric method) and local tests, for instance, visual examination by localized demolition to assess the state of the injection of the grout in the strands in prestressed elements, of the prestressed elements.
- main inspections: they are performed by engineers every year and aim to evaluate the defects and their causes;
- special inspections: they are performed after hazard events and when some anomalies have been reported. These kinds of inspections require detailed evaluations of the state of the defects and a final report that provides morphological indications and descriptions of defects. Based on this report, further surveys, interventions and limitations of the traffic might occur;
- inspections with special vehicles: they allow to check places in the structure that are difficult to reach. An example of these vehicles is the by-bridge platform truck.

The manual provides the condition of the bridge and its elements by means of specific defects cards that allow to evaluate the condition of each part of the bridge. Each card reports the description of the defect and a possible score between 10 and 70. In detail, the scores are identified in the following ranges:

Table 3.4: Defects and score identified by the manual of the surveillance

Defects that do not require interventions	**Defects that don't require short-term interventions**	**Defects that require short-term interventions**
1: the defect is stable 2: the defect can evolve into other defects that don't require interventions		
3: the defect can evolve into other defects that require interventions		
	4: the defect requires long-term interventions 5: the defect requires medium-term interventions	
		6: the defect has an influence on the static behaviour of the bridge, but the safety coefficients are not significantly reduced 7: the defects lead to a significant reduction of the safety coefficients

As a first approximation, short-time, medium-time and long-time periods can be chosen equal to: two years, between two years, five years and more than five years, respectively. In addition, other two parameters can be evaluated in order to help the estimations of the costs of the interventions: (i) the number of the sub-elements, which can be evaluated with respect to each element of the structure, i.e. deck, piers, abutments, etc., that present defects, without considering their extension, and (ii) percentage of the extension of the defects in each of the sub-elements.

Based on these scores, the index quality defined for the typology of the bridge, i.e. viaducts, overpasses, etc., and for the analysed zone, i.e. road trunk can be evaluated. The

index aims at representing the quality of the infrastructure and can be evaluated as follow:

$$I = 100 - \frac{12E + 8D + 4C}{A + B + C + D + E} \cdot 100 \tag{3.4}$$

where the letters represent the number of bridges with scores in fixed ranges, according to the following definitions.

- **A**: Number of bridges with scores in the range 0 and 3
- **B**: Number of bridges with scores equal to 4
- **C**: Number of bridges with scores equal to 5
- **D**: Number of bridges with scores equal to 6
- **E**: Number of bridges with scores equal to 7

However, this approach requires a methodology for assembling the structural elements of different bridges, since it might result as not immediate. All these indexes are then stored in the STONE software where they can be checked in future activities in order to see the quality of the infrastructure network, for example referring to some structural element, typology of the bridge and so on. Another approach proved by the manual is the use of the SAMOA database that reports different evaluation cards for each structural element, which can also be sub-divided into parts. In other words, the defects are better discretized in the different structural elements. In addition, this database has more than 100 defect cards with respect to the STONE database where the defects are grouped for scores (from 1 to 7). The SPEA methods can be framed into a weighted averaging approach.

3.4 Bridge management according to CIAS approach

CIAS, "Centro Internazionale di Aggiornamento Sperimentale-Scientifico" (the International Center for Experimental Scientific Update), is a non-profit organization that carries out a scientific dissemination activity and development of experimentation in the structural and geotechnical field of civil engineering. CIAS developed the manual "Manuale Valutazione dello Stato dei Ponti", for the maintenance and management of existing bridges that aims at: (i) obtain a full survey of the bridges, (ii) to provide a tool for the assessment of the health state of the bridges through the programmed visual inspections, (iii) to provide to the manager of the infrastructural network, informatic support for the management of the existing bridges.

The idea of the manual can be basically subdivided into two parts:

- the survey of the bridge;

- the visual inspection for the damage evaluations.

The first one aims at acquiring all the characteristics of the structure, like geometry, location, etc., that together with the type and the extension of the damages on the structural parts, which are evaluated through the visual inspection, also consents to perform statistical studies.

The first visual inspection (reference for the numerical evaluation of the general conditions) is called primary visual inspection. It allows to classify the bridges according to the state of decay and to establish the frequency of the next inspections. In fact, the manual provides a series of evaluation defect cards, for each structural element. This is a crucial phase that has to be conducted by technicians who are experts in the bridge field. All the information regarding the bridge and the visual inspections are then stored in the software WeBRIDGE.

Following the visual inspections, the numerical method proposed by the manual can be applied. It provides a general index that represents the decaying state of the bridge. The numerical evaluation takes into account the weight G applied to each defect, multiplied for two coefficients, K_1 and K_2, that consider its extension and intensity, respectively. The value of G depends on the evaluation of the defects according to their possible effects on the safety of the structure. In particular, it assumes values: (i) equal to 1 if actually it represents a danger (actual risk), (ii) equal to 2 if it reduces the bearing capacity of the structure (potential risk), equal to 3 if it leads to the presence of others defects (induced risk), equal to 4 if it leads to a high economic cost for its repair. Anyway, it is already assigned to each defect in their evaluation cards. The two coefficients K_1 and K_2 assume values in the range of 0.2 and 1. Then, when it is clear the state of the defects on the structural elements in terms of the introduced parameters, the relative defect *DR* and the absolute defect *DA* can be defined according to the following formula:

$$\begin{aligned} DR &= \sum (G \cdot K_1 \cdot K_2) \\ DA &= \sum (N \cdot G \cdot K_1 \cdot K_2) \end{aligned} \tag{3.5}$$

where *N* represents the number of each structural element.

Based on the *DR* parameter, for each bridge, a hierarchical plan of the interventions can be defined. In detail, for *DR*>25 it is required an experimental campaign to evaluate the static and dynamic capacity of the bridge, with the purpose of the finite element model calibration. Contrarily, for *DR* in the range 0 and 25 it is required an ordinary intervention in order to fix the defects that are emerged during the visual inspections. If the *DR* is less than 5, no interventions are required. The kore of the approach proposed by this manual is the numerical evaluation method which represents an engineering tool that can help in dealing with the complex management and maintenance problem of the existing infrastructural network with rigorous and effective characteristics. The identification of

the state of the decay with its evaluation and classification represents a first step towards the planned management of the existing bridges.

3.5 Bridge management according to the recent Italian guidelines

After recent catastrophic events, difficulties in managing the complex Italian bridge heritage have emerged. In fact, ageing and lack of maintenance over the years led to a heterogeneous problem of management of the existing bridges that requires a certain priority in terms of safety and economic point of view. Thus, starting from May 2020, the Italian Ministry of Infrastructure and Sustainable Mobility has issued the so-called *Guidelines for risk classification and management, safety assessment and monitoring of existing bridges* [21], in the following just guidelines.

The guidelines illustrate a procedure for managing the safety of existing bridges, in order to prevent inadequate levels of damage, making the risk acceptable. It is constituted of three parts:

- census and risk classification;
- safety verification and surveillance;
- monitoring of existing bridges and viaducts.

The risk classification, which is achieved by the determination of attention classes, is based on a multilevel approach. The multilevel approach is a possible solution to manage the high number of Italian bridges. In fact, the complexity and the high cost of inspections, surveys, monitoring and verifications are calibrated by evaluating, even though in an approximate and qualitative way, the actual requirement and urgency according to the current state of the art.

The multilevel approach is based on six levels: **Level 0**, **Level 1**, **Level 2** define the first part, while **Level 3**, **Level 4** and **Level 5** the second one. The third part regarding the monitoring provides an indication for the implementation of a surveillance system. It reports a series of activities that can be applied to bridges in order to improve their knowledge and to better perform the inspections. A surveillance system represents all the surveys, inspections and monitoring activities that have to be performed on existing bridges in order to ensure their availability, functionality and maintenance over the years. The guidelines defined these activities with the so-called risk-based approach, which is based on the attention classes. Thus, in the following, it is reported a brief description of the levels and of the attention classes.

- **Level 0**: census of bridges collecting their main characteristics by means of the analysis of all the available documentation, including technical ones (design reports, interventions, etc.) and administration ones, which consent to reconstruct the applied interventions/retrofitting over the years. In other words, the census of bridges consists in cataloguing all the bridges in order to know the number of structures to be managed and their main characteristics, both from structural elements (geometry) and from road network (type of road in which they are inserted, the site in which it is located, etc.) point of view. The collection of all these data also makes it possible: (i) the creation of a database of Italian bridges, aimed at cataloguing the vast existing infrastructural heritage, (ii) the subdivision of the bridges into macroclasses, and (iii) the identification of an order of priorities useful for planning in-situ visual inspections and starting the activities envisaged by Level 1 of the approach.

- **Level 1**: to be conducted in all the bridges identified in Level 0. It requires visual inspections, surveys of the structure (such as geometric and condition state ones) and of the characteristics of the area from the morphological and hydraulic point of view. The goal is to identify the degradation state and the main structural characteristics of the bridge which are then collected into specific cards. There is one for each type of structural element and constitutive material, such as reinforced concrete abutment, concrete beams, steel beams, etc.. In addition, the cards also report the typical damages that occur for the element under investigation with a score in the range (1,5).

  Severe damages have scores equal to 5 while not severe equal to 1. Defects on structural elements require the identification of their extensions, by means of the coefficient k_1 in the range (0.2,1), and the intensity, by means of the coefficient k_2 in the range (0.2,1).

  Moreover, based on the typology of the bridge, specific critical elements, such as Gerber saddles, prestressing cables, scour at foundations, etc., have to be investigated. In this regard, for post-tensioned concrete bridges built in the 60s/70s, it is fundamental to conduct special inspections in order to identify the state of the prestressing cables. In this part, the guidelines recognise the actual problem in prestressing cables of post-tensioned concrete bridges. Most of them, in fact, could present corrosion in the cables that lead to a strong decrease of capacity.

- **Level 2**: it consents to identify the attention classes of the bridges by means of the analysis of the parameters of hazard, vulnerability and exposure that are determined in the previous levels. This level is the most important of the approach since all future assessments are based on it. The attention class is useful for the definition of the priority of inspections, surveys ad interventions.

The definition of the attention class is based on four types of risk: (i) foundation and structural, (ii) seismic, (iii) landslide and (iv) hydraulic. Each of them is associated to a specific and corresponding attention class.

The attention class of the bridge is then obtained by combining the four attention classes associated to the four types of risk. This operation is performed in a tabular format.

- **Level 3**: it requires the performing of preliminary evaluations with the purpose of correctly understanding the damages and degradations that emerged from Level 1. It is fundamental to evaluate the capacity of the bridge (with reference to the technical code in force at the time of the design phase) with respect to the demand provided by the current technical code. This phase strongly depends on the data acquired in Level 0 and Level 1.

- **Level 4**: it requires the performing of accurate safety assessments according to the Italian technical code [11]. In this regard, there is some peculiarity with respect to

  - the referring time t_{ref} for the evaluation of the stresses (the time in which the safety assessment is satisfied): it can be assumed as a function of the analyses to be carried out. However, a time not higher than t_{ref}, in which structural interventions have to be performed, has to be defined;
  - the influence of the degradation that can reduce the capacity;
  - the evaluation of the loads: the traffic loads defined by the Italian technical codes are valid for new bridges.

  The guidelines provide the corresponding safety factors for each action and reference times. However, they can be reasonably determined with reference to different reference times by adopting the procedures indicated in *fib* Bulletin 80 [22], which in addition, is the approached followed by the guidelines. Briefly, it allows to calculate the safety factors for existing structures with reference to two approaches: (i) the Design Value Method, in which the partial factors are derived from the actual distribution of the variables under examination (i.e. materials, loads, etc.), and (ii) the Adjusted Partial Factor Method (APFM), in which the coefficients provided by the Eurocodes for new structures are modified by the application of the so-called Adjustment coefficients.

  Regarding the latter point, the guidelines define three conditions for bridges: (i) **adequate** if they satisfy the safety assessment with loads and safety factors required by the Italian technical code, (ii) **operative** if they satisfy the safety assessment with loads evaluated according to Italian technical code while the safety factors evaluated with a $t_{ref} = 30$ years, and (iii) **trafficable** if they satisfy the safety

assessment with loads defined by the guidelines and safety factors evaluated with a maximum of $t_{ref} = 5$ years. The trafficable condition requires that during the time assumed as references, limitations on the traffic loads and interventions have to be performed.

Clearly, in the safety assessments that are required at this level, the guidelines are consistent with the requirements of the Italian technical code, and therefore it has to be conducted with reference to the correct "knowledge path" in order to correctly define the Confidence Factors and Confidence Levels that are fundamental in the definition of mechanical parameters adopted in the safety assessments [23].

- **Level 5**: it is applied to bridges that are considered of significant importance. In fact, they require more sophisticated analyses, like the evaluation of the transport relevance, analysing of the interaction between the structure and the road network to which it belongs and the consequences of a possible interruption of the operation of the bridge on the socio-economic context in which it is inserted. However, the guidelines do not explicitly treat this level.

From **Level 0** to **Level 5**, the complexity, the level of detail and the cost of surveys and analyses increase, but the number of bridges on which to apply them, as well as the level of uncertainty of the results obtained, decreases.

As introduced before, Level 2 is the most important and consents to identify the attention class for the bridge under evaluation. The approach defines five attention classes: (i) **high**, (ii) **medium-high**, (iii) **medium**, (iv) **medium-low**, and (v) **low**. For each of them, they are required particular operations in terms of surveys, monitoring and assessments. They are briefly summarized as follows:

- For bridges with high attention class it is required the performing accurate assessments in terms of safety and in-depth analyses of the structural and/or geotechnical characteristics according to Level 4 requirements. Both periodic and special (where it is necessary) inspections and continuous or periodic monitoring systems are required.

- For bridges with medium-high attention class it is required performing of preliminary assessments according to Level 3. In addition, both Periodic and special (where it is necessary) inspections and continuous or periodic monitoring systems are required. The manager of the bridge can decide to apply the requirements of Level 4.

- For bridges with medium attention class it is required the performing of the preliminary assessment of Level 3. If degradation states are identified (through periodic

inspections) also special inspections have to be performed. In addition, the manager of the bridge can decide to install monitoring systems and/or perform safety assessments according to Level 4.

- For bridges with medium-low attention class they are not required further evaluations in addition to those ones already performed (frequent periodical visual inspections).
- For bridges with medium-low attention class they are not required further evaluations in addition to those ones already performed (periodical visual inspections).

4

Damages in existing bridges

Sommario

Questo capitolo descrive le principali cause di crollo per i ponti esistenti distinguendo tra cause interne ed esterne. Successivamente, si cerca di fornire una schematizzazione dei possibili danni a cui i ponti sono soggetti con riferimento a cause, rappresentate dai fenomeni fisici che li generano, ed effetti, rappresentati da diminuzione di capacità e/o aumento della domanda. Infine, alcune delle tipologie di danni vengono contestualizzati con riferimento alla tipologia strutturale dei ponti esistenti.

Summary

This chapter describes the main causes of collapses for existing bridges distinguishing between internal and external causes. Subsequently, a schematization of the possible damages to which bridges are subject with reference to causes, represented by the physical phenomena that generate them, and effects, represented by a decrease in capacity and/or an increase in demand. Finally, some of the types of damage are contextualized with reference to the structural typology of the existing bridges.

4.1 Main causes of bridge failures

The structural behaviour of bridges cannot be considered the same for all bridges: each one is different. To better say it depends on a set of parameters, i.e. geometry, design phases, executive phases, etc, that make it conceivably different. Therefore, each typology of damage that could occur during the service life of a bridge should be considered with reference to several aspects such as constitutive material, typology of damage and its interaction with the type of the bridge, the interactions between damages, etc.. The damages to which an existing bridge can be affected during its service life are multiple and may depend on:

- location of the bridge, i.e. near the sea cost, rainy areas, overpassing of a river, seismic zone, etc.;

- the deterioration of the constitutive material, i.e. concrete, prestressed concrete, steel bars, prestressing cables;
- the typology of the bridge, i.e. static scheme, the geometry of the deck, presence of expansion joints, presence of Gerber saddles, etc.;
- increase of the loads, i.e. traffic.

In addition, the mechanism that governs the occurrence of damages could be very complicated and involves the coexistence of the aforementioned aspects. In fact, based on this coexistence, the damages lead to either operational (functionality) or structural obsolescence. For instance, the structural settlement of a pier leads to an increasing of displacement in the case of a simply supported bridge scheme, which can provide problems in the daily passing of the traffic, while it leads to an increasing of stresses in the case of hyperstatic bridge scheme, which can provide forces that the beam is not adequately reinforced for. As a matter of fact, the identification of cause-effect relationships for damages could be very complicated. For instance, corrosion in the steel bars can be seen as the consequence of material deterioration and the cause of flexural and or shear reduction capacity/damage.

Nevertheless, the main causes of bridge failures, also according to [24], can be subdivided into two main categories: (i) the internal ones and (ii) the external ones. Regarding the first, the following causes can be identified:

- design errors: often an inadequately designed bridge is not able to properly sustain extreme events, i.e. earthquakes, and/or guarantee sufficient safety factors with reference to other problems, i.e. degradation of the constitutive materials;
- lack of maintenance: bridge designers always assume appropriate maintenance in estimating the life of the designed bride. Thus, the main structural element should be made easily accessible for future inspections.

Regarding the external causes:

- flood: the common type of collapse is due to the gradual wearing away of the soil around the piers of the bridge together with an increasing of the external forces on the structural elements;
- scour: in bridges whose structural elements, like piers, are put in place in bed river. In fact, the flowing of the water leads to erosion or removal of a stream bed or bank material from the foundation.
- wind: bridges in windy zones can be subjected to increasing of dynamic loads due to the forced vibration due to wind actions;

- collisions: it may happen that ships, vehicles or trains collide structural elements of a bridge, i.e. vehicles that collide piers of a viaduct that overcomes a highway.
- overload: following the increasing of the static loads, due to retrofitting, changes in the configurations, and traffic loads. In fact, the existing bridge often was designed using different traffic loads with respect to those required by the actual technical codes.
- environmental degradation: the construction materials are subjected to ageing, especially in the bridges which are the kind of structures that are constantly subjected to environmental events, i.e. rain.

4.2 Bridge damages overview: causes and effects, demand and capacity

From a general point of view, it is considered appropriate and more useful to provide a schematization of damages and their possible effects by the integration of them in the context of: (i) an increase in the demand, and (ii) a decrease in the capacity and (iii) physical phenomena that can provoke them. It is worth noting that they are linked through the bridge typology, which involves constitutive materials, geometry and static scheme. Figure 4.1 describes possible relationships between damages.

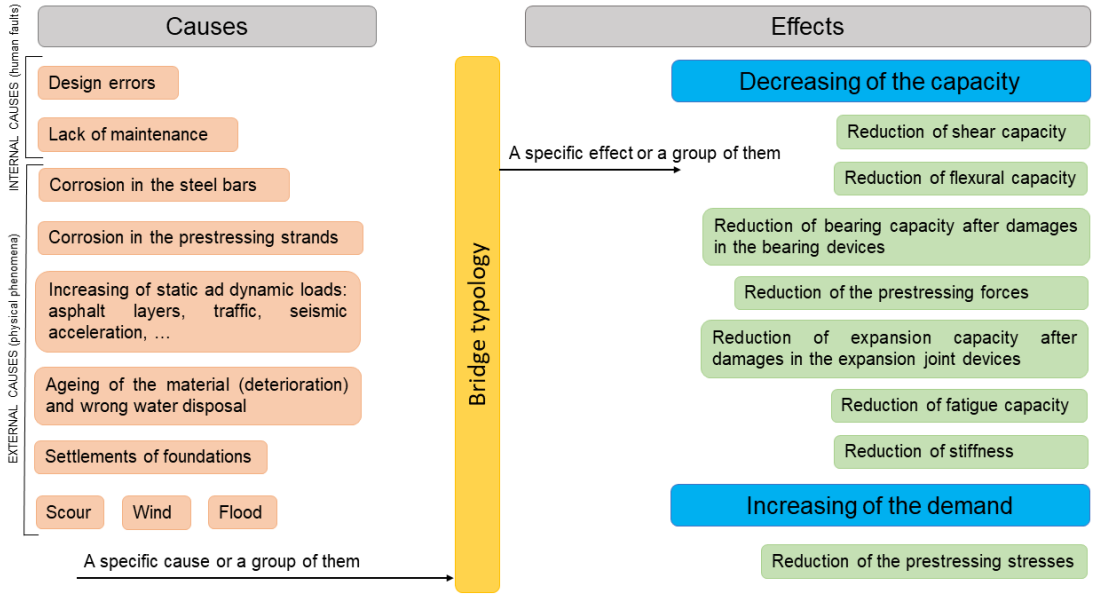

Figure 4.1: A possible schematization of cause-effect relationships for bridge damages

As far as the external causes are concerned, the following physical phenomena may occur:

- Increase of static and dynamic loads: it might lead to overloading with subsequent rupture of the bearing devices. For instance, in the last decades, the actual traffic loads have become higher with respect to those one prescribed by the technical codes in force at the design and construction time. Furthermore, dead loads may change over time, due to the addition of structural and/or not-structural elements, such as New Jersey, asphalt layers, etc..

- Seismic loads: it can lead either to the damage of the structure and/or its components or to partial/total collapses. In fact, for existing bridges built in the last 70s, the seismic design requirements were different with respect to those ones prescribed by the actual technical codes. In addition, sometimes they were not considered at all in the original "static" design phase of the bridge;

- Ageing of the materials: they may provoke their deterioration like cracking in the concrete, corrosion in steel bars and in prestressed cables.

- Wrong water disposal: it leads to the stagnation of the rainwater that can lead to the decay of the structural materials. In fact, the rainwater should be able to autonomously run off the deck thanks to adequate systems.

- Structural settlements: they lead to an increasing of displacement in the case of a simply supported bridge scheme, which can provide problems in the daily passing of the traffic, while they lead to an increasing of stresses in the case of a hyperstatic bridge scheme, which can provide forces that the beam is not adequately reinforced for.

- Scour at bridge foundations placed in riverbed: it leads to the removal of the soil material and sediment from around the bridge foundation (especially with fast-moving water during the event of floods) leaving behind scour holes. The piers can be then subjected to unpredictable changes in support conditions and unexpected water loads, that may even lead to collapse.

- Reduction of the prestressing stresses in structural elements: they are fundamental in the definition of the demand. In fact, it can be seen as the difference between the demand due to the external loads and the capacity due to the prestressing stresses.

As far as the effects are concerned, the following issues may occur:

- Reduction of the flexural and/ or the shear capacity. For instance, related to the material deterioration and to the increasing of the static loads. In fact, the latter

case leads to an increasing of the masses that in turn provoke higher seismic forces for which the structure is not adequate.

- Reduction of the prestressing forces. It is the case, for instance, of the corrosion in the steel bars and prestressing strands, which can lead to losses of strength and ductility and in turn to sudden brittle failure mechanism due to reduced capacity, i.e. the shear ones. Moreover, corrosion in the prestressing strands represents nowadays an important problem in the existing bridge, in particular those that were built with specific post-tension technology. A detailed analysis of this phenomenon and a possible way to model it and consider its effects on the structural behaviour of existing bridges is deeply analysed in part II.

- Expansion joints deterioration: they are necessary at both ends of each bridge span for isostatic simply-supported beams, in correspondence with the Gerber saddles and on the abutments for hyostatic continuous bridge decks. If these kinds of devices are damaged, i.e. due to the increasing of the traffic loads, ageing of their constituent materials, increase of friction coefficient of the steel interfaces, steel corrosion, or missing, i.e. due to the complete covering of the deck with asphalt, the displacement capacity can be reduced.

- Bearing devices deterioration: they are fundamental in the static and seismic behaviour of the bridge. They can include single rollers, pinned connections, multiple sliders, High Damping Rubber Bearing isolators, and friction pendulum devices, such as Curved Surface Sliders. If these kinds of devices are damaged, i.e. due to the ageing of their constituent materials, increase of friction coefficient of the steel interfaces, steel corrosion or undersized with respect to long-term effects, thermal variations, and seismic-induced displacements, the behaviour of the whole bridge can be compromised.

- Reduction of the fatigue capacity: it can be related to the fact that the permissible design stress range (the stress amplitude at which failure occurs for a given number of cycles is the fatigue strength) of a certain constructive detail decreases due to damage.

- Reduction of stiffness: it can be related for instance to material degradation, like cracking in the concrete.

Then, the issues that can be identified according to the possible phenomena above described, are basically related to how the causes (in terms of the physical phenomenon) and the consequences effects (in terms of increasing of the demand and decreasing of the capacity) are influenced by each other. In other words, how each of them, or a group of them, interact and how they can be taken into account in the interpretation of the

structural behaviour of bridges, i.e. in the damage modelling. In fact, related to the type of damage and the type of the bridge, it results to be more appropriate and easier modelling of either the increasing the demand or the reduction of the capacity. For instance, part II is completely devoted to the modelling of the corrosion in prestressed strands with the purpose of providing the reduction effects on their strength and ductility capacities. These effects lead to reductions of the existing bridges, i.e. flexural, rotational, etc., that can be either modelled or measured by means of a specific monitoring system.

Moreover, each bridge, in addition to those above described, can also be affected by specific problems closely related to its typology.

4.3 Damages for each bridge typology

The resistance mechanisms of structures are basically of two types: axial force and bending moment /shear force. This subdivision is important to correctly understand their structural behaviour in terms of possible damages and consecutive effects. Based on these resistance mechanisms the following typologies of bridges can be identified:

- bending moment /shear force resistance mechanism
  - Beams and girders bridges.
  - Rigid frame bridges.
- Axial force resistance mechanism
  - Arch and vaults bridges.
  - Cable-Supported Bridges.

4.3.1 Beams and girders bridges

Beams and girders bridges are structures that are constituted by decks composed of a single beam or by an ensemble of beams where the static scheme can be both isostatic or hyperstatic. These types of bridges are characterized by a well-known structural behaviour and have been widely used in the last decades also involving prestressed concrete. The main problems that might affect these kinds of bridges are basically related to: (i) corrosion of the prestressing strands: it provides a high reduction of strength and ductility capacities of the strands provoking the reduction of the prestressing force in the bridge beams leading to possible sudden collapses. In particular, post-tensioned strands that are not fully injected with mortar can be affected by a high probability of corrosion where mortar injection was not able to cover all cable lengths within the duct. In the case of bridges characterized by beams that cover just one span (isostatic simply-supported

schemes), this could also bring to brittle failure of the beam and thus of considerable portions of the bridge deck.

a

Figure 4.2: Example of corroded strands in the duct of post-tensioned bridge beam

[a] www.fhwa.dot.gov/publications/research/infrastructure/structures/bridge/14039/005.cfm

Modelling of the corrosion in the prestressing strands is a complicated issue that nowadays is still an open research topic. Prestressing forces are at the base of the structural behaviour of prestressed concrete beams. In fact, they allow to exploit the entire transversal cross-section of the beam. Corrosion can strongly reduce the strength and ductility capacities of the strands that are reflected in the prestressing forces configurations. Thus, a decreasing in these forces leads to a reduction of the not-cracked transversal cross-section which can be taken into account by means of a reduction of the inertia characteristics. In addition, as a first approximation, the effects of the corrosion in the strands could be evaluated and modelled considering a reduced moment-curvature diagram taking into account a strand cross-section reduction only.

(ii) Gerber saddles deterioration: it is due to the particular geometry of this structural element which allows the stagnation of the rainwater facilitating the local deterioration of both concrete and reinforcement steel bars.

a

Figure 4.3: Example of deteriorated Gerber saddles in RC road bridges

[a] [25]https://www.mdpi.com/2412-3811/6/2/25

(iii) Foundation vertical settlements in the hyperstatic scheme: they can provoke differential displacement demand at the bridge deck level with consequent unusual changing in the tensional state which can lead to unexpected phenomena, i.e. cracks in parts of beams that are not designed for tension stresses for instance due to the variation, from negative to positive, of the bending moment at the support. Foundation vertical settlements might be easily modelled by introducing elastic settlements in the static scheme of the bridge, i.e. in the finite element model. (iv) Fatigue problems: they are due to load cycles to which the bridge structure is subjected during its service life. In particular, it plays a central role in the suitability of welded and/or bolted connections in steel bridges. Fatigue problems are difficult to evaluate. In general, they require knowledge of the load cycles over the bridge from the construction time until nowadays. Clearly, this information is often unachievable. Thus, the estimations of the traffic loads might be based, for instance, on a certain reduction over the years of the actual traffic passing on the bridge nowadays. The final goal is then the estimation of the remaining fatigue life, on which economic evaluations can be drawn. However, a certain damage to fatigue, for instance in steel bridges that are characterized by many connection joints, can be modelled considering the reduction and/or removal of the connection in the static scheme of the bridge, i.e. in the finite element model.

a

Figure 4.4: Example of a foundation vertical settlements

[a] www.stuff.co.nz/the-press/news/canterbury/9164925/Damaged-bridge-divides-community

4.3.2 Rigid frame bridges

Rigid frame bridges are characterized by hyperstatic schemes where the deck-pier joints play a fundamental role in transmitting bending moment, shear and axial forces. The superstructure and the substructures are continually connected in order to have a monolithic system. Due to hyperstaticity and redundancy of the moment-resisting frame, foundation/soil settlements can provoke differential displacement demand at the deck-pier joints with consequent unusual changing in the tensional state that can lead to the damage of the joints themselves. In addition, due to the frame structural behaviour (high bending moment in correspondence of the joints which have to be able to transfer it to the foundations), the seismic loads can lead to localized damages of the joints that can compromise the static behaviour of the bridge. In fact, the retrofitting of these kinds of bridges according to the seismic standard imposed by the recent codes could result difficult to achieve requiring a high capacity demand for the deck-pier joints.

Arch and vaults bridges are characterized by curved structural elements and they include several types of structural solutions:

- isostatic three-hinges arches;
- hyperstatic two-hinges arches;
- hyperstatic hingeless arches;
- hyperstatic massive - with solid spandrels – masonry or concrete arches;
- tied arches (to be better considered in the cable-supported bridges category);
- hyperstatic three-dimensional vaults and shells.

4.3.3 Isostatic three-hinges arch bridges

Isostatic three-hinges arch bridges need the horizontal reaction (thrust) to be effectively developed by the piers/abutments. Lateral settlements at the foundation level have to be prevented at all costs (meaning that rock soil should be there or deep pile foundations/tie rods provided for) to guarantee the equilibrium of the whole arch (ultimate limit state requirement), and to avoid significant vertical deflections (serviceability limit state requirement). All hyperstatic solutions can suffer both vertical and lateral differential displacements between the two piers/abutments, being subjected to changes in the stresses distribution. All the more reason, differential settlements should be absolutely prevented in vaults and shells. In these cases, the hyperstaticity involves also the transversal dimension of the bridge, in the guise of spatial coactive states hard to be controlled when differential settlements occur. Thus, the settlements are the main causes of damages in

arch and vault bridge structures leading to longitudinal and/or transversal lesions on the materials (concrete, masonry, grout) that provoke reductions of stiffness.

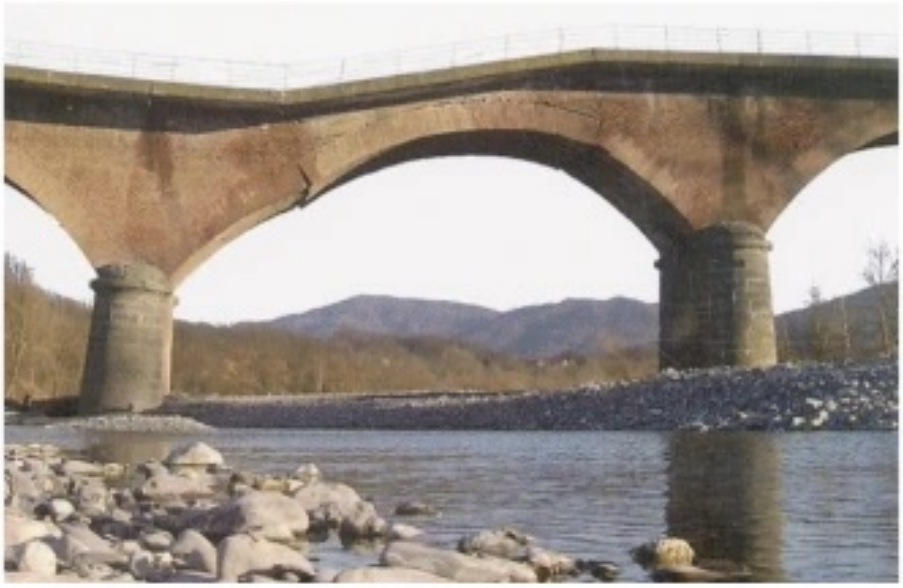

a

Figure 4.5: Example of a pier vertical settlements in an arch masonry bridge

[a] [26]https://link.springer.com/article/10.1007/s11012-021-01397-1

4.3.4 Cable-supported bridges

Cable-supported bridges allow to cover the longest spans. Cables are usually made either of steel or of prestressed concrete. In general, from the shorter to the longer spans, they can be classified as:

- tied arches with the deck at the base of the arch, in which the deck is connected to the main supporting arch by means of vertical or inclined hangers;
- cable-stayed bridges. In the case of steel stays, there could be many of them either in fan or harp arrangement. In the case of prestressed concrete stays, typically they are in reduced number (say 2 or 4, per pylon);
- suspension bridges.

In all cases, the steel cables constituting either the hangers, or the stays, or the main rope and vertical hangers, should be efficient during the entire bridge's life, as well as their connection with other main structural elements. The main issues are then related to cables corrosion and connections deterioration. Furthermore, very specific problems may arise due to wind-induced aero-elastic effects (vortex shedding, Galloping, divergence, flutter), due to the considerable length and slenderness of these structural elements.

4.4 Anomaly detection and damage classification through monitoring systems

For each of the reported damages on existing bridges, prevention (inspections) and maintenance activities, and, if required, intervention strategies, should be put in place. For the correct management of existing bridges, these activities have to be strictly related to each other.

In this context, the monitoring of existing bridges can help, but always with the clear understanding that it is not enough if it is implemented as a standalone tool, without a proper knowledge and deep study of the behaviour of the bridge under examination. In fact, it needs hand calculations and adequate and calibrated numerical models to effectively support the engineers in the actual understanding of the structural behaviour of the bridge and in the identification of its possible anomalies, for instance, related to particular damage scenarios.

In the general framework of Structural Health Monitoring [27], four levels have been widely recognised as possible outcomes of an installed monitoring system (see Table 4.1):

Anomaly detection:

- Level 1: damage existence.

Damage classification:

- Level 2: damage location;
- Level 3: damage type;
- Level 4: damage severity;

Table 4.1: Levels for possible outcomes of an installed monitoring system

Anomaly detection	**Damage classification**		
Level 1: Damage existence	Level 2: Damage location	Level 3: Damage type	Level 4: Damage severity
Supervised Approach: Threshold defined through structural models (structural model-based approach or engineering approach)	**Supervised Approach**: The following tools are needed: Calibrated structural models of the intact bridge; Damage simulation models; Structural models of the damaged bridge; Artificial Intelligence algorithms.	**Supervised Approach**: Idem	**Supervised Approach**: Idem
Not-Supervised Approach: Threshold (iper-parameters) defined through large data collection and statistical tools on the dataset (data-driven approach)			

The so-called "anomaly detection" (Level 1), which is also related to the definition of performance indexes and thresholds values (such as attention, alert and alarm conditions) that can be implemented as parameters to check during the service life of the monitored bridges, can be performed according with the following approaches:

1. Supervised approach (structural-model based or engineering approach): the engineer identifies suitable significant parameters, or a combination of them, for each damage, (e.g. the strain in a certain point of a beam). This activity is based on the knowledge/experience/skill (i.e. the expertise) of the engineer on both structural analysis and phenomena that provoke the damage. In other words, the monitoring data might be enough to discriminate the safe and unsafe states of the bridge, i.e. by comparison of the measured stresses in a certain point of a beam with its permissible value driven by the expert judgment of the engineer. However, also calibrated structural models of the bridge, depending on the type of damage, can be used to set threshold values for the identified parameters. These models in fact allow to study of the effects of damages, which requires their modelling according to the bridge typology and its structural behaviour, on the response parameters that

have either directly measured parameters (in the field by the monitoring system) or indirect ones (obtained from the measured parameters).

2. Not-supervised approach (data-driven approach): this approach is based only on the analysis of the monitoring data measured in long periods and properly processed with statistical tools. A large amount of data is required, to identify reliable statistical thresholds.

The so-called "damage classification" (Levels 2, 3 and 4) is aimed at identifying the damage location, damage type and damage severity. For these activities, the damage modelling introduced within calibrated structural models has the purpose of identifying sets of output parameters related to the location, type and severity of the damage. These parameters will be used to train AI artificial intelligence algorithms, aimed precisely at classifying the damage scenario in terms of location, type and severity.

5

Structural Health Monitoring and maintenance

Sommario

In questo capitolo viene brevemente descritto cosa si intende per Structural Health Monitoring (SHM), introducendo le fasi che dovrebbero essere implementate nella corretta gestione del monitoraggio stesso, anche con riferimento alle attività e i ruoli professionali coinvolti. Successivamente, viene decritto il background teorico di due tecniche di identificazione dinamica ampiamente utilizzate nell'estrazione dei parametri dinamici significativi di una struttura monitorata (frequenze di vibrazione, modi di virbrare e rapporti di smorzamento). Queste sono poi applicate a due casi studio di una passerella in acciaio sita in Pianoro, Bologna, ed un ponte ferroviario sito a Napoli. Inoltre, viene brevemente descritto il background teorico di una tecnica statistica (Principal Component Analysis) spesso utilizzata per rimuovere gli effetti ambientali, come quelli dovuti alla temperatura e all'umidità ad esempio, sui dati di monitoraggio.

Summary

This chapter briefly describes the meaning of Structural Health Monitoring (SHM), introducing the phases that should be implemented in the correct management of the monitoring itself, and also with reference to the activities and involved professional roles. Subsequently, the theoretical background of two dynamic identification techniques widely used in the extraction of the significant dynamic parameters of a monitored structure (frequencies, modal shapes and damping ratios) is described. These are then applied to two case studies of a steel footbridge located in Pianoro, Bologna, and a railway bridge located in Naples. Furthermore, the theoretical background of a statistical technique (Principal Component Analysis) often used to remove environmental effects, such as those due to temperature and humidity for example, on monitoring data is briefly described.

5.1 Phases for a correct Structural Health Monitoring system

Structural Health Monitoring (SHM) aims at giving, at every moment during the life of a structure, a diagnosis of the "state" of the constituent materials, of the different parts, and of the full assembly of these parts constituting the structure as a whole [28]. The state of the structure must remain in the domain specified in the design, although this can be altered by normal ageing due to usage, by the action of the environment, and by accidental events. Thanks to the time-dimension of monitoring, which makes it possible to consider the full history database of the structure, and with the usage of techniques for dynamic identification, i.e. Frequency Domain Decomposition (FDD), and for statistical approaches, i.e. Principal Component Analysis (PCA), it can also provide a prognosis (evolution of damage, residual life, etc.) of structures. SHM can be seen as a decision-making tool for the interventions necessary for existing structures to maintain the code-required safety levels. In other words, a monitoring system is an organized set of measurement tools and instrumentation that is designed and managed in order to obtain field data that, if properly interpreted, can give useful information about the structural behaviour of existing bridges and structures. Therefore, it can help the Owner and the Engineer in the decision-making process, by driving them towards the identification of the best type of intervention for the infrastructure at hand.

It may happen that monitoring systems lead to wrong decisions on the basis of wrong data acquisition or wrong data interpretation. To avoid this and to be effective, the monitoring system of a given existing bridge should consist of the following phases (to which specific activities, different roles and responsibilities of the involved operators correspond):

0. **Preparation**: planning and design of the monitoring system with clear identification of the objectives and of the response parameters to be measured.

1. **Data acquisition**: this phase refers to the operations with which the physical instruments are put in place (implementation) and correctly provide the data of interest (calibration).

2. **Data processing**: this phase refers to the first elaborations, typically made by technicians who installed the instruments, aimed at returning the raw data in an intelligible way (data reported in the correct measure units, removal of spikes and systematic errors in the recorded signal, any correction of the temperature effects).

3. **Extraction of significant response parameters**: this phase corresponds to the mathematical analysis of the recorded signal with the aim of extracting hidden response parameters of the bridge (e.g. frequency, damping, ...). This phase requires

the removal of the thermal effects on the monitoring data. In fact, the measure of the response of the structure could be hidden by the thermal component.

4. **Data clustering**: a collection of all data in a single "tool" usable by specific operators, typically a web platform, which can be inquired to provide a first visualization (e.g. time-history plot) of the results.

5. **Aggregate data reporting**: this term refers to the scheduled operations in which people in charge (typically the company in charge of data clustering) provides reporting containing all the aggregate data obtained from the monitoring system.

6. **Short-term data evaluation**: expeditious evaluations carried out daily/weekly by the so-called "Control room" through the comparison of the data with identified "threshold values" and prescribed "attention bands" (lower and upper bounds), if available. In the event of dangerous scenarios (e.g. exceedance of the "threshold values"), phase 9 has to be considered, keeping into account all implications on the society.

7. **Long-term data interpretation**: this phase refers to periodic evaluations with scheduled reporting (typically half-yearly, yearly, ...), with which the results provided by the monitoring system are analysed and compared (together with those provided by any additional survey campaign). These evaluations require the contextualization of the experimental data in relation to the specific characteristics (history, materials, mechanical and behavioural properties, loading intensities, temperature effects) of the infrastructure at hand. The interpretation of the monitoring data is a complex operation that must be seen with a long-term perspective (reasonably lasting for the entire life of the infrastructure or at least until the structural behaviour stabilizes) and which must necessarily be carried out on the basis of in-depth knowledge of the bridge. In this respect, attention is paid to the fact that this long-term interpretation is not to be confused with the simple aggregate data reporting of the monitoring data referred to in the previous point. The interpretation is aimed at having a meditated picture of the static and dynamic/seismic condition of the infrastructure under control both in the immediate (quarter/semester of reference) but also, and above all, in perspective (i.e. identification of any pathologic changes in the state/conditions of the bridge with reference to its physiological behaviour).

8. **Decision support**: it corresponds to the technical and scientific contributions that the Experts (Engineers and/or Scientific Committee) provide in terms of guidance in the choices made by the Owner (a) in the development of the monitoring system, (b) in the interpretation of the data, (c) in the activation of specific surveys and consultancy studies aimed at planning specific interventions.

9. **Intervention**: in this phase, the possible intervention decided in the previous phase has to be designed and implemented. It is worth noticing that the Owner and the Police, together with the Experts (Engineers and/or Scientific Committee), should temporarily handle the infrastructure both before and during the intervention phase. Typically, two scenarios can be envisaged: (i) closing the access to the infrastructure (full closing), (ii) limiting the traffic on the bridge (partial closing, reduction of weight, reduction of velocity). Consequences on the viability (traffic jams, alternative ways) should be carefully considered since they may have a large impact on the society habits and expectations.

The following table aims at schematizing the above-mentioned phases and at identifying actors, roles and responsibilities as well as the main objectives of each step.

Table 5.1: Schematization of the monitoring activities

	Step	**Phase**	**Actors-Operators**	**Activities-Responsibilities**	**Objectives**
Preparation	0	Preparation	Owner + Engineer + Scientific Committee	Identification of the objectives of the monitoring system	Decision about data to be measured
Anamnesis	1	Data acquisition	Company in charge of the physical monitoring instrumentation	Installation Acquisition	Correct functioning Actual measurements of what expected
	2	Data processing	Company in charge of the physical monitoring instrumentation	Processing Delivery to the web platform	Spikes removal Temperature effects corrections Adequate precision/resolution Transfer speed Adequate connection with the data clustering company

	3	Extraction of significant response parameters	Signal analysis specialist	Signal analysis	Mathematical rigour Correct identification of significant hidden response parameters
	4	Data clustering	Company in charge of the development of the data web-repository (software platform)	Web-repository development Collection Visualization Inquiry	Full collection Safe storage Straightforward tools
	5	Aggregate data reporting	Company (could be the same in charge of the development of the data web-repository)	Periodic report Visualization	Diligence Compliance with deadlines
Diagnosis	6	Short-term data evaluation	People in charge of daily/weekly check of data (“Control Room”)	Daily check Weekly check Comparison of selected data with threshold values	Surveillance Alert Early warning
	7	Long-term data interpretation	Technicians (Engineer / Scientific Committee) in charge of periodic long-term interpretation of data (6/12 months, even more)	Comparative study of the results in the more general context given by deep knowledge of the bridge	Overall understanding of actual behaviour of the infrastructure Engineering judgement for the definition of sound thresholds

	8	Decision support	Engineer + Scientific Committee + Risk manager + Consultants	Synthesis of all information Support to the Owner	Engineering judgement leading to safety conclusions and to the best intervention type
Consequences	9	Intervention	Owner + Police + Experts	No intervention needed Limiting the traffic Closing the infrastructure to traffic	To handle the infrastructure during the intervention design process and implementation

5.2 Possible approaches for the extraction of significant response parameters

From an engineering point of view, the extraction of the significant response parameters represents an important step (phase 3) on which the SHM are based. In this regard, the parameters that describe the dynamic behaviour of the structure, i.e. vibration frequencies, modal shapes, and damping ratios, can be estimated by means of several dynamic identification techniques. They can be divided into two groups: (i) frequency domain techniques and (ii) time domain techniques. With reference to the type of the excitation load, the algorithms for identification of modal properties are divided into: (i) input-output, referred to as Experimental Modal Analysis (EMA), which requires the measurements of the input loads (the dynamic characteristic of the structure are collected from the transfer function between the input and the output responses), and (ii) output-only, referred as Operational Modal Analysis (OMA), which use the measured response of the structure in operational condition and does not require the characterization of the input loads. The EMA approach has been widely used in the last decades in the mechanical engineering field, basically in the study of dynamic behaviour and in the dynamic identification of small elements in lab spaces. However, also experimental campaigns with purposes of dynamic identification through EMA techniques on buildings and bridges have been performed. Since the OMA techniques take advantage of the fact that the monitored structures can stay in the operational conditions, resulting also advantageous from an economic point of view, they have taken hold in recent decades.

One of the most used OMA techniques for the dynamic identification that works in

the frequency domain is the Frequency Domain Decomposition (FDD) [29], [30], [31] that involves computation of the power spectral density matrix and uses singular value decomposition (SVD) to decompose the matrix at every frequency into a set of auto-spectral density functions, each corresponding to a single degree of freedom (SDOF) system. In parallel, in the time domain, the objective is to extract the physical information of the structure under examination from correlation functions. The major difference between the time domain techniques is that they use different ways for the formulation of the regression problem. One of the most diffused techniques is the Stochastic Subspace Identification (SSI), which can be formulated into two types: covariance-driven SSI (SSI-cov) and data-driven SSI (SSI-data). In the last 30 years, the output-only identification technique, such as Frequency Domain Decomposition (FDD) and Stochastic Subspace Identification (SSI) became widely used since they overcame the limitations of the previous techniques in terms of working with closely spaced modes and noise. Thus, nowadays Operational Modal Analysis (OMA) techniques are frequently used in the framework of civil engineering (buildings, bridges, pedestrian bridges, wind turbines, dams, etc.) mechanical engineering and aerospace engineering.

The OMA techniques are based on the following hypotheses: (i) the response of the system to a combination of inputs is equal to the combination of the response to every single input, (ii) the input is assumed to be stationary (it does not change its characteristics over the time) and (iii) the layout of the sensors is well-designed in the sense that it consents the observability of the modes of interests. The key point of the OMA technique resides in the fact that the input is supposed to be white noise, i.e. the PSD is a constant matrix. In other words, this assumption leads to consider that all the modes are equally excited and the output spectrum contains full information about the structure.

5.2.1 Frequency Domain Decomposition

The Frequency Domain Decomposition (FDD) provides very accurate results maintaining a user-friendly approach. It is based on the theoretical relationship in the modal space between the unknown outputs *y(t)* and the modal coordinates *p(t)*:

$$y(t) = [\Phi]p(t) \tag{5.1}$$

where $[\Phi]$ is the Modal Matrix. The correlation matrix of the outputs *y(t)* can be expressed by computing their expected value as follow:

$$[R_{yy}(\tau)] = E[y(t+\tau)y(t)^T] = [\Phi][R_{pp}(\tau)][\Phi]^T \tag{5.2}$$

The Fourier transform of the Eq. 5.2 then results to be:

$$[G_{yy}(j\omega)] = [\Phi][G_{pp}(j\omega)][\Phi]^T \tag{5.3}$$

where $G_{yy}(j\omega)$ and $G_{pp}(j\omega)$ represent the Power Spectral Density (PSD) matrices of the outputs and of the modal coordinates, respectively. Through the Singular Value Decomposition (SVD), the PSD matrix of the outputs ($G_{yy}(j\omega)$) can be factorized as reported in the following formula:

$$G_{yy} = [U][S][V] \tag{5.4}$$

Where the matrices U and V are the unitary matrices that contain the left and right singular vectors and S is a diagonal matrix of the scalar singular values. However, for a Hermitian and positive definite matrix, like the PSD matrix, it results that $U = V$ and the factorization can be written as follow:

$$G_{yy} = [U][S][U] \tag{5.5}$$

From the comparison between Eq. 5.3 and Eq. 5.5 it can be seen the direct relationship between singular vectors and mode shapes. The singular values are related to the modal responses and they can be used to define the spectra of equivalent SDOF systems characterized by the same modal parameters as the modes contributing to the response of the Multiple Degrees of Freedom (MDOF) system under investigation.

Thus, the first step of the technique algorithm is the estimation of the Power Spectral Density (PSD) matrix, for instance by means of the Welch formulation [32]. The PSD of the output is then evaluated at discrete frequencies $f = f_i$ that define the frequency resolution of the final spectra. It is worth noting that the results achieved by using the FDD technique are affected by the frequency resolution. In addition, the important aspect of the SVD decomposition is that, since it provides the singular values arranged in descending order, in each frequency f_i value the first singular value contains the information about the dominant mode at that frequency.

Welch's Method. The signal is divided into L overlapping (by D points) segments of length M. The L segments are then windowed in the time domain by applying a window function (i.e. Hamming, Blackman, Gaussian, etc.). Then the periodogram is calculated by computing the squared magnitude of the Discrete Fourier Transform of the windowed segments. The individual periodograms are then averaged, which reduces the variance of the individual power measurements. The end result is an array of power measurements vs. frequency "bin".

The identification goals using the FDD technique are then achieved by looking at the spectra, as a function of the frequency, of the first singular values. This is the case of well-separated modes, where the contribution of the higher singular values is negligible and the modes identified on the spectra of the first singular value are a good approximation. On the contrary, in the case of close modes, near their natural frequencies, more than two

singular values with not negligible amplitude can be observed. In this case, the modes are identified by looking at the singular values that present higher amplitudes, which might be different from the frequency of the peak. This aspect is due to the fact that the SVD provides orthogonal vectors. In fact, if the experimental mode shapes are orthogonal the obtained estimates are unbiased. On the contrary, if the mode shapes are not orthogonal, the mode shape estimates for the closely spaced modes are biased. However, the estimate of the dominant mode can be considered valid, in fact, the bias mainly affects the weak mode. Finally, the modal shape of each mode is determined by looking at the singular vector, which is stored in the U matrix, associated with the peak of the singular value identified as its natural frequency. Starting from the identified peak, equivalent SDOF systems can be defined. In fact, each of them can be seen as a set of singular values around the peak that are characterized by similar singular vectors. This aspect is used in the so-called Enhanced Frequency Domain Decomposition (EFDD) [33] in order to estimate in addition, the damping ratio. Thus, as the first step the procedure requires the identification of singular vectors around that one corresponding to the peak. A possible choice can be carried out using the so-called Modal Assurance Criterion (MAC) index, which is used to measure the correlation between two modal vectors, according to the following formula.

$$MAC(u_i\phi_k) = \frac{|{u_i}^H \phi_k|^2}{({u_i}^H u_i)({\phi_k}^H \phi_k)} \tag{5.6}$$

where u_i and ϕ_k represent a generic vector at the frequency f_i and the vector representing the $k-th$ mode (it corresponds to the $k-th$ peak).

The MAC assumes, by definition, values in the range [0,1]. In particular, it is equal to 0 when the two vectors under analysis are orthogonal while is equal to 1 when they differ for a scale factor only. The MAC index is used to choose the points of an equivalent PSD SDOF function. In fact, each point corresponds to the singular vectors that have a MAC index that assumes values higher than the so-called rejection level, which is typically adopted equal to 0.8. Thus, the identified equivalent PSD SDOF function can be used to evaluate the modal damping ratio, which can be estimated by using the logarithmic decrement technique applied to its Inverse Fast Fourier Transform (IFFT). The latter, in fact, assumes the shape of an approximated correlation function taken by an equivalent SDOF system in the time domain.

In addition, to estimate the natural frequency independent with respect to the frequency resolution of the spectra, a linear regression on the zero crossing times of the equivalent SDOF system correlation function could be applied.

5.2.2 Covariance-driven Stochastic Subspace Identification

Equations of motion of a Multiple Degree of Freedom (MDOF) are generally expressed in matrix form by the following expression:

$$[M]\ddot{y}(t) + [C]\dot{y}(t) + [K]y(t) = f(t) \tag{5.7}$$

where $\ddot{y}(t)$, $\dot{y}(t)$ and $y(t)$ are the vectors of acceleration, velocity, and displacement, respectively, $[M]$, $[C]$, and $[K]$ denote the mass, damping, and stiffness matrices, $f(t)$ is the forcing vector. State space models are used to convert the second-order problem described by Eq. 5.7 into two first-order problems, defined by the so-called state equation and observation equation. They assume the expressions reported in Eq. 5.8 and Eq. 5.9, respectively.

$$\dot{s}(t) = [A_c]s(t) + [B_c]u(t) \tag{5.8}$$

$$y_o(t) = [C_a]\ddot{y}(t) + [C_v]\dot{y}(t) + [C_d]y(t) \tag{5.9}$$

Where $y_o(t)$ is the vector of the measured outputs, $[C_a]$, $[C_v]$ and $[C_d]$ are the output location matrices for acceleration, velocity, and displacement, respectively. $[A_c]$ and $[B_c]$ are the state matrix and the input influence matrix, respectively. The subscript *c* indicates the continuous time. $s(t)$ is the state vector, which is defined according to Eq. 5.10.

$$s(t) = \begin{Bmatrix} \dot{y}(t) \\ y(t) \end{Bmatrix} \tag{5.10}$$

Detailed mathematical manipulation for obtaining Eq. 5.8 and Eq. 5.9 can be found in [30].

Under the assumption that the input is piecewise constant over the sampling period continuous-time state-space model can be converted to the discrete-time state-space model and assumes the following expression:

$$\begin{aligned} \dot{s_{k+1}} &= [A]s_k + [B]u_k \\ y_k &= [C]s_k + [D]u_k \end{aligned} \tag{5.11}$$

where $s_k = s(k \cdot \Delta t)$ is the discrete-time state vector yielding the sampled displacements and velocities, u_k and y_k are the sampled input and sampled output, respectively, $[A]$ is the discrete state matrix, $[B]$ is the discrete input matrix, $[C]$ is the discrete output matrix and $[D]$ is the direct transmission matrix. However, the system described by Eq. 5.11 is a deterministic model (it is driven by a deterministic input only). Thus, in order

to include stochastic components, the following discrete-time combined deterministic-stochastic state-space model is obtained:

$$\begin{aligned} \dot{s_{k+1}} &= [A]s_k + [B]u_k + w_k \\ y_k &= [C]s_k + [D]u_k + v_k \end{aligned} \tag{5.12}$$

where w_k is the process noise due to disturbances and model inaccuracies, while v_k is the measurement noise due to sensor inaccuracies.

In the context of Operational Modal Analysis (OMA), structures are excited by several inputs that cannot be measured. In other words, the information about the vector u_k is not available and the measured system response is generated by the stochastic processes w_k and v_k only. Therefore, the system is simplified as follows:

$$\begin{aligned} \dot{s_{k+1}} &= [A]s_k + w_k \\ y_k &= [C]s_i + v_k \end{aligned} \tag{5.13}$$

Finally, when a stochastic state-space model is adopted (q. 5.13), the objective is the determination of the matrices $[A]$ and $[C]$ from a large number of measurements of the output y_k. In addition, also the determination of the order *n* of the unknown system is required.

The Covariance-driven Stochastic Subspace Identification (SSI-cov) aims at computing the state space models described by Eq. 5.13 from a given output data assuming white noise for w_k and v_k. The SSI-cov starts from the computation of output correlations of the data collected in the *l* (number of outputs) x *m* (number of elements of each output)$[Y]$ matrix at different time lags *i*, according to the following formula:

$$[R_i] = \frac{1}{m-i}\left[Y_{(1:m-i)}\right]\left[Y_{(1:m)}\right]^T \tag{5.14}$$

where $\left[Y_{(1:m-i)}\right]$ is obtained from the *n x n* data matrix $[Y]$ by removal of the last *i* samples, while $\left[Y_{(1:m)}\right]$ is obtained from $[Y]$ by removal of the first *i* samples. Thus, all the estimated correlations at different time lags are collected in the Toeplitz matrix according to the following expression:

$T \in \mathbb{C}^{p\times p}$ is a Toeplitz matrix if $t_{ij} = t_{i-j}$ for $2p-1$ parameters $t_{1-p_1}, ..., t_{p-1}$. An example for $p = 4$:

$$T = \begin{bmatrix} t_0 & t_{-1} & t_{-2} & t_{-3} \\ t_1 & t_0 & t_{-2} & t_{-2} \\ t_2 & t_1 & t_0 & t_{-1} \\ t_3 & t_2 & t_1 & t_0 \end{bmatrix}$$

$$[T_{1|i}] = \begin{bmatrix} [R_i] & [R_{i-1}] & \dots & [R_1] \\ [R_{i+1}] & [R_i] & \ddots & [R_2] \\ \vdots & \vdots & \ddots & \vdots \\ [R_{2i-1}] & [R_{2i-2}] & \ddots & [R_i] \end{bmatrix} \tag{5.15}$$

The Toeplitz matrix $[T]$ has dimension equal to $(l \cdot i)$ x $(l \cdot i)$ since each correlation matrix $[R_i]$ has dimension *lxl*. For the identification of a system with order *n*, the number of blocks rows has to respect the condition for which $(l \cdot i) \geq n$. Clearly, in practical identification problems, this parameter is unknown and has to be tuned.

After the assembling of the Toplix matrix, considering that the number of outputs l is a constant of the identification problem, the value of *i* that respects the condition with respect to the number of model orders can be set: $i \geq n/l$. In other words, the *i* value is the main parameter to be chosen by users and that has to be well identified. Considering the relationship between the correlations and the state matrix of Eq.5.16, the Toeplitz matrix can be factorized as follow.

$$\begin{gathered} [R_i] = [C][A]^{i-1}[G] \\ \text{where} \\ G = E[s_{k+1} y_k^T] \end{gathered} \tag{5.16}$$

where G is the covariance between the response of the system y_k and the state vector s_{k+1}.

$$[T_{1|i}] = \begin{bmatrix} [C] \\ [C][A] \\ \vdots \\ [C][A]^{i-1} \end{bmatrix} \begin{bmatrix} [A]^{i-1}[G] & \dots & [A][G] & [G] \end{bmatrix} = [O_i][\Gamma_i] \tag{5.17}$$

Where $[A]$ is the state matrix, $[O_i]_{l \cdot i \times n}$ and $[\Gamma_i]_{n \times l \cdot i}$ are the observability and reversed controllability matrices, respectively. It is worth noting that if the condition $l \cdot i \geq n$ is respected, the rank of the Toeplitz matrix is equal to *n* (the Toeplitz matrix results from the product between a matrix with *n* columns and a matrix with *n* rows). Comparing the Singular Value Decomposition (SVD) of the Toeplitz matrix in Eq. 5.18 with its definition reported in Eq. 5.17 it results immediate the estimation of the observability and controllability matrices.

$$[T_{1|i}] = [U][S][V]^T = \begin{bmatrix} [U_1] & [U_2] \end{bmatrix} \begin{bmatrix} [\Sigma_1] & [0] \\ [0] & [0] \end{bmatrix} \begin{bmatrix} [V_1]^T \\ [V_2]^T \end{bmatrix} \tag{5.18}$$

Where the non-zero singular values are decreasingly arranged in the diagonal matrix $[\Sigma_1]$, which has $n \times n$ dimension. The matrices that contain the left and right singular vectors, respectively U and V, have dimensions equal to $(l \cdot i \times n)$ and $(n \times l \cdot i)$. Consequently, the observability and controllability matrices assume the following expressions.

$$\begin{aligned} [O_i] &= [U_1][\Sigma_1]^{\frac{1}{2}}[T] \\ [\Gamma_i] &= [T]^{-1}[\Gamma_1]^{\frac{1}{2}}[V_1]^T \end{aligned} \tag{5.19}$$

The final step is then the estimation of the matrices $[A]$ and $[C]$, which can be done according to different approaches whose detailed expressions can be found in [30]. Finally, the modal parameters can be extracted from those matrices. In fact, the poles in the discrete time are in the diagonal matrix obtained from the eigenvalue decomposition of the state matrix. The conversion of the *p-th* pole corresponding to a physical mode from discrete-time to continuous-time is obtained by Eq. 5.20, which describes a relationship between the pole in the z-domain (discrete) and that one in the Laplace domain (continuous).

$$z_p = e^{\lambda \cdot p \cdot \Delta t} \Rightarrow \lambda_p = \frac{ln(z_p)}{\Delta t} \tag{5.20}$$

Thus, for instance, for the *p-th* mode, the natural frequency, the damped modal frequency, and the damping ratio can be obtained as follow:

$$\begin{aligned} f_p &= \frac{|\lambda_p|}{2\pi} \\ f_{d,p} &= \frac{Imag(\lambda_p)}{2\pi} \\ \xi_p &= -\frac{Real(\lambda_p)}{|\lambda_p|} \end{aligned} \tag{5.21}$$

As described above, the number of modes could be estimated as the rank of the Taopleiz matrix. However, in practical identification problems, this is not possible due to the fact that the singular values that theoretically should be zero (defining of the $[\Sigma_1]_{n \times n}$ in Eq. 5.18 matrix), are not, for instance, due to noise phenomena and modelling inaccuracies. Thus, in practical applications, a range of model order *n* is previously fixed, for instance, higher than two times the number of physical modes of the system within the frequency range under analysis according to [34], and then the number of inputs are identified ($l \cdot i \geq n$). Moreover, the time lag *i* has to be previously set, also based on the experience, in such a way as to allow the identification of the main modes. For instance, [35] suggests to consider the minimum number of correlation points (which are related to the time lag *i*) taking into account that the correlations should contain more than one complete cycle of the largest structure period of vibration.

The introduction of high model order leads to the identification of the so-called spurious modes, which are numerical modes without physical meaning. Typically, the separation between physical and spurious modes is done by means of the stabilization diagram where all the modal parameters coming from the identification are expressed all together. It shows the poles obtained for different model orders as a function of their frequency. Physical modes can be identified from alignments of stable poles with respect to the mode orders. In fact, the spurious modes tend to be more scattered. The construction of the stabilization diagram is based on the comparison of the poles associated with a given model order with those associated with the previous model order. The adopted criteria to identify stable poles are related to the value assumed by the percentage of the difference in two consecutive model orders of the frequency, damping ratio and MAC values. Typically, the following limit percentage are adopted:

$$\left(\frac{|f(n) - f(n+1)|}{f(n)} < 0.01\right) \tag{5.22}$$

$$\left(\frac{|\xi(n) - \xi(n+1)|}{f(n)} < 0.05\right) \tag{5.23}$$

$$\Big[[1 - MAC(\phi_n, \phi_{n+1})] < 0.02\Big] \tag{5.24}$$

Therefore, according to these limits, in the stabilization diagram, the following poles can be identified: (i) stable in frequency: if is respected the Eq. 5.22 only, (ii) stable in damping: if is respected the Eq. 5.23 only, (iii) stable in *MAC* if is respected the Eq. 5.24 only, and (iv) stable: if Eqs. 5.22, 5.23 and 5.24 are simultaneously verified. The stabilization diagram consents to select the poles that reasonably represent the structure physical modes.

5.3 A possible approach to manage the long-term data evaluation

In order to properly perform the monitoring activities, in particular the Long-term data interpretation, the environmental effects on the monitoring data have to be removed. In fact, the structural behaviour measured by the sensors composing the monitoring system is affected by the environment in which the structure is located. As a consequence, the data results are affected by components that are not associated with the structural behaviour only, but also by those ones associated with the interaction of the structure with the environment, i.e. temperature, humidity, and so on. In this regard, Figure 5.1 shows an example of monitoring data (normalized according to Eq. 5.25) that are affected by tem-

perature effects. This is clear from the seasonal behaviour (that seems almost periodic) of the data over the years.

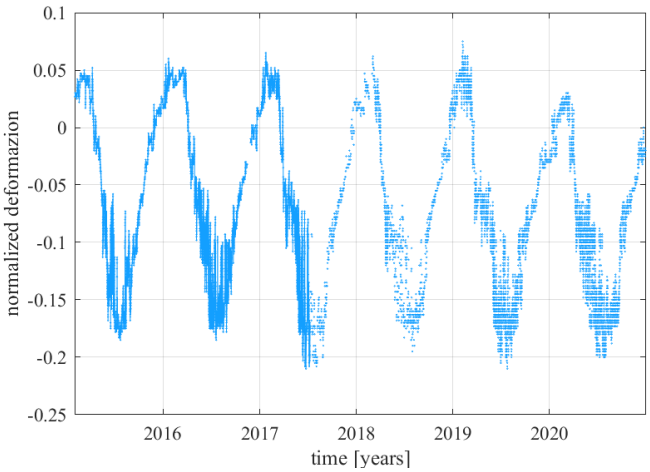

Figure 5.1: Example of monitoring data affected by temperature effects

A possible approach to remove these effects is by means of the application of statistical tools which can be calibrated using the large number of observations coming from the monitoring system. The goal of these approaches is to find relationships between the parameters that describe the structural behaviour of the monitored bridge, which can be either directly measured, like stresses, inclinations, etc., or indirectly calculated like frequency, damping ratios, modal shapes, etc. (for instance with FDD and SSI-cov techniques), with the factors that influence them, like temperature, humidity, etc.. Clearly, this requires the measurements of those independent variables (temperature, humidity, etc.). A widely used statistical tool for this purpose is the Principal Component Analysis (PCA) which is briefly described in the following section.

5.3.1 Principal Component Analysis

Principal Component Analysis (PCA) is probably the oldest multivariate analysis technique. It was first introduced by Pearson (1901)[36], and developed independently by Hotelling (1933) [37]. Like many multivariate methods, it started to be widely used after the advent of electronic computers in the last decades. Nowadays PCA represents a popular technique adopted for the analysis of large data sets with a high number of dimensions. The central idea of principal component analysis is to reduce the dimensionality of a data set in which there are a large number of correlated variables, maintaining as much as possible, the variability present in the data set itself. This reduction is achieved by transforming the variables of the original data set to a new set of variables, the principal components, which are uncorrelated (diagonal covariance matrix), and are ordered in such a way that the first few retain most of the variability that is present in all of the

original variables. The computation of the principal components is given by the solution of an eigenvalue problem for a positive-semidefinite symmetric matrix. The steps towards the computation of the principal components are the following:

- Standardization of the data set *D* of dimensions $m \times n$, which represents the length of the variables (i.e. the time of acquisition) and the number of the variables (i.e. the number of the sensors), respectively. The goal is to standardize the initial variables that are present in the data set so that each one of them contributes equally to the analysis. In fact, they are of different natures with different ranges of definition, i.e. data measured by different sensors of a monitoring system. In other words, they have an initial variability. Since the PCA is sensitive to this initial variability, which means that a variable in a range 0-100 will dominate a variable in a range 0-1, which can lead to biased results, the following formula to standardize the initial variables can be applied:

$$D_{i,st} = \frac{D_i - mean(D_i)}{std(D_i)} \tag{5.25}$$

  Eq. 5.25 leads to a data set that can be transformed in the same scale.

- Computation of the covariance matrix C.

$$[C]_{n\times n} = [D_{st}][D_{st}]^T \tag{5.26}$$

- Computation of the Singular Value Decomposition (SVD) of the covariance matrix $[C]$.

  The objective of the PCA analysis is to compute the matrix that allows to make the following transformation:

$$[P]_{m\times n} = T_{m\times m}[D_{st}]_{m\times n} \Rightarrow [D_{st}] = [T]^T[P] \tag{5.27}$$

  where $[P]$ is the matrix that contains the data projected in the PCA base and $[T]$ is the transformation matrix. By applying the expression reported in Eq. 5.26, the covariance matrix assumes the following expression:

$$[C] = [T]^T[P]([T]^T[P])^T = [T]^T[P][P]^T[T] \tag{5.28}$$

  whose Singular Value Decomposition is:

$$[C]_{n\times n} = [U]_{m\times n}[S]_{n\times n}[V]^T_{m\times n} \tag{5.29}$$

the comparison between Eqs. 5.28 and 5.29 suggests that:

$$[U] = [V]^T = [T]^T \Rightarrow [T] = [U]^T \Rightarrow [P] = [U]^T[D_{st}] \tag{5.30}$$

This linear application allows to represent the variability of the data set (decomposition of the covariance matrix) with their associated weight (the singular values). In addition, since the algorithms for computing the singular value decomposition provide the singular values in descending order, the first element of the diagonal of S coincides with the higher variance of the data, and so on. Thus, a reduction of the data set can be adopted. For instance, the matrix S can be reduced in order to consider variability of the data equal to a certain percentage, i.e. $p_{max} = 95\%$. This means that the reduced $[S_{red}]$ matrix contains the singular values that respect the following equation:

$$p_{max} = \frac{\sum_{i=1}^{K} s_i}{\sum_{i=1}^{n} s_i} \tag{5.31}$$

Clearly, the reduction of the $[S]$ matrix leads to a reduction of the $[U]$ matrix. It is worth to calculate the data set resulting after this reduction in order to compare it with the original data set. The reduced data set $[S_{red}]$, according to Eq. 5.30 assumes the following expression:

$$\overline{[P]}_{k\times k} = \overline{[U]}^T_{k\times m}\overline{[D_{st}]}_{m\times k} \Rightarrow \overline{[D_{st}]} = \overline{[T]}^T\overline{[P]} \tag{5.32}$$

where the superscript $-$ denotes the reduced matrices.

- Computing of the so-called residuals *r*. They can be evaluated as the difference between the original data set and the reduced data set.

$$r = [D_{st}] - \overline{[D_{st}]} \tag{5.33}$$

Eq. 5.33 allows to remove the temperature effects on the data. In fact, those effects are associated to higher variabilities and therefore they are present in both the data sets (original and reduced). In other words, the difference between these data allows to represent the data due to the only structural behaviour (they represent the magnitude of the variation remaining in each sample after projection through the model calculated with the PCA). For a correct removal of the thermal effects, the period of time in which to calculate the reduced transformation matrix has to be at least one year (in such a way as to consider the seasonal effects). From a practice point of view, $\overline{[T]}$ is calculated with reference to the data coming from one year of monitoring, which reasonably can be assumed as a safe state for the structure under

monitoring. However, this is the fundamental passage that also requires calibration, for instance with respect to the percentage of variability to consider in the reduction of the transformation matrix. Since the residuals represent the structural behaviour only, they allow making considerations about the safety of the structure under monitoring. In particular, they consent to highlight anomalies in the structural behaviour that can be associated with changes in the structure configuration with respect to the configuration represented in the year of reference (used to calculate $\overline{[T]}$).

- Identification of anomalies in the structural behaviour by means of the so-called control charts that summarize the information contained in the residuals considering the Hotelling's T^2 value. It represents the distance from the centre of the model (calculated with the PCA analysis) and the data themselves (residuals). T^2 assume the expression:

$$T^2 = (r_i - \mu_{r_i})^T [C](r_i - \mu_{r_i}) \tag{5.34}$$

where $\mu_.$ represents the mean value of $(\cdot)$. Under some statistical assumptions on the data, the T^2 can be expressed by a Fisher distribution that allows to theoretical define the safety regions, which represent the regions beyond which the data might be considered anomalous. However, for practical applications, since there are several uncertainties regarding the statistics of the data, they can be assumed as percentiles of the residuals, i.e. equal to 95%. Figure 5.2 shows an example of the T^2 values associated with the residuals of the data reported in Figure 5.1. The figure also shows the period of one year (green lines) in which the $\overline{[T]}$ has been calculated, and the limit that defines a safety region (95% percentiles of the residual data).

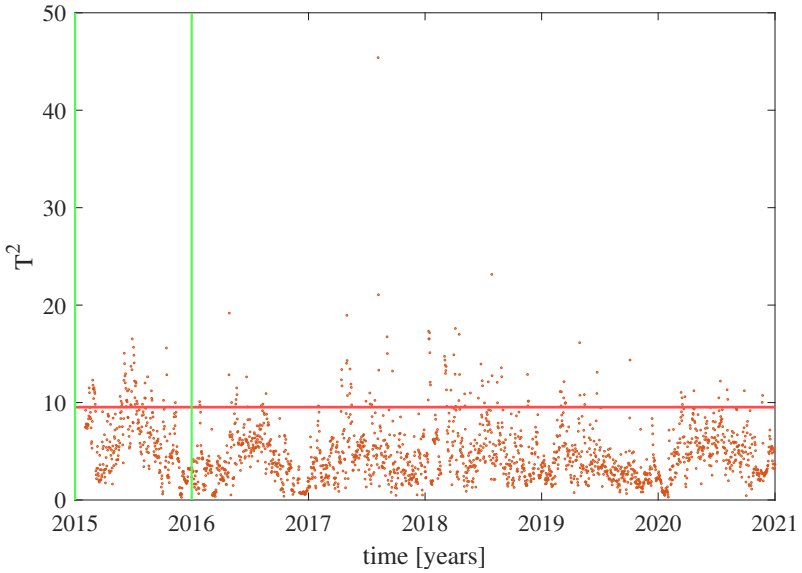

Figure 5.2: Example of T^2 values associated to the residual of monitoring data

The T^2 plot summarizes all the information contained in the residuals associated with the monitoring data emphasizing any present anomalies.

5.4 Example 1: Dynamic identification of a steel pedestrian bridge

In this section is reported an example of the application of the above-described techniques for the dynamic identification of a two-hinge steel pedestrian bridge. The bridge is located in the Savena torrent river park within the municipality of Pianoro, Bologna, Italy and overcomes the river for a length approximately of 62 m. The structure is characterised by two main systems: (i) a lower steel arch with a circle tubular profile of 800 mm in diameter and 14 mm in thickness, and (ii) two circle steel tubular beams of 273 mm in diameter and 6.3 mm in thickness. The arch and the beams are linked by means of transversal circle steel beams of 193 mm in diameter and 6.3 mm in thickness. They are put in place with 2.0 m of spacing. The deck is constituted by a lightened reinforced concrete slab (specific weight of $14kN/m^3$ and cubic characteristic resistance of $350daN/cm^2$) of 15 cm of thickness. A 5 cm thickness of asphalt is placed on the concrete slab. The abutments are manufactured in reinforced concrete with pile foundations of 11 reinforced concrete piles of circular cross-sections with 800 mm in diameter and 14 m in length. Figure 5.3a shows the lateral view of the bridge while 5.3b shows the middle span cross-section.

(a) Lateral view of the pedestrian bridge

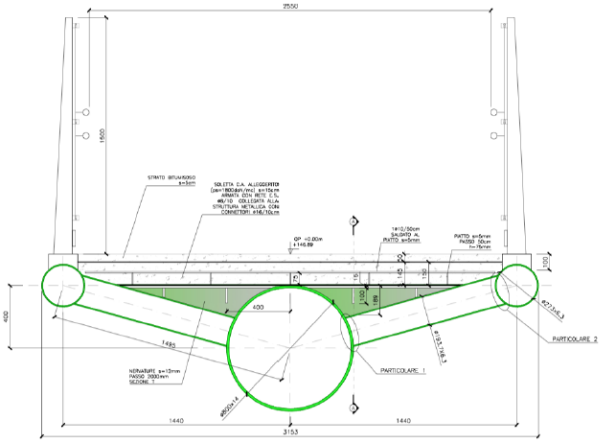

(b) Middle-span cross-section of the pedestrian bridge

Figure 5.3: Lateral view and a cross-section of the pedestrian bridge

In order to apply the Frequency Domain Decomposition (FDD) and Covariance-driven Stochastic Subspace Identification (SSI-Cov) techniques, 20-minute ambient vibration

measurements without interrupting the functionality of the bridge, have been performed. The acquisition system was constituted by four triaxial accelerometers positioned on the bridge deck, as shown in Figure 5.4. The sampling frequency was 400 Hz with a low-pass filter application provided by the acquisition system. The measuring points identified by the positions of the accelerometers were chosen in order to be able to identify the first four modal shapes of the arch structure of the bridge that basically are related to the first modes of an arch beam.

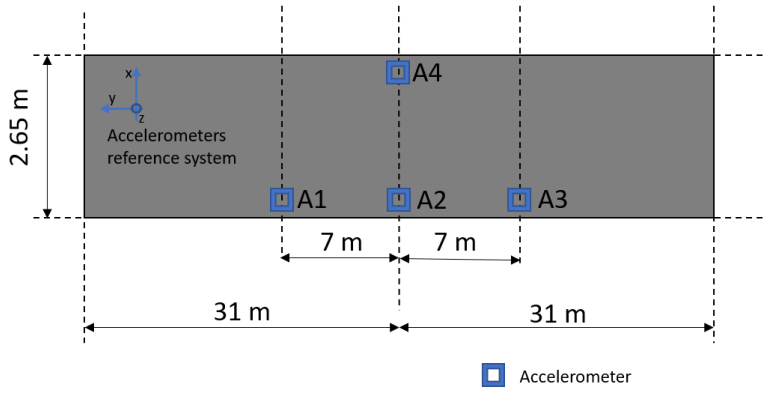

Figure 5.4: Position of the accelerometers on the bridge deck

In this regard, was helpful the finite element model of the pedestrian bridge. In fact, it allows to better visualize the modal shapes in order to correctly locate the accelerometers. The observability of the modes of interest, in fact, is one of the important assumptions in the OMA techniques. However, it provides just an overview of the dynamic behaviour of the bridge since it has to be calibrated with reference to the performed dynamic tests. In the identification process, since the frequencies of the bridge are below 10 Hz, a decimation procedure has been applied to the measured accelerations in order to reduce the sampling frequency from 400 Hz to 20 Hz.

5.4.1 FDD application

The estimation of the spectrum matrix was achieved by applying the Welch average by dividing the time series of the acceleration signals, of a total length of 25 minutes, in segments of a number of samples that lead to a frequency resolution of 0.01 Hz, considering an overlap of 50% between the segments and using Hamming windows to reduce the leakage. Figure 5.5 shows the accelerations and the spectra of the singular values for two cases: (i) the signals as measured and (ii) the signals after removing the part of the acceleration due to external loading (during measurements of few pedestrians and cyclists crossed the bridge).

As it can be seen from the figure, the spectra results to be highly influenced by the pedestrian loads. For this reason, all the analyses have been performed taking into account

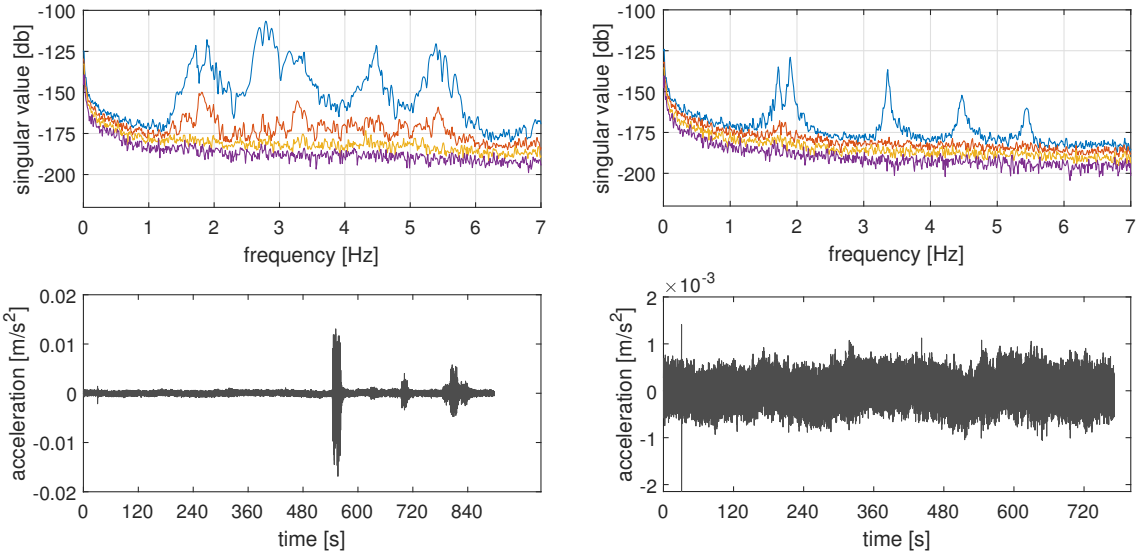

(a) Spectra plot considering all the accelerations measurements

(b) Spectra plot without the part of the acceleration due to external loading

Figure 5.5: Spectra plots of the singular values

the signals after removing the parts of the acceleration due to the external loading (Figure 5.5b). Finally, the final spectra allows to identify five vibration modes, whose shapes are estimated by taking the singular vector corresponding to the identified peak frequency, according to the procedure reported in the previous sections.

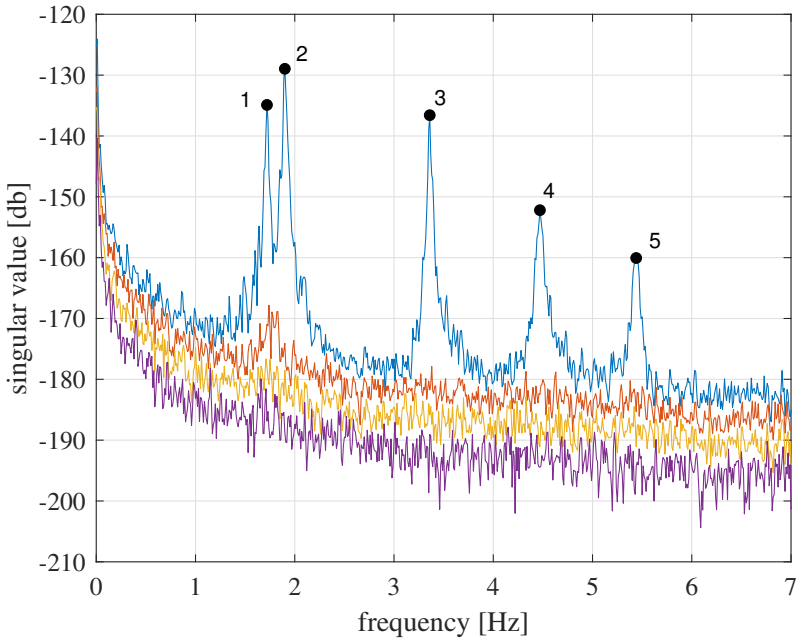

Figure 5.6: Identified peaks on the first singular value spectra

As it can be seen from the spectra (Figure 5.6), the 5 modes, which are identified by

the five peaks (blue line), result to be well-separated. In fact, the amplitude of the other singular values is negligible. Thus, the identification has been achieved by looking at the first singular value. The identified frequencies are reported in Table 5.2.

Table 5.2: Identified frequencies according to FDD technique

Mode	**Frequency [Hz]**
1	1.72
2	1.90
3	3.36
4	4.47
5	5.44

In the following are then reported the associated mode shapes also compared with the results achieved with the finite element model. The coloured circles represent the accelerometers adopted for ambient vibration acquirement. In the model, the arch and the transversal beams were modelled with beam elements, while the deck (concrete slab and asphalt) was modelled with shell elements. The restraints are not symmetric, in the sense that one side of the deck has pinned connections while the other is fully restrained. The arch joints are fully restrained (due to the fact that in operational conditions the hinges behave with a higher degree of constraint, i.e. friction). This asymmetry in the restraints is motivated by the asymmetry in the experimental modes.

- **Mode 1**

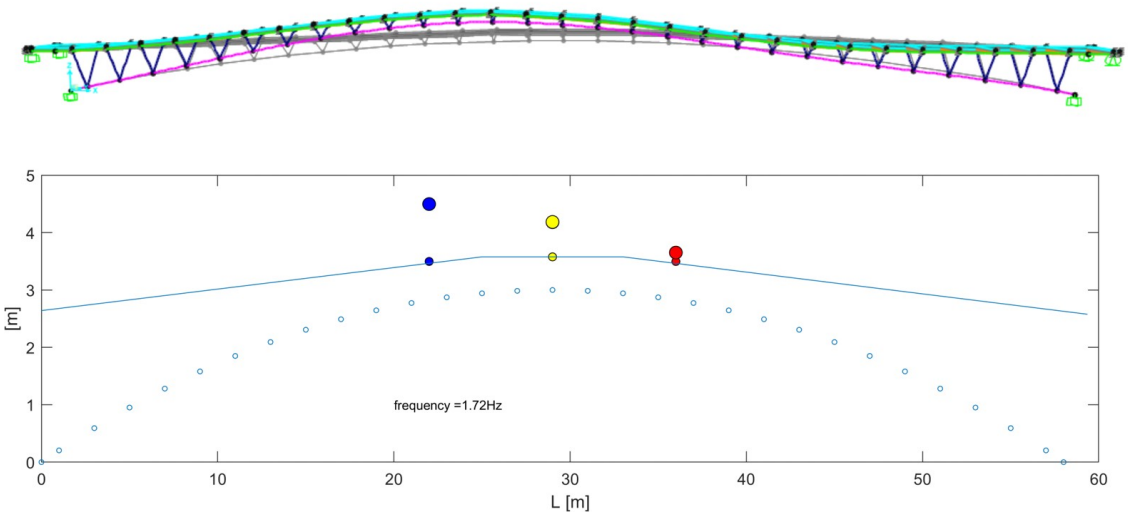

Figure 5.7: Comparison between experimental and numerical 1^{st} mode shape

- **Mode 2**

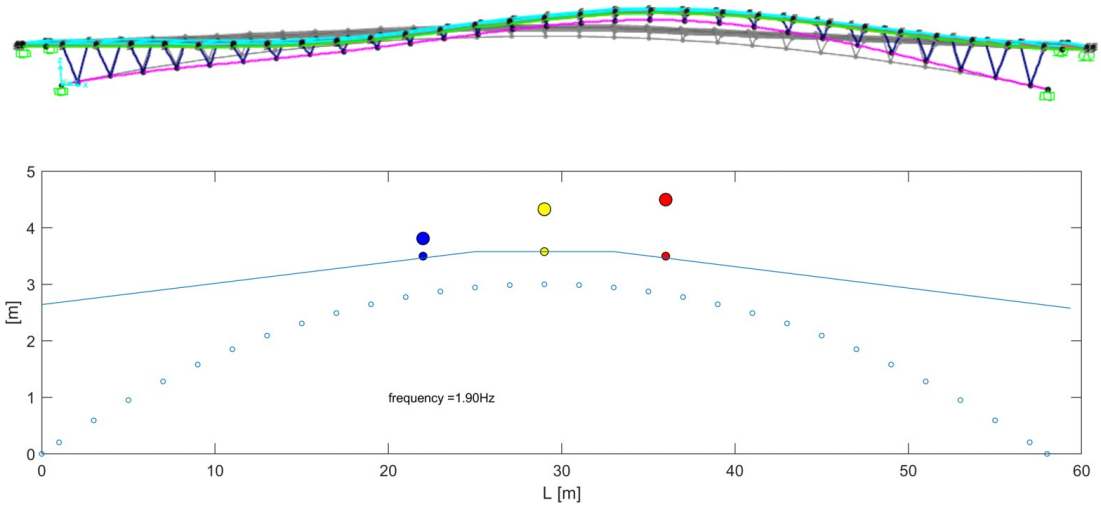

Figure 5.8: Comparison between experimental and numerical 2^{nd} mode shape

- **Mode 3**

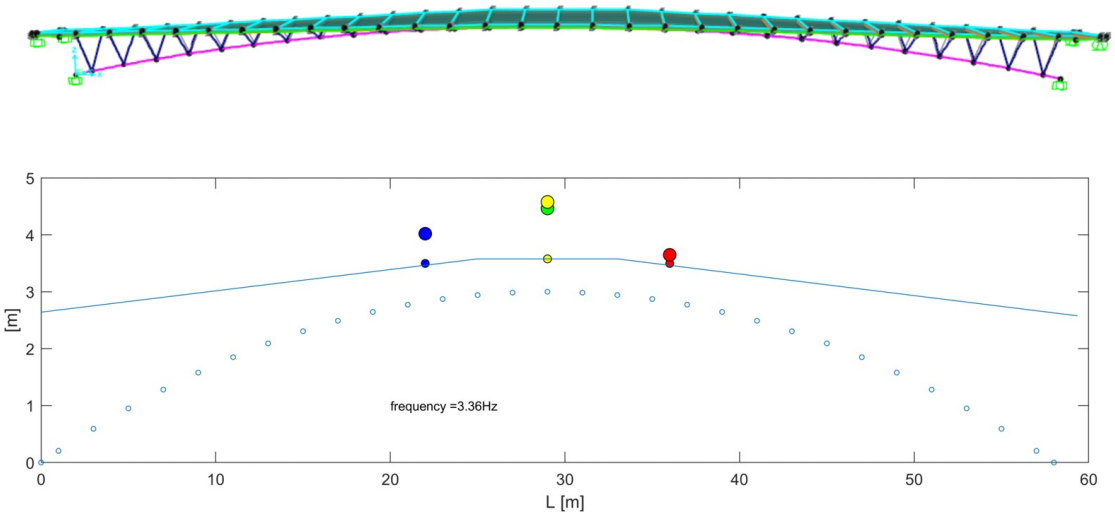

Figure 5.9: Comparison between experimental and numerical 3^{rd} mode shape

- **Mode 4**

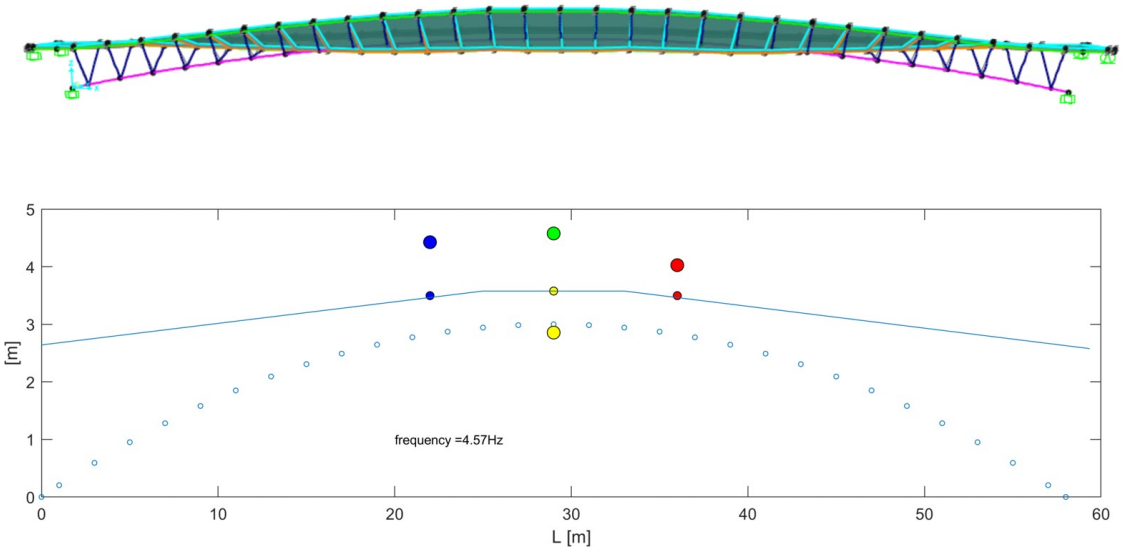

Figure 5.10: Comparison between experimental and numerical 4^{th} mode shape

5.4.2 SSI-cov application

The SSI-cov algorithm has been applied by introducing a time lag of *5 s*. This means that 100 correlation points have been considered (20 Hz sampling frequency). This time

lag corresponds to almost 10 cycles of the lower frequency ($1/1.72Hz \simeq 0.58s$). Figure 5.11 shows the stabilization diagram resulting from the output of the technique, adopting the limit reported in Eqs. 5.22, 5.23 and 5.24.

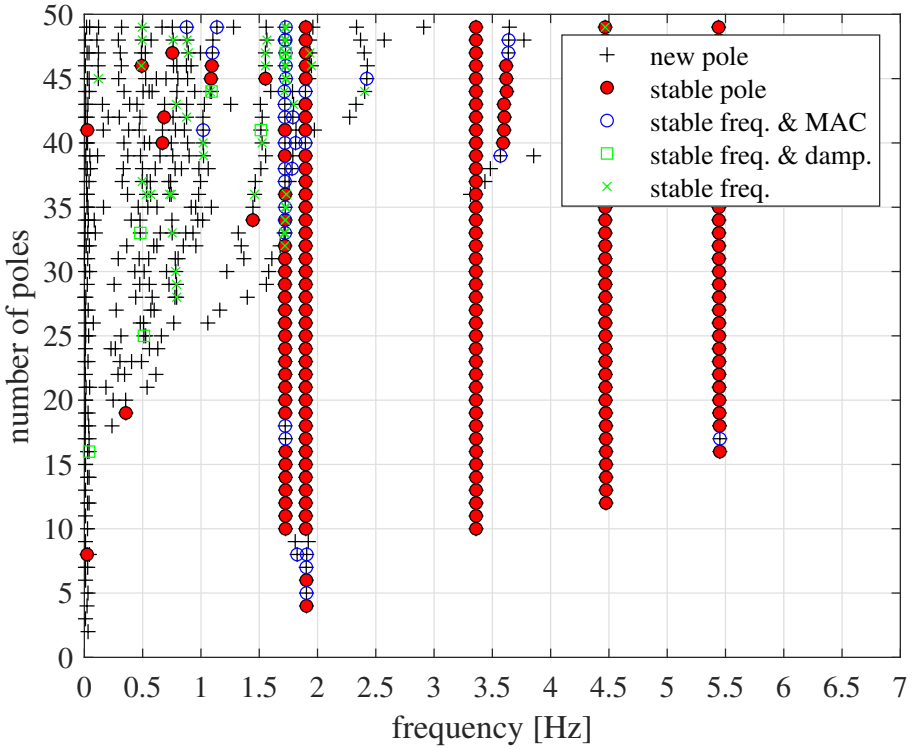

Figure 5.11: Stabilization diagram

The stabilization diagram allows to identify the modes that reasonably represent the physical modes of the bridge. The following modes can be extracted from the diagram.

Table 5.3: Identified frequencies according to SSI-cov technique

Mode	**Frequency [Hz]**
1	1.723
2	1.898
3	3.359
4	4.469
5	5.444

- **Mode 1**

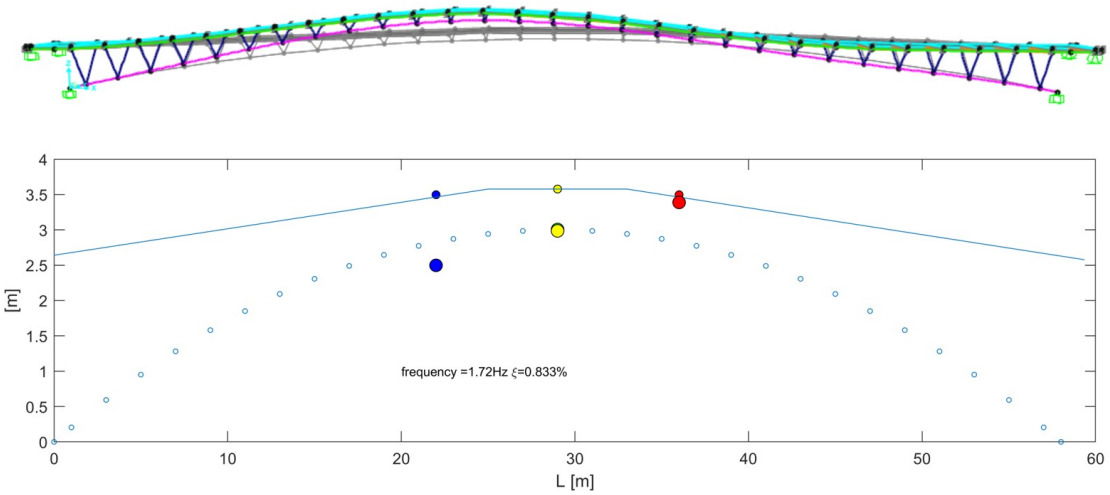

Figure 5.12: Comparison between experimental and numerical 1^{st} mode shape

- **Mode 2**

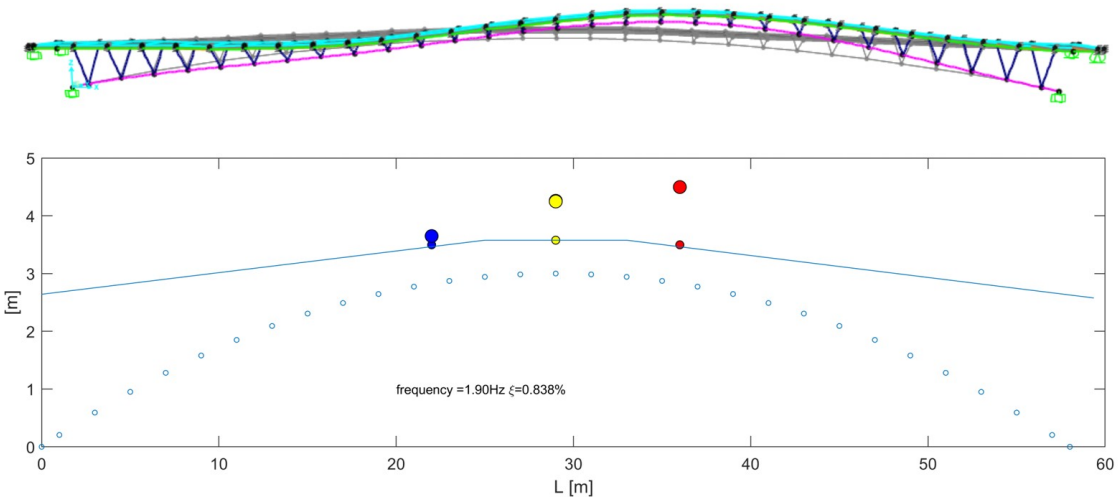

Figure 5.13: Comparison between experimental and numerical 2^{nd} mode shape

- **Mode 3**

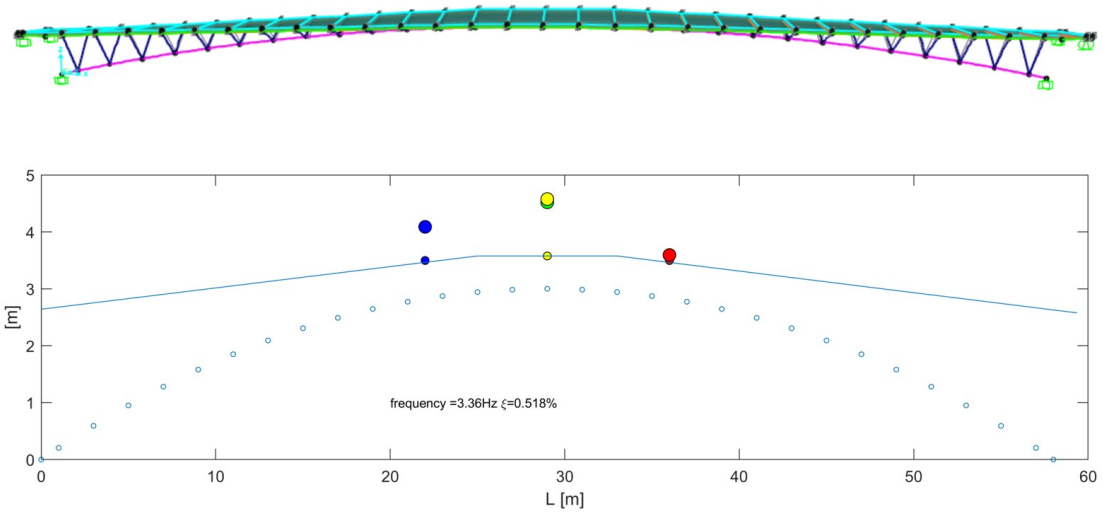

Figure 5.14: Comparison between experimental and numerical 3^{rd} mode shape

- **Mode 4**

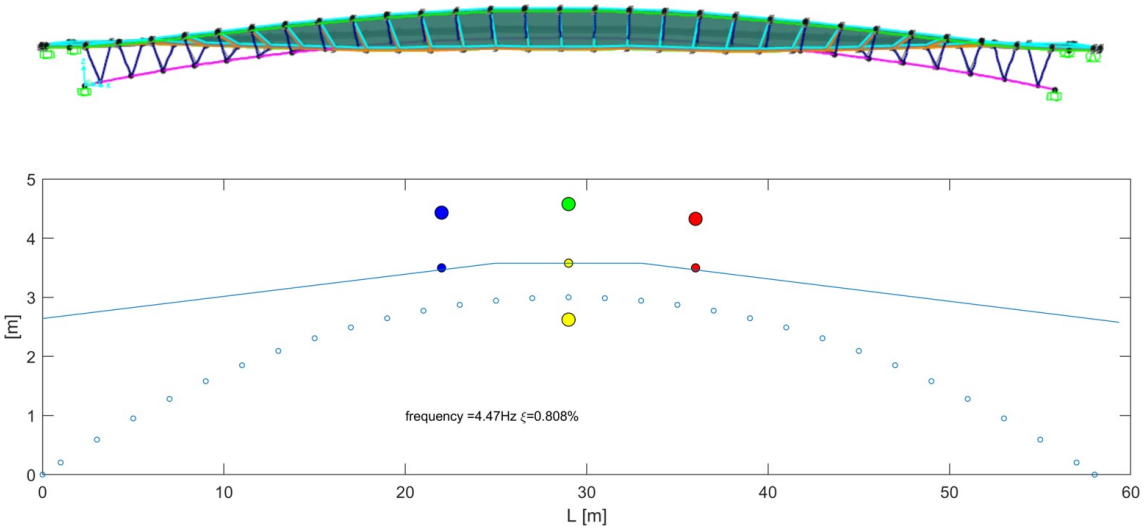

Figure 5.15: Comparison between experimental and numerical 4^{th} mode shape

5.4.3 Sensitivity analyses

As it can be seen from the comparison of the mode shapes, there is a good agreement between the experimental and numerical modes. However, a calibration of the finite element model is needed. In fact, the values of the frequencies present differences. In order

to calibrate the model, which is an operation often called modal updating, parametrical analyses through the finite element model have been carried out. These analyses have been performed thanks to the OAPI functions in Sap2000[1] that allow to study the effects of the variation of the parameters on the structural analysis, i.e. modal analysis.

In this regard, with reference to two limits restrain conditions of the restrained joints: (i) fully-restrained and (ii) hinges-restrained, sensitivity analyses varying the joints stiffness, the Young modulus and the unit weight of the concrete have been performed. Figure 5.18 summarizes the two restrain conditions and the parameters that have been varied in the sensitivity analyses.

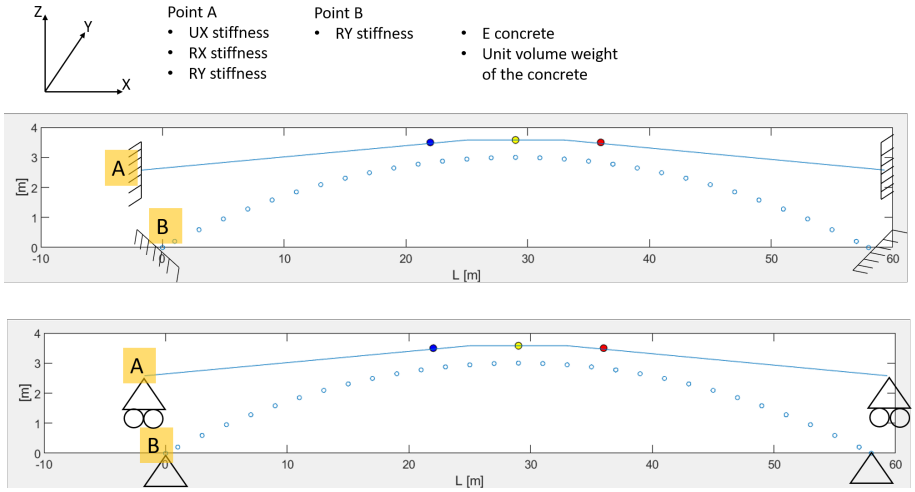

Figure 5.16: Two limit cases considered for the sensitivity analysis of the finite element model

Figure 5.17 and Figure 5.18 report the results of the sensitivity analyses with reference to the parameters that have an influence on the modal shapes only: (i) the Young Modulus of the concrete, (ii) the unit volume weight of the concrete, (iii) the translational stiffness *UX* and the rotational stiffness *RY* (point B).

[1]CSI, "SAP2000 Integrated Software for Structural Analysis and Design", Computers and Structures Inc., Berkeley, California.

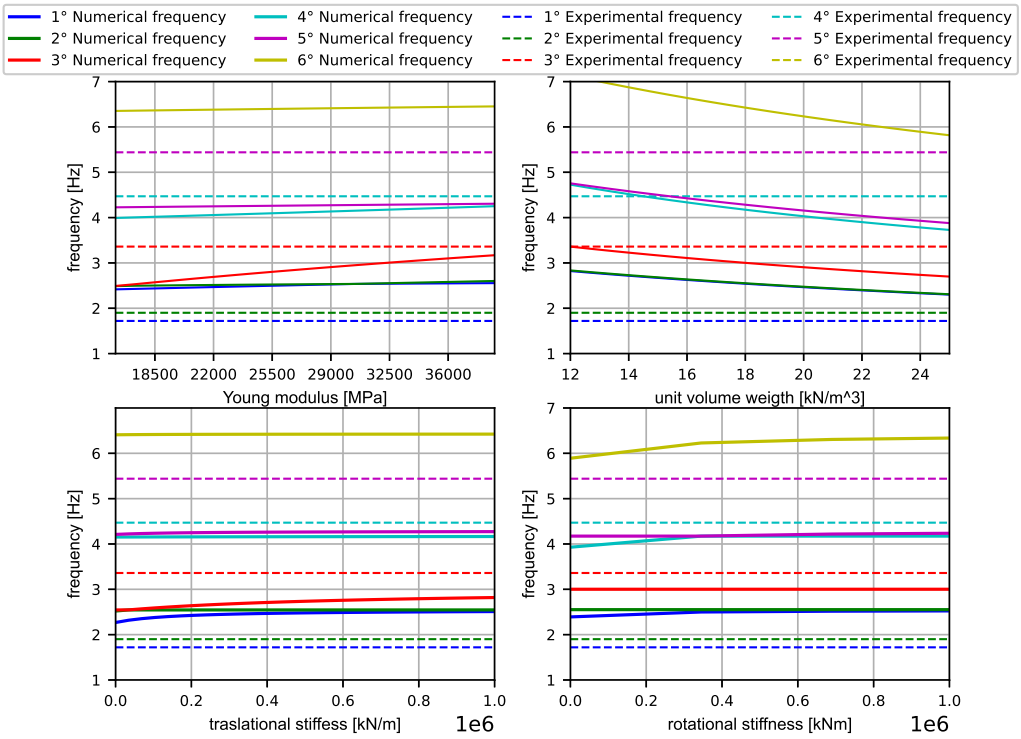

Figure 5.17: Sensitivity analyses results for the fully-restrained condition

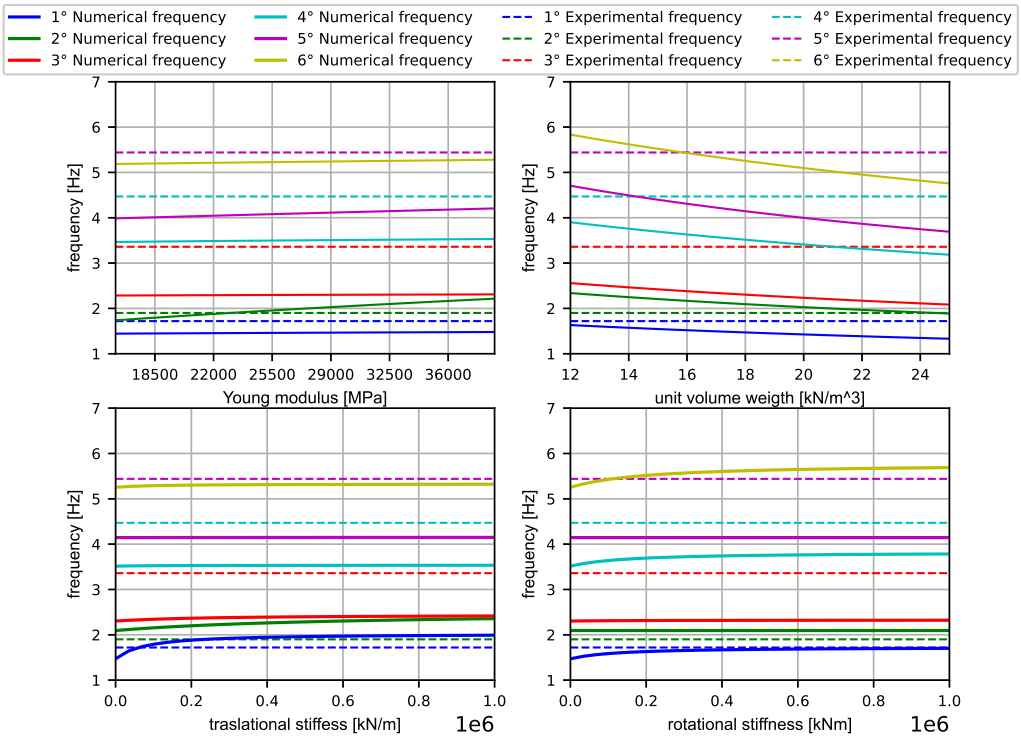

Figure 5.18: Sensitivity analyses results for the hinges-restrained condition

After the identification of the main parameters that govern the dynamic behaviour of the bridge they can be introduced as variables in the model updating process whit reference to the n identified modes, for instance, with a typical approach of minimizing a cost function, also called the objective function. This function typically assumes the following expression:

$$\sum_{i=1}^{n} w_{f,i} \cdot \left(\frac{f_{i,exp} - f_{i,fem}}{f_{i,exp}} \right)^2 + \sum_{i=1}^{n} w_{MAC,i} \cdot (1 - MAC_i) \tag{5.35}$$

where $w_{f,i}$ and $w_{MAC,i}$ indicate the weight that can be applied to the frequency and MAC, respectively. $f_{i,exp}$ and $f_{i,fem}$ are the identified and the numerical frequencies, respectively. The Modal Assurance Criteria, between $f_{i,exp}$ and $f_{i,fem}$, can be calculated according to expression 5.6. However, this step is already ongoing, since the setup of the acquirement system was constituted by 4 accelerometers and it does not allow to correctly update the model.

5.5 Example 2: Dynamic identification of a railway pre-stressed concrete bridge

In this section it is reported an example of the application of the above-described techniques for the dynamic identification of a railway post-tensioned concrete viaduct. It belongs to the railway line Roma-Formia-Napoli, Italy and overcomes the A1 highway in the Napoli municipality. The bridge, which was built in 1976, consists of seven 35.10 m long straight simple supported caisson beams. A schematic view of the viaduct is reported in Figure 5.19. It is characterized by the typical configurations adopted in the construction of most of the Italian bridges built in the 60-70s. Figure 5.20 reports its longitudinal profile and the transversal cross-section of the caisson beam.

Figure 5.19: View of the railway post-tensioned concrete viaduct

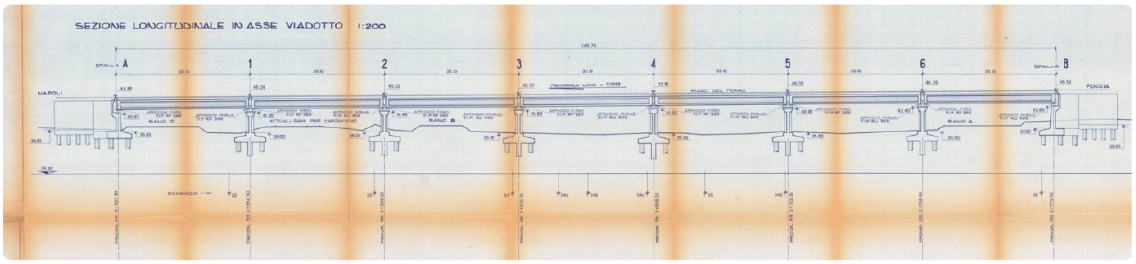

(a) Longitudinal profile

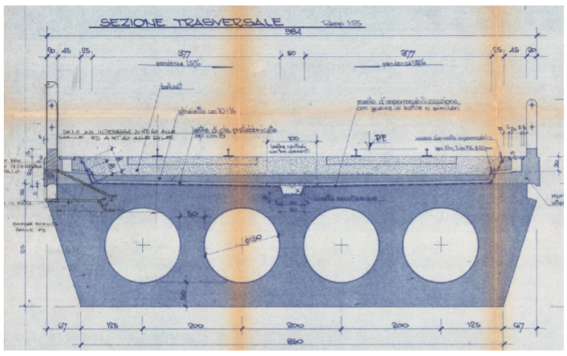

(b) Transversal cross-section of the caisson beam

Figure 5.20: Original technical drawing of the railway post-tensioned concrete viaduct

Each beam is post-tensioned by means of the presence of curvilinear harmonic steel wires with 8mm diameter. In particular, they follow four different layouts (α, β, γ and δ) along the longitudinal extension of each beam, as reported in Figure 5.21.

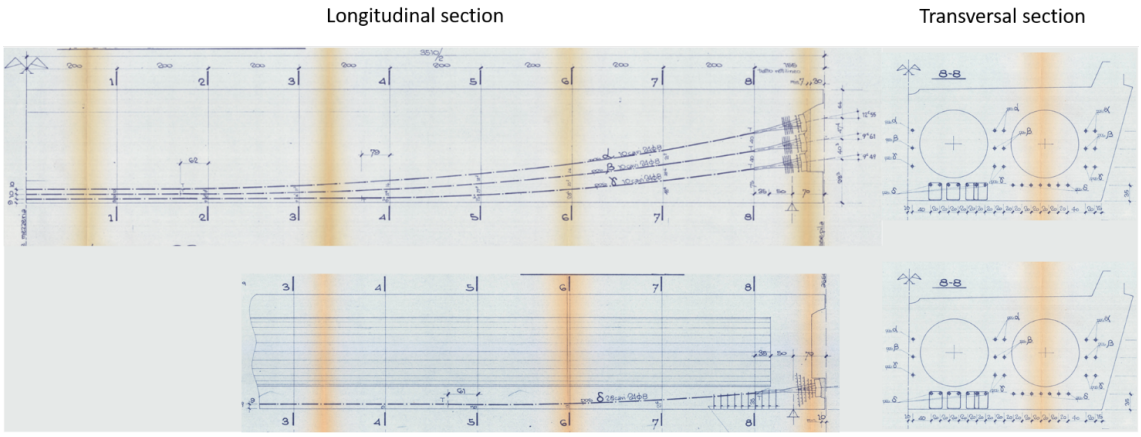

Figure 5.21: Cables layout along the post-tensioned beams

The supports at each extremity of a beam are constituted respectively by four bearing devices that fix the displacement in all directions and bearing devices that allow the longitudinal displacements. The static scheme provided by the supports is the typical isostatic simple-supported scheme. Piers and abutments are on pile foundations.

In 2022, the National railway company decided to install a static and dynamic monitoring system on two of the seven beams of the viaduct in order to identify its structural behaviour and to manage its conditions over the next years, in terms of maintenance, retrofitting, and future interventions. The monitoring system consists of several sensors, including strain gauges, inclinometers, accelerometers, thermocouples, laser barriers (to identify the passing of the trains) and displacement sensors. Figure 5.22 reports a schematization of the sensors that are installed in the two monitored beams.

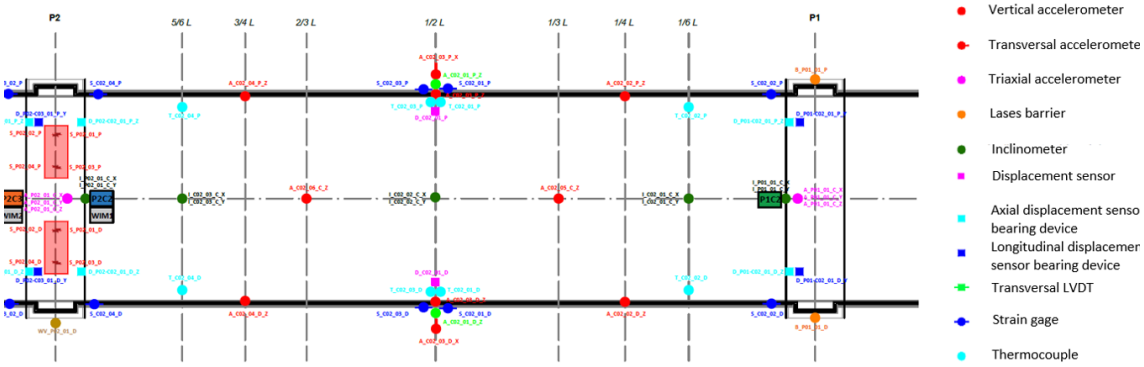

Figure 5.22: Layout of the sensors installed on one of the two monitored spans

Until now, the system is still in a checking phase and requires further calibrations and tuning activities. For instance, in order to remove the effects of the temperature on the monitoring data, i.e. according to the PCA theory discussed before, the amount of the acquired data has to be enough to consider the seasonal effects. However, several data are already available and dynamic identification techniques can be applied. This activity, in fact, allows to calibrate a finite element model of the viaduct that will be fundamental in the future monitoring phases. In this regard, in the present case, only the data dynamically acquired by the accelerometers (red circles in Figure 5.22) during operational conditions of the viaduct have been considered. The sampling frequency is 200 Hz.

5.5.1 FDD application

The estimation of the spectrum matrix was achieved by applying the Welch average by dividing the time series of the acceleration signals, of a total length of 40 minutes, in segments of a number of samples that lead to a frequency resolution of 0.05 Hz, considering an overlap of 50% between the segments and using Hamming windows to reduce the leakage. Figure 5.23 the spectra of the singular values.

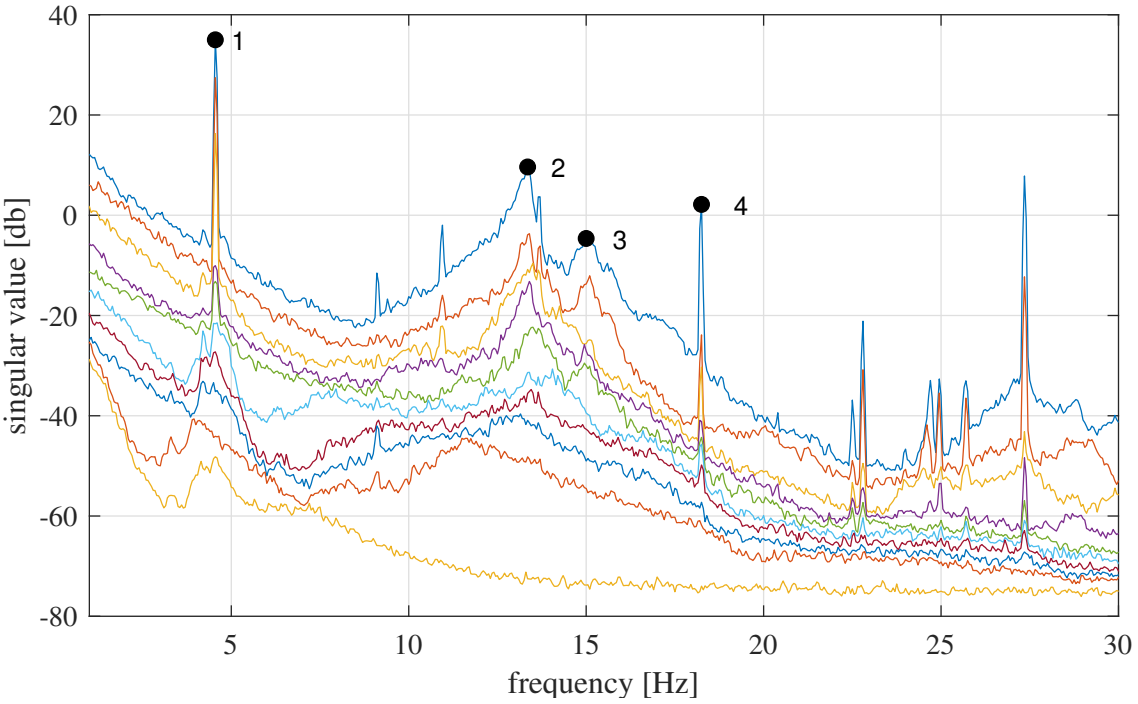

Figure 5.23: Spectra plot of the singular values

As it can be seen from Figure 5.23 also the other singular values with respect to the first one present not negligible values around the peak that can be identified as modes. This could lead to unbiased modal shapes, however, their frequency values can be assumed valid. In this regard, Table 5.4 reports the first four identified frequencies in the range of (0 Hz,30 Hz).

Table 5.4: Identified frequencies according to FDD technique

Mode	**Frequency [Hz]**
1	4.55
2	13.35
3	15.00
4	18.25

However, the modal shapes that correspond to the identified peak on the spectra assume high complex values that do not allow to correct identify their modal shapes. This aspect requires further studies that are currently ongoing.

5.5.2 SSI-cov application

The SSI-cov algorithm has been applied by introducing a time lag of *3 s*. This time lag corresponds to almost 10 cycles of the lower frequency ($1/4.55Hz \simeq 0.22s$). Figure 5.24 shows the stabilization diagram resulting from the output of the technique, adopting the limit reported in Eqs. 5.22, 5.23 and 5.24.

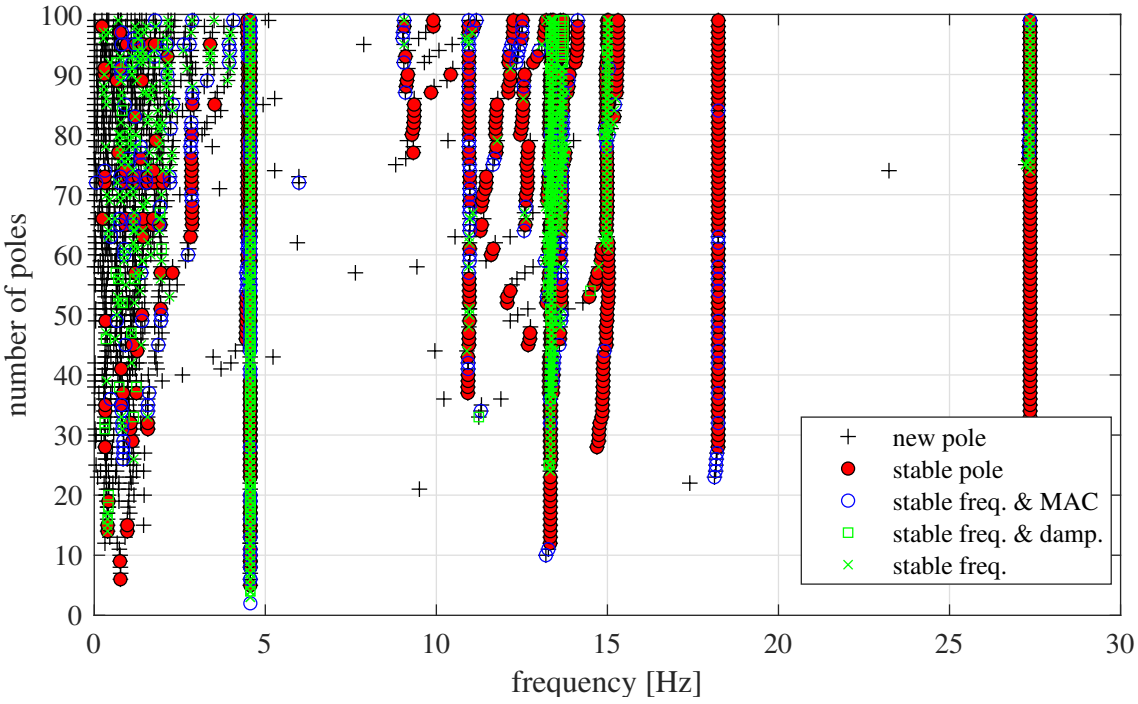

Figure 5.24: Stabilization diagram

The stabilization diagram shows that the frequencies identified by the FDD techniques appear stable and could be real modes of the structure. However, the poles in the range 10-20 Hz still have to be well characterized.

5.6 Concluding remarks of the chapter

The chapter has reported the phases that should be conducted in the correct management of monitoring systems. Each phase is described in terms of the specific activities, different roles and responsibilities of the involved operators. Two examples of techniques that can be implemented for the extraction of the significant response parameter from the dynamic data coming from monitoring systems have been described. Thus, these techniques, the Frequency Domain Decomposition (FDD) and the Covariance-driven Stochastic Subspace Identification (SSI-cov) have been applied to the measurements acquired on a steel pedestrian bridge in Pianoro, Italy. Parametric analyses on the Finite Element

Model of the bridge have been performed in order to identify the parameters that govern the dynamic behaviour of the bridge and that can be tuned in order to calibrate the model itself. However, this step is already ongoing, since the setup of the acquirement system was constituted by 4 accelerometers and it does not allow to correctly update the model.

In addition, the chapter also reports the theoretical description of the Principal Component Analysis, which is a widely used technique for removing the environmental effects, like those one related to temperature, humidity, etc., on the monitoring data.

6

Intervention strategies

Sommario

Questo capitolo descrive brevemente alcune possibili strategie di intervento sui ponti esistenti necessarie per ripristinare i livelli di sicurezza richiesti, sia dal punto di vista statico che sismico.

Summary

This chapter briefly reports some possible intervention strategies on existing bridges necessary in case to restore the required safety levels, both from a static and seismic point of view.

If the existing bridge is no more able to satisfy some functionality requirements or it shows an evident reduction of the strength capacity of some structural elements (e.g. due to deterioration of the materials, damage caused by environmental actions and/or abnormal operating and use situations, etc.), an expert judgement, sometimes requiring a structural safety assessment, is necessary in order to establish whether:

- the functional obsolescence is moderate or severe;
- the structural obsolescence is moderate or severe;
- the use of the bridge can continue without interventions;
- it is necessary to restore full functionality or to increase structural safety through major or minor interventions.

6.1 Intervention strategies from static point of view

The safe static behaviour of an existing bridge is fundamental and has to be always guaranteed. For instance, the following interventions can be applied:

- replacing of the bearing devices;

- increasing of strength of selected structural elements (deck, piers) by means of composite materials;
- increasing of the foundation capacities;

6.2 Intervention strategies from seismic point of view

Seismic actions could represent high demanding loads that a bridge has to sustain. The solutions mostly adopted to intervene on existing bridges, from a seismic point of view are:

- introducing special bearing devices currently available on the market, like isolators (High Rubber Damping Bearing or Curved Surface Sliders), eventually with the addition of shock-transmitters and dampers.
- traditional solutions that provide increasing of strength and ductility, like interventions with composite materials and reinforcement of the substructures.

The typologies of seismic intervention basically depend on the static scheme of the bridge. For instance, the seismic upgrading of a rigid frame bridge often requires the increasing of strength of the most stressed points, like the connections between the deck and the piers. Regarding the seismic upgrading of existing bridges through isolators, in the part III is described a simplified procedure is described which identifies the proper isolator system with an application to a reinforced concrete bridge.

Part II

Corrosion in wires and strands

7

Methodological approach

Sommario

Questo capitolo introduce il problema della corrosione nei trefoli e descrive i principali approcci e risultati disponibili in letteratura in merito alle modalità di analisi di trefoli corrosi e all'interpretazione di risultati sperimentali.

Sulla base di questi ultimi, emerge come la riduzione di resistenza nei trefoli corrosi dipenda da ulteriori fenomeni rispetto alla sola riduzione di sezione trasversale.

A partire quindi da questa osservazione, viene presentato brevemente l'approccio metodologico (dettagliato nei capitoli successivi) utilizzato nel cercare di modellare la corrosione in fili e trefoli al fine di fornire degli strumenti ingegneristici utili ai fini progettuali e di valutazioni di sicurezza.

Summary

This chapter introduces the problem of corrosion in strands and describes the main approaches and results available in the literature, regarding the methods of analysing corroded strands and the interpretation of experimental results.

In this regard, it emerges that the reduction of strength in corroded strands depends on further phenomena in addition to the reduction of the cross-section area only.

Therefore, starting from this observation, the methodological approach (detailed in the following chapters) in trying to model corrosion in wires and strands is briefly presented in order to provide engineering tools useful for design purposes and safety assessments.

7.1 Scientific background

Cementitious grouting of the steel strands in post-tensioned prestressed concrete beams is essential to provide their permanent protection against corrosion. In fact, they are highly vulnerable to corrosion phenomena, which can strongly reduce their strength and ductility capacities leading to sudden failures. The recent catastrophic collapse of the Polcevera

bridge [1] and subsequently, extended bridge inspections on Italian bridges [38] highlighted that several post-tensioned beams present lacks in the grout, which trigger the formation of corrosion in the steel strands. Steel seven-wire strands are often used in reinforced concrete structures. They are constituted by a straight central wire, often indicated as king-wire, and six external wires twisted into helicoidal shapes. Since they are made up of high-strength steel they are commonly used both in pre-tensioned and post-tensioned elements, such as bridge beams.

Localized corrosion phenomena may be particularly dangerous for such elements given the high difficulty in their detection, especially when dealing with long bridge beams. They can interest both the longitudinal and transversal directions of strands and might be characterized by uniform or specific complex shapes, depending on the chemical conditions during corrosion phenomena. Their presence might, therefore, detrimentally influence the strength of the strand.

Thus, the availability of reliable engineering tools enabling the estimation of the maximum strength of corroded strands accounting for the geometry of the corrosion and the characteristics of the steel material represents nowadays one of the main challenges for the structural engineering community.

According to the available studies, three approaches can be identified:

- assessment based on the results of numerical analyses carried out with sophisticated finite element models capable of accounting for the real corrosion configuration;
- assessment based on the results of experimental tensile tests on corroded wires and strands aimed at obtaining reduction/correlations relationships based on the main mechanical parameters and the main information regarding the corrosion extent;
- assessment based on simplified analytical models taking into account the geometry of corrosion and the steel material parameters.

These approaches are summarized in Figure 7.1.

On one hand, numerical finite element modelling of corroded strands, which are available for instance in [39] and [40], require complete knowledge of the corrosion geometry. However, nowadays this information is still difficult to obtain. In this regard, [40], [41] proposed analytical formulas for the estimation of the section loss in corroded wires. As a matter of fact, this approach can be directly adopted after collapses when the geometry of the corrosion can be directly measured on the field. This leads to the fact that the approach of using complete and sophisticated numerical models results difficult to be used as an engineering prediction tool.

On the other hand, several experimental campaigns on corroded wires and strands that take into account both real and artificial corrosion have been conducted. The behaviour of corroded strands, collected from existing bridges, has been studied in [40],[3],[42], [43],

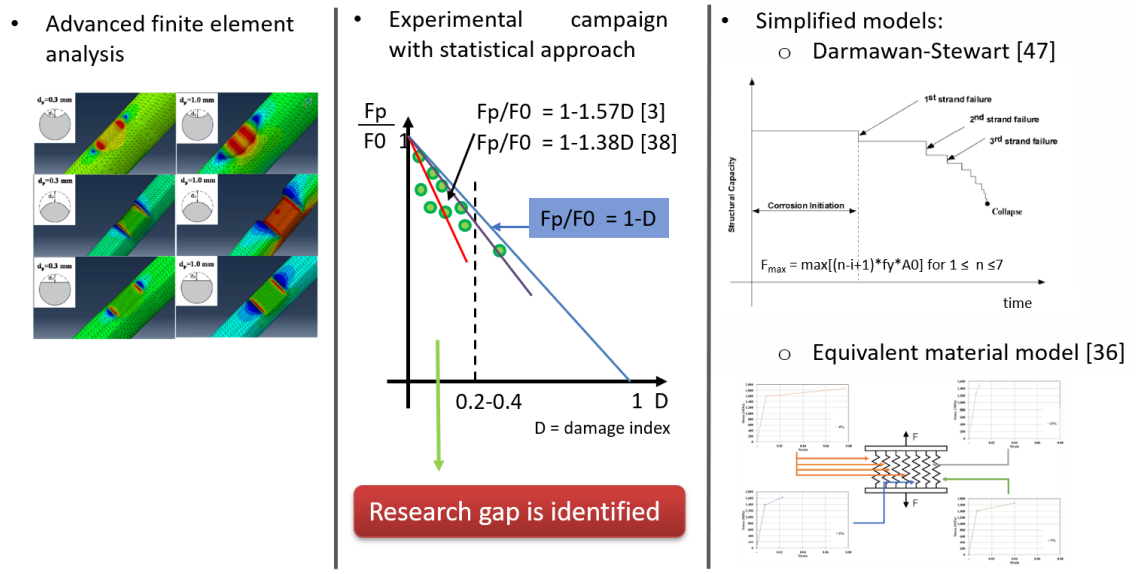

Figure 7.1: Summary of the possible approaches to manage corrosion phenomena in strands

[44], by means of tensile tests. In addition, experimental results of artificial corroded strands are available in [45], [46] and [47], where also analytical modelling of corrosion introducing a damage constitutive model is reported. In addition, [48] introduces a constitutive model for corroded strands, taking into account the pit type morphologies proposed by [40] comparing the results of the model with experimental tensile tests. Recently, [49] proposed a simplified model for the evaluation of the residual mechanical response of corroded strands providing a formulation based on a single input parameter represented by the maximum penetration depth on the most corroded wire. Similarly, [50] reports a probabilistic study of the corrosion pits introducing a constitutive model of corroded strands.

However, typically a linear correlation between the ultimate force measured during the tests and the total reduction of the cross-section of the most corroded wire is provided. This is due to the assumption, often confirmed by experimental evidence, that the first wire failure occurs in correspondence of the most corroded one and that it corresponds to the maximum force in the strand.

However, trends of the force reduction as a function of the cross-section loss in the strand are also available. The latter representation results to be a more complete description of the force reduction in corroded strands and is the one that will be used in this work. Basically, what has been done seems to be limited for three reasons: (i) the tested specimens had reductions of the cross-section area in a specific range, typically 20-30%, (ii) the analytical formulations are limited to consider the maximum strength of the strands corresponding to the most corroded wire, and (iii) the results depend on the specific test configuration setup. Although tests on wires and strands, both with real and artificial

corrosion, were conducted, analytical formulations are still limited. These formulations should be able to provide an estimation of the strength in corroded strands taking into account the geometry of the corrosion in the wires constituting the strand and the steel material properties. Examples of analytical models are shown in [48], [49] and [51]. However, the latter model is circumscribed to the case of the brittle behaviour of wires.

The peak force of corroded strands (F_p), for instance, measured during pulling tests, can be represented as a function of a synthetic parameter of damage D , related to the global reduction of the cross-section area. In fact, $D = 1 - A/A_0$, where A and A_0 indicate the residual and the intact cross-section area of the strand, respectively. This representation is available [40], [3], [43], [44], [46] [50], [48]. However, the current state of the art shows that the peak force seems to be influenced by further effects that have not been deeply analysed so far. In fact, the maximum force measured during tensile tests does not agree with the prediction provided by the linear formulation given by the reduction of the cross-section area only (dashed black line in Figure 7.2. As observed also by [40] the amount of decrease in tensile strength is larger than the amount of decrease in the reduction in cross-sectional area.

This effect is graphically explained in Figure (1) where the tensile tests results are identified by the green circles ($F_{p,EXP}$). F_p and F_0 are the maximum force (peak force) in corroded strands and the maximum force in not-corroded ones, respectively. In addition, Figure 7.2 reports also some example of linear correlation of the experimental data, usually provided by their interpolation and often representing a damage index until 20-40 $\%$.

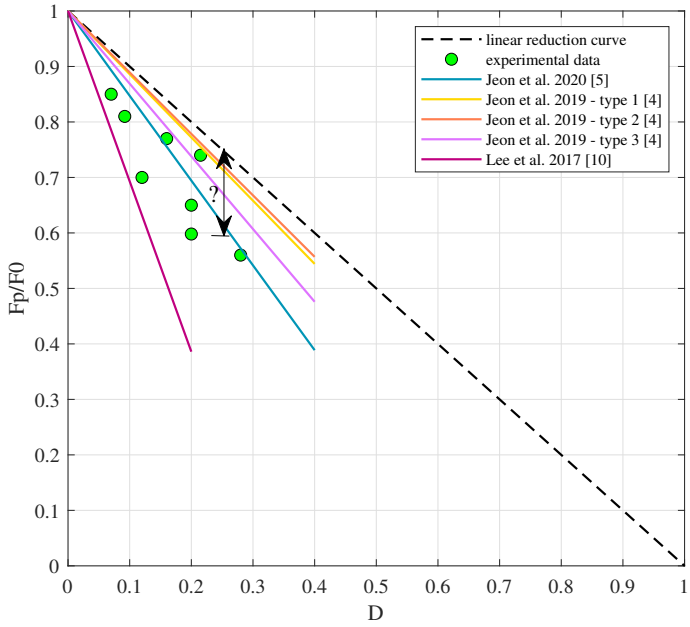

Figure 7.2: Results of some experimental tensile tests on corroded seven-wire strands available in the literature

The linear correlations between ultimate force and corrosion level in strands are typically expressed by the following formula:

$$F_{p,\alpha} = F_0(1 - \alpha \cdot D) \tag{7.1}$$

The parameter α depends on the experimental data and may assume values in the range (1.31 [40], 3.07 [46]). The different amount of dispersions for the same damage index suggests that the peak forces reduction might be affected also by further parameters such as the variability of the corrosion in the wires. As a matter of fact, a reliable expression of the strength reduction in corroded seven-wire strands, which should be valid in the entire domain of the damage index D, is still missing. Thus, this work aims at providing a complete strength reduction curve for corroded seven-wire strands by means of a new resistance model that is able to represent the dispersion in the peak force by means of introducing a new function depending on the variability of the corrosion in the wires. In addition, this new model should allow to characterize the effects of localized corrosion on the mechanical behaviour of corroded strands evaluated through force-displacement relationships (which are shown in chapters 8,9 and 10).

7.2 Problem formulation

Post-tensioned beams can be affected by lack of injections in the grout of the duct containing prestressing steel strands. Figure 7.3 shows how this problem has been schematized in this work. The behaviour of these post-tensioned beams can be seen as represented by the series system between intact zones and corroded zones where the lack of injection occurred. Thus, in this kind of problem, the study of the mechanical behaviour of the strands in the corroded zones has been first performed.

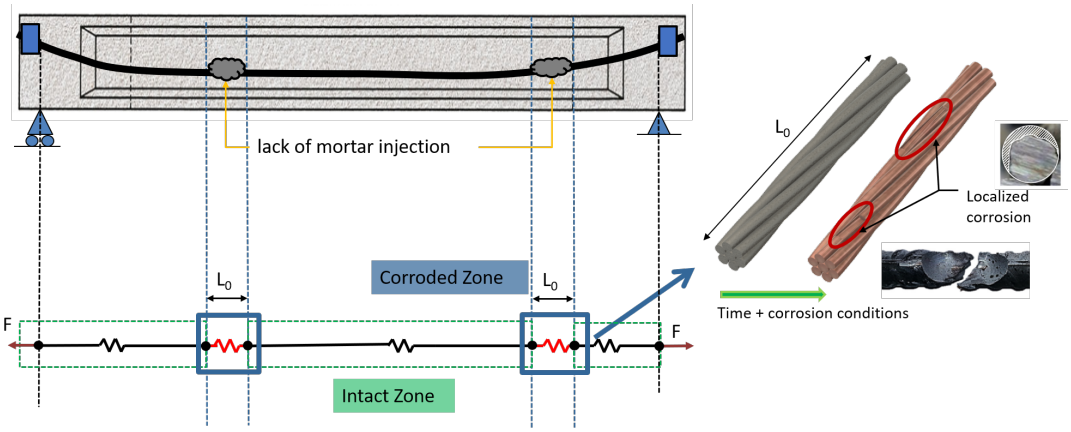

Localized corrosion picutures taken from [52]

Figure 7.3: Schematization of lack of injections in post-tensioned beams

Localized corrosion along the longitudinal and transversal directions of strands is characterized by uniform or specific complex shapes, however, for the sake of introducing simplified analytical models, they are often approximated by analytical configurations, which allows the calculation of the cross-section loss.

In this work, the cross-section reduced area due to corrosion is introduced by means of a simplified model for the corrosion geometry that considers both the longitudinal and the transversal corrosion extension. The model is based on the key parameters:

- the adimensional reduction of cross-section area $\rho_i = A_i/A_{0i}$, where A_{0i} and A_i indicate the not-corroded and the residual cross-section areas of the i-th wire, respectively;
- the adimensional corrosion length $\lambda_i = L_c/L_0$, where L_0 and L_C represent the reference length and the corrosion length, respectively.

The reference length represents the portion of wires or strands for which lack of grouting occurred, and therefore the portion where the corrosion can develop, while the corrosion length represents the length of the corroded part.

Thus, when the geometry of the corrosion is defined, corroded and not-corroded parts can be identified and their mechanical behaviour is expressed in terms of force-displacement relationships.

Consequently, the corroded wire is modelled as a series system between those identified springs (corroded and not-corroded parts) in terms of force-displacement relationships according to the representation reported in Figure 7.4.

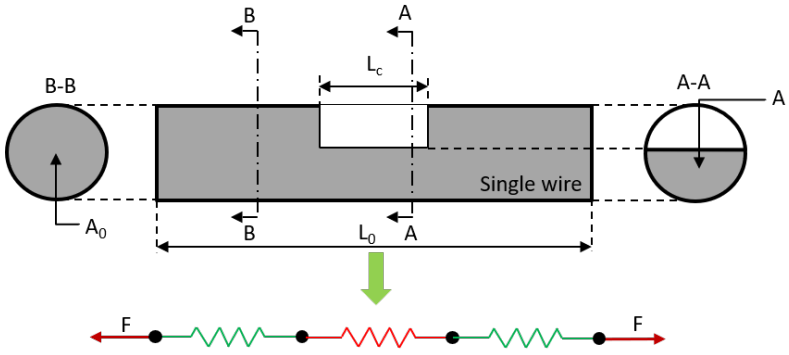

Figure 7.4: Model for the geometry of the corrosion in corroded single wires

Finally, the mechanical behaviour of corroded seven-wire strands is modelled by means of the parallel system between corroded and not-corroded wires in terms of force-

displacement relationships as shown in Figure 7.5. As a result, the force-displacement relationship of the corroded strand allows to identify the peak force (strength) and the ultimate displacement (ductility, if referred to the yielding displacement) that will be analysed in detail in this work. It is worth pointing out that the peak force of a corroded seven-wire strand might be in between a lower bound estimation, provided by the brittle behaviour of the wires (i.e. Darmawan-Stewart model), and the fully ductile behaviour of the wires.

The effects of the geometry of corrosion in the strands are summarized by means of three synthetic parameters:

- the adimensional corrosion length λ_i;
- the mean corrosion level ρ_M;
- the group coefficient ρ_G.

In particular, the characterization and the study of the "group coefficient" represent the original result of this work that together with a new resistance model, which is introduced in chapter 10, allows the achievement of the set objectives by means of the analysis of the peak force provided by the parallel model. The group coefficient can be seen as the product of two other coefficients: the minimum group coefficient $\rho_{Gmin}(D, COV_{\rho_i})$, which describes a completely brittle behaviour of the wires, and the model coefficient $\eta(D, COV_{\rho_i}, \lambda_i, \mu_\epsilon)$, which accounts for a ductile behaviour of the wires. In other words, it can be seen as the coefficient to apply to the lower bound estimation of the group coefficient in order to consider a certain ductility level.

After the characterization of the analytical expression of the lower bound estimation of the group coefficient ρ_{Gmin}, several Monte-Carlo simulations of corroded seven-wire strands have been performed in order to estimate the model coefficient η.

Hence, the simulation results allowed to characterize the model coefficient η in order to apply two different procedures:

- procedure a) considering λ_i as unknown: it could be the case of lack of knowledge of the corrosion extension;
- procedure b) considering λ_i as known: it could be the case of a complete characterization of the extension of the corrosion.

The application of the resistance model according to deterministic and probabilistic approaches lead to the definition of the strength and the ultimate displacement (ductility) reduction curves, and design-oriented results (safety factors and combination coefficients) based on the probability functions of the peak force of corroded strands, respectively. The idea is summarized in the following table.

Table 7.1: Summary of the application of the introduced resistance model

	Peak strength model			
	Deterministic approach		*Probabilistic approach*	
F_0	Calculated			
ρ_M	Calculated and/or estimated, i.e. experience, measurements			
ρ_{Gmin}	Calculated as discussed in chapter 10			
η	λ_i is known Polynomial expression as a function of λ_i	λ_i is unknown Constant value	λ_i is known PDF	λ_i is unknown PDF as a function of λ_i

The statistical description of the group coefficient ρ_G as a function of the damage index D, with reference to different percentiles, provides the possibility to define different strength reduction curves that directly allow evaluating the estimation of the strength of the corroded strands considering the geometry of corrosion, the mechanical parameter of the steel material and a certain ductility level. In other words, they allow to apply the introduced resistance model in a deterministic approach.

Parallel to the strength reduction curve, also ultimate displacement reduction curves providing useful information regarding the available ductility for corroded seven-wire strands have been obtained and shown in chapter 11. They consent to calculate reduced sigma-epsilon relationships for the steel material according to the damage index of the strand. This result allows to evaluate the reduction of the bending moment capacity of post-tensioned beams, for instance through the bending moment-curvature diagram, as illustrated in chapter 12.

The statistical description of the model coefficient η, in terms of probability and cumulative density functions, results central in the application of the introduced resistance model in a probabilistic approach. In fact, it consents to calculate the peak strength probability density function that allows to define useful design-oriented results, like safety factors and combination coefficients. This is deeply analysed in chapter 10.

Figure 7.5 summarizes the theoretical path followed for defining the probabilistic and the deterministic approaches taking into account the new resistance model and the lower bound estimation of the minimum group coefficient.

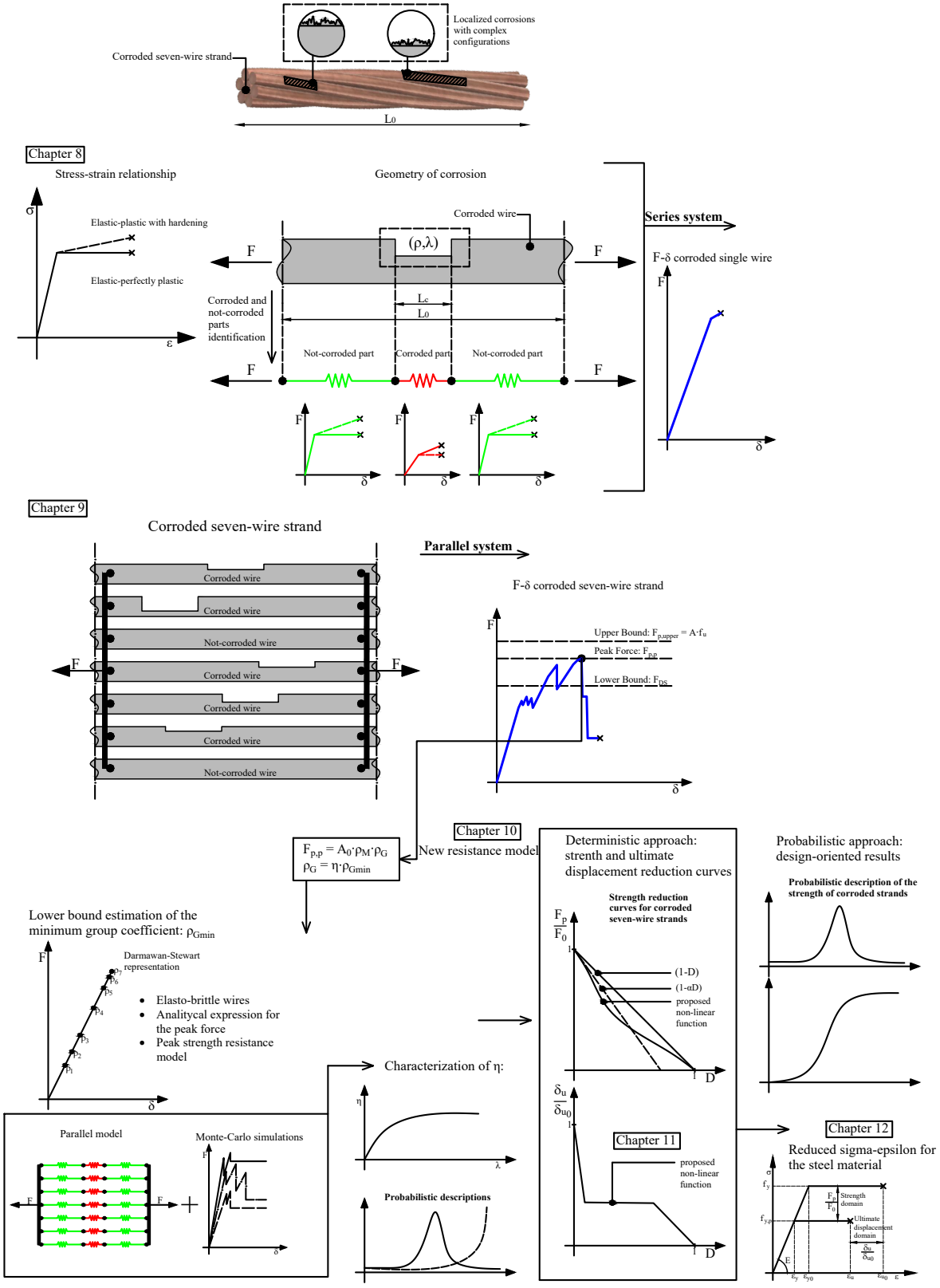

Figure 7.5: Graphical outline of the methodological approach applied for the evaluation of corrosion in wires and strands

8

Mechanical behaviour of corroded wires

Sommario

Questo capitolo presenta la modellazione analitica di fili corrosi. Nel modello vengono introdotti i parametri che verosimilmente ne governano il suo comportamento meccanico. Tali parametri riguardano la geometria di corrosione, in termini di riduzione trasversale di area e di estensione longiturinale, e i parametri costitutivi del materiale acciaio, quali la duttilità e il rapporto di incrudimento. Gli effetti di questi parametri sul comportamento meccanico di fili corrosi, valutato mediante diagrammi forza-spostamento, sono emersi da una serie di analisi parametriche condotte tramite il modello meccanico del filo corroso introdotto.

Summary

This chapter presents the analytical modelling of corroded single wires. The parameters that may govern the mechanical behaviour of corroded wires that are introduced in the model concern the geometry of the corrosion, in terms of transversal cross-section reduction and longitudinal extension, and the constitutive parameters of the steel material, such as ductility and hardening ratio. The effects of these parameters on the mechanical behaviour of corroded wires, evaluated by means of force-displacement relationships, emerged from a series of parametric analyses conducted using the introduced mechanical model of corroded wire.

The parameters that might influence the mechanical behaviour of corroded wires and strands are necessarily related to the mechanical behaviour of steel material and the geometrical configuration of the corrosion. The mechanical behaviour of the steel material is here represented by two stress-strain relationships: (i) elastic - perfectly plastic behaviour and (ii) bilinear with hardening behaviour. Figure 8.1a shows the parameters that define the sigma-epsilon relationships of the steel material. They are the yield stress f_y, the ultimate stress f_u, the yield strain ϵ_y and the ultimate strain ϵ_u.

As far as the bilinear with hardening steel material relationship is concerned, the hardening coefficient r defines the slope of the sigma-epsilon after the yield point as a percentage of the Young modulus E. The geometrical configuration of the corrosion in the wires

is here described by two key-parameters: (i) the adimensional reduction of cross-section area ρ_i and (ii) the here proposed adimensional corrosion length λ_i.

The proposed mechanical model of the corroded single wire is based on the following main assumptions:

- the wire is straight and subjected to tension force only;
- the corrosion model provides cross-section reduction both in transversal and longitudinal direction;
- the wire is described as an equivalent series system composed by the corroded and not-corroded parts that can be identified along the reference length;
- the mechanical behaviour of the corroded wire is represented by a force-displacement relationship that also accounts analytically for the corrosion effect on the elastic stiffness

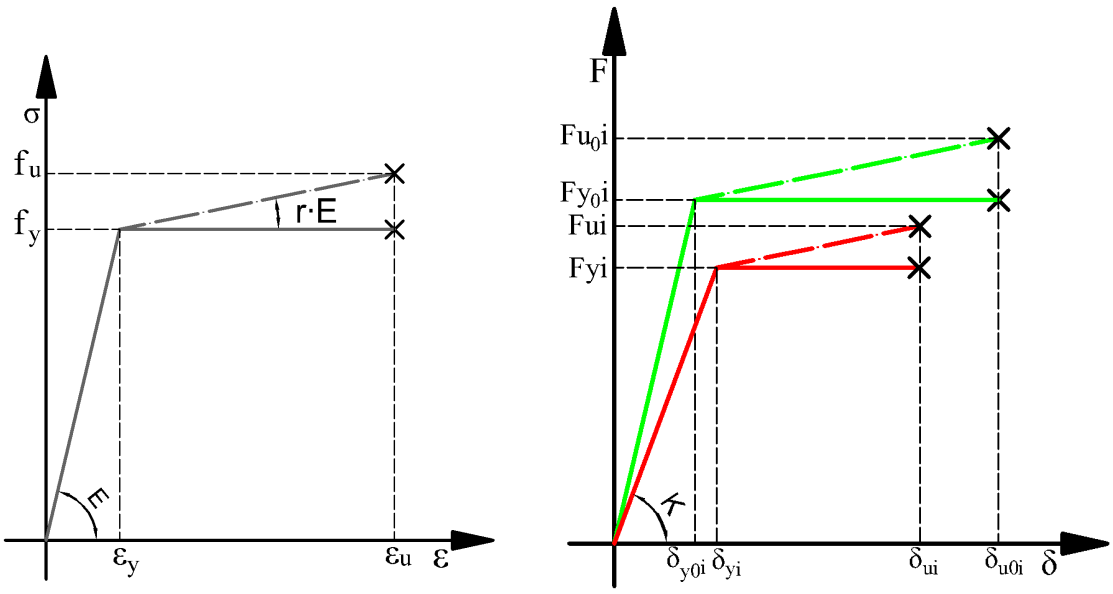

(a) sigma-epsilon relationships of the steel material

(b) qualitative force-displacement relationships of the corroded and not-corroded wire

Figure 8.1: Sigma-epsilon relationships of the steel material and qualitative force-displacement relationships of corroded and not-corroded wires

Figure 8.1b reports qualitative force-displacement relationships of corroded (green lines) and not-corroded (red lines) wires highlighting the main parameters that characterize their shape. They are yield forces F_{y0i} and F_{yi}, the ultimate forces F_{u0i} and F_{ui}, the yield displacements δ_{y0i} and δ_{yi}, and the ultimate displacement δ_{u0i} and δ_{ui}. The subscript

0 indicates the not-corroded configuration while the subscript i indicates that it is referring to the wire. The elastic stiffness K_i is referred to the corroded wire.

8.1 Analytical model with elasto-plastic material

The mechanical behaviour of a corroded wires can be expressed in terms of force-displacement relationships. Considering the geometry of the corrosion and the elastic-perfectly plastic steel material, from the properties of series systems, the elastic stiffness, the yield force, the yield displacement, the ultimate force and the ductility of a corroded wire can be expressed in a closed form as follow, respectively:

$$K_i = \frac{E \cdot A_{0i}}{L_0} \left[\frac{1}{1 + \lambda_i \left(\frac{1}{\rho_i} - 1 \right)} \right] \tag{8.1}$$

$$F_{yi} = \rho_i \cdot f_y \cdot A_{0i} \tag{8.2}$$

$$\delta_{yi} = \frac{F_{yi}}{K_i} \tag{8.3}$$

$$\delta_{ui} = \delta_{yi} + (\epsilon_u - \epsilon_y) \cdot \lambda_i \cdot L_0 \tag{8.4}$$

$$\mu_{\delta_{ui}} = 1 + \frac{\epsilon_u - \epsilon_y}{\epsilon_y} \frac{\lambda_i}{\rho_i \left[1 + \lambda_i \cdot \left(\frac{1}{\rho_i} - 1 \right) \right]} \tag{8.5}$$

It is worth noting that Eqs. 8.1, 8.2, 8.3 are also valid for elastic-perfectly plastic with hardening steel material and that the plastic deformation, according to Eq. 8.4 occurs in the corroded part only.

Figures 8.2a and 8.2b report the ductility of the corroded wire given by Eq. 8.5, compared with the ductility of the not-corroded wire, which corresponds to the material ductility $\mu_\epsilon (\mu_{\delta_0} = \mu_\epsilon)$, for a fixed value of material ductility $\mu_\epsilon = 10$ (harmonic steel) in a three-dimension and two-dimension ductility domains, respectively.

It can be seen from Figure 8.2, that the reduction of the ductility in a corroded wire is governed by the coupling of the two parameters of the adimensional reduction of cross-section area ρ_i and the adimensional corrosion length λ_i. In particular, it assumes a high non-linear behaviour for small values of the parameters (ρ_i, λ_i). In other words, the geometry of the corrosion can strongly govern the mechanical behaviour of a corroded wire, especially for localized corrosion. Similar behaviours can be observed in the other parameters as well.

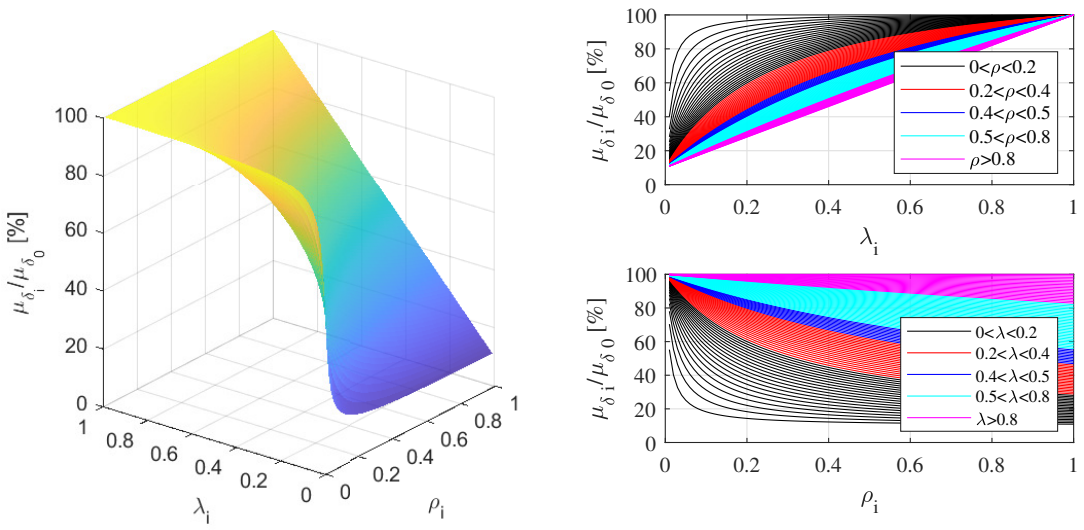

(a) 3d trend

(b) 2d trend

Figure 8.2: Reduction of the ductility in corroded wires as a function of the adimensional reduction of cross-section area and adimensional corrosion length

8.2 On the influence of the hardening ratio and the material ductility

To highlight the effects of the steel material and the geometrical configurations of the corrosion on the mechanical response of a corroded single wire, several parametrical simulations have been carried out. In particular, for the steel material, they are considered two values of material ductility: (i) $\mu_\epsilon = 10$ as representative of harmonic steel and (ii) $\mu_\epsilon = 10$ as representative of mild steel. In addition, they are taken into account three values of the hardening coefficient: 0 % (elastic-perfectly plastic), 0.5 % and 1.5%. As far as the geometrical configuration of the corrosion, for each value of the dimensional corrosion extension λ_i different ρ_i values in the range (0,1) have been considered.

Figure 8.3 and Figure 8.4 report the results of the parametrical simulations of corroded wires for the case of $\lambda_i = 0.01$ and $\lambda_i = 0.15$ in terms of force-displacement relationships, respectively. The results are shown normalized with respect to the not-corroded wire ($\rho_i = 1$) dividing the forces by the yield force $F_{y0,i}$ and the displacement by the yield displacement $\delta_{y0,i}$. In other words, it is made equal to (1, 1) the yielding point of the not-corroded wire. The figures show the force-displacement results considering elastic-perfectly plastic and elastic-plastic with hardening stress-strain relationships for the two values of material ductility.

Figure 8.3 and Figure 8.4 clearly show that the different configurations (in terms of r and μ_ϵ) lead to different results in terms of maximum force, yield and ultimate displacement. They allow identifying two different behaviours of the wires characterized

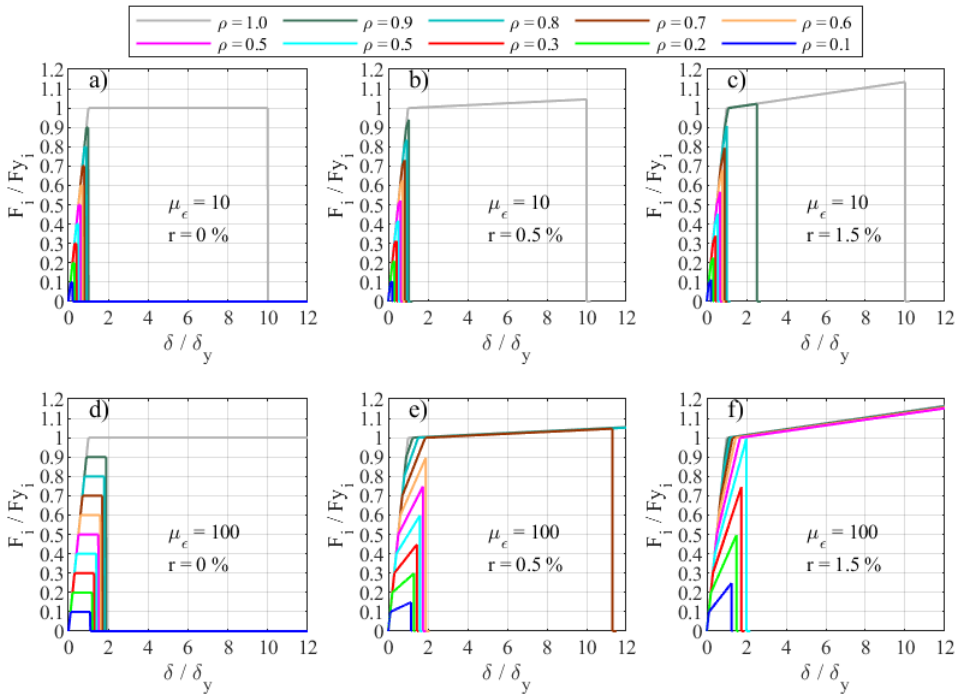

Figure 8.3: Results of parametrical simulations of corroded wires characterized by $\lambda_i = 0.01$ in terms of force-displacement relationships: (a) ($\mu_\epsilon = 10, r = 0\%$), (b) ($\mu_\epsilon = 10, r = 0.5\%$), (c) ($\mu_\epsilon = 10, r = 1.5\%$), (d) ($\mu_\epsilon = 100, r = 0\%$), (e) ($\mu_\epsilon = 100, r = 0.5\%$), (f) ($\mu_\epsilon = 100, r = 1.5\%$)

by $r > 0$. The first one is represented by a bilinear behaviour with the collapse due to the complete plasticization of the corroded part only, while the not-corroded part remains within the elastic behaviour. The second one is represented by a trilinear behaviour with two consecutive changes in the slope of the diagram after the yielding point. This behaviour occurs because the collapse involves a partial plasticization of the not-corroded part in addition to the full plasticization of the corroded part, thus leading to a higher ductile behaviour. In other words, an exploitation of the post-yielding branch response of the not-corroded part is observed.

This "post-yielding response exploitation" leads to larger ultimate displacement (ductility) and, for $r > 0$, also to increased maximum force, describing the capacity of the corroded wire to exceed the yielding force of the not-corroded one. This depends on the specific combination of the values of r and μ_ϵ. In addition, it results to be high depending also on the λ_i value, as shown by comparing Figure 8.3 with Figure 8.4. In fact, the higher the adimensional extension λ_i, which describes a higher ductility in the corroded part, the higher the capacity to exploit the post-yielding branch response of the not-corroded part.

The post-yielding response exploitation can also occur for small values of λ_i. In the case of limited material ductility, which is the case of harmonic high-strength steel used in prestressed concrete structures, this effect strongly depends on the coupling between ρ_i

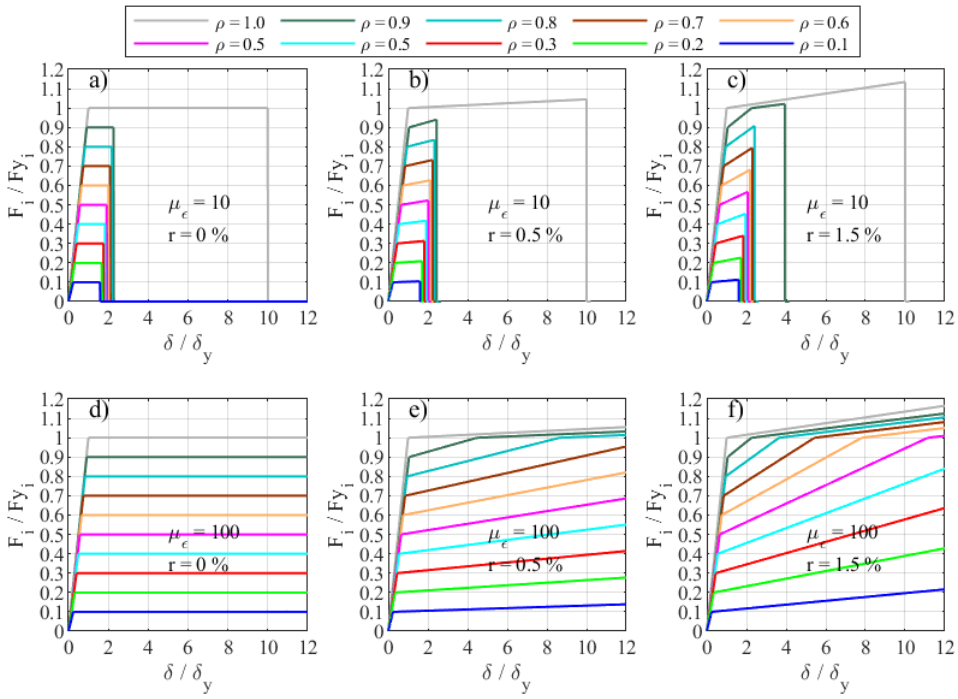

Figure 8.4: Results of parametrical simulations of corroded wires characterized by $\lambda_i = 0.15$ in terms of force-displacement relationships: (a) ($\mu_\epsilon = 10, r = 0\%$), (b) ($\mu_\epsilon = 10, r = 0.5\%$), (c) ($\mu_\epsilon = 10, r = 1.5\%$), (d) ($\mu_\epsilon = 100, r = 0\%$), (e) ($\mu_\epsilon = 100, r = 0.5\%$), (f) ($\mu_\epsilon = 100, r = 1.5\%$)

and λ_i. In particular, as reported in Figure 8.3, for small values of ρ_i, it can be observed only for high values of hardening coefficient (i.e. $r = 1.5\%$). In other cases, the plastic deformation involves only the corroded part. This phenomenon leads to very brittle behaviour for the corroded wire. Moreover, also the material ductility μ_ϵ plays a very important role in the mechanical response of corroded wires, in fact, the higher the material ductility, the higher the maximum force.

Accounting for the combination of the three parameters $\rho_,\lambda_i$ and μ_ϵ can provide a better description of the behaviour of corroded wires with respect to the usual estimation. Indeed, typically, as a first approximation, the force-displacement response of the corroded wire can be estimated with reference to the corroded part only: specifically, the maximum force of a corroded wire can be obtained with reference to the cross-section reduction of the corroded part only (i.e. $F_{u,i} = \rho_i f_y A_{0,i}$).

The main results of the simulations are here summarized and subdivided with the behaviour classes for the steel material. Assuming an elastic-perfectly plastic material (hardening coefficient $r = 0\%$):

- the peak force of corroded wires results to be independent with the adimensional corrosion length λ_i. In these cases, it can be assumed as a function only of the adimensional reduction of cross-section area ρ_i.

- The ultimate displacement of corroded wires results to be independent with the adimensional reduction of cross-section area ρ_i. In these cases, it can be assumed as a function only of the adimensional corrosion length λ_i.
- The ductility of the material μ_ϵ leads to an increase in the ductility of the corroded wires.

Assuming an elastic-plastic material (hardening coefficient $r \neq 0$):

- The effect of the coupling of ρ_i and λ_i can provide a post-yielding response exploitation of the not-corroded part leading to higher peak force and ultimate displacement with respect to the ones of the corroded part, which can represent a first approximation of the mechanical behaviour of a corroded wire.
- For high values of ρ_i, the post-yielding response exploitation appears clear also for small values of hardening coefficient (i.e. $r = 0.5\%$), but it depends on the λ_i and ρ_i values.
- For small values of ρ_i, the same effect takes place only for higher values of r and λ_i . In other words, a particular coupling of ρ_i and λ_i might provide a post-yielding response exploitation of the not-corroded part leading to an increase in the performance of the corroded wire.

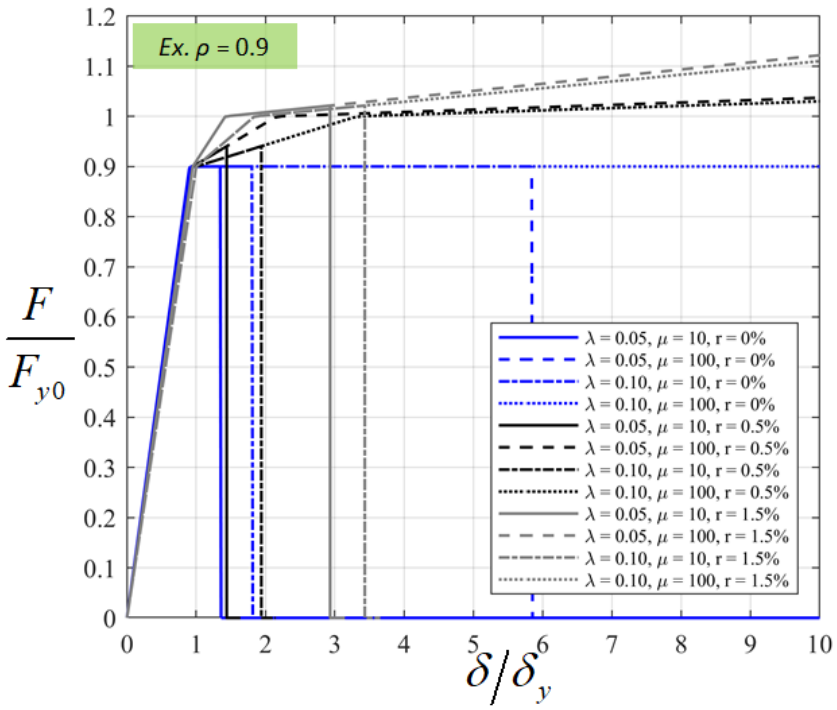

Figure 8.5: Comparison of the parametric force-displacement relationships of corroded wires

Figure 8.5 summarises the force-displacements relationships obtained from the parametric study with reference to the case of $\rho_i = 0.9$ with $\lambda_i = 0.05$ and $\lambda_i = 0.1$. It empathizes the discussed reducing effects both of the strength and of the ductility. The diagrams are expressed with reference to the not-corroded case.

Therefore, from this first parametric study carried out on the single wire, the following considerations can be drawn: (i) a particular coupling of ρ_i and λ_i might lead to a post-yielding response exploitation of the not-corroded part that allows the capacity of the corroded wire to exceed the one of the corroded parts, (ii) the maximum force and the ultimate displacement for the case of limited material ductility and small hardening coefficient are governed by the adimensional reduction of cross-section area ρ_i and the adimensional corrosion length λ_i, respectively, (iii) accounting for λ_i allows to model the wire embrittlement caused by the corrosion.

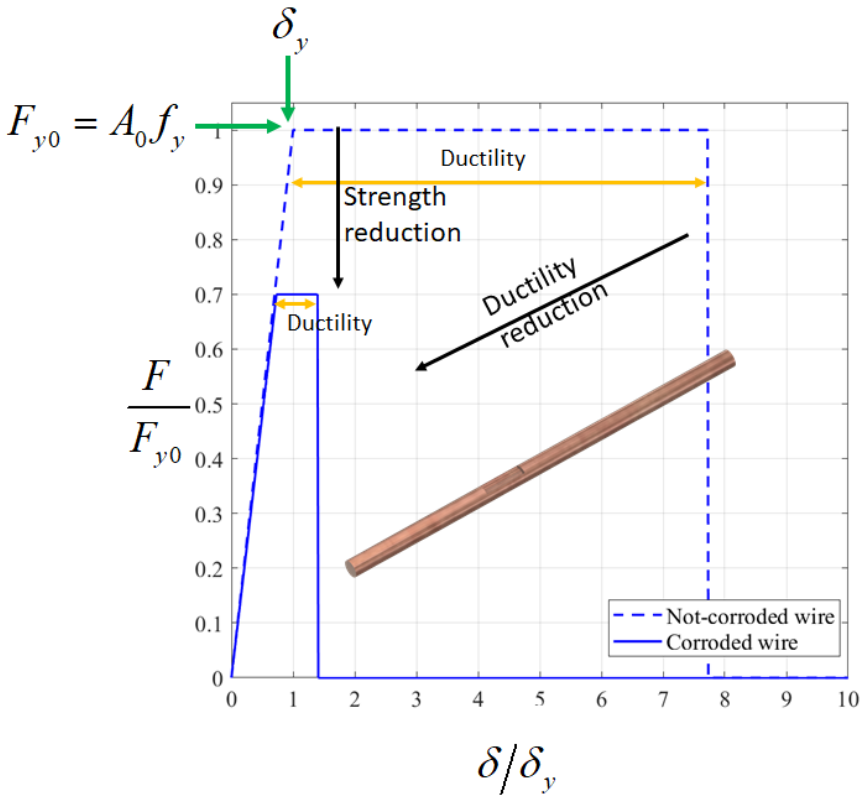

Figure 8.6: Schematization of the strength and ductility reductions in corroded wires

Figure 8.6 summarises the identified effects due to corrosion on the force-displacement of a corroded single wire. In particular, it empathizes the reductions both of the strength and of the ductility in case of an elastic-perfectly plastic steel material. The diagrams are expressed with reference to the not-corroded case.

9

Mechanical behaviour of corroded seven-wire strands

Sommario

Questo capitolo presenta due modelli analitici per tefoli corrosi. Il primo prevede un comporamento elasto-fragile dei fili corrosi mentre il secondo consente di tenere conto dell'effettivo diagramma forza-spostamento dei fili corrosi costitutiscono il trefolo. Gli effetti dovuti alla variabilità della corrosione nei fili sul comportamento meccanico di trefoli corrosi sono emersi da uno studio parametrico relativo a specifici scenari di trefoli corrosi. Tali effetti conducono ad un ulteriore riduzione di resistenza dei trefoli che dipende dalla geometria di corrosione.

Summary

This chapter presents two analytical models for corroded strands. The first concerns an elastic-fragile behaviour of the corroded wires while the second allows taking into account the effective force-displacement diagram of the corroded wires whose constitute the strand. The effects due to the variability of corrosion in the wires on the mechanical behaviour of corroded strands have emerged from a parametric study related to specific scenarios of corroded strands. These effects lead to a further reduction of the strength of the strands which depends on the geometry of the corrosion.

In this chapter, they are reported two models for corroded strands that are frequently used in this work. The first one has been described by Darmawan and Stewart [51] and provides a simple analytical formulation to estimate the peak strength in corroded strands considering a completely brittle behaviour in the wires (brittle model). The second one is a parallel model, similarly adopted by [40], in which the geometry of the corrosion, according to the idealization constituted by the two key-parameter ρ_i and λ_i, and the mechanical parameters of the steel material are introduced. The parallel model provides a peak force that is in between a lower bound estimation provided by the brittle model and the upper bound estimation provided by the ductile model ($F_{upper} = Af_u$). On one hand, the brittle model allowed to analytically develop the minimum group coefficient ρ_{Gmin} as

discussed in section 10.5. On the other hand, the parallel model allowed to study of the influence of the single parameters constituting the corrosion (i.e. geometry and variability of the corrosion) and the steel material (ductility and hardening ratio) on the mechanical behaviour of the corroded strands.

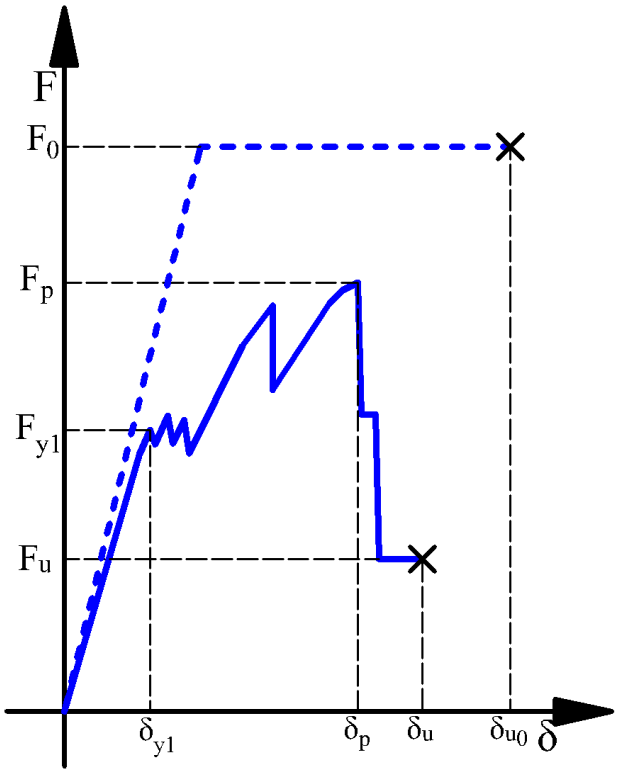

Figure 9.1: Qualitative force-displacement relationship of a corroded seven-wire strand

Figure 9.1 shows qualitative force-displacement relationships of a corroded seven-wire strand (continued line) compared with the not corroded one characterized by an elastic-perfectly plastic steel material(dashed line). This is typically characterized by some key parameters: (i) a series of yield points, i.e. (δ_{y1}, F_{y1}), that describes the progressive collapses of the wires, (ii) the peak point (δ_p, F_p) that is the maximum point of the diagram, and (iii) the ultimate point (δ_u, F_u). Duals points can be identified for the not-corroded strands: the peak force F_0 and the ultimate displacement δ_{u0}. This chapter is focused on the study and characterization of the peak point, taking into account the force only. In other words, an extensive analytical and numerical study on peak force F_p has been carried out. It is worth noting that in a parallel model, which is the model that will be deeply developed and used in this work, the ultimate displacement of a corroded strand is the same of that one of the more ductile wires in the strand itself.

In addition, it is worth noting that similarly to wire ropes, in seven-wire strands, two kinds of progressive collapses can be identified: (i) due to the changing of geometrical

configuration: after the first wire break, the geometry of the strand changes and a progressive collapse of the wires, due to geometrical effects only, can occur. In fact, the mechanical behaviour of helicoidal strands and ropes may become very complicated [53]. (ii) Due to localized corrosion: it is considered and deeply analysed in this work. Regarding the first point, it is important to clarify that the change of the geometry after a wire collapse is more significant in wire ropes where its effects lead to increasingly local phenomena related to flexural, shear and torsional effects. In other words, in seven-wire strands, the further effects on the peak force reduction due to the changing of the geometry after a wire collapse, together with those introduced in this chapter, assume a negligible contribution. However, this aspect will be the objective of future studies.

9.1 The Darmawan-Stewart model for brittle material

The Darmawan-Stewart model provides an analytical expression for the peak force in corroded strands constituted by a certain number of wires. The hypothesis considered by the model are:

- equal stiffness in all the wires;
- the elasto-brittle behaviour of the wires;
- progressive collapses of the wires according to the adimensional reduced cross-section area values.

The expression for the peak force assumes the following expression:

$$F_{p,DS} = max\left[(n_w - i + 1)\rho_i \frac{F_0}{n_w})\right] \tag{9.1}$$

where the adimensional reduction of cross-section areas ρ_i are in ascending order. Figure 9.2 summarizes the model idea: they are considered different strands configurations according to the ρ_i wires values in ascending order, and then the maximum of their peak force provides the peak force of the corroded strand.

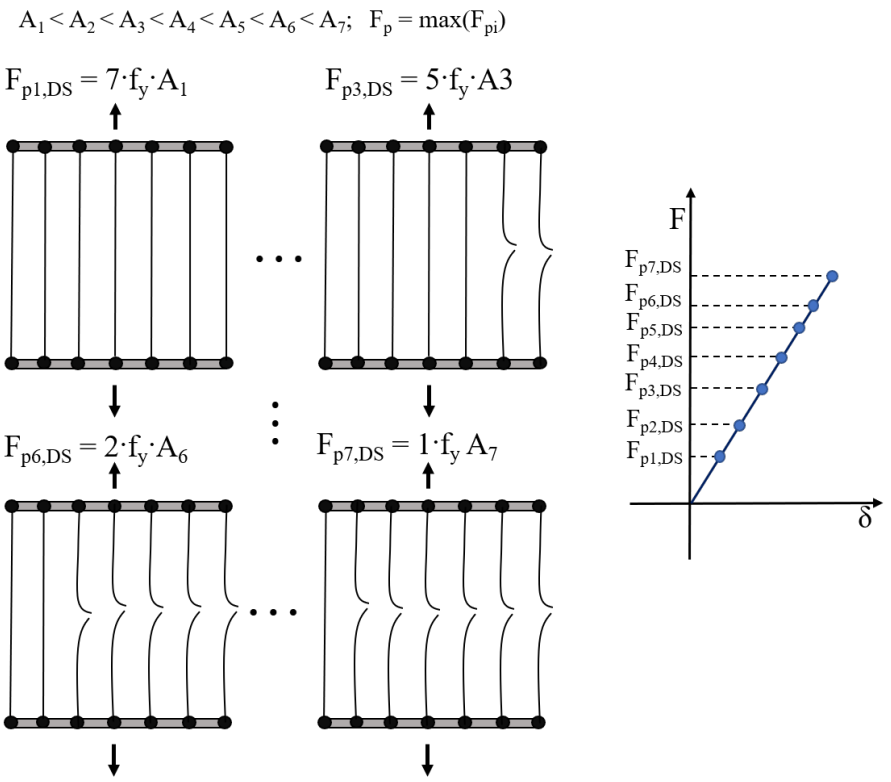

Figure 9.2: Mechanical idealization of the Darmawan-Stewart model

9.2 The parallel model for the elasto-plastic material

The parallel mechanical model of a corroded straight seven-wire strand is based on the following main assumptions:

- the wires composing the strand are straight and subjected to tension forces only;
- any kind of interaction (e.g., friction) between the wires is neglected;
- the strand is described as a parallel system between the equivalent series systems representing the wires (according to their mechanical behaviour described in chapter 8);
- the mechanical behaviour of a corroded seven-wire strand is represented by a force-displacement relationship;
- all the wires are characterized by the same diameter.

As a result of the characterization of the mechanical behaviour of the single wire, the parallel model provides the force-displacement of corroded strands taking into account the geometry of the corrosion, which is described by the two key-parameter ρ_i and λ_i,

and the steel material parameters that describe its sigma-epsilon relationship. The model considers the parallel system of the equivalent spring representing the corroded wires. In addition, it considers the effects of corrosion on the elastic stiffness of the wires. Figure 9.3 reports a schematic representation of the parallel model and a possible result in terms of force-displacement relationship, respectively.

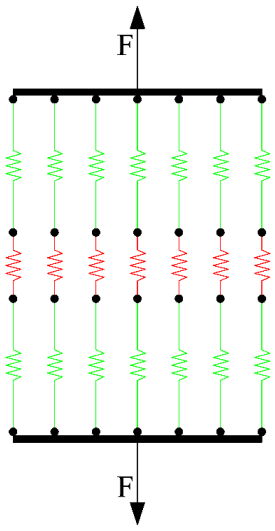

(a) Mechanical idealization

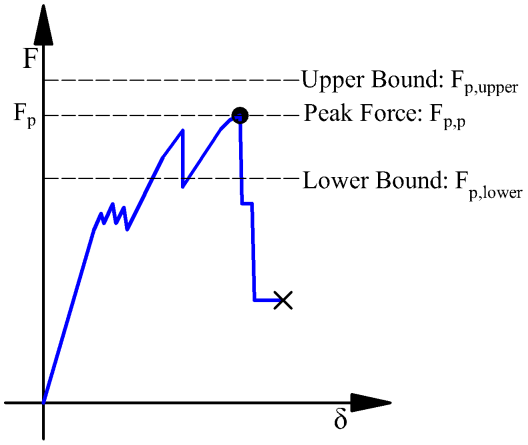

(b) qualitative force-displacement relationship of a corroded seven-wire strand

Figure 9.3: Mechanical idealization and a qualitative force-displacement relationship given by the parallel model

As an important result, as it can be seen from Figure 9.3, the model here presented is able to describe the typical mechanical behaviour of strands under tensile loads, which is characterized by a progressive collapse of the wires whose are constituted. The parameter of interest on which this work is focused is the peak force measured on the force-displacement relationship provided by the model ($F_{p,p}$). In addition, Figure 9.3 reports also both the lower and upper bounds among which the peak force is included. Valid expressions for the two limits are the following: (i) Darmawan-Stewart model prevision for the lower bound $F_{p,DS}$ and (ii) fully-ductile model prevision for the upper bound prevision $F_{p,upper} = Af_u$.

9.3 On the influence of the variability of the corrosion in the wires

Since this model has been implemented by coding, parametric studies have been carried out in order to (i) study the influence of the single parameters constituting the corrosion (i.e. geometry and variability of the corrosion) and the steel material (ductility and hardening ratio) on the mechanical behaviour of the corroded strands, and (ii) for characterizing the new resistance model introduced in chapter 10. As far as the first objective is concerned, seven possible scenarios of corrosion in the strands reported in Table 9.1 have been taken into account. In this regard, each scenario has been simulated considering a distribution of corrosion in such a way as to have the mean corrosion level $\rho_M = 0.5$ with different levels of variability of the corrosion (which is evaluable through their variability, that can be quantified by the coefficient of variation COV_{ρ_i} of the ensemble of the seven corrosion levels of the single wires constituting the whole strand) and the adimensional corrosion extension λ_i in the range (0,1) with a reference length $L_0 = 1m$. The mean corrosion level and the variability of the corrosion in the wires are defined as follows:

$$\rho_M = \frac{\sum_{j=1}^{n_w} A_{i,j}}{\sum_{j=1}^{n_w} A_{0i,j}} = \frac{\sum_{j=1}^{n_w} A_{0i,j} \cdot \rho_{i,j}}{\sum_{j=1}^{n_w} A_{0i,j}} = \frac{A_{0i,j} \sum_{j=1}^{n_w} \rho_{i,j}}{n_w A_{0i,j}} = \frac{\sum_{j=1}^{n_w} \rho_{i,j}}{n_w} = m_{\rho_i} \tag{9.2}$$

$$COV_{\rho_i} = \frac{\sqrt{\frac{\sum_{j=1}^{n_w} (\rho_{i,j} - m_{\rho_i})^2}{n_w - 1}}}{m_{\rho_i}} \tag{9.3}$$

It is worth noting that since all the wires are characterized by the same diameters (it is justified by the small differences between the diameter of the king-wire and those of the external wires) the mean corrosion level is equal to the mean of the corrosion. On the contrary, it corresponds to the weighted average of the adimensional reduced cross-section areas.

Table 9.1: Seven different scenarios of corroded seven-wire strands

Scenario	ρ_1	ρ_2	ρ_3	ρ_4	ρ_5	ρ_6	ρ_7	ρ_M	COV_{ρ_i}
1. S1	0.50	0.50	0.50	0.50	0.50	0.50	0.50	0.50	0
2. S2	0.41	0.44	0.47	0.50	0.53	0.56	0.59	0.50	0.129
3. S3	0.35	0.40	0.45	0.50	0.55	0.60	0.65	0.50	0.216
4. S4	0.20	0.30	0.40	0.50	0.60	0.70	0.80	0.50	0.432
5. S5	0.15	0.20	0.25	0.50	0.75	0.80	0.85	0.50	0.606
6. S6	0.10	0.20	0.40	0.50	0.60	0.70	1	0.50	0.611
7. S7	0.05	0.20	0.35	0.50	0.65	0.80	0.95	0.50	0.648

Figure 9.4 and Figure 9.5 report the force-displacement relationships obtained with the application of both the parallel model and the Darmawan-Stewart model (horizontal lines) to the identified scenarios, for the case of $\lambda = 0.01$ and $\lambda = 0.15$. They are normalized with respect to the not-corroded strand dividing the forces by the yield force $F_{y0} = A_0 f_y$ and the displacement by the yield displacement δ_{y0}. In other words, it is made equal to (1, 1) the yielding point of the not-corroded strand. The figures show the force-displacement results considering elastic-perfectly plastic and elastic-plastic with hardening stress-strain relationships for the two values of material ductility. The hardening coefficients have been considered equal to 0.5% and 1.5%.

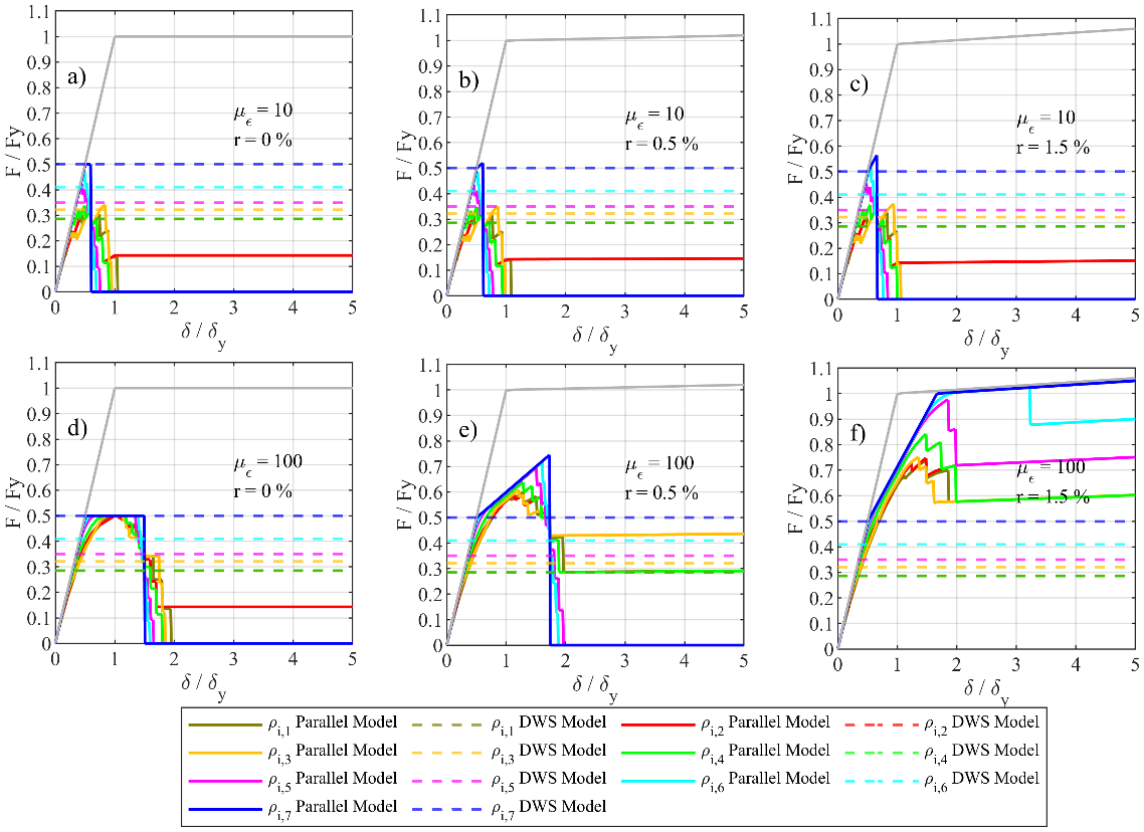

Figure 9.4: Results of parametric simulations of fixed scenarios of corroded seven-wire strands characterized by $\lambda_i = 0.01$ in terms of force/displacement relationships: (a) ($\mu_\epsilon = 10, r = 0\%$), (b) ($\mu_\epsilon = 10, r = 0.5\%$), (c) ($\mu_\epsilon = 10, r = 1.5\%$), (d) ($\mu_\epsilon = 100, r = 0\%$), (e) ($\mu_\epsilon = 100, r = 0.5\%$), (f) ($\mu_\epsilon = 100, r = 1.5\%$)

Figure 9.4 and Figure 9.5 show that the proposed parallel model is able to simulate the typical force-displacement relationship of corroded wire strands that are characterized by progressive collapses of the single wires. It is also worth noting that, for a fixed value of λ_i (especially for small values), the behaviour of corroded strands might be different according to the corrosion distribution in the wires, which is evaluable through their variability. In fact, the peak force and ultimate displacement given by force-displacement

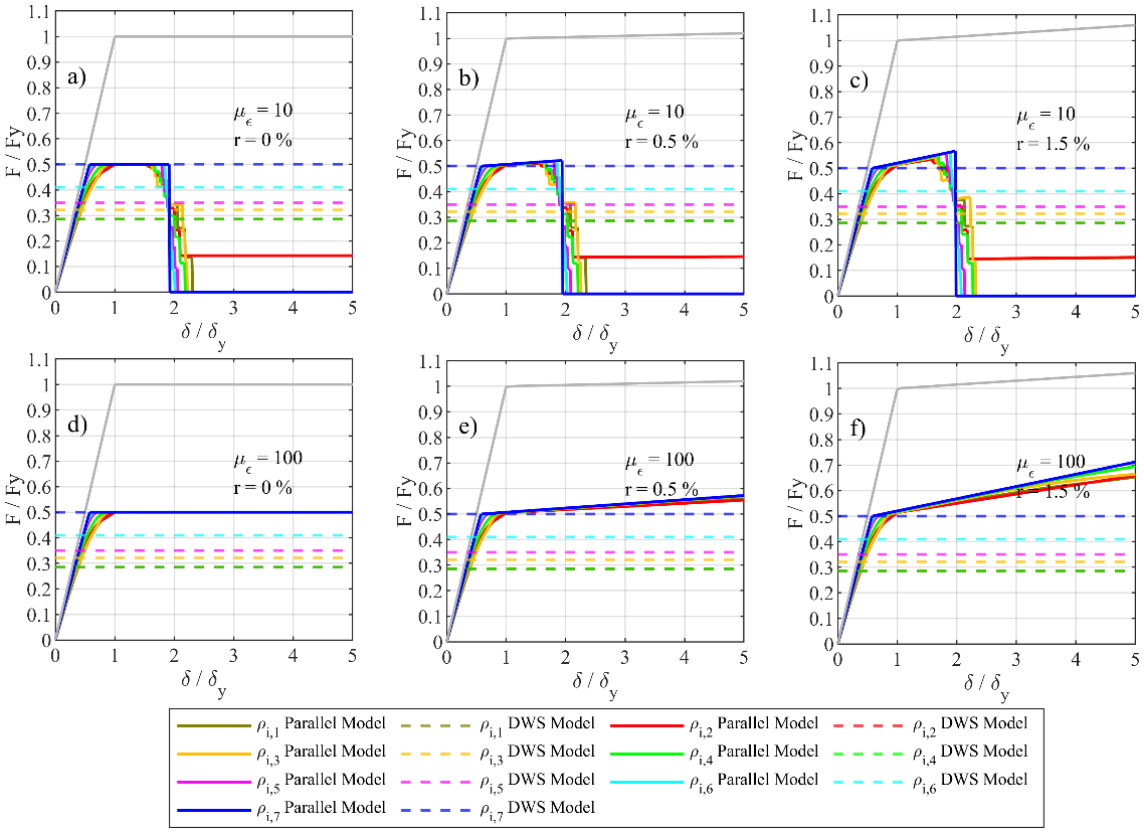

Figure 9.5: Results of parametric simulations of fixed scenarios of corroded seven-wire strands characterized by $\lambda_i = 0.15$ in terms of force/displacement relationships: (a) ($\mu_\epsilon = 10, r = 0\%$), (b) ($\mu_\epsilon = 10, r = 0.5\%$), (c) ($\mu_\epsilon = 10, r = 1.5\%$), (d) ($\mu_\epsilon = 100, r = 0\%$), (e) ($\mu_\epsilon = 100, r = 0.5\%$), (f) ($\mu_\epsilon = 100, r = 1.5\%$)

relationships of the strand characterized by $COV_{\rho_i} = 0.129$ (light blue line) are different than those ones of the strand characterized by $COV_{\rho_i} = 0.129$ (yellow line), even though the strands were characterized by the same mean corrosion level. This suggests that the reductions in the peak force and ultimate displacement are influenced by both the corrosion mean level ($\rho_M = 0.5$) and the variability in the corrosion of the wires (different COV_{ρ_i}). In particular, as it can be seen from Figure 9.4 the effects of the variability are much more significant in strands characterized by small values of λ_i (localized corrosion), where the interaction with ρ_i is higher. In other words, the ductility in the wires is not enough to enable the strand achieving the maximum force given by the mean corrosion level, which is, on the contrary, evident for higher values of λ_i reported in Figure 9.5. Such first results, which require further investigation as shown in chapter 10, allows highlighting the importance of considering both parameters ρ_i and λ_i of the wires (and not only ρ_i), in the mechanical behaviour of corroded seven-wire strands. Furthermore, the hardening effect is limited for small material ductility (i.e. high strength steel with $\mu_\epsilon = 10$), whilst it leads to higher maximum force and higher ultimate displacement for large material ductility (i.e. mild steel with $\mu_\epsilon = 100$).

In other words, the behaviour of corroded seven-wire strands made up of high strength steel is well represented by an elastic-perfectly plastic constitutive model. On the contrary, for elastic-perfectly plastic steel material with high values of material ductility μ_ϵ, the peak force depends only on the mean corrosion level ρ_M, in fact, the ductility content in the wires is enough to achieve the yielding stress. This is valid also if, in addition, high values of the adimensional corrosion length λ_i are considered.

As a matter of fact, the peak force in corroded seven-wire strands, considering an elastic-perfectly plastic with hardening steel material, as shown in Figure 9.4 and Figure 9.5, always depends on the variability of the corrosion in the wires.

Figure 9.6a reports the reductions of the peak force of corroded strands identified by the seven scenarios reported in Table 9.1 considering an elastic-perfectly plastic steel material with ductility $\mu_\epsilon = 10$.

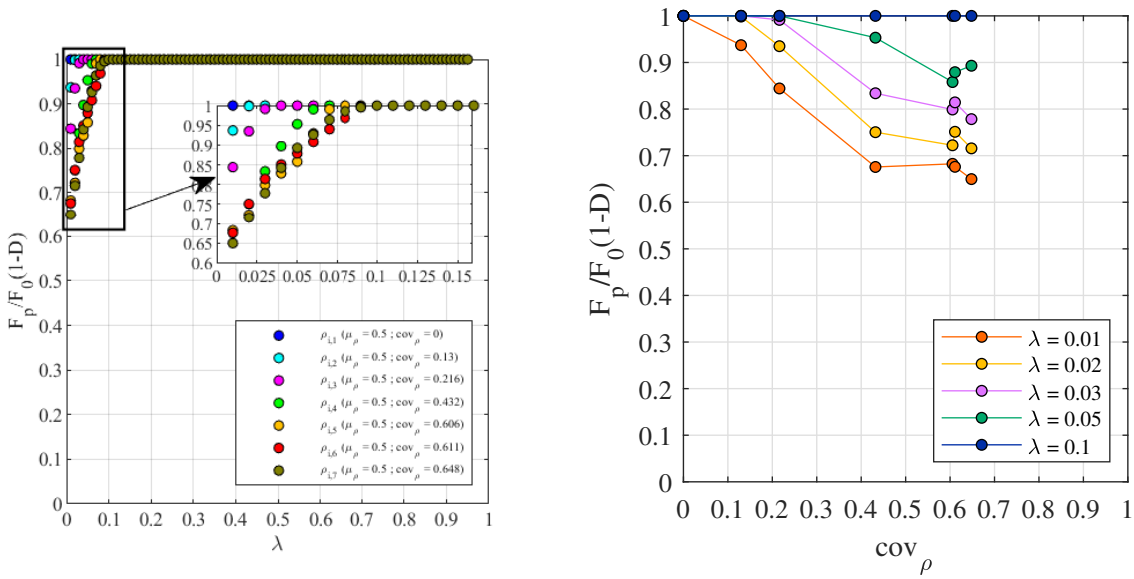

(a) Peak force as a function of the adimensional corrosion extension

(b) Peak force as a function of the coefficient of variation of the corrosion in the wires

Figure 9.6: Peak force reduction in corroded strands of the seven scenarios reported in Table 9.1 considering an elastic-perfectly plastic steel material with ductility $\mu_\epsilon = 10$

As it can be seen from Figure 9.6a, the higher the variability of the corrosion in the wires the higher the reduction of the peak force in the strand. Furthermore, for small values of λ_i (localized corrosion) the reduction is strongly dependent on the variability in the corrosion, while after a specific value around 0.1, this effect fails since all the wires have sufficient ductility to achieve the yielding stress. As a matter of fact, this important aspect should be considered in the evaluation of the strength capacity of a corroded strand. Figure 9.6b reports the trend taken by the reduction of the peak force with the coefficient of variation of the corrosion in the wires confirming that this variability has an important effect on the peak force in corroded strands. In addition, Figure 9.6b summarizes the

important aspects that have been obtained from this study regarding the peak force in corroded strands: (i) it decreases with an increasing of the variability of the corrosion in the wires, and (ii) it decreases with a decreasing of the adimensional corrosion extension λ_i.

Figure 9.7 reports the ultimate displacement δ_u identified in the seven scenarios reported in Table 9.1 with reference to the case of elastic-perfectly plastic steel material with ductility $\mu_\epsilon = 10$. The ultimate displacement is expressed with respect to the ultimate displacement of the not-corroded strand $\delta_{u0} = \epsilon_u \cdot L_0$.

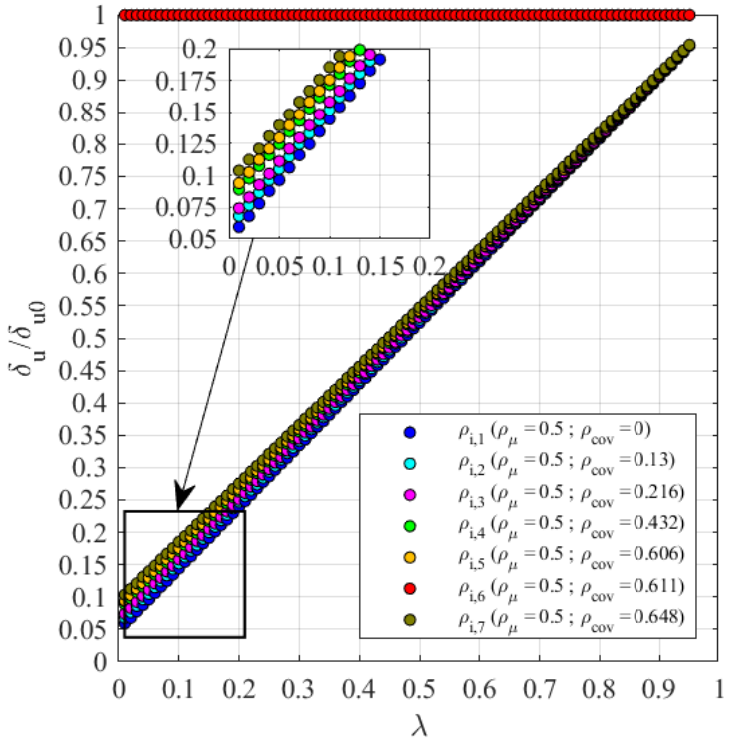

Figure 9.7: Ultimate displacement of the strands in the seven scenarios as a function of the adimensional corrosion extension

As it can be seen from the Figure 9.7, the ultimate displacement increases with the increasing of the adimensional corrosion extension. In fact, it governs the ductility in the wires and allows to model the embrittlement in the wires due to corrosion. In addition, the ultimate displacement tends to increase with an increasing of the variability of the corrosion in the wires. The sixth scenario, which is characterized by a not-corroded wire, shows, as expected, no reduction of the ultimate displacement. In fact, in the parallel model, the ultimate displacement of the strand corresponds to the ultimate displacement of the more ductile wire. However, do not consider the effects of variability of the corrosion in the wires on the ultimate displacement of the strand could be accepted from a safety point of view.

Figure 9.8 summarises the identified effects due to corrosion on the force-displacement of a corroded seven-wire strands. In particular, it empathizes the reductions both of the strength and of the ductility in case of an elastic-perfectly plastic steel material. The diagrams are expressed with reference to the not-corroded case.

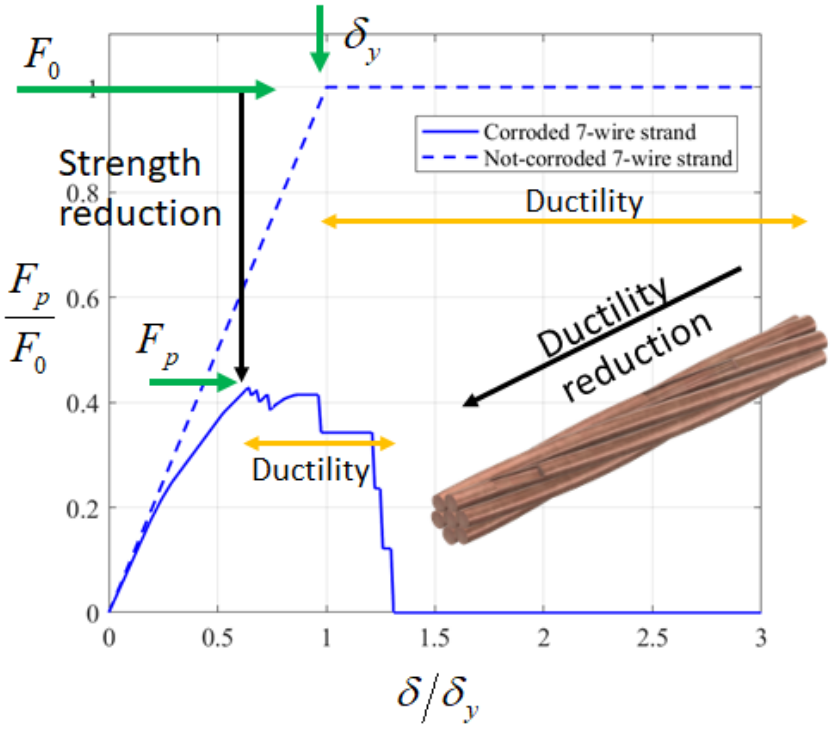

Figure 9.8: Schematization of the strength and ductility reductions in corroded seven-wire strands

In conclusion, the parametric study allows to make the following considerations: (i) the mechanical behaviour of a corroded strand is highly governed by the geometrical configuration of the corrosion in the wires, and by the ductility and hardening capacities of the steel material. In particular, their coupling might not be negligible in the evaluation of the peak force and the ultimate displacement. (ii) To consider either elastic-perfectly plastic or elastic-plastic with hardening steel material is comparable if the ductility of the material is low, which is also the case of wire strands, (iii) the corrosion distribution in the wires provides a further reduction on the peak force in addition to that one due to the reduction of the cross-section area and in the ultimate displacement, (iv) for a fixed value of λ_i, the higher the variability of the corrosion, the higher the reduction of the peak force and the lesser is the reduction of the ultimate displacement, and (v) the further reductions in the peak force and in the ultimate displacement due to the variability in the wires decreases with an increasing of the adimensional corrosion extension λ_i.

10

Peak strength resistance model

Sommario

In questo capitolo viene introdotto un nuovo modello di resistenza per trefoli corrosi. Tale modello introduce un parametro atto a rappresentare gli effetti della variabilità della corrosione nei fili sulla risposta meccanica di trefoli corrosi. Il modello introdotto è applicato secondo due approcci, quello deterministico e quello probabilistico, e secondo due procedure dipendenti dalla conoscenza dettagliata o meno della geometria di corrosione.

I paramtetri del modello vengono calibrati mediante simulazioni di Monte Carlo di trefoli corrosi, sfruttando le modellazioni di fili e trefoli mostrate nei capitoli precedenti.

Sulla base dei risultati delle simulazioni, viene infine proposto un dominio di resistenza per trefoli corrosi che tiene conto sia della geometria di corrosione che dei parametri costitutivi del materiale acciaio.

La descrizione probabilistica del modello di resistenza introdotto ha permesso la definizione di parametri di verifica e di progetto, ad esempio i fattori di sicurezza, per tener conto della presenza di corrosione nei trefoli nelle verifiche di sicurezza.

Tutti i risultati sono riportati in forma tabellare nell' Appendice A.

Summary

In this chapter, a new resistance model for corroded strands is presented. This model introduces a parameter able to represent the effects of corrosion variability in the wires on the mechanical response of corroded strands. The introduced model is applied according to two approaches, the deterministic and the probabilistic one, and according to two procedures depending on the knowledge of the geoemtry of the corrosion.

The model parameters are calibrated by means of several Monte Carlo simulations of corroded strands, taking into account the models of corroded wires and strands shown in the previous chapters.

Based on the results of the simulations, resistance curves for corroded strands are finally proposed which takes into account both the corrosion geometry and the constitutive parameters of the steel material.

The probabilistic description of the resistance model introduced has allowed the definition of safety and design factors, for instance the safety factors, to take into account the corrosion in the strands in the safety assessments.

All the results are reported in tabular form in the Appendix A.

10.1 The proposed model and the approaches

The expression for the peak force reported in Eq.7.1 has some limitations in its definition, in fact, it is defined only for limited cases of damage index (up to 20-40%) and provides no physical results (negative force reductions) for damage index higher than a fixed value that depends on the α parameter. In addition, it is not able to describe the dispersion in the peak force reduction for the same value of D, also shown in some experimental campaigns [40], [3], [43]. Therefore, here is introduced a resistance model for corroded strands introducing a new coefficient that accounts for the variability of the corrosion in the wires. Since this coefficient is supposed to represent the effects of the group of wires in a corroded strand, in terms of corrosion variability, it is referred to it as the group coefficient ρ_G. The physical meaning of this coefficient is that in a corroded seven-wire strand not all the wires, according to the corrosion geometry, might reach the yield stress, leading to a premature collapse of the wires themselves, which provides a peak force that cannot be described by simply considering the mean corrosion level only. This result is also suggested by the parametric study shown in section 9.2.

10.2 The peak strength resistance model

The peak strength resistance model here proposed, therefore, assumes the following expression:

$$\begin{aligned} F_{p,p}(\rho_M, \rho_G) &= F_0 \cdot \rho_M \cdot \rho_G \\ F_{p,p}(\rho_M, \rho_G) &= F_0 \cdot \rho_M \cdot \rho_G(\rho_M(m_{\rho_i}), COV_{\rho_i}, \lambda_i, \mu_\epsilon) \\ F_{p,p}(\rho_M, \rho_G) &= F_0 \cdot \rho_M \cdot \rho_{Gmin}(\rho_M(m_{\rho_i}), COV_{\rho_i}) \cdot \eta(\rho_M(m_{\rho_i}), COV_{\rho_i}, \lambda_i, \mu_\epsilon) \end{aligned} \tag{10.1}$$

where $\rho_M = \rho_M(m_{\rho_i})$ and $\rho_G = \rho_G(COV_{\rho_i})$, accounting for the mean corrosion level and the dispersion of the corrosion in the set of the n_w values of corroded areas, respectively. In addition, the group coefficient is a function of the damage index D (mean corrosion level), the ductility in the wires and the material ductility. It can be seen as the product of the other two coefficients: the minimum group coefficient $\rho_{Gmin}(D, COV_{\rho_i})$

and the model coefficient $\eta(D, COV_{\rho_i}, \lambda_i, \mu_\epsilon)$. In other words, it can be seen as made up of two contributions related to a completely brittle behaviour (ρ_{Gmin}) and to a ductile one (η):

$$\rho_G = \rho_{Gmin} \cdot \eta \tag{10.2}$$

From a qualitative point of view, the group coefficient should have two boundary conditions in $D = 0$ and $D = 1$ that are cases characterized by no variability in the corrosion, which corresponds to $COV_{\rho_i} = 0$. In these cases, no further reduction in the peak force due to variability of corrosion occurs, then, the group coefficient is equal to one.

Accordingly, the objectives are now to estimate the minimum group coefficient ρ_{Gmin} and the model coefficient η. In fact, these coefficients are the unknowns in Eq. 10.1, since the peak force of the not-corroded strand F_0 and the mean corrosion level ρ_M can be calculated. In this regard, section 10.6 shows the analytical lower bound estimation of the group coefficient and section 10.5 describes the estimation of the model coefficient by means of several Monte Carlo simulations of corroded seven-wire strands.

10.3 The approaches for the model parameters

The resistance model can be applied according to the following approaches:

- the deterministic one that can be used for a direct estimation of the strength of corroded seven-wire strands by directly applying the Eq.10.1:
  - the mean corrosion level is reasonably estimated $\Rightarrow \rho_M$;
  - the peak force of the not-corroded strand is calculated $\Rightarrow F_0$;
  - the minimum group coefficient is calculated by applying Eq.10.3 $\Rightarrow \rho_{Gmin}$;
  - the model coefficient can be calculated thanks to its expressions that have been obtained by the fitting procedure of the Monte Carlo simulations results. These functions for all the damage index values are reported in Appendix A $\Rightarrow \eta$;
- the probabilistic one that can be used for providing a statistical representation of the peak force as discussed in detail in section 10.7.2. Through the representation of the variables (or some of them) that define the resistance model as random variables, it is possible to characterize the variability of the peak strength of corroded seven-wire strands:
  - the mean corrosion level ρ_M can be assumed as deterministic variable;

- the peak force F_0 of the not-corroded strand is equal to $A_0 \cdot f_y$. The cross-section area A_0 of the not corroded strand can be assumed as a deterministic variable while the yielding stress of the steel material f_y is a random variable;
- the minimum group coefficient ρ_{Gmin} can be assumed as deterministic variable;
- the model coefficient η can be assumed as random variable. Its probability density functions have been obtained by the fitting procedure of the Monte Carlo simulations results. These functions for all the damage index values are reported in Appendix A.

In both approaches, the geometrical configuration of the corrosion and the mechanical parameters of the steel material are taken into account by means of the cross-section reduction of the strand (through the mean corrosion level ρ_M) and the adimensional extension reduction λ_i. As far as the latter parameter is concerned, two procedures can be identified for the application of the introduced resistance model:

- procedure a) considering λ_i as unknown: it could be the case of lack of knowledge of the corrosion extension;
- procedure b) considering λ_i as known: it could be the case of a complete characterization of the extension of the corrosion.

10.4 Approaches and procedures to estimate the model parameters

From a practical point of view, the two procedures differ from each other with respect to the set of simulations data that are used in their estimations. In fact, the procedure for λ_i unknown takes into account all the set of the simulated λ_i values, while the other procedure considers the exact value of the simulated λ_i.

Therefore, the achieved results in this work are in terms of ρ_{Gmin} and η, which assumes different expression according to the two approaches and the two procedures:

- deterministic approach:
  1. values of η that is independent with respect to λ_i value (procedure for λ_i unknown). It assumes constant values.
  2. values of η that is dependent with respect to λ_i value (procedure for λ_i known). It assumes polynomial expression as a function of λ_i.
- probabilistic approach:

1. probability density functions of the model coefficient η that are independent with respect to λ_i (procedure for λ_i unknown);
2. probability density functions of the model coefficient η that are dependent with respect to λ_i (procedure for λ_i known);
3. design-oriented results based on the probability functions of the peak force of corroded seven-wire strands. This is obtained considering both the types of the probability density functions of the model coefficient η (λ_i unknown and λ_i known)

Table 10.4 summarizes the two approaches and the two procedures for the application of the proposed model.

Table 10.1: Summary of the results for the application of the introduced resistance model

	Peak strength model (Eq.10.1)			
	Deterministic approach		*Probabilistic approach*	
F_0	Calculated			
ρ_M	Calculated and/or estimated, i.e. experience, measurements			
ρ_{Gmin}	Calculated by Eq.10.3			
η	λ_i is known Polynomial expression as a function of λ_i	λ_i is unknown Constant value	λ_i is known PDF	λ_i is unknown PDF as a function of λ_i

10.5 Brittle material assumption: lower bound estimation of the group coefficient

Assuming that the group coefficient has the minimum value in the brittle case, the Darmawan-Stewart model is used to estimate analytically its lower bound. In this regard, the estimation has been carried out considering the following points:

- considering a uniformly distributed corrosion in the wires of the strand whose amplitude is described by the parameter p. The corrosion in the wires has mean value m_{ρ_i};
- equalling the analytical peak force given by the Eq. 9.1 with that one given by the Eq. 10.1;

- solving of this new equation with respect to ρ_{Gmin} that is the only unknown in the equation.

In this section is reported the final expression of the ρ_{Gmin} while the complete methodology adopted for its estimation is reported in Appendix B. However, it is considered appropriate to provide some consideration about the final expression of the ρ_{Gmin} reported in Eq. 10.3. In this regard, Eq. 10.3 is obtained by considering the corrosion in the wires uniformly distributed in the domain $(m_{\rho,i} - p, m_{\rho,i} + p)$ and characterized by the maximum variability (case of $p = p_{max}$).

$$\begin{cases} \rho_{Gmin} & = (n_w - i_{max} + 1)\left[\dfrac{2p_{max}}{n_w - 1}(i_{max} - 1) + (m_{\rho_i} - p_{max})\right]\dfrac{1}{m_{\rho_i} n_w} \quad p_{max} > p_{min} \\ \rho_{Gmin} & = \dfrac{(m_{\rho_i} - p_{max})}{m_{\rho_i}} \quad p_{max} \leq p_{min} \end{cases} \tag{10.3}$$

Detailed analytical developments and analytical expressions for the index that provides the maximum force i_{max}, the minimum and maximum amplitudes p_{min} and p_{max}, are reported in Appendix B. The expression of the lower bound estimation of the group coefficient represents a general expression that can be applied to strands characterized by different numbers of wires also characterized by different diameters (in the present case $m_{\rho_i} = \rho_M$).

Figure 10.1a shows the coefficient of variation of the corrosion in the wires as a function of the damage index. As it can be also seen the assumption of uniform distribution of corrosion provides a plateau value for a damage index higher than 0.5 and with decreasing trend according to an increase in the number of the wires in the strand. Figure 10.1b reports the minimum group coefficient as a function of the coefficient of variation of the corrosion in the wires showing that the higher the variability in the corrosion the lesser the minimum group coefficient. This result confirms that high variability in the corrosion might provide a further reduction of the peak force in the strand. In addition, the minimum group coefficient tends to a plateau value equal to 0.5 for a higher value of the number of wires. This aspect is clear from Figure 10.1c.

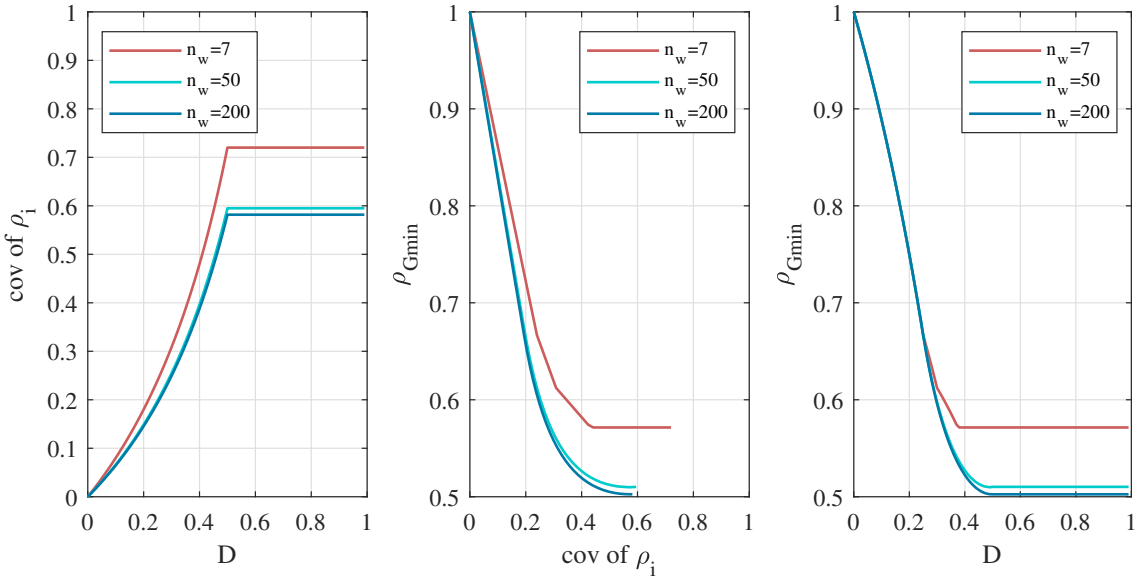

Figure 10.1: Variability of the corrosion in the wires: (a) coefficient of variation of the corrosion in the wires as a function of the damage index (b) ρ_{Gmin} as a function of the coefficient of variation of the corrosion in the wires and (c) ρ_{Gmin} as a function of the damage index

Therefore, according to these aspects, the following observations can be done: (i) ρ_{Gmin} decreases with increasing *COV* values, (ii) for large *COV* values, ρ_{Gmin} assumes a minimum value that depends on the number of wires in the strands, (iii) the minimum value assumed by ρ_{Gmin} decreases with increasing of the total number of wires, (iv) ρ_{Gmin} decreases with increasing damage index *D*, achieving a minimum value for *D* around 0.5. This result confirms that high variability in the corrosion might provide a further reduction of the peak force in the strand.

10.6 Statistical evaluation of the model coefficient and the group coefficient

In order to estimate the model coefficient η, which describes all the effects on the peak force of corroded strands that are not taken into account by ρ_{Gmin}, i.e. ductility in the wires (taking into account λ_i), not-uniformity of the corrosion domain, etc., several Monte-Carlo simulations have been carried out. In fact, until now η is the only unknown of Eq.10.1. The simulations were characterized by the following assumptions:

- the strands are constituted by seven wires;
- the parallel model described in section 9.2 was assumed for the corroded strands;

- the wires were constituted by elastic-perfectly plastic steel material with low material ductility $\mu_\epsilon = 10$ (strands are typically constituted by harmonic steel) since considering either elastic-perfectly plastic or elastic-plastic with hardening steel material is comparable in the study of their mechanical response through force-displacement relationships (as shown in section 8.2);
- the reference length $L_0 = 1m$;
- the reductions of the cross-section area in the wires were randomly generated in order to have a damage index in the range (0,1);
- the adimensional corrosion lengths λ_i were generated in the range (0,0.1) and assumed equal for all the wires in each generation of the corroded strands.

Figure 10.2 summarizes the theoretical path that has been applied to estimate the model coefficient η, which corresponds to that one of the group coefficient ρ_G since $\rho_G = \eta \cdot \rho_{Gmin}$.

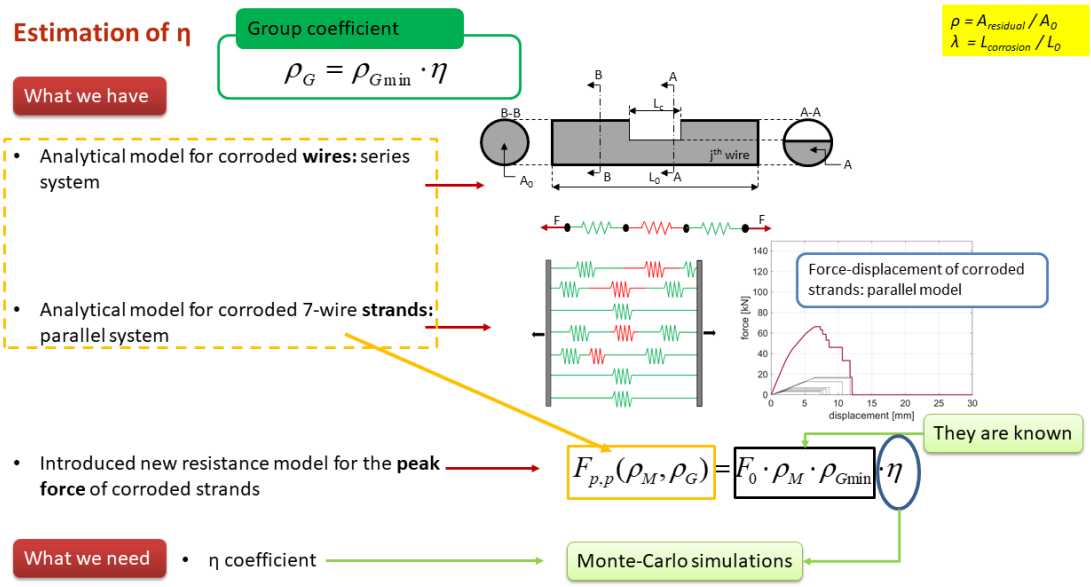

Figure 10.2: Theoretical path applied for the estimation of the model coefficient η

Figure 10.3a shows the results of the simulations highlighting as the model coefficient η tends to be less variable according to an increase of the adimensional corrosion length λ_i and to reach a maximum value equal to $1/\rho_{Gmin}$ (i.e. equal to $1/0.57 = 1.75$ in case of $D = 0.5$). In addition, it can be identified a fixed value of λ_i at which η shows a plateau value equal to $1/\rho_{Gmin}$ according to the damage index scenario. If this adimensional corrosion length value is indicated with $\overline{\lambda_i}$, in the cases characterized by $\lambda_i > \overline{\lambda_i}$ the

ductility of the wires is able to reach the maximum force and the model coefficient η can be assumed equal to $1/\rho_{Gmin}$.

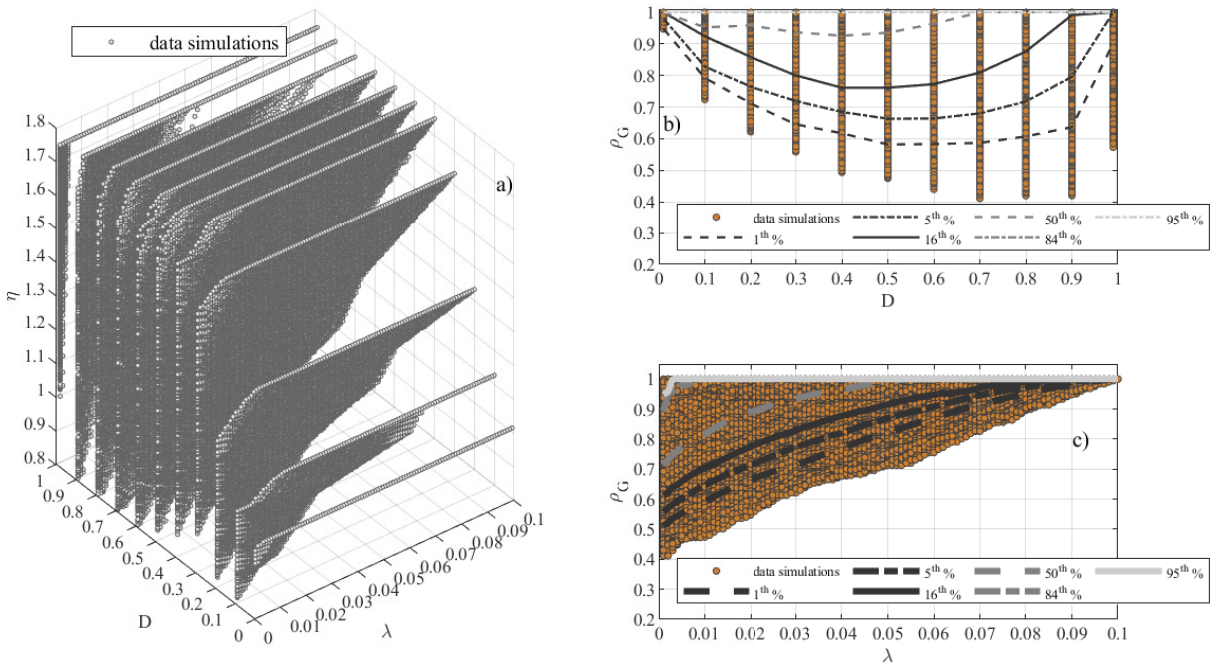

Figure 10.3: Results of the simulations: (a) 3d plot of the model coefficient η, (b) statistical distribution of the group coefficient as a function of D for all the λ_i values; (c) statistical distribution of the group coefficient as a function of λ_i for all the D values

Figure 10.3b reports the statistical distribution of the group coefficient percentiles as a function of the damage index for all the adimensional corrosion length λ_i values. From a qualitative point of view, it shows that the group coefficient assumes values equal to 1 in the limit case of no variability in the wires, which means the cases of $D = 0$ and $D = 1$. In addition, Figure 10.3c, which reports the statistical distribution of the group coefficient percentiles as a function of the adimensional corrosion length λ_i for all the damage index scenarios, shows that the effects of the variability in the wires tend to be negligible when the adimensional corrosion length λ_i increases.

As a result, it is clear that: (i) the effects of the variability of the corrosion in the wires are higher for small values of λ_i, as also introduced in section 9.2, (ii) since higher percentiles describe the configuration in which the strands have a higher ductility (they reach $\rho_G = 1$ for a higher value of λ_i) they can be used for describing different ductility contents in the strands and (iii) the statistic of the group coefficient tends to change with an increase of the adimensional corrosion length λ_i. Clearly, all these aspects are worth also for the model coefficient η, according to Eq. 10.1. In this regard, Figure 10.4 reports

the trends taken both by the standard deviation and by the coefficient of variation of the model coefficient η, related to the case of $D = 0.5$.

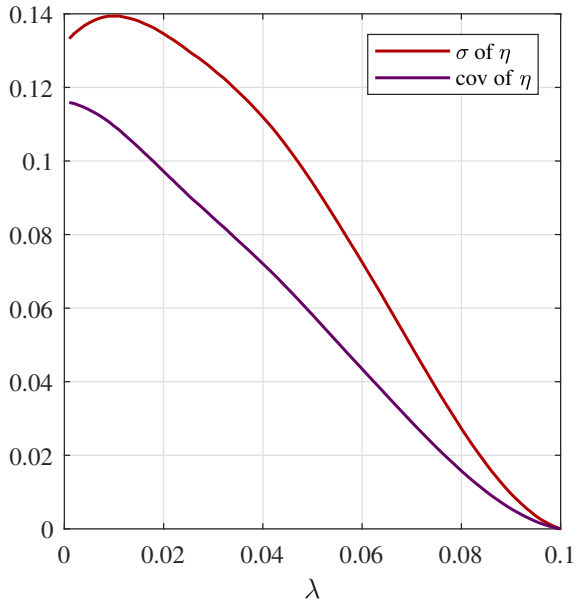

Figure 10.4: Trends of the standard deviation and the coefficient of variation of the model coefficient η with the adimensional corrosion length λ_i

Looking in detail at the variation of the probability density function, Figure 10.5a and Figure 10.5b report the relative frequency histogram of the model coefficient η corresponding to $\lambda_i = 0.03$ and $\lambda_i = 0.07$, respectively, 5^{th}, 16^{th}, 84^{th} and 95^{th} percentiles calculated on their respective simulations and a fitting with the normal and the scaled beta distributions. The beta probability density function is defined in the range [0,1], and then its parameters have been determined by a scaling operation on the coefficient model η values dividing them for $max(\eta)$. Thus, the new beta probability density function can be obtained by rescaling the identified function in order to obtain the integral of its probability density function equal to 1.

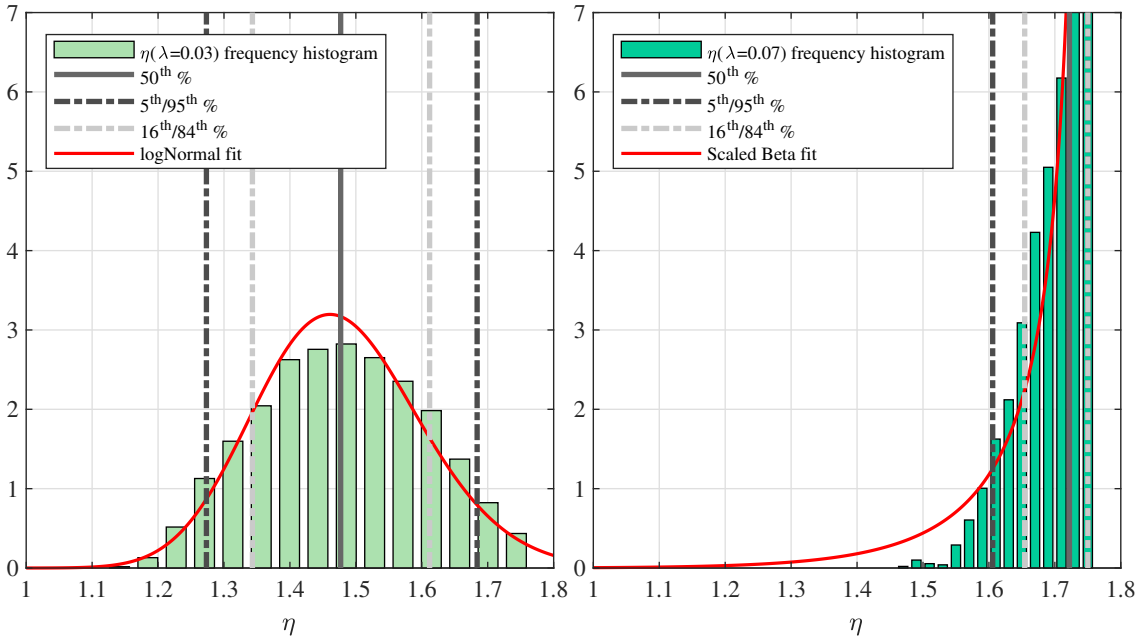

(a) $\lambda_i = 0.03$ (b) $\lambda_i = 0.07$

Figure 10.5: Statistical properties of the model coefficient η

Furthermore, Figure 10.5 shows that for small values of λ_i the statistic of the model coefficient η is well-represent by the logNormal function. On the contrary, for values of λ_i that tends to $\overline{\lambda_i}$, negatively skewed distributions seem to be more appropriate. In other words, the safety level evaluation of corroded seven-wire strands can be different according to the statistic of η.

To better explain the two procedures, Figure 10.6 shows both the case of deterministic and probabilistic approaches for the case of $D = 0.5$. In particular, Figure 10.6a shows the results of the deterministic approach in which the percentiles of the model coefficient assume constant values (λ_i is unknown and the simulations results of its entire set are considered) and polynomial expressions (λ_i is known and the simulations results of their fixed values are considered), respectively. Similarly, Figure 10.6b shows the results of the probabilistic approach in terms of suggested probability density function fit for the model coefficient η, corresponding to the entire set of λ_i (unknown), for $\lambda_i = 0.03$ and for $\lambda_i = 0.07$.

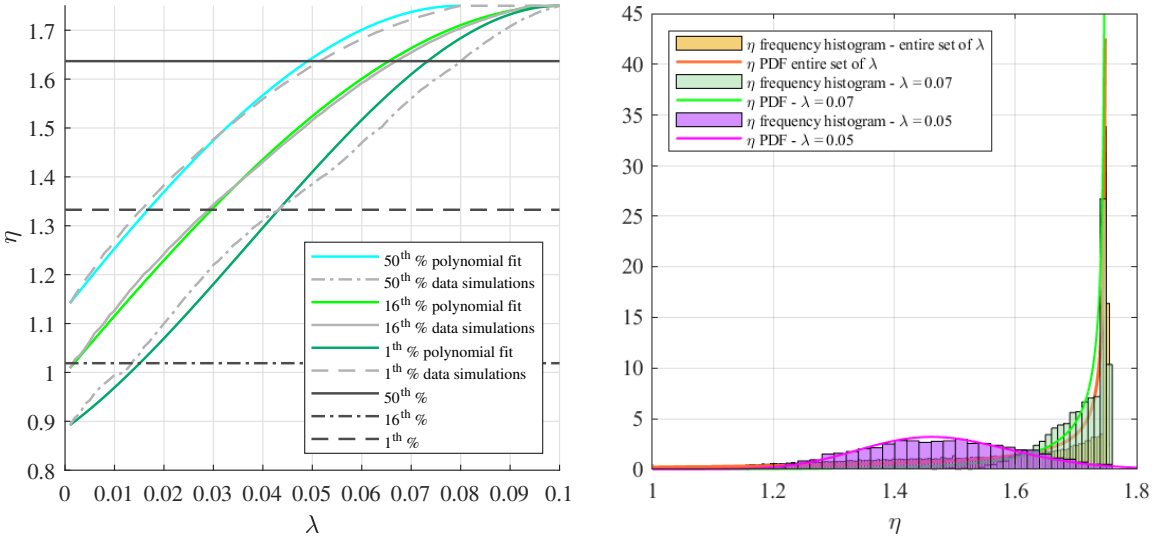

(a) Deterministic approach

(b) Probabilistic approach

Figure 10.6: Procedures (a) for λ_i known and (b) for λ_i unknown in the case of $D = 0.5$

As far as the deterministic approach in Figure 10.6a is concerned, it is clear that considering the results without taking into account the exact value of λ_i can lead to an excessive evaluation of the model coefficient η in the cases of brittle corroded strands (characterized by low values of λ_i), which can provide an overestimation of the peak force. Vice versa, for the cases of ductile corroded strands (characterized by high values of λ_i) it suggests values for the model coefficient η that can provide an underestimation of the peak force.

In detail, a summary of the simulation results for all the damage index scenarios and for all the available λ_i values is reported in Appendix A, for both the approaches and procedures.

10.7 Results of the analyses carried out

As described in the previous section, two approaches can be identified and each of them can be applied with reference to two procedures: (i) for λ_i unknown and (ii) for λ_i known.

10.7.1 Deterministic approach and strength reduction curves proposal

In the deterministic approach all the functions that define the peak strength of corroded seven-wire strands, given by Eq.10.1, can be assumed as deterministic variables. Thus,

the following point can be recognized:

- the mean corrosion level is reasonably estimated $\Rightarrow \rho_M$;
- the peak force of the not-corroded strand is calculated $\Rightarrow F_0$;
- the minimum group coefficient is calculated by applying Eq.5.28 $\Rightarrow \rho_{Gmin}$;
- the model coefficient can be calculated thanks to the functions obtained by the fitting procedure of the Monte Carlo simulations results depending on the λ_i (unknown or known). These functions for all the damage index values are reported in Appendix A $\Rightarrow \eta$.

  In particular:

  1. values of η that is independent with respect to λ_i value (procedure for λ_i unknown). It assumes constant values.
  2. values of η that is dependent with respect to λ_i value (procedure for λ_i known). It assumes polynomial expression as a function of λ_i.

In this section is presented a proposal of strength reduction curves considering the deterministic approach for the procedure of λ_i unknown (which means to consider all the simulations results in terms of λ_i since they represent the worse situation). The strength reduction curve represents an important engineering tool that provides the amount of strength reduction in corroded strands due to the presence of corrosion. According to the resistance model in Eq.10.1, the strength reduction $F_{p,p}/F_0$ can be defined as follow:

$$\begin{aligned} F_{p,p} &= F_0 \cdot \rho_M \cdot \rho_G \\ \frac{F_{p,p}}{F_0} &= \rho_M \cdot \rho_G \\ \frac{F_{p,p}}{F_0} &= (1-D)\rho_G \end{aligned} \tag{10.4}$$

Therefore, the first step to represent the strength reduction curve is to evaluate the group coefficient ρ_G for the entire damage index domain, as reported in Figure 10.7. In particular, the figure also reports the 1^{st}, 5^{th} and 16^{th} percentiles with their second-order and sixth-order polynomial fit and the ρ_{Gmin} analytical trend. As it can be seen, the fitting with a sixth-order polynomial provides the best fit for all the percentiles. However, since the group coefficient ρ_G cannot assume values bigger than 1, the case of the sixth-order polynomial fit of the 16^{th} percentile should be put equal to 1 for damage index in the range of (0.9-1), where it assumes values slightly higher than 1. Thus, considering this approximation, in the following, only the sixth-order polynomial fits are considered.

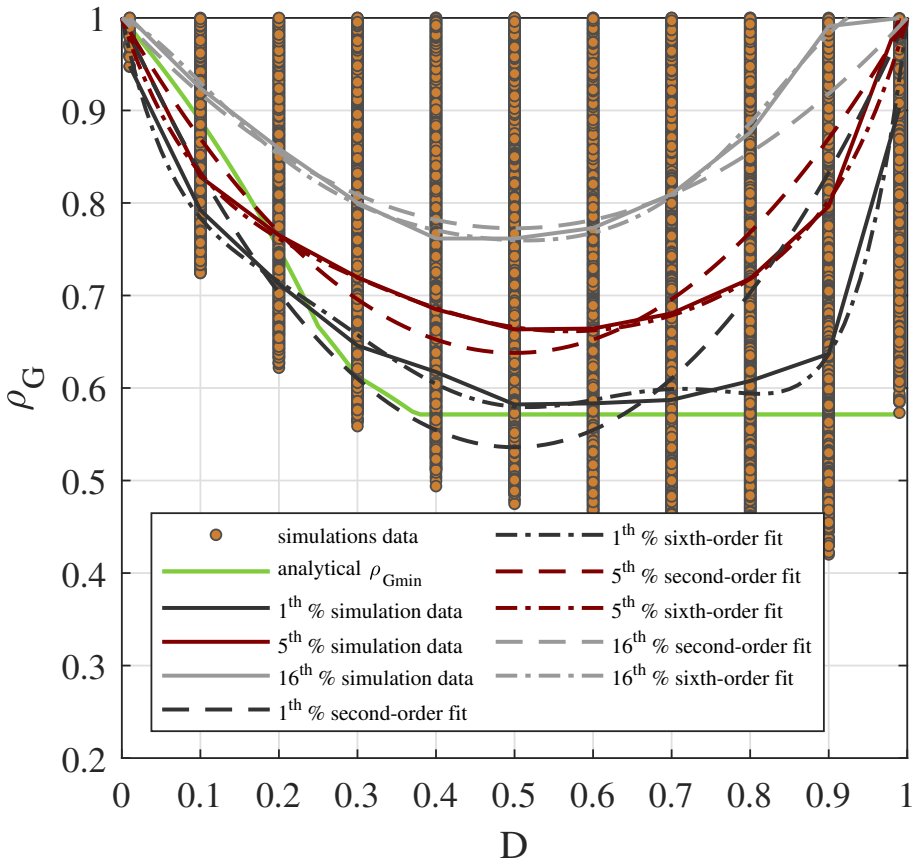

Figure 10.7: Group coefficient as a function of the damage index

It is worth noting that the lower bound estimation of the group coefficient seems to be higher for damage index up to 0.20, with respect to the prevision given by the 5^{th} and 1^{st} percentiles.

This aspect is due to the fact that for strands characterized by a small amount of corrosion is much more difficult to have the maximum variability in the corrosion of the wires, which is one of the hypotheses for the analytical estimation of the ρ_{Gmin}. However, the 1^{st} percentile represents a good approximation of the group coefficient for representing seven-wire strands characterized by small values of λ_i (brittle strands). On the other hand, the 5^{th} and 16^{th} percentiles can be used for estimating the behaviour of corroded seven-wire strands characterized by a certain ductility level. The polynomial fittings are characterized by the following expressions:

$$\begin{cases} 1^{st} \Rightarrow \rho_G = 61.37D^6 - 172.87D^5 + 186.46D^4 - 96.81D^3 + 25.75D^2 - 3.94D + 1 \quad R^2 = 0.99 \\ 5^{th} \Rightarrow \rho_G = 15.76D^6 - 47.92D^5 + 58.55D^4 - 36.03D^3 + 12.24D^2 - 2.60D + 1 \quad R^2 = 0.99 \\ 16^{th} \Rightarrow \rho_G = -20.10D^6 + 55.06D^5 - 57.04D^4 + 28.09D^3 - 5.65D^2 - 0.36D + 1 \quad R^2 = 1 \end{cases} \tag{10.5}$$

Figure 10.8 shows the strength reduction curves for corroded seven-wire strands by applying Eq. 10.5. This is a fundamental result of this work that can be useful for the assessment of the residual strength of corroded seven-wire strands taking into account the geometry of the corrosion and the steel material properties. The Figure reports the curves as directly evaluated from the Monte-Carlo simulations and from their identified percentiles of Eq. 10.4. In addition, it also reports some analytical linear fittings, which are based on experimental tensile tests, available in the literature.

The proposal strength reduction curves represent a lower bound estimation of the peak strength reduction in corroded seven-wire strands measured during some experimental campaigns. In fact, some of those corroded seven-wire strands could be characterised by different amounts of ductility, which makes it possible that the reductions are lesser than those described by the 16^{th} percentile. As discussed before, the here proposed curves represent the application of the deterministic approach considering all the sets of the adimensional corrosion extension λ_i (λ_i unknown). This leads to an overestimation of the reduction of the peak force (worse case), which could be the difference with the case of the three models proposed by [40]. Further simulations considering the exact values of the adimensional corrosion extension λ_i (λ_i known) are currently ongoing.

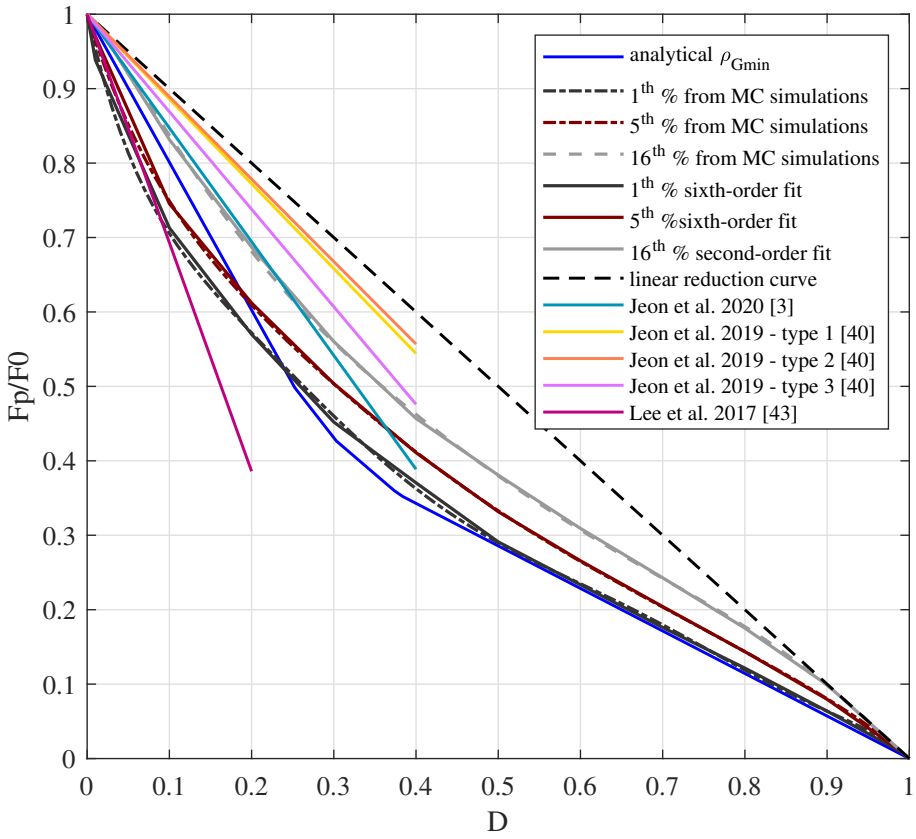

Figure 10.8: Strength reduction curves of corroded wire strands as a function of the damage index

Clearly, according to the results shown previously in the parametrical study of section 9.2, an increase of the ductility in the corroded wires corresponds to an increase in the peak force in the strand that is observable also in the strength reduction curves. In fact, the higher the percentile of the model coefficient η the lower the peak force reduction.

The proposal curves in Figure 10.8 present two important aspects: (i) they are defined in the entire damage index domain, (ii) they respect two physical boundary conditions respectively in $D = 0$ (where no damage occurs, then no reduction of the strength is manifest) and $D = 1$ (where the damage is complete, then no strength capacity is possible).

The expressions of the strength reduction curves with reference to the $1^{st}\%$, $5^{th}\%$ and $16^{th}\%$ can be obtained applying Eq.10.4 and Eq.10.5. Thus, they assume the following expressions:

$$\begin{cases} 1^{st} & \Rightarrow \dfrac{F_p}{F_0} = (1-D)\cdot[61.37D^6 - 172.87D^5 + 186.46D^4 - 96.81D^3 + 25.75D^2 - 3.94D + 1] \\ & R^2 = 0.99 \\ 5^{th} & \Rightarrow \dfrac{F_p}{F_0} = (1-D)\cdot[15.76D^6 - 47.92D^5 + 58.55D^4 - 36.03D^3 + 12.24D^2 - 2.60D + 1] \\ & R^2 = 0.99 \\ 16^{th} & \Rightarrow \dfrac{F_p}{F_0} = (1-D)\cdot[-20.10D^6 + 55.06D^5 - 57.04D^4 + 28.09D^3 - 5.65D^2 - 0.36D + 1] \\ & R^2 = 1 \end{cases} \tag{10.6}$$

In conclusion, the proposed strength reduction curves represent interesting engineering tools for the design and safety evaluations of corroded seven-wire strands. However, their comparison with the results of experimental tensile tests on corroded seven-wire strands will be the object of future work and studies.

10.7.2 Probabilistic approach

In the probabilistic approach the functions that define the peak strength of corroded seven-wire strands (or some of them), given by Eq.10.1, can be assumed as random variables. The result of this approach is the description of the statistic of the introduced parameter η. In particular, the achieved results of this work are presented in terms of its probability functions and the consequent probability functions of the peak force of corroded strands that allow to identify design-oriented parameters.

The resistance function of corroded strands, according to the resistance model, assumes a formal aspect reported in Eq. 10.7.

$$R = R(A_0, f_y, \eta) = \rho_M \cdot \eta \cdot \rho_{Gmin} \cdot A_0 \cdot f_y \tag{10.7}$$

In this work, in order to determine the probability functions of the peak force given by the resistance model defined by Eq. 10.7 four hypotheses have been done:

1. the resistance R is a function of deterministic and random variables;
2. the yield stress of the steel material f_y, and the model coefficient η are considered random variables;
3. the not-corroded area of the wires A_0 (it is typically characterized by a small coefficient of variation, below 1%), the mean corrosion level ρ_M and the minimum group function ρ_{Gmi} are considered as deterministic variables;
4. the functions that define the resistance R can be assumed as independent variables.

In addition, the probability density function of the yield stress can be assumed as logNormal with a mean value equal to 1700 MPa and a coefficient of variation equal to 5%. Instead, the model coefficient η has a probability density function reported in Appendix A, chosen according to the two procedures for λ_i unknown and for λ_i unknown. The not-corroded strand area can be assumed, for instance, equal to $87.96mm^2$ (seven wires with a diameter of $4mm$) and the minimum group function ρ_{Gmin} assumes values given by Eq. 10.3 according with the mean corrosion level.

For the sake of clarity, the following notation is here introduced: (i) the resistance function $R = Y_1$; (ii) the random variable $f_y = X_2$ and (iii) the random variable $\eta = X_3$. Thus, after some analytical manipulations, the probability density and cumulative distribution functions of the resistance of corroded seven-wire strands can be obtained by the following integral expression.

$$
\begin{aligned}
f_{Y_1}(y_1) &= \int_1^{1/\rho_{Gmin}} f_{X_2}\left(\frac{y_1}{y_2 \cdot A_0 \cdot \rho_M \cdot \rho_{Gmin}}\right) \cdot f_{X_3}(y_2) \cdot \frac{1}{y_2 \cdot A_0 \cdot \rho_M \cdot \rho_{Gmin}} \cdot dy_2 \\
F_{Y_1}(y_1) &= \int f_{Y_1}(y_1) \cdot dy_1
\end{aligned}
\tag{10.8}
$$

Figure 10.9 reports both the probability and cumulative density functions given by the cases of λ_i unknown and λ_i known: $\lambda_i = 0.03$ and $\lambda_i = 0.07$, considering the scenario of damage index $D = 0.5$.

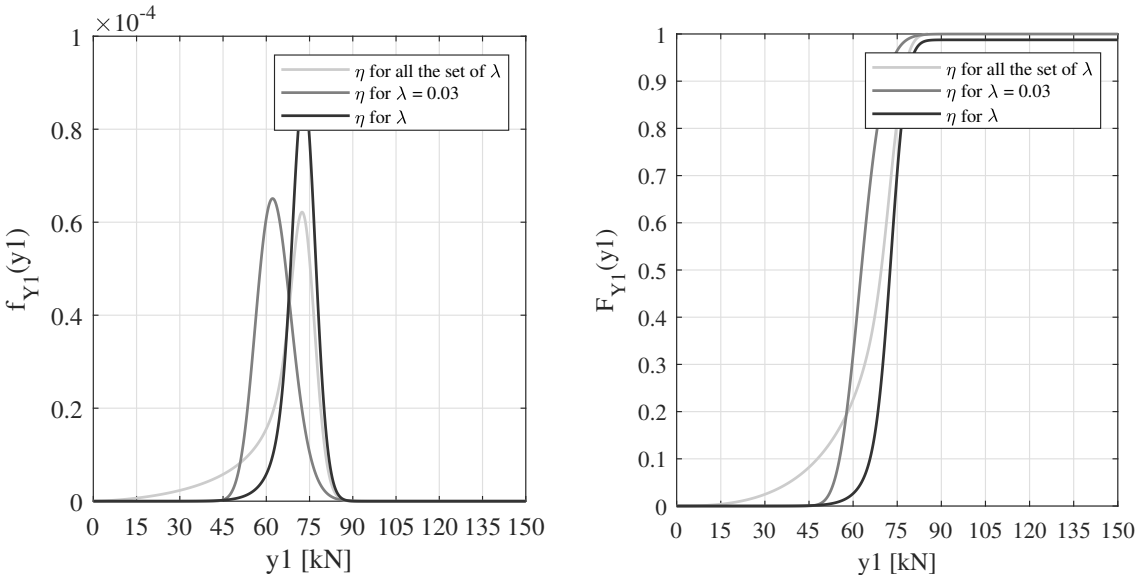

(a) resistance probability density function

(b) resistance cumulative density function

Figure 10.9: Probability functions of corroded seven-wire strands in the case of $D = 0.5$

As shown in Figure 10.9 the knowledge of the corrosion in terms of the adimensional corrosion length λ_i leads to a better estimation of the resistance of corroded strands. Evaluating the resistance probability functions considering a fixed value of λ_i leads to a reduction of the collapse probability of corroded strands. In addition, as results clear from Figure 10.9b, the higher the adimensional corrosion length λ_i the lower the collapse probability of corroded strands, according to λ_i effects discussed in section 9.2.

According to the Annex C of EN 1990 [54], a formulation to compute the design value of a random variable, based on the type of distribution and the probability of failure chosen for the design purposes can be applied. In the present case, the evaluations have been performed considering a probability of having a more unfavourable value of 0.1%, typically assumed when dealing with ultimate limit states, and corresponding to a target reliability index β equal to 3.8. In fact, the design value of the considered state can be evaluated assuming the FORM sensitivity factor equal to 0.8 (design resistances).

In this regard, useful results from the resistance probability functions, with reference to $A_0 = 87.96mm^2$ and $n_w = 7$, are summarized in Table 10.2, in terms of the resistance characteristic value, which is evaluated as the cumulative probability equal to 5%, and the resistance design value, which is evaluated as the cumulative probability equal to 0.1%. In addition, Table 10.2 also reports the same results considering the resistance design value evaluated as the probability equal to 1%, the corrosion characteristic coefficient and the resistance safety factors. The subscripts *k* and *d* denote the characteristic and design value of the random variable, respectively. The corrosion characteristic coefficient k_{corr}, which might be higher than one due to the fact that the reduction of the strength is already provided by η_k, ρ_M and ρ_G, is estimated from the simulations in order to be applied in

the design phases (to estimate the design value of the strength) according to the following formula:

$$R_d = k_{corr} \cdot \frac{f_{y,k} \cdot A_0 \cdot \eta_k \cdot \rho_M \cdot \rho_{Gmin}}{\gamma} \tag{10.9}$$

Appendix A reports the estimated k_{corr} and γ values for all the damage index D and the adimensional corrosion extension λ_i scenarios.

Table 10.2: Design-oriented results from the peak strength probability density function

Cumulative Curve	λ_i unknown	$\lambda_i = 0.03$	$\lambda_i = 0.07$
Resistance characteristic value R_k [kN]	38.30	53.45	62.85
Resistance design value $R_{d,0.1\%}$ evaluated to CDF = 0.1 % [kN]	8.95	46.40	45.75
Resistance design value $R_{d,1\%}$ evaluated to CDF = 1 % [kN]	21.55	49.99	55.58
Resistance safety factor $\gamma = R_k/R_{d,0.1\%}$	4.30	1.16	1.37
Resistance safety factor $\gamma = R_k/R_{d,1\%}$	1.78	1.07	1.13
Corrosion characteristic coefficient for the strength parameters $k_{corr} = R_k/(f_{y,k} \cdot A_0 \cdot \eta_k \cdot \rho_M \cdot \rho_{Gmin})$	1.08	1.18	1.06

As it can be seen from the results in Table 10.2, in the case of $D = 0.5$, the resistance safety coefficients assume high different values according to the λ_i configuration. In fact, when the adimensional extension of the corrosion λ_i is unknown the resistance safety coefficient can assume values higher than three times the value that it assumes for the cases of known. In other words, in order to have a safe level according to technical codes (i.e. EN 1990 [54]) it is required a reduction of the resistance parameters of more than four times. These results confirm that the knowledge of the geometry of the corrosion leads to a more precise safety assessment of the resistance of corroded seven-wire strands. On the other hand, the approach can be applied considering a higher value of the probability of having more unfavourable cases, i.e. 1%, which, of course, leads to a lesser resistance safety factor and might be a good compromise for the safety evaluation of corroded seven-wire strands resistance. In this section, in order to explain the approach, just 3 cases of λ_i have been presented, however, Appendix A reports the probability functions given by Eqs. 10.8 and the design-oriented results, for the two procedures of λ_i unknown and λ_i known, for all the values of the damage index.

In conclusion, the following outcomes can be drawn: (i) the lack of knowledge in the geometry of the corrosion can strongly reduce the resistance of corroded seven-wire

strands and (ii) the probabilistic approach here presented allows evaluating the resistance probability functions of corroded seven-wire strands and the calculation of safety factors considering two procedures that take into account the cases of λ_i unknown and λ_i known. This result may be useful both from a design and safety assessment point of view.

11

Ultimate displacements and ductility

Sommario

Questo capitolo riporta i domini di spostamento ultimo per trefoli corrosi stimati a partire dalle simulazioni Monte Carlo di tefoli corrosi descritte nel capitolo precedente. Tali domini permettono di stimare lo spostamento utlimo di trefoli corrosi (e quindi di valutare la duttilità disponibile) tenendo conto sia della geometria di corrosione che dei parametri costitutivi del materiale acciaio. I domini vengono espressi in termini di diversi percentili e rappresentano degli utili strumenti ingegneristici sia ai fini progettuali che di valutazioni di sicurezza.

Summary

This chapter reports ultimate displacement reduction curves for corroded strands estimated from the Monte Carlo simulations of corroded strands described in the previous chapter. These curves allow to estimate the ultimate displacement of corroded strands (and therefore to evaluate the available ductility) taking into account both the corrosion geometry and the constitutive parameters of the steel material. They are expressed in terms of different percentiles and represent useful engineering tools both for design purposes and for safety assessments.

The reduction of the ultimate displacement of corroded seven-wire strands emerged from the Monte Carlo simulations presented in section 10.6. As explained, the simulated corroded seven-wire strands were characterized by the adimensional corrosion extension λ_i in the range (0,0.1). In fact, the value $\lambda_i = \overline{\lambda_i} = 0.1$, leads to enough ductility in the wires that allows to reach the condition $F_{p,p} = F_0$. In other words, the peak force of the corroded strand is equal to the peak force of the not-corroded one.

Nevertheless, according to the results discussed in chapter 8 and chapter 9, a value of λ_i lesser than 1 leads always to a brittle behaviour in wires and strands.

11.1 The complete reduction curves

Thus, in order to fully characterize the ultimate displacements of corroded strands, the simulations should consider the variation of the adimensional corrosion extension λ_i

in the range (0,1) as reported in Figure 11.1. The figure, in addition, reports the $1^{st}\%$, $5^{th}\%$, $16^{th}\%$ percentiles measured taking into account all the simulated λ_i (procedure for λ_i unknown) and their fitting with second-order polynomial functions, which are reported in Eq.11.1.

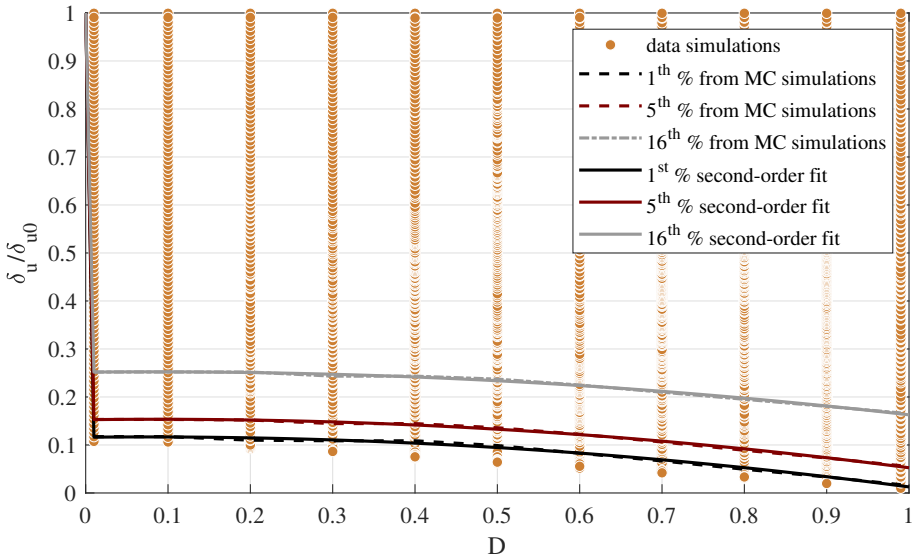

Figure 11.1: Complete ultimate displacement reduction curves

As it can be seen from the figure, the curves have to assume a value equal to 1 in case of $D = 0$, which means no corrosion in the strand (then no reductions of ductility), while they assume an almost constant value until $D = 0.5$ then decreases with an increasing of the damage index. These results confirm that the adimensional corrosion extension λ_i has an important impact on the ultimate displacement of corroded strands that strongly reduces their ductility capacity. In fact, looking at the percentiles, which represent the ultimate displacements associated with small values of λ_i (localized corrosion), there is a high reduction also for small values of the damage index.

$$\begin{cases} 1^{st} \Rightarrow \dfrac{\delta_u}{\delta_{u0}} = -0.121D^2 + 0.018D + 0.116 \quad R^2 = 0.99 \text{ for } D \geq 0.01 \\ 5^{th} \Rightarrow \dfrac{\delta_u}{\delta_{u0}} = -0.121D^2 + 0.021D + 0.153 \quad R^2 = 1 \text{ for } D \geq 0.01 \\ 16^{th} \Rightarrow \dfrac{\delta_u}{\delta_{u0}} = -0.106D^2 + 0.017D + 0.252 \quad R^2 = 1 \text{ for } D \geq 0.01 \end{cases} \tag{11.1}$$

11.2 The reduced reduction curves

In order to be consistent with the strength reduction curves (λ_i in the range (0,0.1)), the ultimate displacement reduction curves have been redefined in the same range of λ_i

(Figure 11.2). This slightly changes the lower percentiles since they are associated with the lower values of λ_i. Eqs.11.2 reports the expressions of the second-order polynomial fit of the percentiles associated with the reduced ultimate displacement reduction curves.

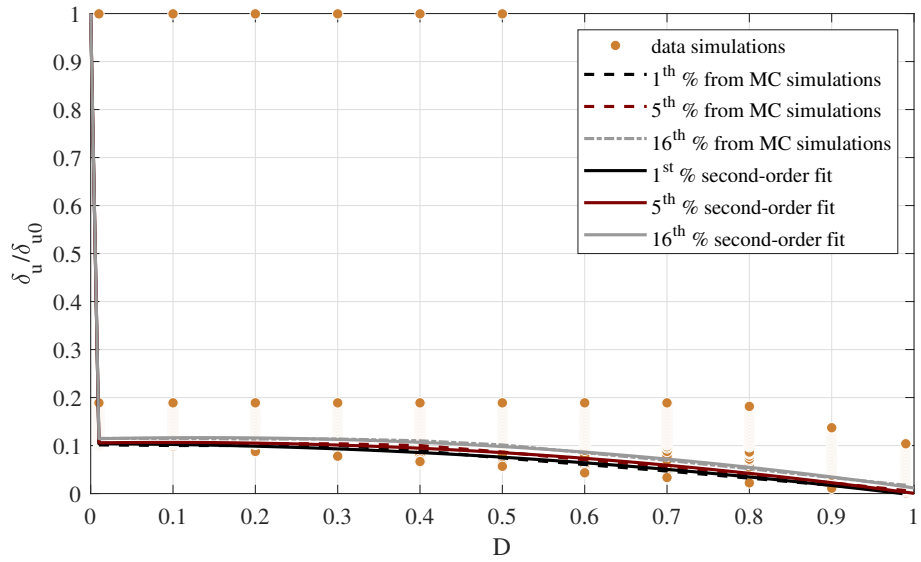

Figure 11.2: Ultimate displacement reduction curves

As it can be seen from the curves in Figure11.2, the simulations were characterized by few points leading to no reduction in the ultimate displacement. This is due to the random generation of the corroded strands. In fact, in order to simulate a certain damage index, in particular the small values, some wires could be not-corroded. This leads to an ultimate displacement of the corroded strand equal to that of the not corroded wire (parallel system model). However, this does not make big changes in the percentiles.

$$\begin{cases} 1^{st} \Rightarrow \dfrac{\delta_u}{\delta_{u0}} = -0.102D^2 + 0.005D + 0.104 \quad R^2 = 0.99 \text{ for } D \geq 0.01 \\ 5^{th} \Rightarrow \dfrac{\delta_u}{\delta_{u0}} = -0.129D^2 + 0.024D + 0.105 \quad R^2 = 0.99 \text{ for } D \geq 0.01 \\ 16^{th} \Rightarrow \dfrac{\delta_u}{\delta_{u0}} = -0.141^2 + 0.038D + 0.114 \quad R^2 = 1 \text{ for } D \geq 0.01 \end{cases} \tag{11.2}$$

The reduction curves represent an important engineering tool for the design and safety evaluations of corroded seven-wire strands. They allow to estimate the ductility capacity of corroded strands taking into account the geometry of the corrosion and the steel material parameters.

In conclusion, until now, the reduction of the peak force and the ultimate displacement of corroded seven-wire strands are described by their respective reduction curves as functions of the damage index. The next chapter shows a possible their implementation in the definition of a reduced sigma-epsilon relationship for the steel material in order to take into account corrosion in the structural behaviour of post-tensioned beams.

12

Corrosion effects on the structural behaviour of prestressed concrete elements

Sommario

In questo capitolo viene presentato un possibile approccio per valutare gli effetti dovuti alla presenza di trefoli corrosi sulla capacità di elementi in calcestruzzo armato precompresso. In particolare, tenendo conto di una legge costitutiva del materiale acciaio ridotta a causa della corrosione, tali effetti possono essere valutati mediante lo studio del conseguente diagramma momento-curvatura ridotto di una sezione inflessa o mediante diagramma sforzo assiale-deformazione ridotto nel caso di un elemento teso. La riduzione della legge costitutiva del materiale acciaio può essere stimata a partire dai domini di resistenza e di spostamento ultimo per trefoli corrosi ottenuti nei capitoli precedenti.

Summary

In this chapter a possible approach to evaluate the effects due to the presence of corroded strands on the capacity of prestressed concrete elements is presented. In particular, taking into account a constitutive law of the steel material reduced due to corrosion, these effects can be evaluated by studying the resulting reduced moment-curvature diagram of a given cross-section or by the reduced axial stress-strain diagram in the case of a tense element. The reduction of the constitutive law of the steel material can be estimated starting from the strength and ultimate displacement reduction curves for corroded strands obtained in the previous chapters.

12.1 The reduced sigma-epsilon relationship for the steel material

In the previous chapters, the force-displacement relationships of corroded seven-wire strands have been discussed and characterized. They take into account the geometry of

the corrosion, by means of the cross-section reduction and the adimensional corrosion extension, and the steel material parameters that define its sigma-epsilon relationship. The peak force measured from the force-displacement relationships of corroded seven-wire strands has been described through a new resistance model introduced in Eq.10.1. Thus, several Monte Carlo simulations of corroded strands allowed to fully characterize the model parameters and the following proposal curves:

1. the strength reduction curves (see Figure 10.8) that describe the peak force reduction as a function of the damage index *D*;
2. the ultimate displacement reduction curves (see Figure 11.2) that describe the ultimate displacement reduction (ductility reduction) as a function of the damage index *D*.

From a practical point of view the reduction curves allow to estimate the strength and the ductility of corroded strands, with different confidence levels, simply by the knowledge of the cross-section reduction of the strands through the mean corrosion level ρ_M ($D = 1 - \rho_M$).

In this chapter, a possible implementation of these results is presented. The idea is to characterize the reduced sigma-epsilon constitutive law of the steel material in order to take into account the effects of the corrosion in the bending moment-curvature diagram. In fact, the equivalent sigma-epsilon constitutive law can be obtained starting from the reduction of the peak strength:

$$\frac{F_p}{F_0} = \frac{\rho_M \cdot \rho_G \cdot f_y \cdot A_0}{f_y \cdot A_0} = \frac{f_{y,p}}{f_y} \tag{12.1}$$

where $f_{y,p}$ represents the reduced yielding stress. Similarly, the reduction of the ultimate displacement δ_u of corroded strands is related to the reduction of the ultimate stress ϵ_u of the steel material:

$$\frac{\delta_u}{\delta_{u0}} = \frac{\epsilon_u \cdot L_0}{\epsilon_{u0} \cdot L_0} = \frac{\epsilon}{\epsilon_{u0}} \tag{12.2}$$

where ϵ_{u0} indicates the ultimate stress of the steel material with reference to the not-corroded configuration.

Figure 12.1 reports the two reduction curves obtained and presented in the previous chapters.

It is worth noting that the ultimate displacement curves represent those one corresponding to the range of simulated λ_i in the range (0,0.1). In fact, this is consistent with the strength curves assumptions. Figure 12.2 shows the reduced sigma-epsilon relationship based on the values of the curves.

It is to be noted that the Young modulus of the steel has been considered not degraded due to corrosion.

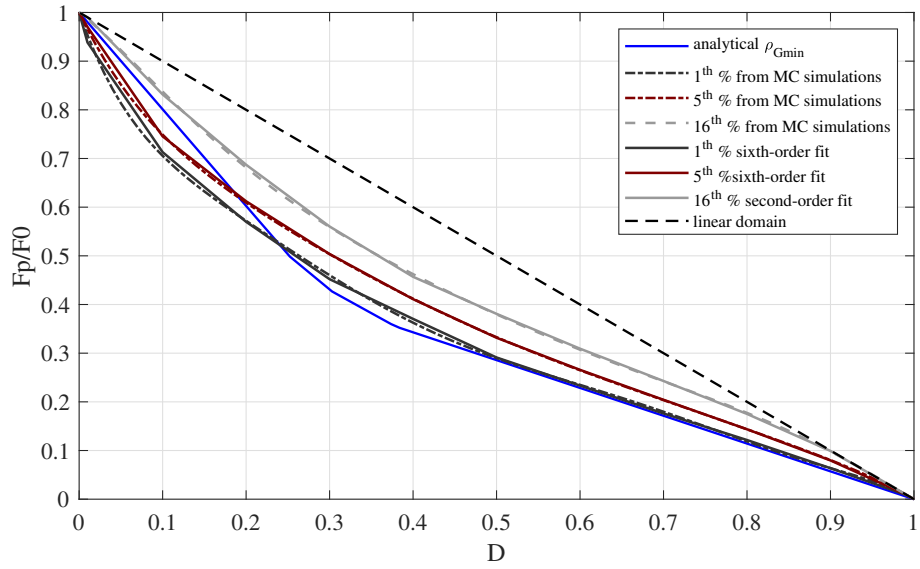

(a) Strength reduction curves

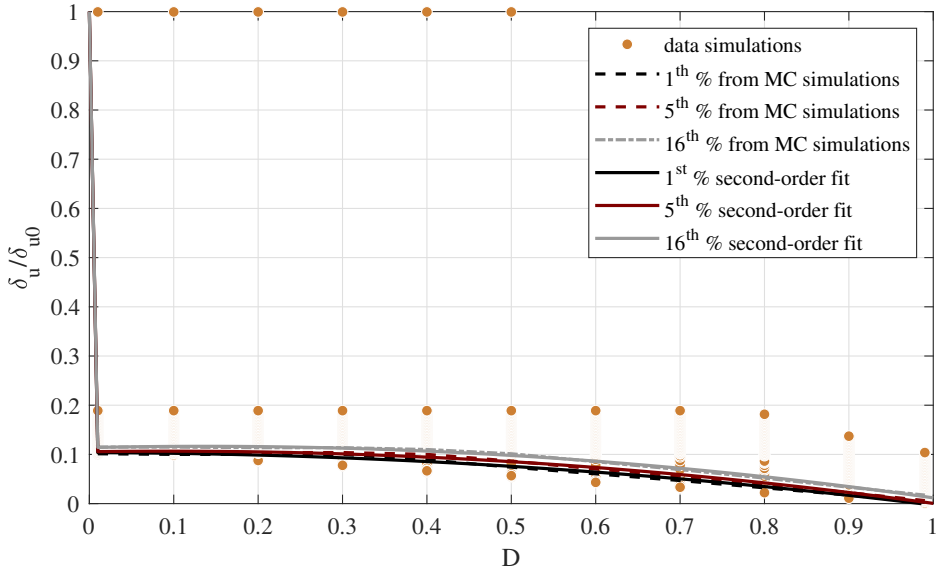

(b) Ultimate displacement reduction curves

Figure 12.1: Reduction curves for corroded seven-wire strands

As a matter of fact, the reduction curves can be also used for cables that are constituted by several seven-wire strands, which is the typical configuration of post-tensioned beams in bridges. In fact, their behaviour can be seen again as that one of a parallel system between the strands. In other words, ρ_M represents the mean corrosion level of the corroded cable. This assumption leads to the validity of the obtained strength and ultimate displacement reduction curves obtained for single seven-wire strands even for cables constituted by several seven-wire strands.

However, to be rigorous, the reduction curves should be obtained considering the exact value of the number of wires in the cable, according to the procedure presented in

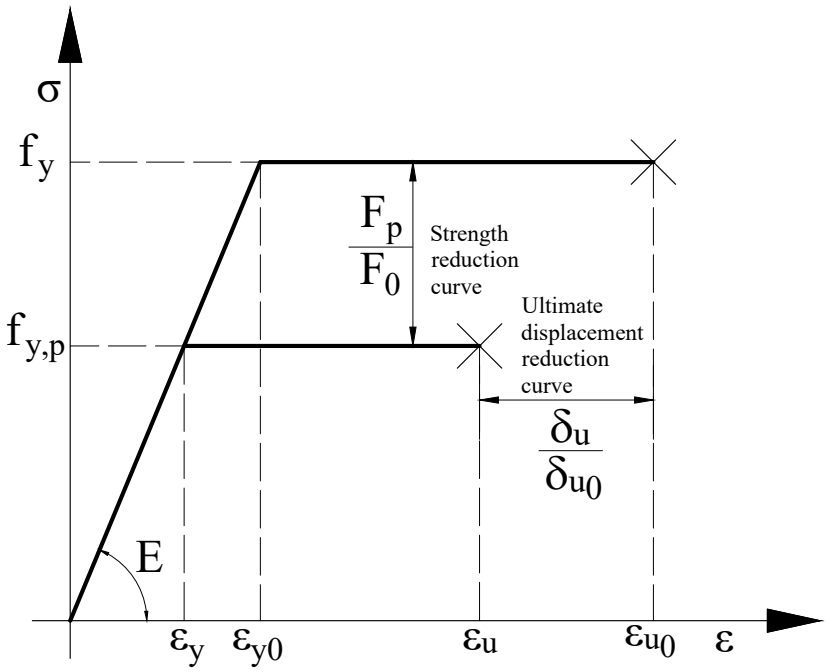

Figure 12.2: Reduction of the sigma-epsilon relationship for the steel material

chapter 10, taking into account the exact value of the group coefficient $\rho_G = \eta \cdot \rho_{Gmin}$. Nevertheless, the lower bound estimation of the group coefficient tends to a plateau value equal to 0.5 for high values of the number of wires (see Figure 10.1). Thus, the differences in terms of strength and ultimate displacement reduction curves are minimal.

12.2 The bending moment-curvature diagram

The next step to take into account the effects of corroded strands on the structural behaviour of post-tensioned elements is to implement the reduced sigma-epsilon relationship for the steel material in the evaluation of their capacity, for instance by means of the bending moment-curvature diagram. In this regard, the following hypotheses have to be considered in the calculation of the resistance bending moment as a function of the curvature:

- plane sections remain plane (plane sections preservation);
- non-linear behaviour of the constitutive materials;
- perfect bonding between steel and concrete;
- tensile strength of concrete equal to zero.

From a practical point of view, the bending moment-curvature diagram for a given cross-section can be obtained by imposing the curvature value (displacement control approach) and then performing the equilibrium between the concrete and steel stresses and calculating the resulting bending moment. At each curvature level, the strains in the materials have been checked with reference to their sigma-epsilon relationships (the reduced one in the case of corroded prestressing steel).

In order to give an idea of the possible way to proceed, let's consider a post-tensioned concrete beam with a rectangular cross-section characterized by a base $B = 30$ cm and a height $H = 60$ cm without reinforced steel (Figure 12.3b). The prestressing force is provided by 10 seven-wire strands (each seven-wire strand has a cross-section area $A_s = 87.96mm^2$).

The concrete is characterized by a characteristic cylinder compressive strength $f_{ck} = 45$ MPa, which means a design value $f_{cd} = 25.5$ MPa [11], while the prestressing steel has a design yielding stress $f_{yd} = 1700$ MPa, Young modulus $E = 210000$ MPa and material ductility $\mu_\epsilon = 10$ ($\epsilon_{ud} = 10 \cdot \epsilon_y = 10 \cdot f_{yd}/E = 8.1\%$). In fact, the Technical code (paragraph 11.3.3.2 [11]) requires an ultimate design strain for prestressing steel $\epsilon_{ud} \geq 0.9 \cdot 3.5 = 3.15\%$. The sigma-epsilon relationships for the constitutive materials are reported in Figure 12.3a.

Supposing a lack of injection along the duct containing the 10 seven-wire strands, which leads to the presence of corrosion in the prestressing strand, for instance, due to a cross-section reduction equal to 30% (which means a corrosion mean level $\rho_M = 0.7 \Rightarrow D = 1 - \rho_M = 0.3$) the reduced yielding stress and the reduced ultimate strain for the steel material can be estimated through Eqs. 10.6 and 11.2, respectively. With reference to the the 5^{th} percentile the following reductions can be estimated:

- reduced yielding stress: $\frac{F_p}{F_0}|_{D=0.3} = 0.503 \Rightarrow \frac{f_{yp}}{f_y} = 0.503 \Rightarrow f_{yp} = 0.503 \cdot f_y = 855.1$ MPa;
- reduced ultimate displacement: $\frac{\delta_u}{\delta_{u0}}|_{D=0.3} = 0.101 \Rightarrow \frac{\epsilon_u}{\epsilon_{u0}} = 0.101 \Rightarrow \epsilon_u = 0.101 \cdot \epsilon_{u0} = 0.101 \cdot 8.1\% = 0.818\%$.

Where for the yielding stress and the ultimate strain of the steel material have been considered their design values: $f_y = f_{yd}$ and $\epsilon_u = \epsilon_{ud}$. In other words, the safety coefficient on the steel material has been assumed as unaffected by the corrosion.

Thus, the reduced sigma-epsilon for the prestressing steel assumes the values reported in Figure 12.4.

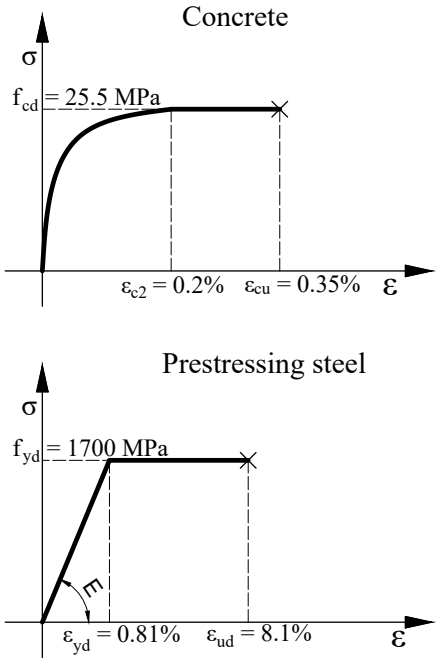

(a) Sigma-epsilon relationships of the constitutive materials

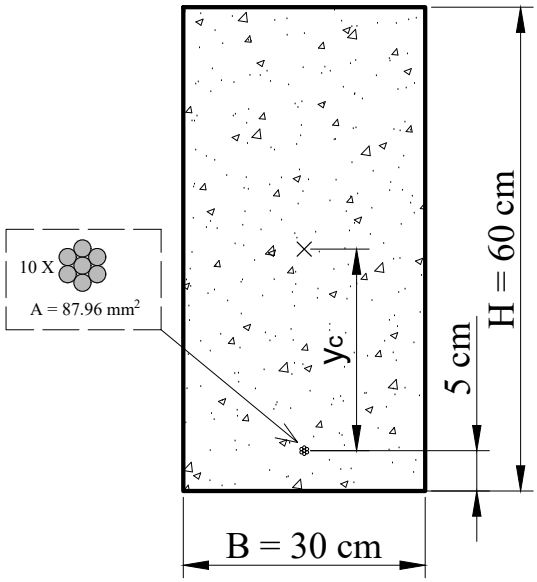

(b) Cross-section of the post-tensioned beam

Figure 12.3: Sigma-epsilon relationships of the constitutive materials and cross-section of the beam

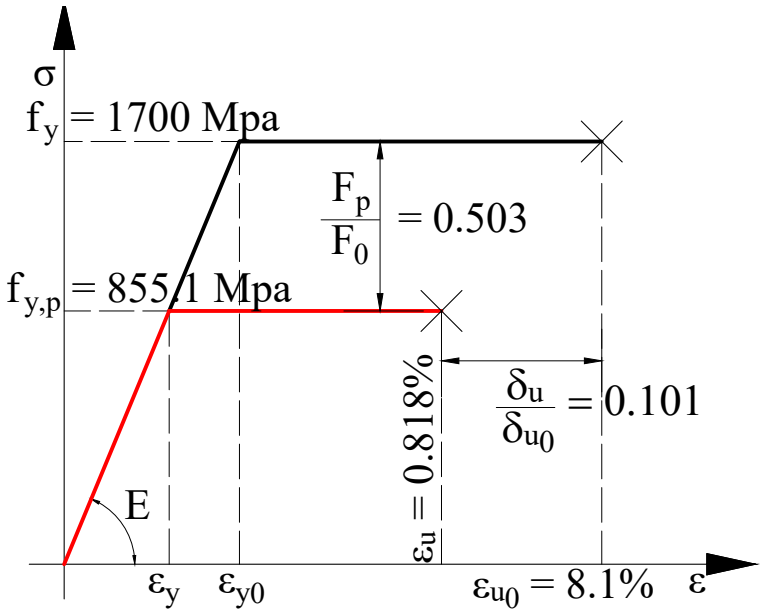

Figure 12.4: Reduced sigma-epsilon relationship for D = 0.3

Following these results, the presence of corroded strands may change the behaviour of a given cross-section in a post-tensioned beam. In fact, the reduction in both the cross-

section area of the prestessing steel strands and in the sigma-epsilon relationship for the steel material can lead to the embrittlement of the cross-section that reaches the collapse in correspondence to the cracking bending moment. This is due to the fact that the prestressing forces fail and, after the cracking of the concrete, the beam is no more able to support the external loads. Consequently, the strength and the ductility of the beam with corroded strands is strongly reduced.

Moreover, the same idea can be also applied to prestressed elements subjected to axial force only.

13

Summary of the results obtained

In the previous chapters mechanical models for corroded wires and strands have been presented introducing a new resistance model for corroded strands that considers the effects of the variability of the corrosion in the wires constituting the whole strands. It takes into account both the geometry of the corrosion, which is described in longitudinal and transversal extensions by means of the adimensional corrosion extension λ_i and the adimensional reduction of the cross-section area ρ_i, and the steel material properties, in terms of its sigma-epsilon laws.

By means of these mechanical models, the effects of corrosion on the force-displacement response of both steel wires and strands have been investigated. The importance of the single parameters constituting the corrosion (i.e. geometry and variability of the corrosion) and the steel material (ductility and hardening ratio) on the mechanical behaviour of the corroded strands emerged from parametric studies. The following conclusions can be drawn.

Regarding the single wire:

- The effect of the coupling of ρ_i and λ_i can provide a post-yielding response exploitation of the not-corroded part leading to higher maximum force and ultimate displacement with respect to the ones of the corroded part, which can represent a first approximation of the mechanical behaviour of a corroded wire.
- For high values of ρ_i, the post-yielding response exploitation appears clear also for small values of hardening coefficient (i.e. $r = 0.5\%$), but it depends on the λ_i and μ_ϵ values.
- For small values of ρ_i, the same effect takes place only for higher values of r and λ_i. In other words, a particular coupling of ρ_i and λ_i might provide a post-yielding response exploitation of the not-corroded part leading to an increasing of the performance of the corroded wire.

Regarding the corroded seven-wire strand:

- The mechanical force-displacement response appears further depending on the corrosion variability in the wires.

- The reductions in the maximum force and ultimate displacement are provided both from the corrosion mean level and from the variability in the corrosion of the wires.
- For a fixed λ_i value, the higher the variability, the higher the reduction of the strand maximum force.
- For a fixed λ_i value, the higher the variability, the lesser the reduction of the ultimate displacement.
- The further reduction in the peak force due to the variability in the wires decreases with an increasing of the adimensional corrosion extension λ_i.
- The further reduction in the ultimate displacement due to the variability in the wires increases with an increasing of the adimensional corrosion extension λ_i.
- The hardening effect is limited for small material ductility (i.e. high strength steel with $\mu_\epsilon = 10$), whilst it leads to higher maximum force and higher ultimate displacement for large material ductility (i.e. mild steel with $\mu_\epsilon = 100$). In other words, the behaviour of corroded seven-wire strands made up of high-strength steel is well represented by an elastic perfectly plastic constitutive model.
- For elastic-perfectly plastic steel material with high values of material ductility μ_ϵ, the peak force depends only on the mean corrosion level ρ_M, in fact, the ductility content in the wires is enough to achieve the yielding stress. This is valid also if, in addition, high values of the adimensional corrosion length λ_i are considered

Finally, the parametric study here presented led the foundations for the development of engineering tools for the estimation of the strength capacity of corroded seven-wire strands based on the introduction of the new resistance model that takes into account the variability of the corrosion in the wires, by means of the group coefficient. In this respect, an analytical estimation of its lower bound is provided by using the Darmawan-Stewart model, which considers brittle strands, while its characterization for ductile behaviour is provided through several Monte-Carlo simulations. In addition, two approaches have been introduced, whose main results are provided in tabulated form reported in Appendix A, for the evaluation of the peak force of corroded seven-wire strands: the probabilistic and the deterministic ones.

From the results obtained by the application of the probabilistic approach, it is emerged that the safety coefficients of the resistance of corroded seven-wire strands assume highly different values according to the λ_i configuration. In fact, when the adimensional extension of the corrosion λ_i is unknown the resistance safety coefficient can assume values higher than three times the values that it assumes for the cases of λ_i known. These results confirm that the knowledge of the geometry of the corrosion leads to a more precise

safety assessment of the resistance of corroded seven-wire strands. In other words, the lack of knowledge of the geometry of the corrosion can strongly reduce the resistance of corroded seven-wire strands.

Moreover, strength and ultimate displacements reduction curves proposals for corroded seven-wire strands that take into account both the geometry of the corrosion and the steel material parameter are provided. They can represent interesting tools in the design and safety assessment process of corroded strands. However, their comparison with the results of experimental tensile tests on corroded seven-wire strands will be the object of future work and further studies.

As a matter of fact, the new resistance model here introduced is able to represent the variability often shown in experimental tensile tests of corroded seven-wire strands. It is worth noting that the application of the approaches here proposed (deterministic and probabilistic ones) is current ongoing also considering configuration in terms of different geometry of the corrosion and different material constitutive laws.

The aforementioned Appendix A is organized for increasing values of the damage index *D*. For each of them, it reports the following results:

- **Deterministic approach**: fitting results of different percentiles of the model coefficient η for the procedure of λ_i unknown, in which it assumes constant values, and for the procedure of λ_i known, in which it assumes polynomial expressions as a function of λ_i.
- **Probabilistic approach**:
  - results of the probability density function of the model coefficient η for the procedure of λ_i unknown and for the procedure of λ_i known. Basically, it assume LogNormal or Beta probability functions.
  - design-base results based on the probability functions of the peak force of corroded seven-wire strands for the procedure of λ_i unknown and for the procedure of λ_i known.

Here in the following it is reported an example of the tabular form results that are reported in Appendix A for the case of $D = 0.5$.

The strength and the ultimate displacement reduction curves allowed to estimate a reduced stress-strain relationship for the prestressing steel, in order to take into account the effects of the corrosion in the strands on the structural behaviour of post-tensioned elements. In fact, the reduced bending moment-curvature diagram that accounts for the corrosion effects can be used to perform a safety assessment of existing bridges and could be of support for possible identification of corrosion in monitoring activities. In fact, the changing of curvature due to the corrosion could be a parameter to be monitored by SHM systems.

Deterministic approach

- **Procedure (a): λ is unknown** $\Rightarrow \eta = C$

Percentile	**C**
50^{th}	1.64
16^{th}	1.33
1^{th}	1.02

- **Procedure (b): λ is known** $\Rightarrow \eta(\lambda) = C_1\lambda^3 + C_2\lambda^2 + C_3\lambda + C_4$ for $\lambda \leq \lambda_{lim}$

Percentile	C_1	C_2	C_3	C_4	λ_{lim}	R^2
50^{th}	-436.18	-27.25	12.73	1.13	0.08	1
16^{th}	-301.06	-15.10	12.05	1.00	0.1	1
1^{th}	-989.39	111.36	7.41	0.89	0.1	0.98

Probabilistic approach

- **Procedure (a): λ is unknown**

  $\beta(a = 2.48, b = 0.26)$

- **Procedure (b): λ is known**

λ	**Probability function of η**
0.001	$logN(\mu = 0.133, \sigma = 0.1152)$
0.01	$logN(\mu = 0.235, \sigma = 0.1098)$
0.02	$logN(\mu = 0.321, \sigma = 0.0977)$
0.03	$logN(\mu = 0.386, \sigma = 0.0851)$
0.04	$logN(\mu = 0.438, \sigma = 0.0730)$
0.05	$logN(\mu = 0.479, \sigma = 0.0593)$
0.06	$\beta(a = 8.33, b = 0.40)$
0.07	$\beta(a = 10.36, b = 0.26)$
0.08	$\beta(a = 18.16, b = 0.19)$
0.09	$\beta(a = 65.69, b = 0.16)$
0.10	-

Table 13.4: Design-oriented results from the peak strength probability density function for the case of $D = 0.5$

Cumulative Curve	**Resistance characteristic value R_k [kN]**	**Resistance design value $R_{d,0.1\%}$ evaluated to CDF = 0.1 % [kN]**	**Resistance design value $R_{d,1\%}$ evaluated to CDF = 1 % [kN]**	**Resistance safety factor $\gamma = R_k/R_{d,0.1\%}$**	**Resistance safety factor $\gamma = R_k/R_{d,1\%}$**	**Corrosion characteristic coefficient $k_{corr} = R_k/(f_{y,k} \cdot A_0 \cdot \eta_k \cdot \rho_M \cdot \rho_{Gmin})$**
λ_i unknown	39.90	9.35	22.57	4.27	1.77	1.08
$\lambda_i = 0.001$	39.63	33.04	36.37	1.20	1.09	1.23
$\lambda_i = 0.01$	44.31	37.25	40.83	1.19	1.09	1.23
$\lambda_i = 0.02$	49.17	42.00	45.65	1.17	1.08	1.21
$\lambda_i = 0.03$	53.44	46.38	49.99	1.15	1.07	1.19
$\lambda_i = 0.04$	57.23	50.42	53.91	1.13	1.06	1.17
$\lambda_i = 0.05$	60.72	54.35	57.63	1.12	1.05	1.15
$\lambda_i = 0.06$	59.60	39.25	50.55	1.52	1.18	1.07
$\lambda_i = 0.07$	63.70	46.51	56.48	1.37	1.13	1.06
$\lambda_i = 0.08$	66.78	56.83	62.96	1.18	1.06	1.04
$\lambda_i = 0.09$	68.41	63.48	66.06	1.08	1.04	1.01

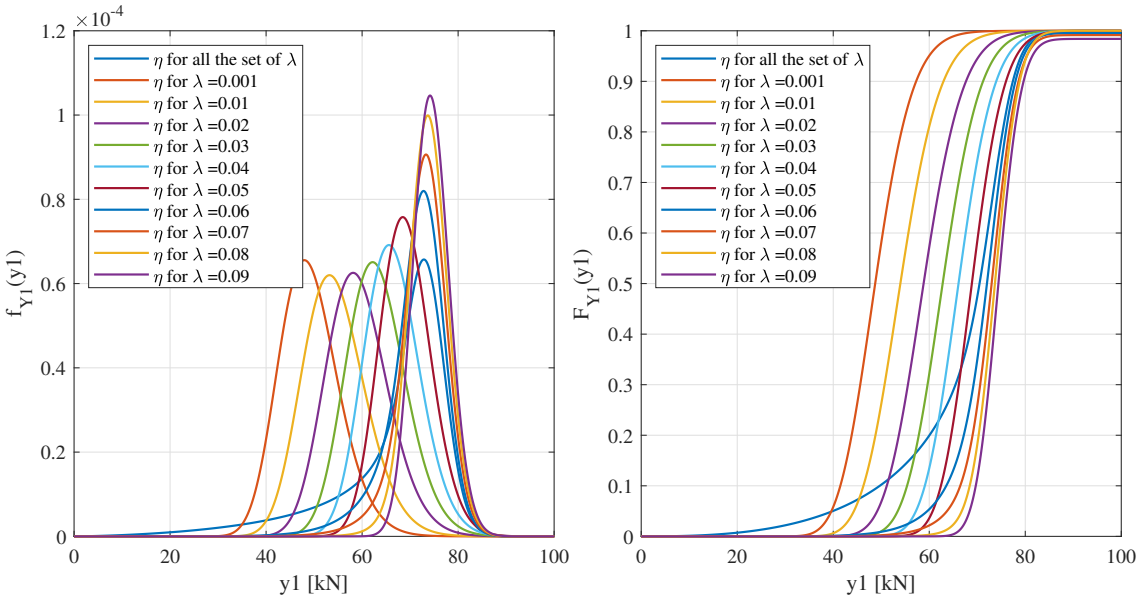

(a) Resistance probability density functions (b) Resistance cumulative density functions

Figure 13.1: Probability functions of corroded seven-wire strands for different values of λ_i and $D = 0.5$

Part III

Seismic upgrading through deck isolation

Sommario

Questa parte riporta un esempio di isolamento sismico di un impalcato da ponte, rispetto alle sottostrutture (pile e spalle), tramite isolatori elastomerici in gomma (High Rubber Damping Bearing - HDRB). Vengono descritti il ponte caso studio e la definizione degli input sismici. La modellazione del ponte caso è stata effettuata sia tramite un modellazione agli elementi finiti, a molti gradi di libertà, sia mediante mondelli minimi a pochi gradi di libertà, 4 nella direzione longitudinale e 5 in quella trasversale.

Viene dettagliata una procedura semplificata per l'identificazione delle caratteristiche di rigidezza degli isolatori, necessaria ad individuare il corretto dispositivo sul presente sul mercato.

L'effetto delle diverse modellazioni del comportamento degli isolatori elastomerici è emersa da analisi time-history condotte con il modello agli elementi finiti del ponte caso studio.

Gli effetti dovuti alla componente verticale del sisma sono stati studiati tramite analisi time-history e con spettro di risposta, valutando inoltre l'efficacia nel considerare tali effetti combinando le due tipologie di analisi o tramite analisi dinamiche complete.

Gli effetti della variabilità del modulo di elasticità tangenziale della mescola, costituente la gomma gli isolatori, sulla risposta strutturale del ponte isolato è emersa da analisi time-history condotte mediante i modelli minimi del ponte caso studio. Dallo studio della diversa variabilità dei parametri di risposta (spostamento degli isolatori, in sommita delle pile e delle spalle) si sono definiti i valori di Upper & lower bounds utili a fini progettuali.

Summary

This part reports an example of seismic upgrading through deck isolation, with respect to the substructures (piles and abutments), by means of High Rubber Damping Bearings (HDRB).

The case-study bridge has been modelled through a finite element model, with many degrees of freedom, and through minimal systems with few degrees of freedom, 4 in the longitudinal direction and 5 in the transversal one.

A simplified procedure is detailed for the identification of the horizontal stiffness of the isolators necessary to identify the correct device on the market.

The effects of the different modelling of the behaviour of the isolators emerged from time-history analyses conducted through the finite element model of the case-study bridge.

The effects due to the vertical component of the seismic actions have been studied through time-history and response spectrum analyses, also evaluating the effectiveness of considering these effects by combining the two types of analyses or through complete dynamic analyses.

The effects the variability of the shear modulus of the rubber material of the HDRB isolators on the structural behaviour of the isolated bridge emerged from time-history analyses conducted through the minimal systems. The analyses of the different variability in the response parameters (displacement of the isolators, at the top of the piles and abutments) allowed to to define the values of Upper & lower bounds useful for design purposes.

14

Seismic upgrading solutions

14.1 Context and objectives

The dynamic and seismic behaviour of bridges is governed by the connection system ("bearings layout") between the superstructure (deck) and the substructures (piers and abutments). Among all possible traditional and innovative solutions [55], [56] nowadays the seismic isolation [57],[58] of the bridge deck with respect to the substructures is widely used for both the seismic design of new bridges and the seismic retrofit of existing ones. Even though in the last years the adoption of Curved Surface Sliders is fast increasing [59], High Damping Rubber Bearings (HDRBs) still represent a viable choice [60].

The analyses presented in this part are placed in the contest of the Network of the University Laboratories of Seismic Engineering (Reluis) project. It is an inter-university consortium that aims to co-ordinate the activities of the University Laboratories of Seismic and Structural Engineering in the field of Seismic and Structural Engineering in accordance with the specific national and international research programs. In the contest of the research activities regarding seismic isolation, several analyses on a case-study RC bridge have been carried out. The main objectives were:

- definition of rapid design rules for the isolation system with elastomeric devices to be adopted for the seismic upgrading of bridges, in order to give a useful tool for an initial evaluation of the geometric and mechanical characteristics of the devices.
- Verification of the effectiveness of the combination between purely horizontal time/history analyses (with accelerograms) and purely vertical linear dynamic analysis (carried out with spectrum) with respect to the reference case with simultaneous actions (accelerograms simultaneously applied both in the horizontal and vertical direction), assuming the average values of the mechanical properties of the devices.
- Investigation of the effects, in terms of displacements, of the variability of the shear modulus of the rubber material of HDRBs. Thus, to provide coefficients to be applied to the displacement response parameters obtained using the mean value of the shear modulus, including the Upper and Lower Bound coefficients, which are useful for design purposes.

The results of the above-described objectives are reported in the chapters 16, 18 and 19, respectively.

15

The case-study RC bridge

15.1 Description of the case-study RC bridge

The considered bridge is characterised by a continuous deck over four equal spans, for a total length L = 180 m (Figure 15.1). The three piers are characterised by different heights, equal to 8 m, 20 m and 10 m (Figure 15.2). The configuration is thus symmetric with reference to the longitudinal direction, while it is slightly eccentric with reference to the transversal direction. The RC caisson deck is 11.50 m wide and 0.50 m thick (Figure 15.3a), whilst the RC piers have a squared cellular cross-section with side length equal to 1.75 m and thickness equal to 0.30 m (Figure 15.3b). On the top of the piers there are RC prismatic transversal elements with a rectangular cross-section of 2.00 m x 1.90 m and a length of 6.40 m, which provide the support base for the isolators. There are two isolators for each pier and for the two abutments, for a total number of ten isolators. Concrete class is C40/50. The bridge is supposed to be located in L'Aquila, Italy. The weight of the RC structural elements is 37723 kN, whilst the weight of the non structural elements (slope screed and bituminous layers, such as waterproofing, binder and wear layer) is 10624 kN. Consequently, the total dead load of the bridge is 48347 kN. The static loads acting on the bride are reported in the following table.

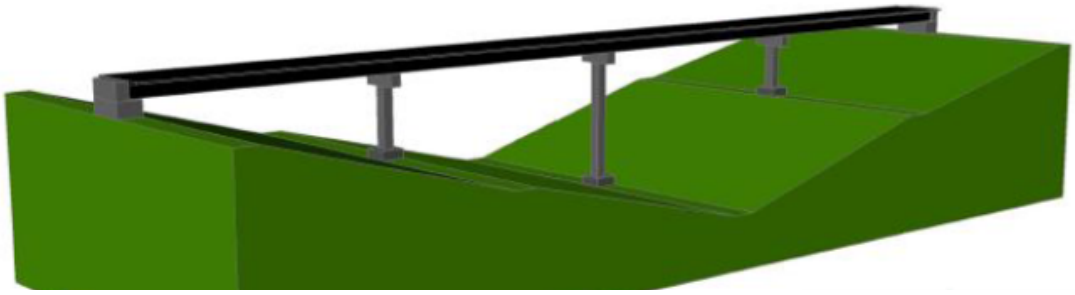

Figure 15.1: 3D sketch of the case-study bridge

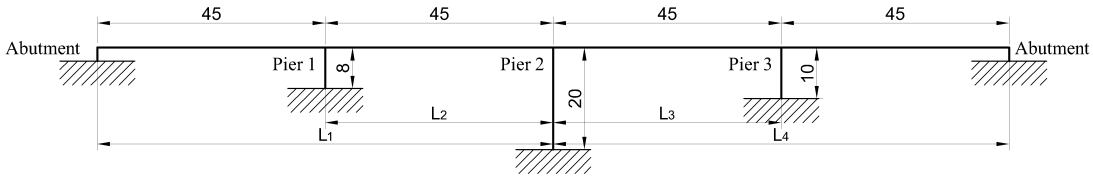

Figure 15.2: Schematised longitudinal view of the case-study bridge

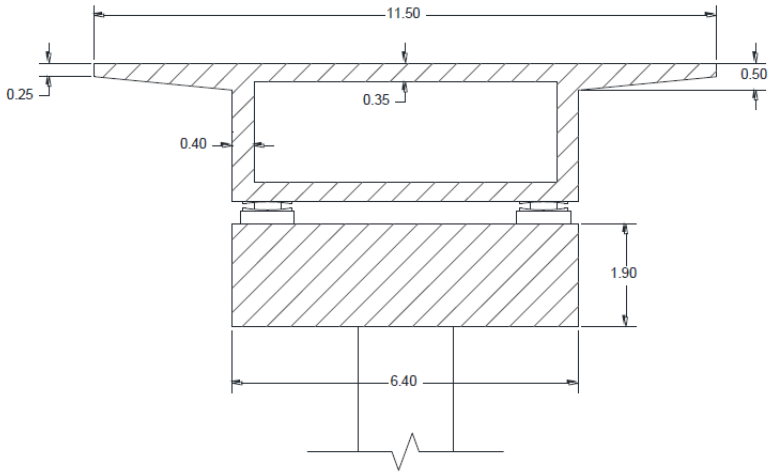

(a) Cross-section of the caisson

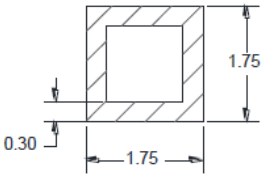

(b) Cross-section of the three RC piers

Figure 15.3: Cross-sections of the caisson and the piers

The three piers are characterized by the following capacity curves, which are valid in both the directions (the piers have a squared cross-section).

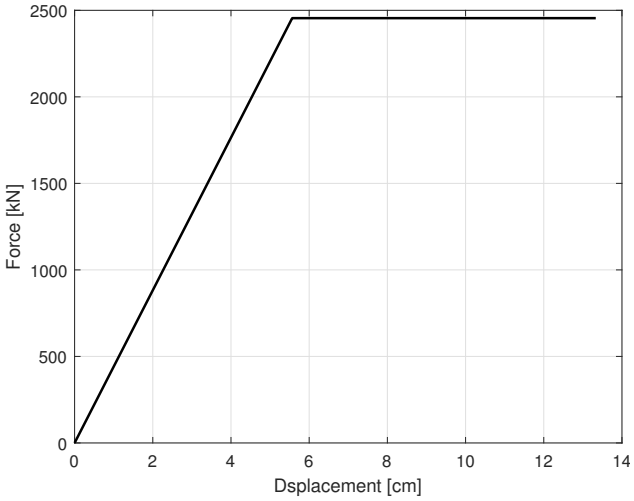

(a) Pier 1 - 8m high

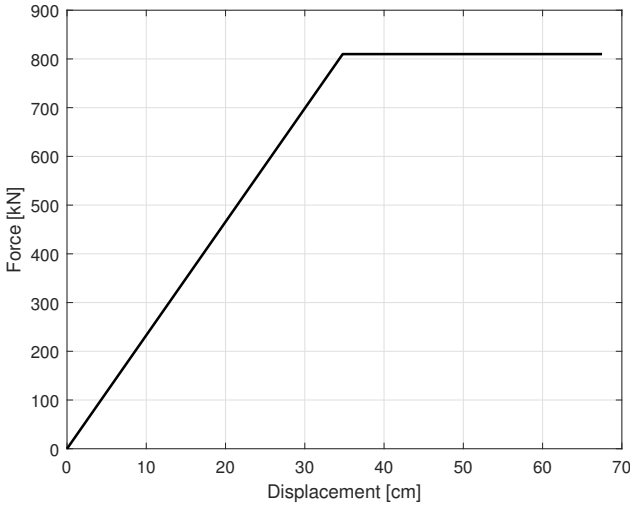

(b) Pier 2 - 20m high

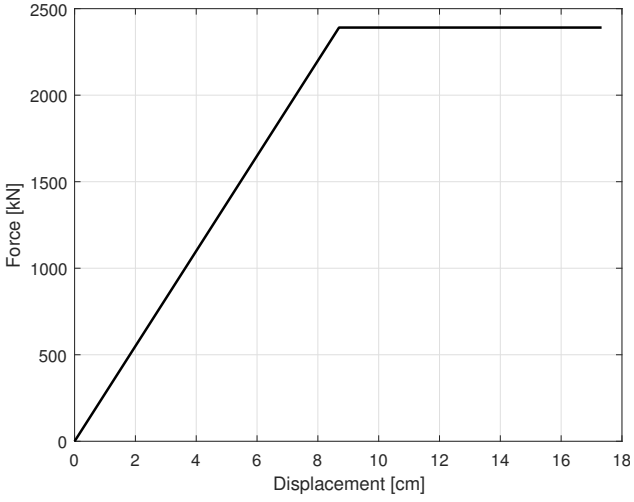

(c) Pier 3 - 10m high

Figure 15.4: Capacity curves of the piers

15.2 Seismic input

The pseudo-acceleration elastic response spectrum of the horizontal component of the earthquake input corresponding to the site of L'Aquila (Italy), to a nominal life of 100 years, to a construction class IV (strategic bridge), to a reference period of the seismic action of 200 years, to the seismic Collapse Limit State (earthquake return period equal to 2475 years), and to a damping ratio equal to 5% is reported in Figure 15.5, according to the seismic input definition provided by the Italian code [11]. The seismic actions have been considered both in horizontal and vertical directions. Peak ground acceleration is equal to 0.459g ans 0.419, respectively. The maximum (plateau) spectral acceleration is equal to 1.103g and 0.879g respectively.

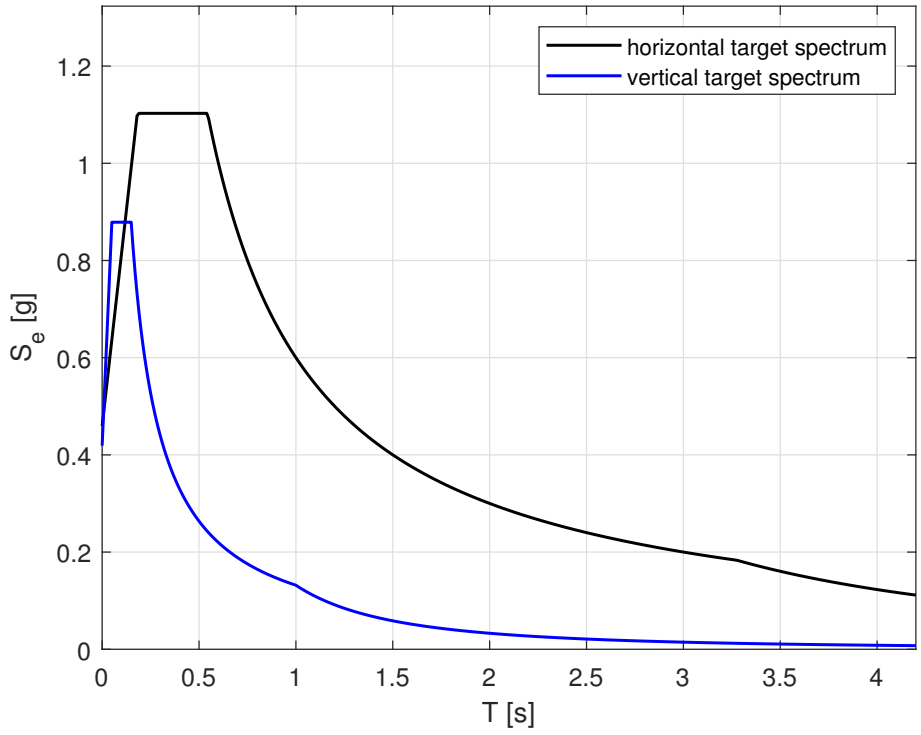

Figure 15.5: Horizontal and vertical elastic spectra

Table 15.1 summarizes the dependent and independent spectral parameters adopted for the definition of the elastic spectra.

Table 15.1: Spectral parameters for L'Aquila site

Dependent spectral parameter	**Horizontal independent spectral parameter**	**Vertical independent spectral parameter**
$a_g = 0.419g$	$S_s = 1.0966$	$S_s = 1.$
$F_o = 2.458$	$S_t = 1$	$S_t = 1$

$T_c^* = 0.384s$	$C_c = 1.451$	
$F_v = 2.097$	$T_B = 0.184s$	$T_B = 0.05s$
	$T_C = 0.544s$	$T_C = 0.15s$
	$T_D = 3.276s$	$T_D = 1s$

where a_g is the peak ground acceleration, F_o is the maximum value of the amplification factor of the horizontal acceleration spectrum (while F_v is for the vertical one), T_c^* is the reference value for determining the beginning of the period of the constant spectral velocity branch of the acceleration spectrum, S_s is the stratigraphic amplification coefficient, S_t is the topographic amplification coefficient, T_B is the lower limit of the period of the constant spectral acceleration branch, T_C is the upper limit of the period of the constant spectral acceleration branch and T_D is the value defining the beginning of the constant displacement response range of the spectrum.

To perform time-history analyses seven natural earthquakes have been chosen in such a way as to result compatible with the 5% damped elastic spectrum, i.e. the mean spectrum given by the seven spectra of the seismic records (grey lines in Figure 15.10) is between 0.95 and 1.30 times (blue lines) the target spectrum (green line), in the period range indicated by the code (red lines). Clearly, in order to achieve the compatibility required by the code scale factors on the seismic events can be applied. The earthquakes that have been chosen respect the compatibility both in the horizontal and vertical directions of the seismic input. Figure 15.6 and Figure 15.8 report the seven natural earthquakes in the horizontal and vertical directions (together with their respective elastic spectrum) that have been chosen, emphasizing the Peak Ground Acceleration (PGA).

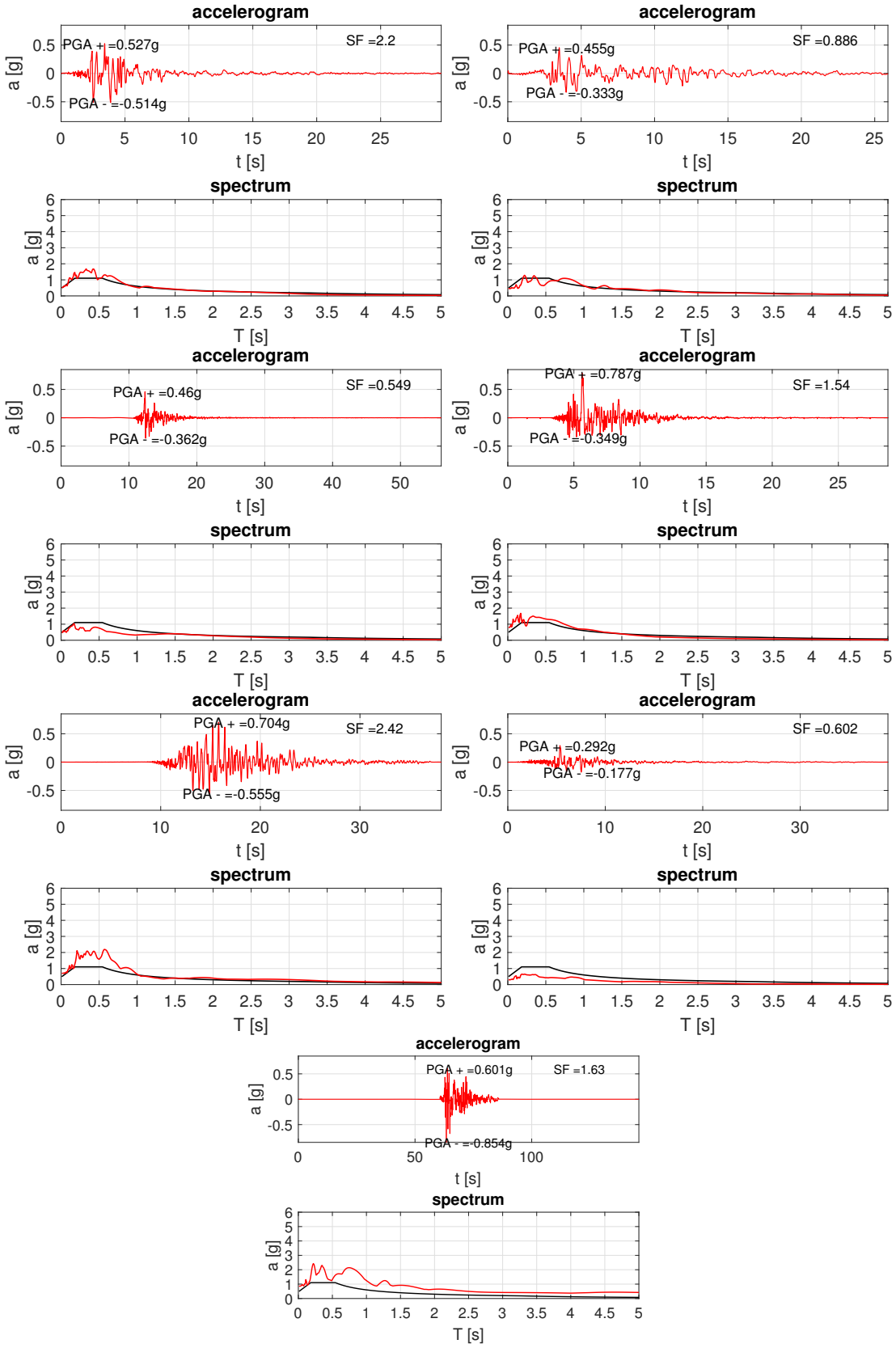

Figure 15.6: Horizontal accelerograms and their corresponding spectra

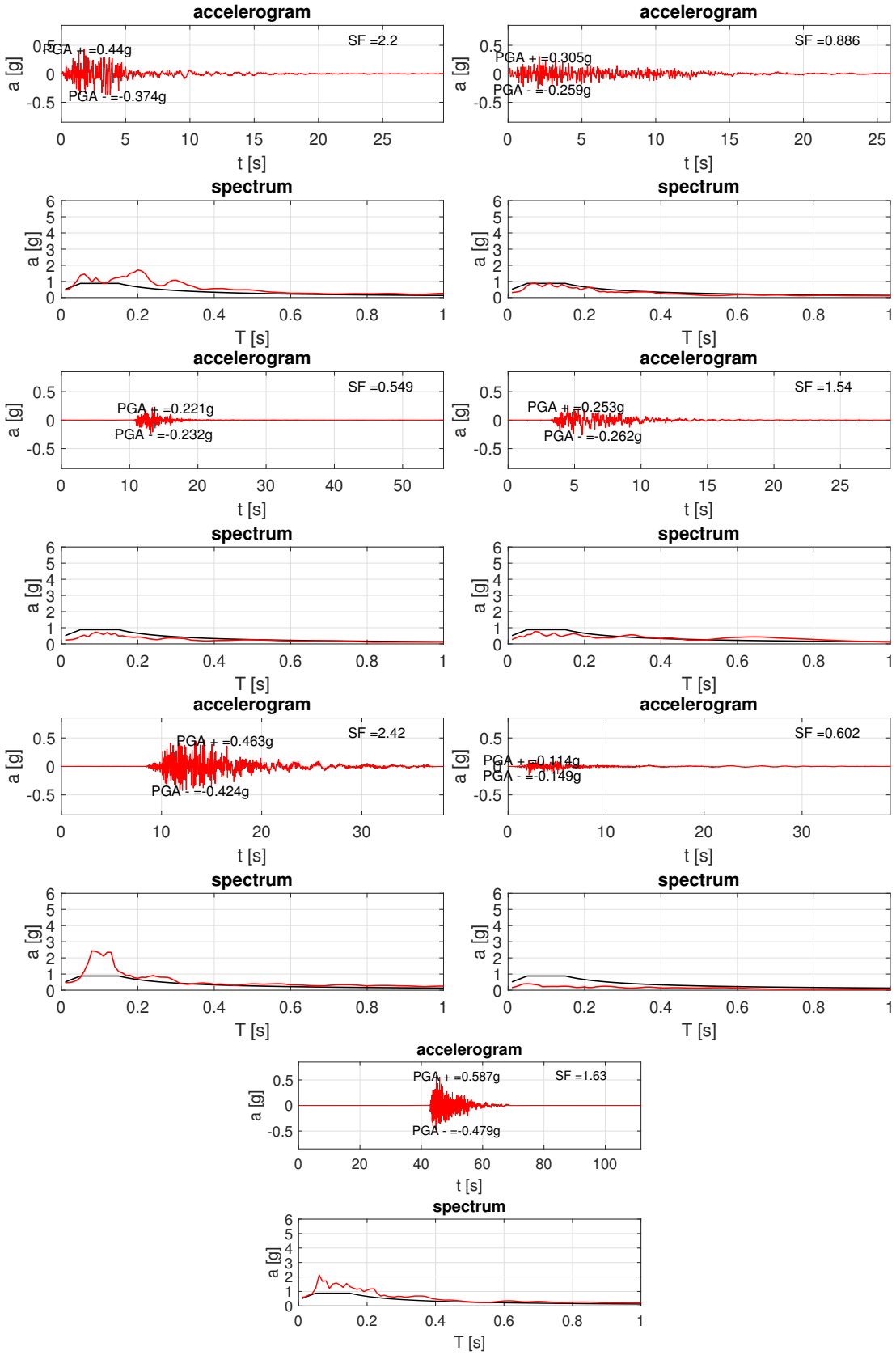

Figure 15.8: Vertical accelerograms and their corresponding spectra

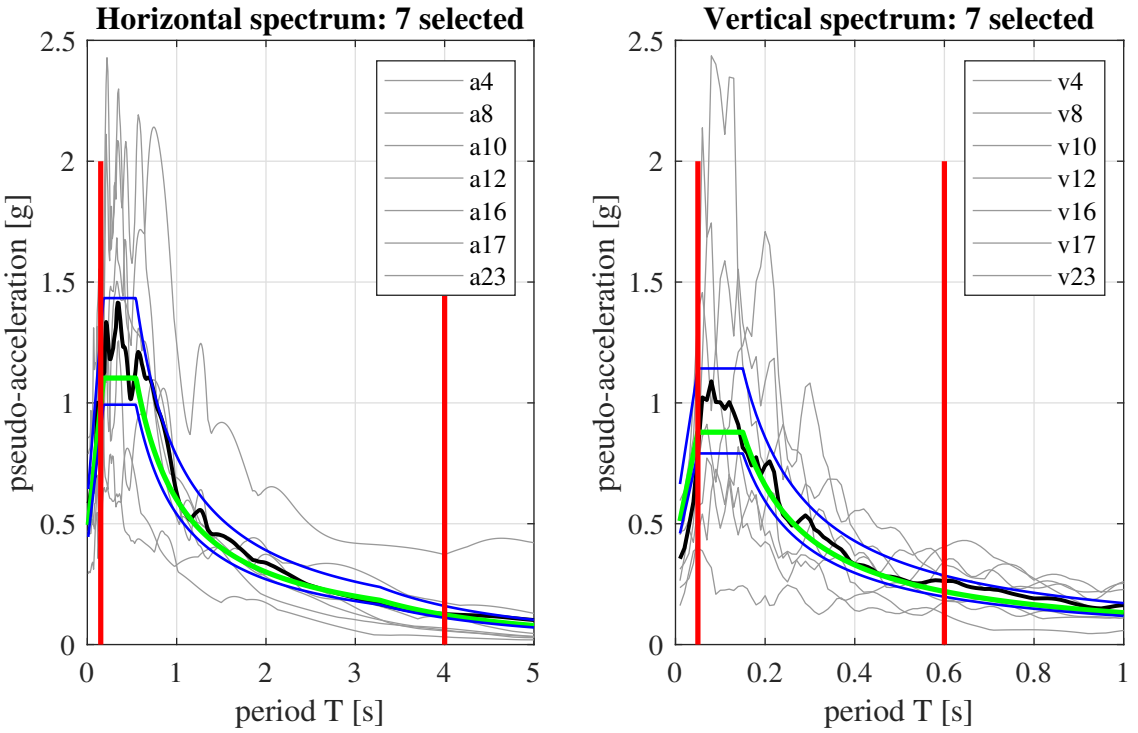

Figure 15.10: Compatibility of the seven spectra in both the horizontal and vertical direction in the range that is of interest for the case-study bridge

15.3 Models of the isolated bridge

Different models are possible for the isolated bridge depending on the objective of the analysis: (i) a Single-Degree-Of-Freedom (SDOF) idealisation, representing the deck mass connected through the lateral stiffness of the isolation system to the substructures (assumed as fixed); (ii) minimal systems, that describe the behaviour of the deck and the piers by means of a reduced number of degrees of freedom [56]; (iii) Finite Element models, that describe the bridge behaviour by means of several nodes and beam and/or shell elements. The first one is usually sufficient for the dimensioning of the isolation system. The second one allows to perform time-history analyses with lower computational effort than the third one. In the minimal systems, the masses that define the degrees of freedom in the equations of motion are the mass of the deck and the masses of each half pier (the remaining parts are assumed to be directly transferred to the ground base).

15.3.1 Minimal systems

The minimal systems used for the evaluation of the seismic response of the bridge along the two directions (u referring to longitudinal displacements and v referring to transversal displacements) are schematized in Figure 15.11 and Figure 15.12, respec-

tively.

- along the (symmetric) longitudinal direction, the minimal system is composed of four degrees of freedom: the displacement of the deck (u_{deck}) and the three displacements of the top of the piers (u_{pier1}, u_{pier2}, u_{pier3});
- along the (slightly eccentric) transversal direction, the minimal system is composed of five degrees of freedom: the displacement of the deck (v_{deck}), the three displacements of the top of the piers (v_{pier1}, v_{pier2}, v_{pier3}), and the in-plane rotation of the deck (ϕ_{deck}).

The equations of motion of the minimal systems in the time domain, along the two directions assume the expressions reported in Eqs.15.1 and 15.2, respectively.

Longitudinal direction

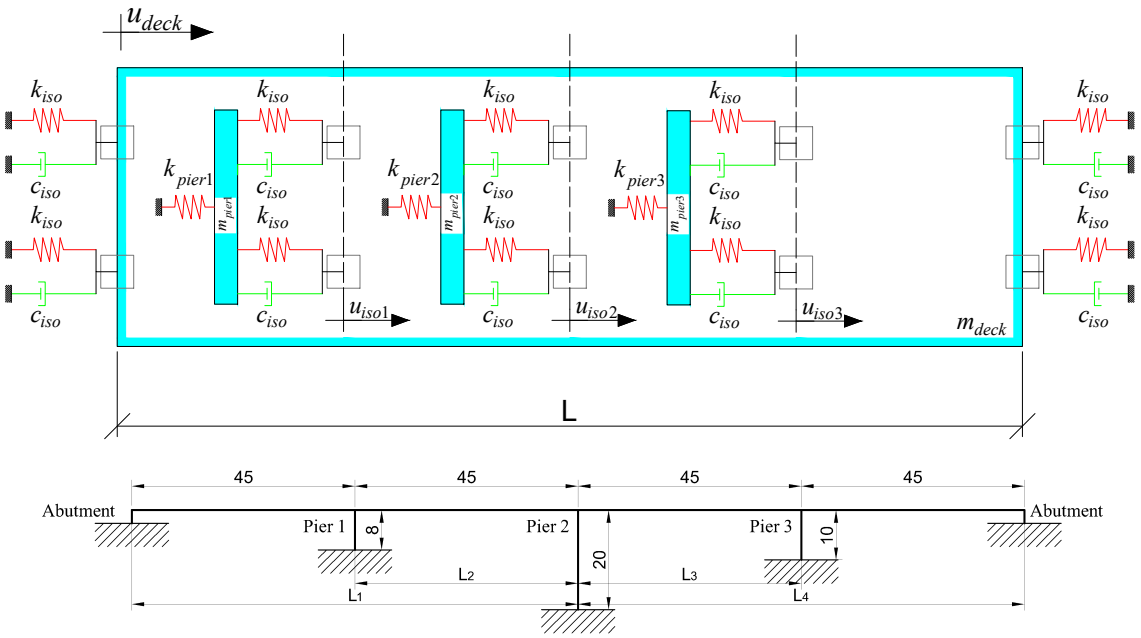

Figure 15.11: Schematization of the minimal system along the longitudinal direction

$$
\begin{aligned}
[M]\{\ddot{u}\} + [C]\{\dot{u}\} + [K]\{u\} &= p(t) \\
\begin{bmatrix} m_{deck} & 0 & 0 & 0 \\ 0 & m_{pier_1} & 0 & 0 \\ 0 & 0 & m_{pier_2} & 0 \\ 0 & 0 & 0 & m_{pier_3} \end{bmatrix} &\begin{bmatrix} \ddot{u}_{deck} \\ \ddot{u}_{pier_1} \\ \ddot{u}_{pier_2} \\ \ddot{u}_{pier_3} \end{bmatrix} + \\
\begin{bmatrix} n_{iso} \cdot c_{iso} & -2c_{iso} & -2c_{iso} & -2c_{iso} \\ -2c_{iso} & 2c_{iso} & 0 & 0 \\ -2c_{iso} & 0 & 2c_{iso} & 0 \\ -2c_{iso} & 0 & 0 & 2c_{iso} \end{bmatrix} &\begin{bmatrix} \dot{u}_{deck} \\ \dot{u}_{pier_1} \\ \dot{u}_{pier_2} \\ \dot{u}_{pier_3} \end{bmatrix} + \\
\begin{bmatrix} n_{iso} \cdot k_{iso} & -2k_{iso} & -2k_{iso} & -2k_{iso} \\ -2k_{iso} & 2k_{iso} + k_{pier_1} & 0 & 0 \\ -2k_{iso} & 0 & 2k_{iso} + k_{pier_2} & 0 \\ -2k_{iso} & 0 & 0 & 2k_{iso} + k_{pier_3} \end{bmatrix} &\begin{bmatrix} u_{deck} \\ u_{pier_1} \\ u_{pier_2} \\ u_{pier_3} \end{bmatrix} = \begin{bmatrix} 1 \\ 1 \\ 1 \\ 1 \\ 0 \end{bmatrix} p(t)
\end{aligned}
\tag{15.1}
$$

where the vectors $\ddot{u}$, $\dot{u}$, u and $p(t)$ denote the horizontal acceleration of the DOFS along the longitudinal direction, the horizontal velocity of the DOFS along the longitudinal direction, the horizontal displacements of the DOFS along the longitudinal direction and the external excitation along the longitudinal direction, respectively.

Transversal direction

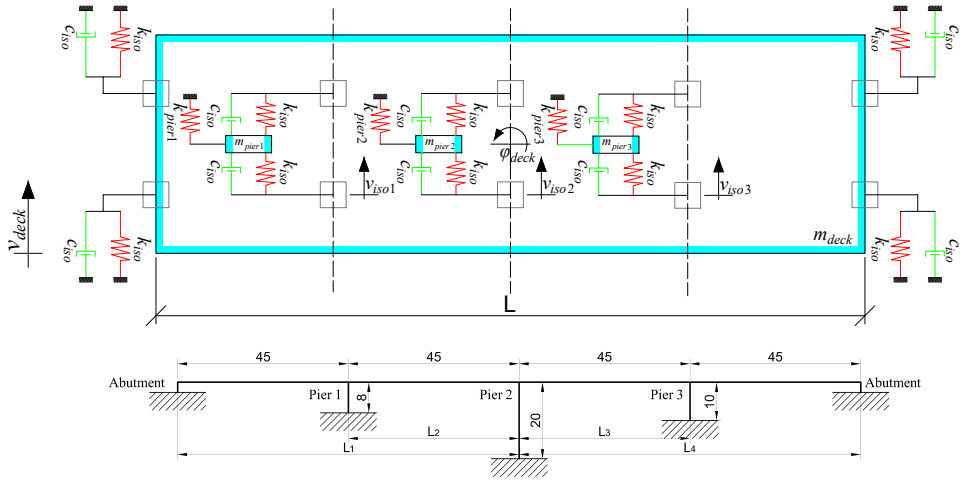

Figure 15.12: Schematization of the minimal system along the transversal direction

$$[M]\{\ddot{v}\} + [C]\{\dot{v}\} + [K]\{v\} = p(t)$$

$$\begin{bmatrix} m_{deck} & 0 & 0 & 0 & 0 & \\ 0 & m_{pier_1} & 0 & 0 & 0 & \\ 0 & 0 & m_{pier_2} & 0 & 0 & \\ 0 & 0 & 0 & m_{pier_3} & 0 & \\ 0 & 0 & 0 & 0 & 0 & m_{rot} \end{bmatrix} \begin{bmatrix} \ddot{v}_{deck} \\ \ddot{v}_{pier_1} \\ \ddot{v}_{pier_2} \\ \ddot{v}_{pier_3} \\ \ddot{\phi}_{deck} \end{bmatrix} +$$

$$\begin{bmatrix} n_{iso} \cdot c_{iso} & -2c_{iso} & -2c_{iso} & -2c_{iso} & \sum_{i=1}^{5} 2c_{iso} \cdot L_i \\ -2c_{iso} & 2c_{iso} & 0 & 0 & 2c_{iso} \cdot L_2 \\ -2c_{iso} & 0 & 0 & 0 & 2c_{iso} \cdot L_3 \\ -2c_{iso} & 0 & 0 & 0 & 2c_{iso} \cdot L_4 \\ \sum_{i=1}^{5} 2c_{iso} \cdot L_i & 2c_{iso} \cdot L_1 & 2c_{iso} \cdot L_2 & 2c_{iso} \cdot L_3 & \sum_{i=1}^{5} 2c_{iso} \cdot L_i^2 \end{bmatrix} \begin{bmatrix} \dot{v}_{deck} \\ \dot{v}_{pier_1} \\ \dot{v}_{pier_2} \\ \dot{v}_{pier_3} \\ \dot{\phi}_{deck} \end{bmatrix} +$$

$$\begin{bmatrix} n_{iso} \cdot k_{iso} & -2k_{iso} & -2k_{iso} & -2k_{iso} & \sum_{i=1}^{5} 2k_{iso} \cdot l_i \\ -2k_{iso} & 2k_{iso} + k_{pier_1} & 0 & 0 & 2k_{iso} \cdot L_2 \\ -2k_{iso} & 0 & 2k_{iso} + k_{pier_2} & 0 & 2k_{iso} \cdot L_3 \\ -2k_{iso} & 0 & 0 & 2k_{iso} + k_{pier_3} & 2k_{iso} \cdot L_4 \\ \sum_{i=1}^{5} 2k_{iso} \cdot L_i & 2k_{iso} \cdot L_2 & 2k_{iso} \cdot L_3 & 2k_{iso} \cdot L_4 & \sum_{i=1}^{5} 2k_{iso} \cdot L_i^2 \end{bmatrix} \begin{bmatrix} v_{deck} \\ v_{pier_1} \\ v_{pier_2} \\ v_{pier_3} \\ \phi_{deck} \end{bmatrix} = \begin{bmatrix} 1 \\ 1 \\ 1 \\ 1 \end{bmatrix} p(t)$$

$$\text{where: } L_i = \begin{bmatrix} L_1 \\ L_2 \\ L_3 \\ L_4 \\ L_5 \end{bmatrix} = \begin{bmatrix} 90mm \\ 45m \\ 0m \\ 45m \\ 90m \end{bmatrix} \tag{15.2}$$

where the vectors $\ddot{v}$, $\dot{v}$, v and $p(t)$ denote the horizontal acceleration of the DOFS along the transversal direction, the horizontal velocity of the DOFS along the transversal direction, the horizontal displacements of the DOFS along the transversal direction and the external excitation along the transversal direction, respectively. The vector L_i represents the longitudinal distances between the isolators and the centre of the deck. The rotational mass m_{rot} has been evaluated as the sum of the rotational masses associated to the portions of the mass deck that can be assumed transferred to each couple of isolators. It can be evaluated according to the following formula:

$$m_{rot} = \frac{m_{deck}}{8} \cdot L_1^2 + 2 \cdot \frac{m_{deck}}{8} \cdot L_2^2 + 2 \cdot \frac{m_{deck}}{8} \cdot L_3^2 + \frac{m_{deck}}{8} \cdot L_4^2 \tag{15.3}$$

The systems of Eqs. 15.1 and 15.2 can be solved by means of the Newmark's method (box che lo descrive) adopting constant mean acceleration hypothesis between two consecutive steps of the method. In fact, this implies that the method is stable for any Δt, no matter how large, and the accuracy depends only on the size of the Δt [61].

15.3.2 Finite element model

The finite element model has been created in Sap2000[1] and concerns frame (often indicated simply as beam) elements for the structural elements, i.e. deck and piers, and link elements for the isolator devices. In this regard, a frame element, which is modelled as a straight line connecting two points, uses a three-dimensional beam formulation that includes the effects of biaxial bending, torsion, axial deformation and biaxial shear deformations. A link element is assumed to be composed of six separate "springs" one for each of six deformational degrees of freedom (axial, shear, torsion, and pure bending) that are independent (the deformation in one degree of freedom does not affect the behaviour of the others). For the High Damping Rubber Bearing devices, adopted in this study, the springs representing the two shear deformations have plasticity properties (see Figure 15.13) while the remaining four deformations have linear stiffness properties. The plasticity model is based on the hysteretic behavior proposed by [62] and [63], and recommended for base isolation analysis by [64].

Since the vertical dynamic behaviour (vertical modal shapes) strongly depends on the deck configuration, its discretization is characterized by 45 beam elements for each span (which means 1 m long beam elements). The piers have been modelled by one single element, in fact, the horizontal behaviour of the bridge is separated respect to that of the deck due to the introduction of the isolators. The identified isolator devices have been modelled by means of link elements that describe their constitutive law in terms of force-displacement relationship (the isolator have been identified with the simplified procedure

[1] CSI, "SAP2000 Integrated Software for Structural Analysis and Design", Computers and Structures Inc., Berkeley, California.

that is described in the following section). In this regard, the typical experimental behaviour of HDRB devices is characterized by non-linear force-displacement behaviour that shows reduced stiffness following the first higher one. However, this behaviour is well represented by an equivalent bi-linear model (see Figure 15.13). Nevertheless, this behaviour is often simplified with an equivalent linear one characterized by a stiffness identified through a mean design displacement. However, in the fem analyses both the constitutive laws of the isolator devices have been implemented. It should be noted that the obtained numerical results are always affected by model (epistemic) uncertainties that lead to unavoidable discrepancies between the theoretical predictions, either analytical or numerical, and the actual response of the structure (especially in the case of non-linear models [65]) which hence should be considered in design applications.

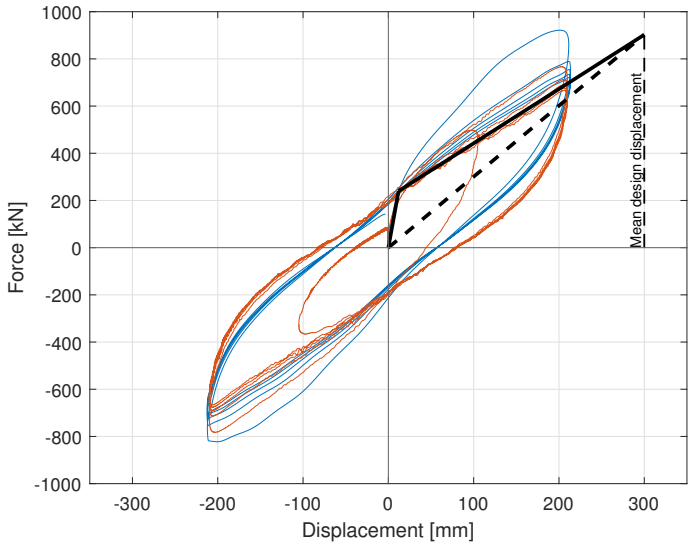

Figure 15.13: Force-displacement relationship of the SI-N 1000/210

Figure 15.14 shows some view of the finite element model of the isolated bridge.

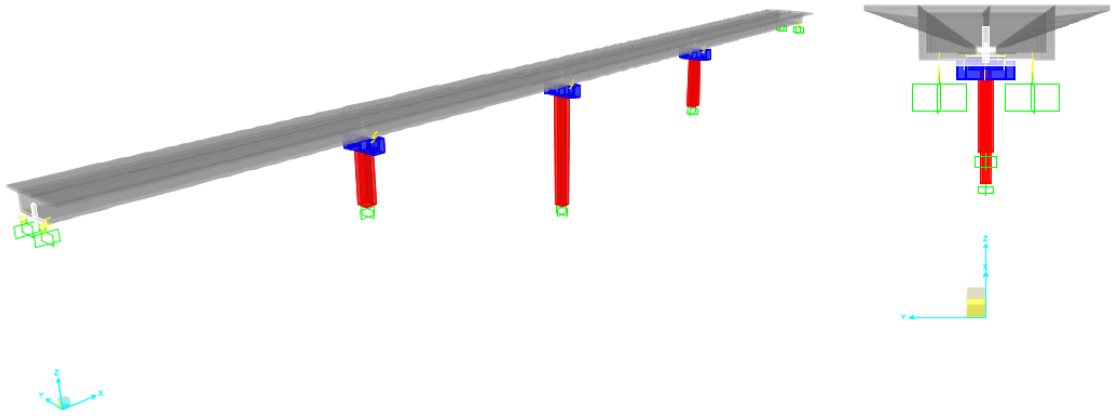

Figure 15.14: Finite element model of the isolated bridge

In the following are reported the first three modal shapes obtained from the model. They are characterized by longitudinal ($2.915Hz$), transversal ($2.836Hz$) and torsional ($2.076Hz$) deformed shapes, respectively. In addition they result to be completely uncoupled.

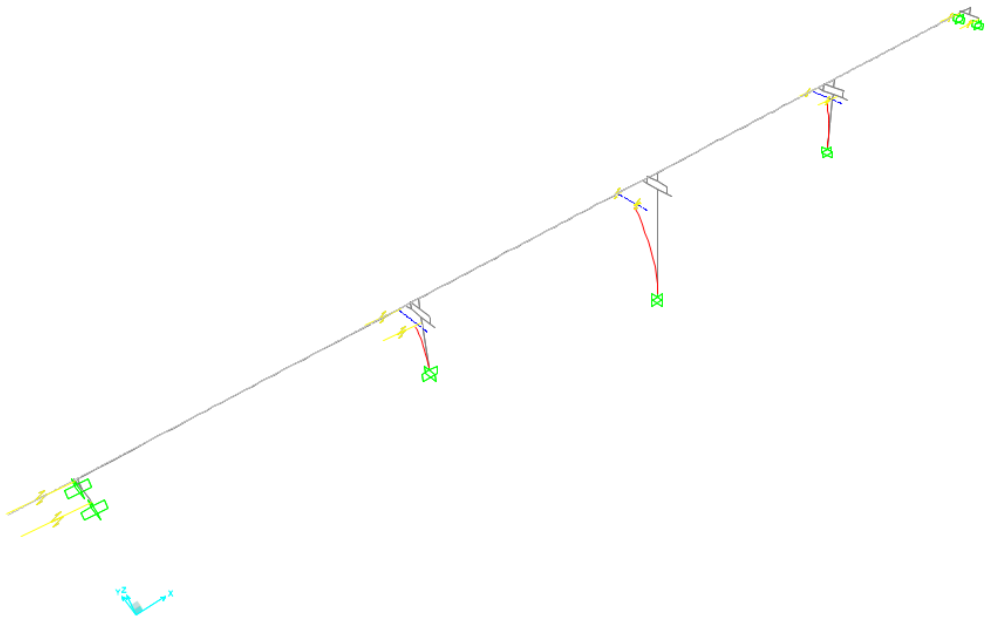

Figure 15.15: Deformed shape of the first mode $2.915Hz$

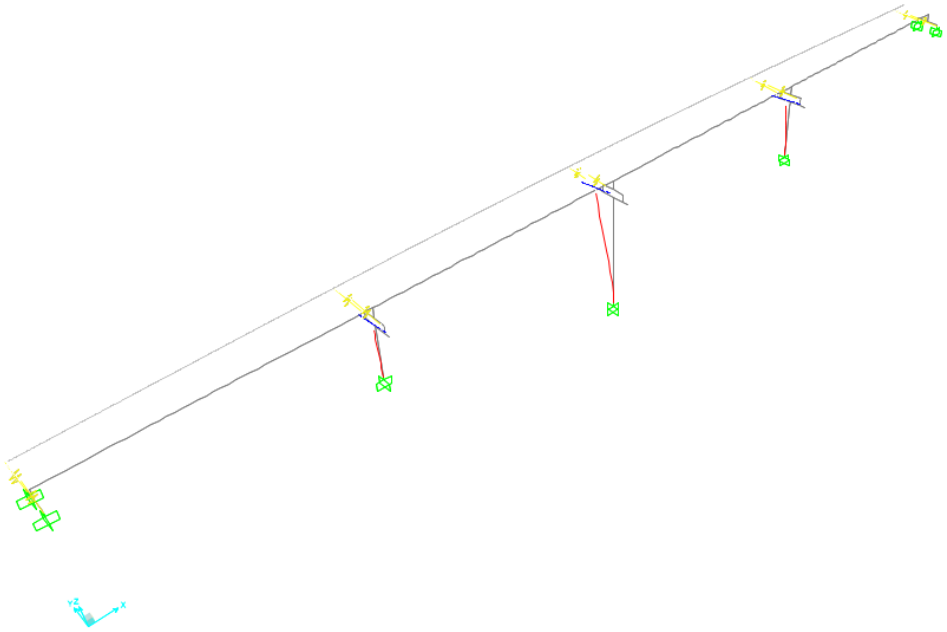

Figure 15.16: Deformed shape of the second mode $2.836Hz$

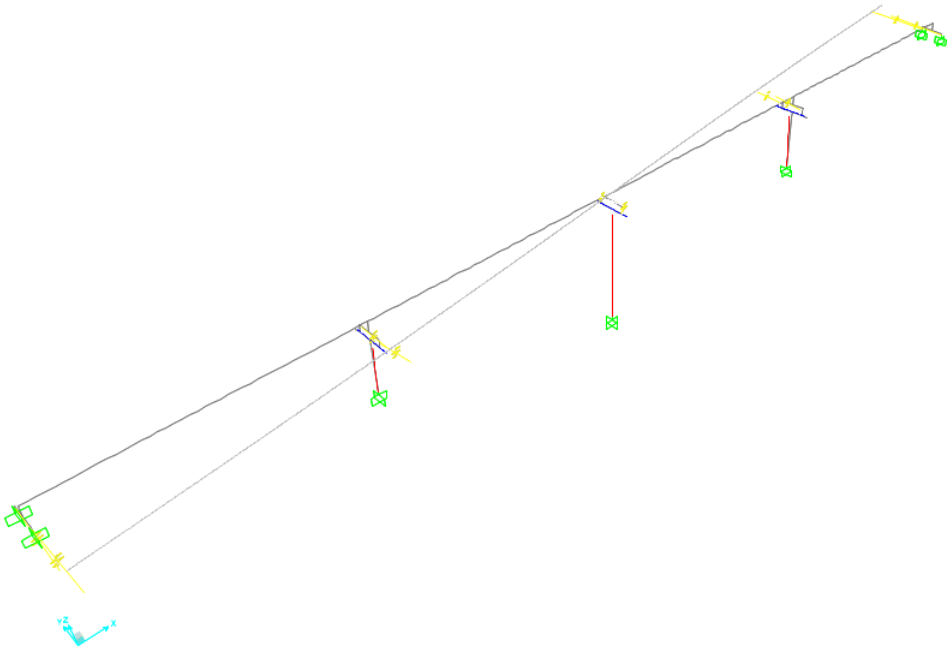

Figure 15.17: Deformed shape of the third mode $2.076Hz$

16

Identification of HDRB isolators

16.1 The simplified procedure

The isolation system (to be placed between the deck and the substructures) has been pre-identified according to a simplified procedure based on the SDOF idealization, in which the degree of freedom is represented by the horizontal displacement of the deck. The SDOF model consists of the mass of the deck (m_{deck}) concentrated at the deck level. The stiffness ($k_{iso,tot}$) and the damping coefficient ($c_{iso,tot}$) are provided by the isolation system, which is made of ten devices. Since they work in a parallel system, the values of the stiffness and the damping coefficient of the equivalent SDOF model are given by the sum of the stiffness values and the damping coefficient values of the ten isolators, respectively.

The simplified procedure is based on the following hypotheses: (i) the deck is rigid in both horizontal (longitudinal and transversal) directions, (ii) the piers are rigid in the vertical (axial) direction, (iii) the target lateral deformation γ_{iso} of the isolator is imposed to be equal to the height h_{iso} of the isolator itself (i.e. shear deformation $\gamma_{iso} = d_{iso}/h_{iso}$ equal to 100%, where d_{iso} is the displacement of the isolator), (iv) the shear modulus of the rubber material that governs the lateral stiffness of the isolator is assumed in the range 0.7-1.0 MPa (this corresponds to a normal rubber and to a damping ratio ξ_{iso} of the isolation system around 10%), (v) the total damping coefficient provided by the isolation system is evaluated as: $c_{iso,tot} = 2 \cdot m_{desk} \cdot \omega_{iso} \cdot \xi_{iso}$ (where ω_{iso} is the fundamental circular frequency of the isolated bridge and ξ_{iso} is the damping ratio), (vi) the isolators have radial symmetry (i.e. the procedure keeps its validity along the two horizontal directions). The procedure is summarized in the following steps:

1. Choice of the target period T_{iso} for the isolated bridge, typically in the range 2.5-3.5 s.

2. Evaluation of the spectral acceleration corresponding to the target period: $S_a(T_{iso})$. Note that it has to be evaluated on the 10%-damped elastic spectrum since an isolation system usually provides a damping ratio ξ_{iso} of around 10%.

3. Evaluation of the spectral displacement:

$$S_d(T_{iso}) = \frac{S_a(T_{iso})}{\omega_{iso}^2} = S_a(T_{iso} \cdot (T_{iso}/2\pi)^2 \tag{16.1}$$

Then, assuming that $\gamma_{iso} = d_{iso}/h_{iso} = 100\%$ leads to:

$$h_{iso} = d_{iso} = S_d(T_{iso}) \tag{16.2}$$

4. Choice of the diameter of the isolator in order to avoid instability phenomena. The ratio between diameter D_{iso} and height h_{iso} should be larger than 2.0 [66],[59]. Therefore a typical relationship is:

$$D_{iso} = 2.5 \cdot h_{iso} \tag{16.3}$$

5. Calculation of the lateral stiffness of the isolator k_{iso} according to the following formula.

$$k_{iso} = \frac{m_{deck} \cdot \omega_{iso}^2}{n_{iso}} \tag{16.4}$$

where n_{iso} is the total number of isolators.

6. check that the shear modulus G falls within the assumed range (0.7-1.0 MPa):

$$G = \frac{4K_{iso}\chi_v h_{iso}}{\pi D_{iso}^2} \tag{16.5}$$

where χ_v represents the shear shape factor. If the hypothesis is not satisfied, then *G* is taken equal to 1.0 MPa and the diameter of the isolator is calculated as:

$$\overline{D} = 2\sqrt{\frac{K_{iso}\chi_v h_{iso}}{\pi G(=1MPa)}} \tag{16.6}$$

7. Check that the isolator shear displacement roughly respects the assumption $\gamma_{iso} = d_{iso}/h_{iso} = 100\%$ (made in Step 3).

8. Evaluation of the maximum vertical axial force on the isolators. They have to carry out the function of support during the entire life of the bridge both in static conditions, with reference to the Ultimate Limit State (ULS), and in seismic conditions, with reference to the Collapse Limit State (CLS). The axial force can be evaluated either according to tributary areas afferent to each isolator or by means of a numerical model.

9. Check that the isolators satisfy the two conditions: in terms of target lateral stiffness k_{iso} (Steps 1-7) and in terms of axial force capacity (Step 8). If this latter is not not satisfied, then the geometric characteristics of the isolators should be updated.

The procedure is summarized in Figure 16.1.

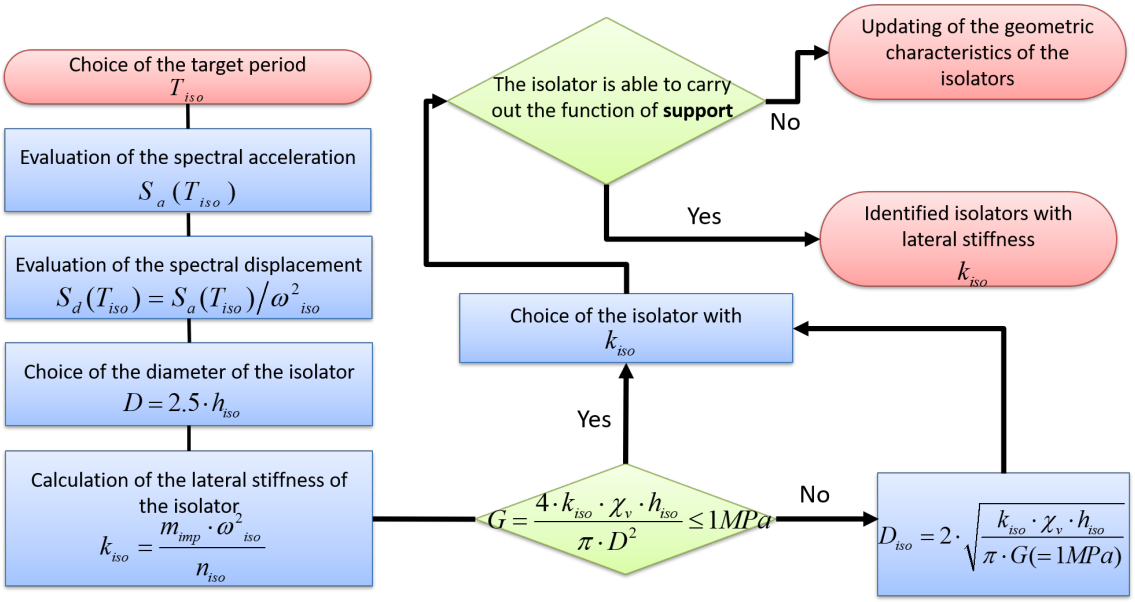

Figure 16.1: Flowchart of the simplified procedure for the identification of HDRBs isolator

16.2 Identification of the isolators for the case-study bridge

The procedure has been applied to the case-study bridge. The following data have been adopted: the horizontal elastic spectrum represented in Figure 15.5 reduced to account for a damping ratio of 10%, $m_{deck} = 4717.4\ t$, $T_{iso} = 3.25\ s$, $n_{iso} = 10$. The following outcomes have been obtained: $h_{iso} \simeq 400\ mm$, $D_{iso} \simeq 1000\ mm$, $k_{iso} = 1.763$ *kN/mm*, $G = 1.00$ *MPa*, $c_{iso} = 182.4$ *kN m/s*. However, the isolator obtained following Steps 1-7 does not satisfy the axial force capacity condition (Step 8). Therefore, the geometric charactersitics have been slightly changed to meet this condition (the height has been reduced). The following final properties for each single isolator have been thus identified: $h_{iso} = 326\ mm$, $D_{iso} = 1000\ mm$, $k_{iso} = 2.99$ *kN/mm*, $G = 0.8$ *MPa*, $c_{iso} = 202$ *kN m/s*, leading to $T_{iso} = 2.50\ s$ for the SDOF idealisation, to $T_{iso} = 2.78\ s$ for the minimal system along the longitudinal direction (roughly including the flexibility of the three piers), and to $T_{iso} = 2.92\ s$ for the more refined FE model (also including the flexibility of the deck and a better representation of the piers behaviour).

Table 16.1 reports the results of the procedure applied in longitudinal direction for a target period of the isolated bridge in the range 2.5 s and 3.0 s. In addition, it also reports the effective period of the bridge resulting from a modal analysis of the corresponding minimal system, which has been calibrated by means of a modal analysis through the finite element model, considering isolators characterized by the stiffness resulting from the simplified procedure. In fact, in the simplified procedure the stiffness of the piers is not considered. On the other hand, the minimal system with four degrees of freedom is then more flexible and provides a higher first period of vibration.

Table 16.1: Output of the simplified procedure

$T_{target}[s]$	$T_{effettive}[s]$	$k_{iso}[kN/m]$	$D_{iso}[cm]$	$G[MPa]$	$h_{iso}[cm]$
2.50	2.82	2979.79	112.72	1	30.44
2.55	2.87	2864.08	111.61	1	31.05
2.60	2.92	2754.98	110.53	1	31.66
2.65	2.97	2652.00	109.48	1	32.27
2.70	3.02	2554.69	108.46	1	32.88
2.75	3.07	2462.63	107.47	1	33.49
2.80	3.12	2375.46	106.51	1	34.10
2.85	3.16	2292.85	105.57	1	34.70
2.90	3.21	2214.47	104.65	1	35.31
2.95	3.26	2140.04	103.76	1	35.92
3.00	3.31	2069.30	102.90	1	36.53
3.05	3.36	2002.01	102.05	1	37.14
3.10	3.41	1937.95	101.22	1	37.75
3.15	3.46	1876.91	100.42	1	38.36
3.20	3.51	1818.72	99.63	1	38.97
3.25	3.56	1763.19	98.94	1	39.58
3.30	3.61	1710.16	99.73	0.96	39.89
3.35	3.66	1659.49	99.73	0.93	39.89
3.40	3.70	1611.04	99.73	0.90	39.89
3.45	3.75	1564.69	99.73	0.88	39.89
3.50	3.80	1520.30	99.73	0.85	39.89

Therefore, according to the results of the procedure the choice of the isolator stiffness k_{isdo} associated to a certain target period, leads to a higher effective period due to the presence of piers in the system. However, the goal of the procedure is to easily provide a rapid idea of the stiffness that is required to the isolator devises in order to achieve a certain period of vibration.

As described above, in the steps of the simplified procedure, the maximum normal stress acting on the elastomeric isolators must first be checked. This value, together with the horizontal translation stiffness value required for the isolators allows to identify the most suitable device among those available on the market. With referring to: static loads G_1 and G_2, traffic loads $Q_{traffic}$, wind load Q_{wind}, breaking load Q_{brak} and seismic load E, the load combinations at the ultimate limit states assume the following expressions:

$$
\begin{aligned}
&ULS_1\text{: } \gamma_{G_1}G_1 + \gamma_{G_2}G_2 + \gamma_{Q_{traffic}}Q_{traffic} + \psi_{02}\gamma_{Q_{wind}}Q_{wind} \\
&ULS_2\text{: } \gamma_{G_1}G_1 + \gamma_{G_2}G_2 + \psi_{01}\gamma_{Q_{traffic}}Q_{traffic} + \gamma_{Q_{wind}}Q_{wind} \\
&ULS_3\text{: } \gamma_{G_1}G_1 + \gamma_{G_2}G_2 + \psi_{11}\gamma_{Q_{traffic}}Q_{traffic} + \psi_{02}\gamma_{Q_{wind}}Q_{wind} + \psi_{03}\gamma_{Q_{break}}Q_{break} \\
&ULS_4\text{: } \gamma_{G_1}G_1 + \gamma_{G_2}G_2 + \psi_{01}\psi_{11}\gamma_{Q_{traffic}}Q_{traffic} + \gamma_{Q_{wind}}Q_{wind} + \psi_{03}\gamma_{Q_{break}}Q_{break} \\
&ULS_5\text{: } \gamma_{G_1}G_1 + \gamma_{G_2}G_2 + \psi_{01}\psi_{11}\gamma_{Q_{traffic}}Q_{traffic} + \psi_{02}\gamma_{Q_{wind}}Q_{wind} + \gamma_{Q_{break}}Q_{break} \\
&CLS_x\text{: } G_1 + G_2 + E_x \\
&CLS_y\text{: } G_1 + G_2 + E_y
\end{aligned}
\tag{16.7}
$$

where the safety coefficient γ and the combination coefficient ψ assume the values reported in the technical code [11].

Table 16.2 reports the maximum axial force in the isolators corresponding to the combinations load.

Table 16.2: Maximum axial force in the isolators in ULS

Combintion	**Maximum axial force in the isolators [kN]**
ULS_1	11837.00
ULS_2	11323.00
ULS_3	11200.00
ULS_4	10846.00
ULS_5	10716.00
CLS_x	6637.00
CLS_y	8674.00

In addition, also the temperature effects on the horizontal displacements have to be taken into account. The horizontal displacement due to the thermal deformation of the deck considering $\Delta T = 30°$ is equal to 5.4 cm ($\alpha \Delta T L = 10^{-5} \cdot 30° \cdot 180m$). This value has to be added to the displacement demand due to the seismic loads.

A possible solution of a device that satisfies the two main requirements of vertical bearing capacity and lateral stiffness is, for example, that represented by the *SI-N*

1000/210 isolator produced by the Italian company FIP MEC s.r.l.. For the present case the axial loads in the isolators were predominant in the choice of their geometry. In fact, due to the particular configuration of the isolators on the top piers (see Figure 15.3a), which are characterized by two devices put in place with almost $5m$ of distance between them, the transversal seismic loads generate high axial force in the two isolators. However, the procedure provides a starting point that could be iteratively changed in order to satisfy all the structural requests.

17

Evaluation of the effects of the force-displacement constitutive law of the isolators

17.1 The force-displacement constitutive law of the isolators

As introduced before, the isolator devices have been introduced in the model by means of two constitutive laws

- bi-linear force-displacement relationship;
- equivalent linear force-displacement relationship.

It is referred to those configurations as non-linear isolators (in the following expressed as iso-NL) and linear isolators (in the following expressed as iso-L), respectively.

17.2 Analyses carried out

The effect due to the differences between the two constitutive laws, emerged from time-history analyses with the seven accelerograms identified in section 15.2 along the longitudinal and transversal directions. They have been carried out through the finite element model of the case-study bridge considering modal-type solution and assuming a damping ratio equal to 5% for all the modes.

17.3 Results obtained

The demand (in terms of displacement and force) was calculated in terms of "average values of the 7 maximums" (measured during the 7 accelerograms) since the technical codes [11] allows the use of the average values in the design phase for the case of a group

of 7 accelerograms. The reported isolator displacements represent the displacement in the isolator itself and corresponds to the relative displacement between the deck and top of the piers (and between the deck and the abutment). In particular, along the longitudinal direction, Figure 17.1 and Figure 17.2 show the displacements and the shear forces in the isolators and of the top piers, respectively. Similarly, Figure 17.3 and Figure 17.4 show analogues results along the transversal direction.

In conclusion, from the analyses emerged that the two constitutive laws for the isolator are comparable. In addition, the isolators allow to strongly reduce the shear demand in the structural elements with an increase of the displacement. However, the displacement demand in the piers do not lead to plastic deformation, in fact, they are always lesser then the corresponding yielding force for each pier (Figure 15.4).

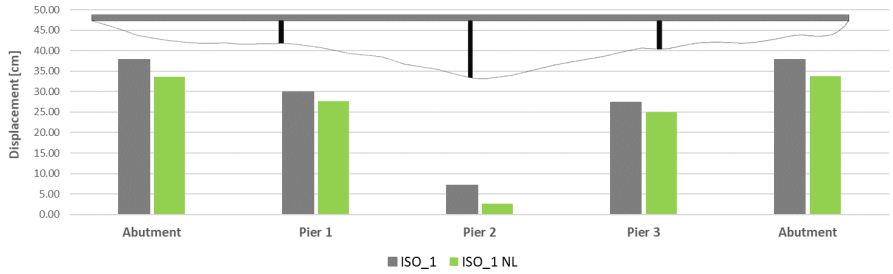

(a) Structural element displacements

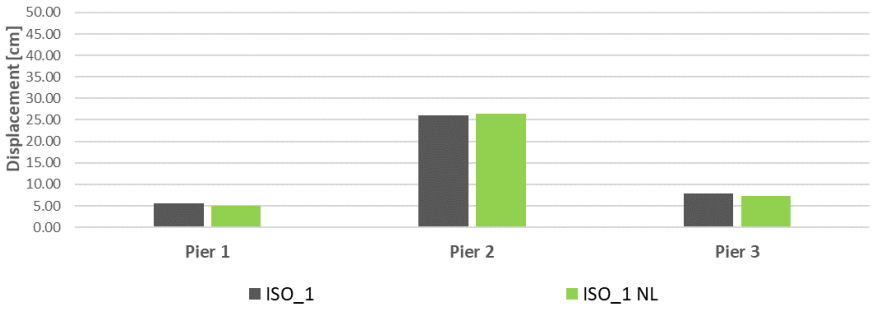

(b) Isolators displacements

Figure 17.1: Horizontal displacement results from the longitudinal time-history analyses

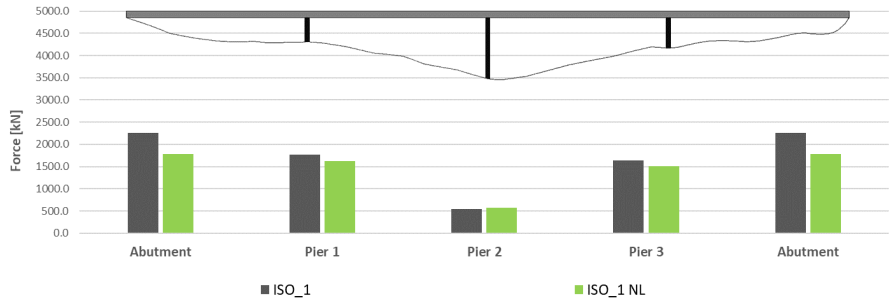

(a) Structural element shear forces

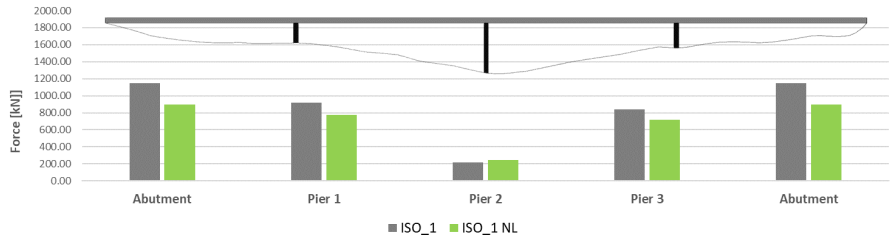

(b) Isolators shear forces

Figure 17.2: Longitudinal shear results from the longitudinal time-history analyses

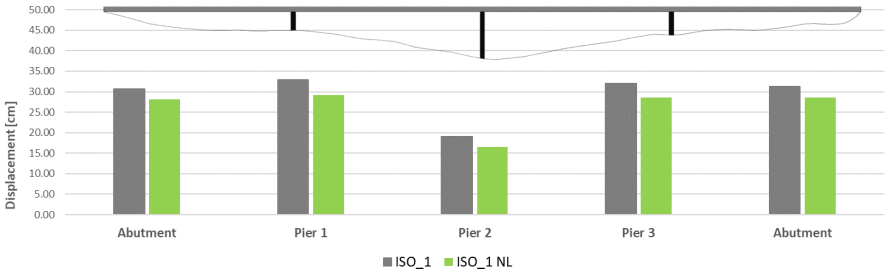

(a) Structural element displacements

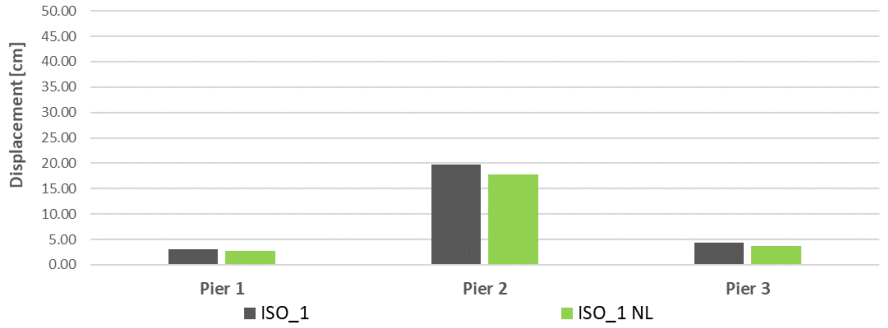

(b) Isolators displacements

Figure 17.3: Horizontal displacement results from the transversal time-history analyses

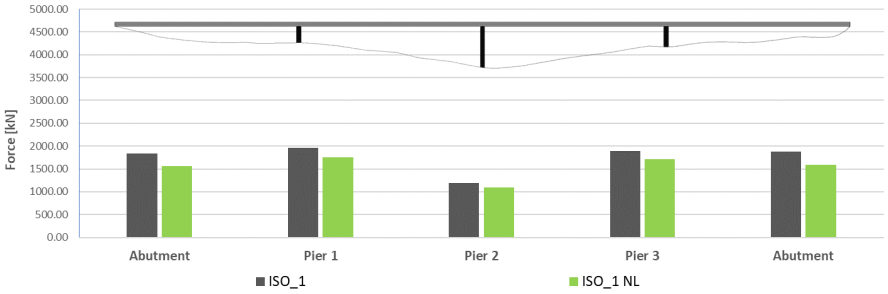

(a) Structural element shear forces

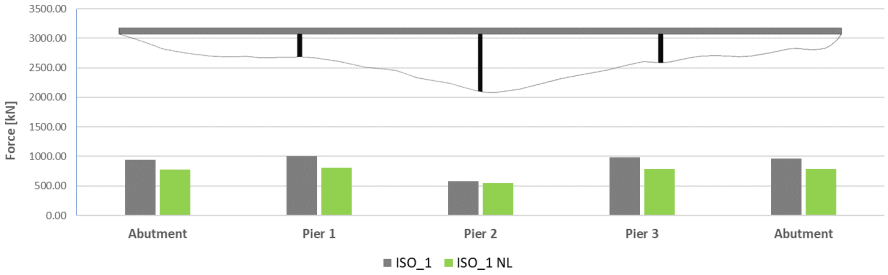

(b) Isolators shear forces

Figure 17.4: Transversal shear results from the transversal time-history analyses

18

Evaluation of the effects due to the vertical component of the seismic input

18.1 Coupling between horizontal and vertical components of the seismic action

Seismic actions are characterized by horizontal and vertical components. This chapter presents a series of analyses conducted on the case-study bridge taking into account the above-mentioned components with the following possible analyses:

- not-coupled analyses: seismic loads applied separately in the three directions and then combined with specific rules;
- coupled analyses: seismic loads applied simultaneously in horizontal (longitudinal or transversal) and vertical directions.

The objectives of this study are to highlights (i) the effects of the vertical component and (ii) the effectiveness of the rules adopted for taking into account the vertical component itself by means of not-coupled analyses.

18.2 Analyses carried out

The effect of the vertical component of the seismic action emerged from two types of analyses conducted through the finite element model of the case-study bridge:

- time-history analyses;
- response spectrum analyses.

The adopted accelerograms and sprectrum are those that have been identified in section 15.2.

According to the technical codes [67], [11] the results of time-history analyses can be summarized by considering the mean value of the maximum (in absolute value) effects measured in each analysis. A summary of the analyses carried out and the adopted nomenclature is reported in the following.

- **not-coupled analyses**. Time history analyses are indicated with nomenclature *TH* followed by the number of the accelerogram (from 1 to 7 in horizontal (H) and vertical directions (V)). Response spectrum analyses are indicated with nomenclature *Spectrum* followed by the direction of the seismic action (horizontal (H) and vertical (V) ones).

Table 18.1: Summary of not-coupled analyses in horizontal (H) and vertical directions (V)

n	Type of analysis	X direction	Y direction	Z direction	Results
1	TH – H1	✓	×	×	
2	TH – H2	✓	×	×	
3	TH – H3	✓	×	×	TH-X
4	TH – H4	✓	×	×	
5	TH – H5	✓	×	×	
6	TH – H6	✓	×	×	
7	TH – H7	✓	×	×	
8	Horizontal response spectrum analysis	✓	×	×	Spectrum-X
9	TH – H1	×	✓	×	
10	TH – H2	×	✓	×	
11	TH – H3	×	✓	×	TH-Y
12	TH – H4	×	✓	×	
13	TH – H5	×	✓	×	
14	TH – H6	×	✓	×	
15	TH – H7	×	✓	×	
16	Horizontal response spectrum analysis	×	✓	×	Spectrum-Y
17	TH – V1	×	×	✓	
18	TH – V2	×	×	✓	
19	TH – V3	×	×	✓	TH-Z
20	TH – V4	×	×	✓	

21	TH – V5	×	×	✓	
22	TH – V6	×	×	✓	
23	TH – V7	×	×	✓	
24	Vertical response spectrum analysis	×	×	✓	Spectrum-Z

- **Coupled analyses**. The adopted nomenclature depends on the type of the analyses that are considered in the coupling and it is reported in the following list.

  – **Full Time-History analyses**: accerograms are applied in both horizontal and vertical directions.

    1. X Time-History + Z Time-History : **Full TH-XZ**
    2. Y Time-History + Z Time-History : **Full TH-YZ**

Table 18.2: Summary of coupled time-history analyses in horizontal (H) and vertical directions (V)

n	Type of analysis	X direction	Y direction	Z direction
1	TH - H1+V1	✓	×	✓
2	TH - H2+V2	✓	×	✓
3	TH - H3+V3	✓	×	✓
4	TH - H4+V4	✓	×	✓
5	TH - H5+V5	✓	×	✓
6	TH - H6+V6	✓	×	✓
7	TH - H7+V7	✓	×	✓
1	TH - H1+V1	×	✓	✓
2	TH - H2+V2	×	✓	✓
3	TH - H3+V3	×	✓	✓
4	TH - H4+V4	×	✓	✓
5	TH - H5+V5	×	✓	✓
6	TH - H6+V6	×	✓	✓
7	TH - H7+V7	×	✓	✓

  – **Time-History-Spectrum combination**: in horizontal direction it is applied the corresponding accelerogram, while in the vertical direction it is applied the spectrum. The combinations of the effects have been done by applying: (i) the Square Root of the Sum of the Square (SRSS) rule as reported by the Eurocode 8 part 2 paragraph 4.2.1.4 [67], and (ii) the rule proposed by the Italian technical code, paragraph 7.3.5 [11] that requires the combination of

the effects with the application of the coefficients equal to 1 and 0.3.

1. X Time-History + Z Spectrum (Combination effects: SRSS): **SRSS-XZ**
2. X Time-History + Z Spectrum (Combination effects: 1-0.3): **(1-0.3)-XZ**
3. X Time-History + Z Spectrum (Combination effects: 0.3-1): **(0.3-1)-XZ**
4. Y Time-History + Z Spectrum (Combination effects: SRSS): **SRSS-YZ**
5. Y Time-History + Z Spectrum (Combination effects: 1-0.3): **(1-0.3)-YZ**
6. Y Time-History + Z Spectrum (Combination effects: 0.3-1): **(0.3-1)-YZ**

Table 18.3: Summary of coupled time-history analyses in horizontal direction (H) and response spectrum analysis in vertical direction (V)

n	Combination	Mean of the 7 TH - X direction	Mean of the 7 TH - Y direction	Mean of the 7 TH - Z direction	Response spectrum Z direction
1	SRSS: X TH + Z SP	✓	×	×	✓
2	1-0.3: X TH + Z SP	1	×	×	0.3
3	0.3-1: X TH + Z SP	0.3	×	×	1
4	SRSS: Y TH + Z SP	×	✓	×	✓
5	1-0.3: Y TH + Z SP	×	1	×	0.3
6	0.3-1: Y TH + Z SP	×	0.3	×	1

18.3 Results obtained

The results are reported in terms of displacement and shear demands in the isolator and in the piers, along the longitudinal and transversal directions. The reported isolator displacements represent the displacement in the isolator itself and corresponds to the relative displacement between the deck and top of the piers (and between the deck and the abutment).

For the not-coupled analyses along the longitudinal direction, Figure 18.1 and Figure 18.2 show the displacements and the shear forces of the top piers and in the isolators, respectively. Similarly, Figure 18.3 and Figure 18.4 show analogues results along the transversal direction. Figure 18.5 and Figure 18.6 report a comparison of the axial force in the isolators along the two directions. It also takes into account the effects of the static loads.

For the coupled analyses along the longitudinal direction, Figure 18.7 and Figure 18.8 show the displacements and the shear forces of the top piers and in the isolators, respectively. Similarly, Figure 18.9 and Figure 18.10 show analogues results along the

transversal direction.

Not-coupled analyses

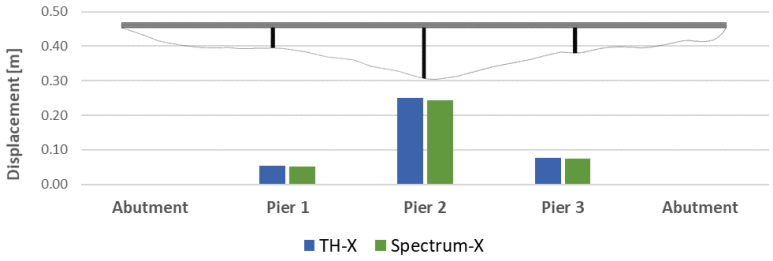

(a) Structural element

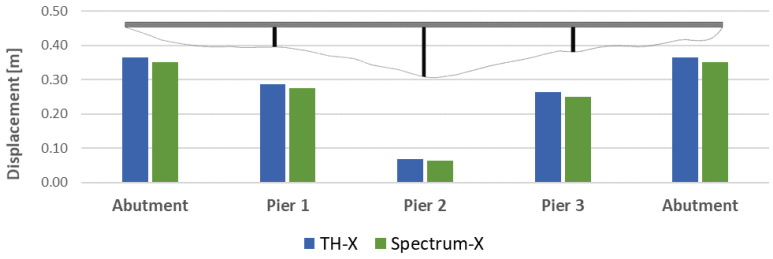

(b) Isolators

Figure 18.1: Horizontal displacement results from the longitudinal not-coupled time-history and response spectrum analyses

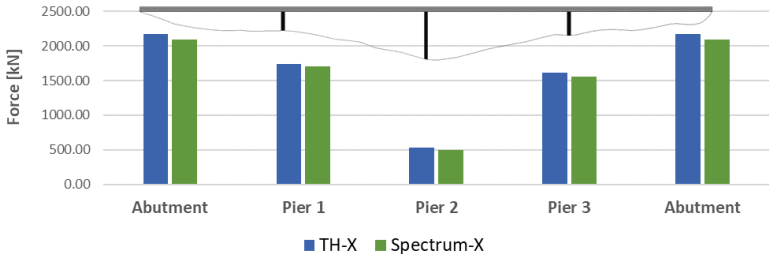

(a) Structural element

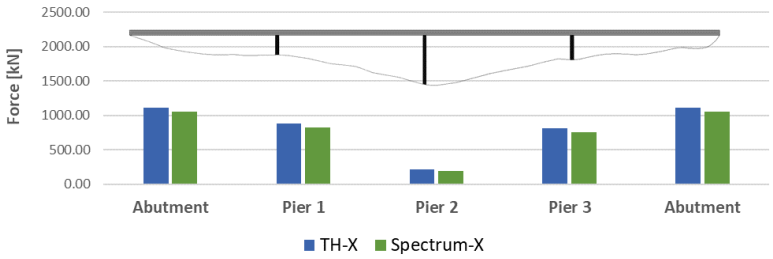

(b) Isolators

Figure 18.2: Longitudinal shear results from the longitudinal not-coupled time-history and response spectrum analyses

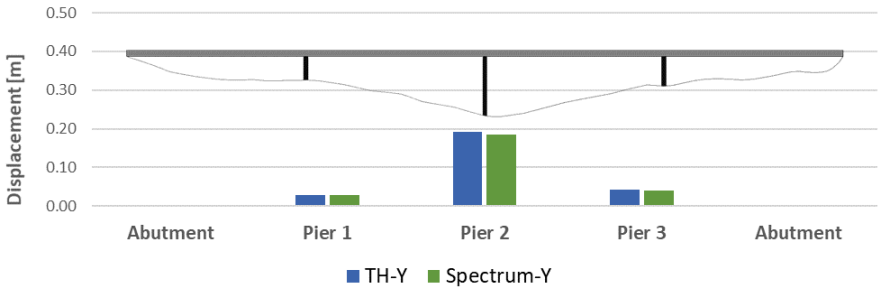

(a) Structural element

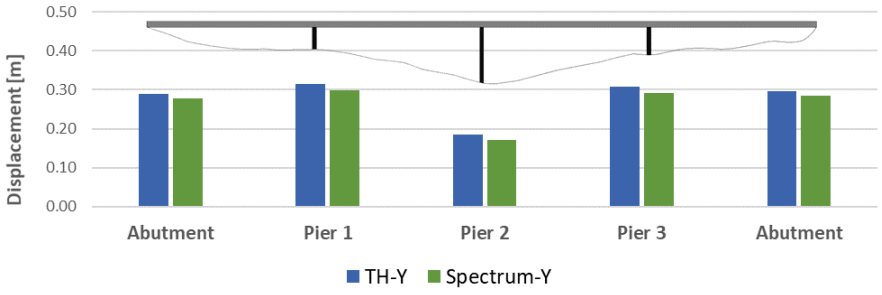

(b) Isolators

Figure 18.3: Horizontal displacement results from the transversal not-coupled time-history and response spectrum analyses

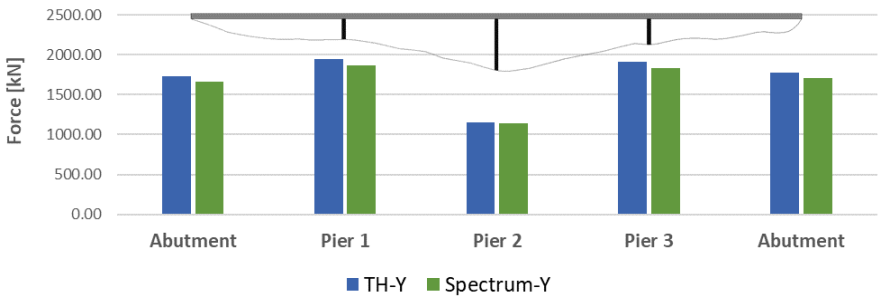

(a) Structural

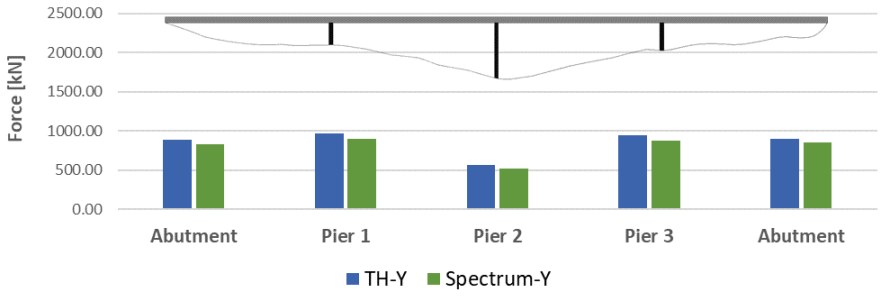

(b) Isolators

Figure 18.4: Longitudinal shear results from the transversal not-coupled time-history and response spectrum analyses

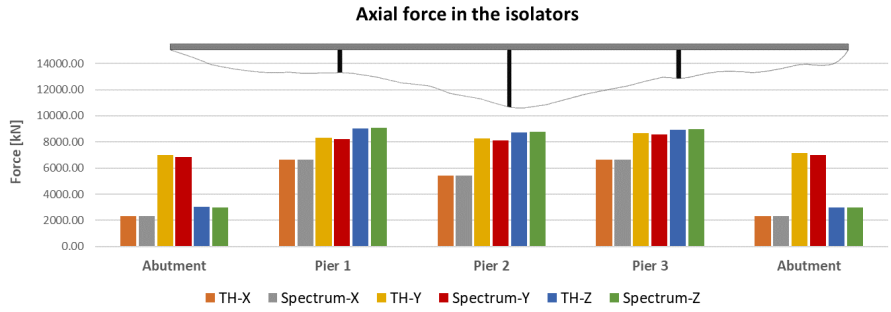

Figure 18.5: Comparison of the axial force in the isolators in the longitudinal not-coupled analyses

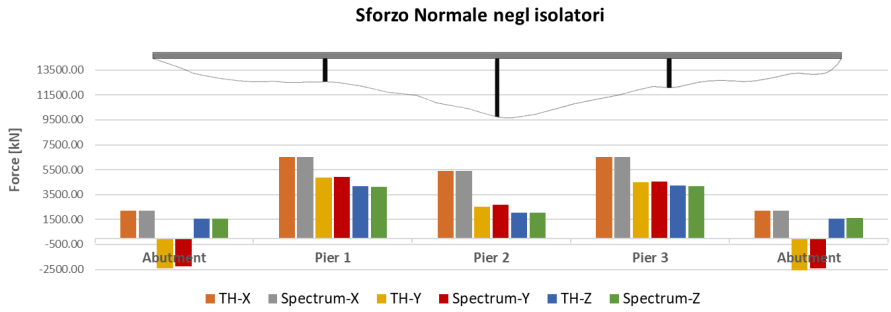

Figure 18.6: Comparison of the axial force in the isolators in the transversal not-coupled analyses

In conclusion, from the results it is clear that the behaviour of the bridge results to be uncoupled (this was also clear from the modal analysis) and that the two types of analyses (time-history and response spectrum) are comparable. In addition, due to the particular configuration of the bridge along the transversal direction (two isolators for each pear at a distance around 5m) the analyses along the transversal direction provoke high axial force in the isolator. Even though this configuration should be avoided, the displacements and the forces in the structural elements and in the isolators are in according with their capacities. The displacement demand in the piers do not lead to plastic deformation since their are always lesser then the yielding force for each pier (Figure 15.4).

Coupled analyses

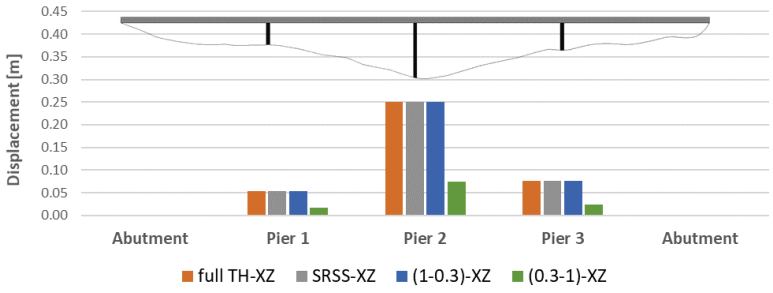

(a) Structural element

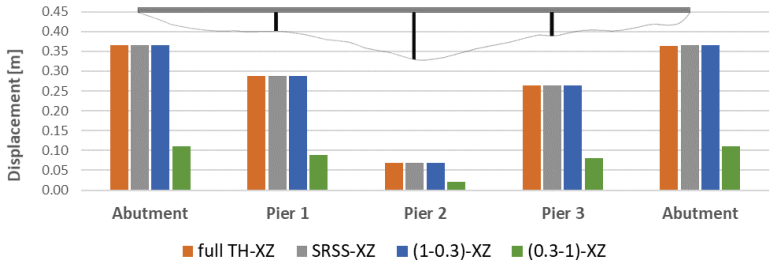

(b) Isolators

Figure 18.7: Horizontal displacement results from the longitudinal coupled analyses

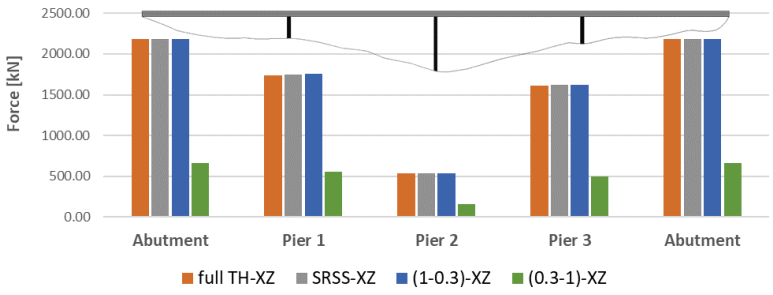

(a) Structural element

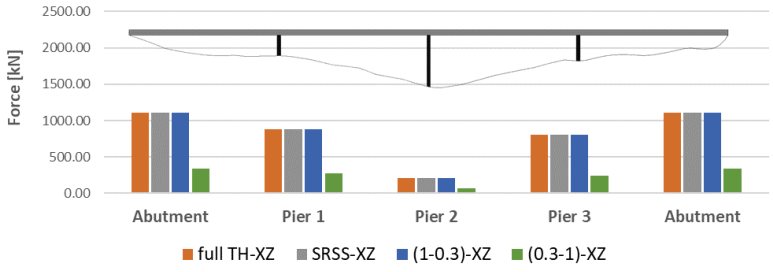

(b) Isolators

Figure 18.8: Axial force results from the longitudinal coupled analyses

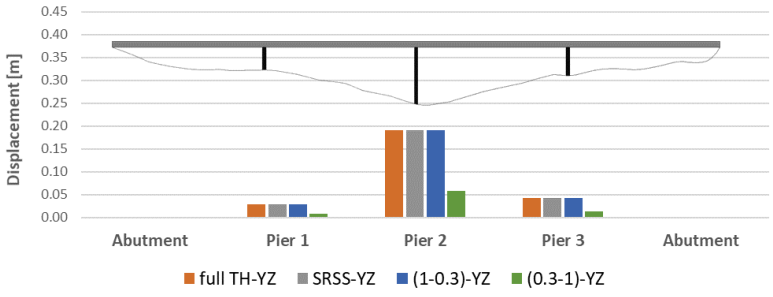

(a) Structural element

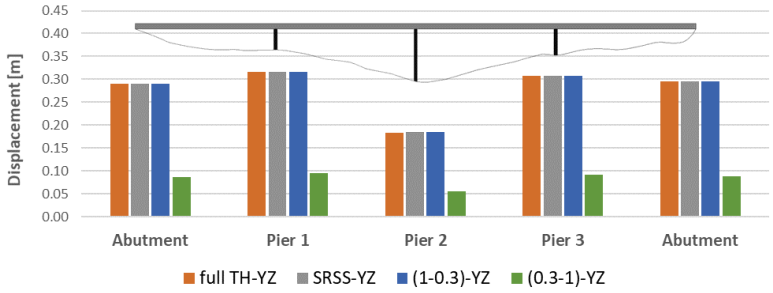

(b) Isolators

Figure 18.9: Horizontal displacement results from the transversal coupled analyses

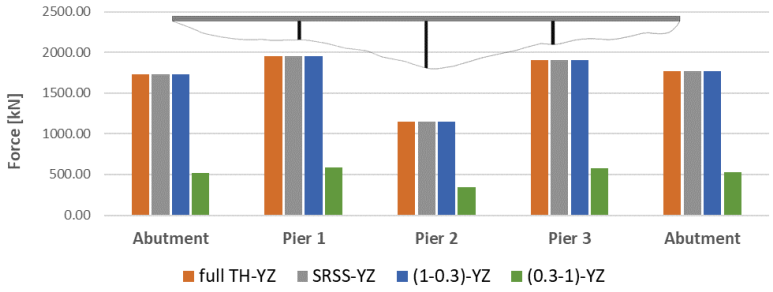

(a) Structural element

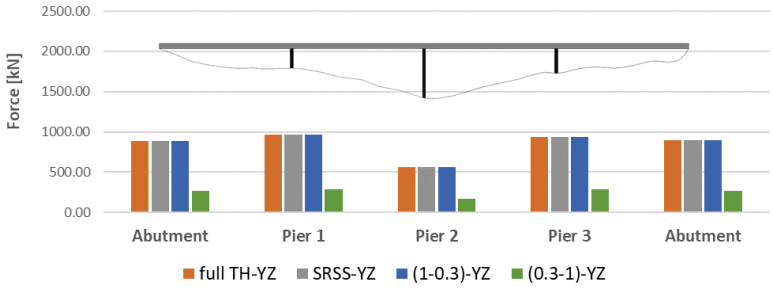

(b) Isolators

Figure 18.10: Axial force results from the transversal coupled analyses

In conclusion, analogues consideration with respect to the non-coupled analyses can be drawn. In addition, from the obtained results the two approaches provided by the Eurocode 8 and by the Italian technical code, for taking into account of the spatiality of the seismic events, are comparable.

19

Evaluation of the effects due to the variability in the material properties of the rubber of the isolators

Design of HDRB isolation system is typically conducted by practitioners assuming a deterministic value of the shear modulus of the rubber material of the HDRB devices [59]. However, it is a random variable with a non-negligible coefficient of variation, that can be reasonably described by a Gaussian distribution, as highlighted by the analysis of the results of several experimental campaigns carried out for commercial orders at various laboratories [66].

Minimal models are able to well represent the dynamic behaviour of the bridge both in longitudinal and transversal direction. This aspect is relevant in performing parametric analyses of the parameters that may be considered important in the dynamic behaviour of the bridge. In fact, the minimal systems are constituted by few degrees of freedoms and require low computational effort in the execution of dynamic analyses. In this regard, the effects of the aleatory variability in the shear modulus G of the rubber material of the HDRB isolators have been investigated by means of time-history dynamic analyses carried out using the minimal systems detailed in section 15.3.1 and the seven seismic records described in section 15.2.

19.1 Hypotheses on the isolator devices

The isolators identified in section 16.2 are constituted by rubber layers with mean shear modulus G equal to 0.8 MPa and equivalent viscous damping ratio of around 10%. Consequently, G is assumed as a random variable characterized by a normal distribution with mean value equal to 0.8 MPa and coefficient of variation equal to 14.5% (as per the results of experimental campaigns carried out for commercial orders at various laboratories, see [66]). The following assumptions have been made:

- The shear modulus G is the parameter that mainly governs the mechanical behaviour of the isolator device.

- A linear relationship is assumed between the rubber shear modulus *G* and the horizontal stiffness k_{iso} of the isolator device:

$$G = \left(\frac{4 \cdot \chi_v \cdot h_{iso}}{\pi \cdot D_{iso}^2} \right) k_{iso} \tag{19.1}$$

  where the geometric parameters of the isolator have been considered as deterministic.

- The variability of the shear modulus has been taken into account by acting directly on the mean horizontal stiffness of the isolator device ($k_{iso,mean} = 2.99 kN/mm$ corresponding to a mean shear modulus equal to 0.8 MPa) by means of an adimensional factor *g*, for which a normal distribution has been assumed:

$$\begin{aligned} k_{iso} &= g \cdot k_{iso,mean} \\ g &= N(\mu = 1, \sigma = 14.5\%) \end{aligned} \tag{19.2}$$

- A number of 10000 realizations of the normal random variable corresponding to multiplication factor *g* have been randomly generated and seven time-history simulations have been carried out (with the seven seismic records) for each realisation.

- The damping coefficient of the isolator devices has been updated after each realisation adopting the equivalent SDOF model and assuming a damping ration equal to $\xi_{iso} = 10\%$:

$$\begin{aligned} \omega_{iso} &= \sqrt{\frac{n_{iso} \cdot k_{iso}}{m_{deck}}} \\ c_{iso} &= \frac{2 \cdot \xi_{iso} \cdot \omega_{iso} \cdot m_{deck}}{n_{iso}} \end{aligned} \tag{19.3}$$

- The same damping coefficient c_{iso} has been assumed in both longitudinal and transversal directions.

19.2 Hypotheses on the minimal systems

The minimal models in the two direction have been calibrated on the basis of the results of the modal analysis conducted on the complete FEM model of the bridge under examination, which differs from the minimum models in considering a distributed mass of the deck. Table 19.1 shows the comparison between the vibration periods obtained with the minimum models and those obtained with the FEM model, both in the longitudinal and transverse direction.

Table 19.1: Comparison between the modal analysis results of finite element model and minimal models

	longitudinal direction X		**transversal direction Y**	
Mode	4 DOFS minimal system	FEM	5 DOFS minimal system	FEM
1	2.781	2.915	2.656	2.836
2	0.650	0.655	2.176	2.076
3	0.323	0.324	0.168	0.169
4	0.263	0.266	0.546	0.542
5	/	/	0.215	0.213

19.3 Analyses carried out

Figure 19.1 shows the histogram of the relative frequencies of the sample of the randomly generated 10,000 realizations, which have mean value equal to 1 and coefficient of variation equal to 14.4% (compared to the 14.5% target).

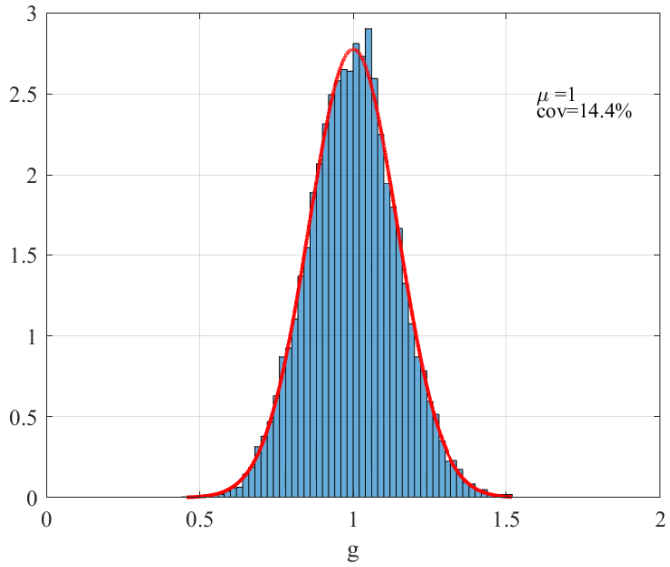

Figure 19.1: Histogram of the relative frequencies of the sample of the 10000 realizations of g

Therefore, the following minimal systems corresponding to this set of samples of the factor g can be defined: (i) 10000 minimal models with 4 DOFS in longitudinal direction, and (ii) 10000 minimal models with 5 DOFS in transversal direction. Thus, for each of

the 20000 models, 7 time-history analyses with natural accelerograms have been carried out. To sum up, a total number of 140000 numerical simulations have been performed:

1. Group of analyses 1: 70000 analysis along the longitudinal direction, conducted on 10000 minimal models with 4 DOFS assuming the 7 natural accelerograms as input.

2. Group of analyses 2: 70000 analysis along the transversal direction, conducted on 10000 minimal models with 5 DOFS assuming the 7 natural accelerograms as input.

The results are expressed in terms of mean displacement of each degree of freedom of the two minimal systems along the two directions. For each direction, it is evaluated as the mean of the seven maximum values of the displacement obtained during the seven accelerograms. With reference to the nomenclature introduced in Figure 15.11 and Figure 15.12, the attention has been paid on the following displacements:

- $u_{isoAB} = u_{deck}$ and $v_{isoAB} = v_{deck}$ are the displacements sustained by the isolators on the abutments that coincide with the displacements of the deck with respect to the abutment. They represent the displacement of the first degree of freedom of the minimal systems (gdl_1);

- $u_{iso1} = u_{deck} - u_{pier1}$ and $v_{iso1} = v_{deck} - v_{pier1}$ are the longitudinal and transversal displacements sustained by the isolators on pier 1 that coincide with the relative displacements of the deck with respect to the top of pier 1. The displacement of the top pier 1 represents the second degree of freedom of the minimal systems (gdl_2);

- $u_{iso2} = u_{deck} - u_{pier2}$ and $v_{iso2} = v_{deck} - v_{pier2}$ are the displacements sustained by the isolators on pier 2. The displacement of the top pier 1 represents the third degree of freedom of the minimal systems (gdl_3);

- $u_{iso3} = u_{deck} - u_{pier3}$ and $v_{iso3} = v_{deck} - v_{pier3}$ are the displacements sustained by the isolators on pier 3. The displacement of the top pier 3 represents the fourth degree of freedom of the minimal systems (gdl_4);

Figure 19.2 reports a schematization of the degrees of freedom associated to the minimal systems in the longitudinal and transversal direction.

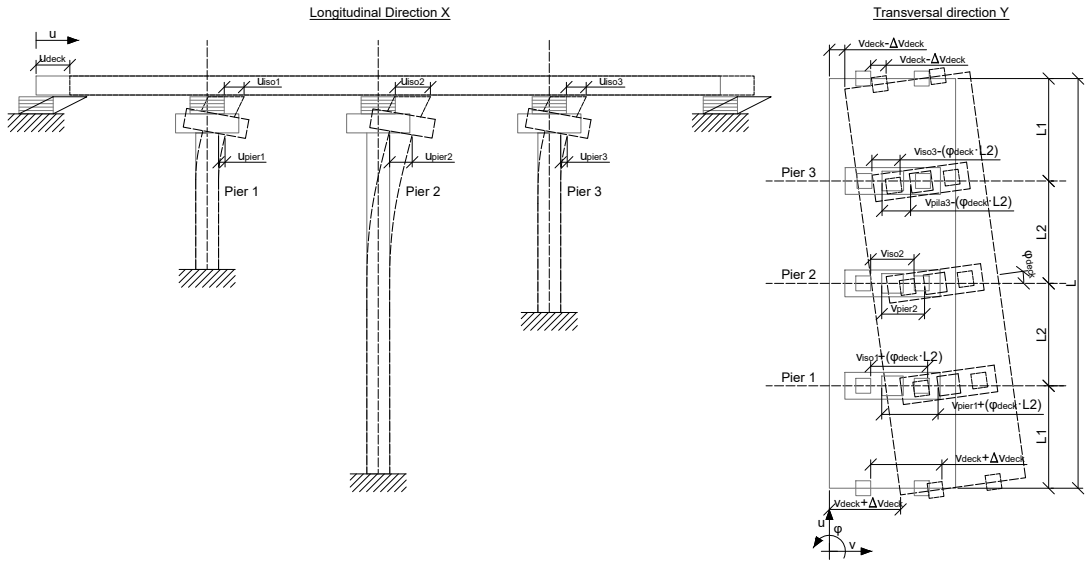

Figure 19.2: Schematization of the degrees of freedom associated to the minimal systems

For each one of the above-mentioned displacements, a set of 10000 mean displacement values (mean of the seven maximum values obtained for the seven accelerograms) are obtained. Each set is considered as a sample of a random variable whose distribution is unknown and has to be identified. A fitting has been then performed of the relative frequency histogram of each set of 10000 values of the above-mentioned displacements with the Probability Density Function that better represents the set itself. The best fitting has been conducted by considering four well-known Probability Density Functions (PDFs): (i) Normal, (ii) LogNormal, (iii) Weibull, (iv) Extreme Values and (v) Gamma [68].

19.4 Results of the analyses

19.4.1 Results along the longitudinal direction

Figure 19.3 reports the results of the simulations in longitudinal direction (X) of the displacement of the structural elements (deck, and top of the piers). They are reported in terms of relative frequency histograms of the displacements and their fitting with the five theoretical density functions, in terms of probability and cumulative ones.

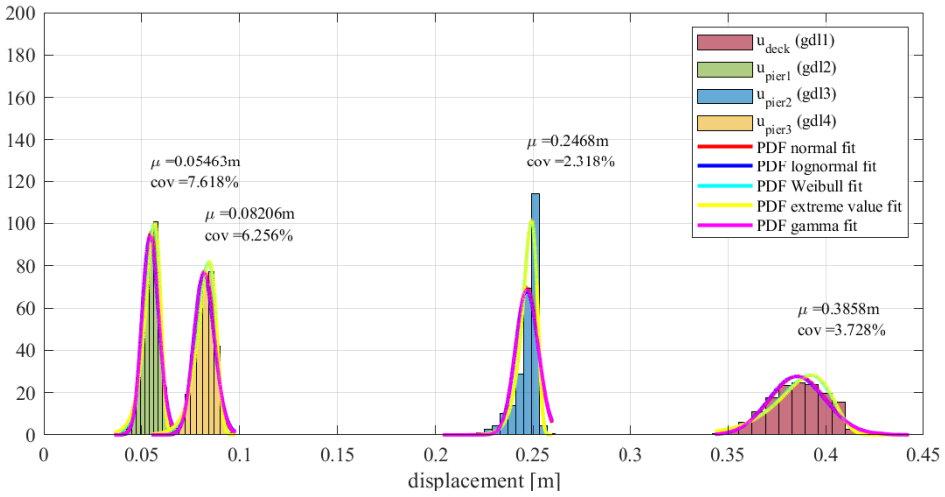

(a) Frequency histogram and theoretical Probability Density Functions

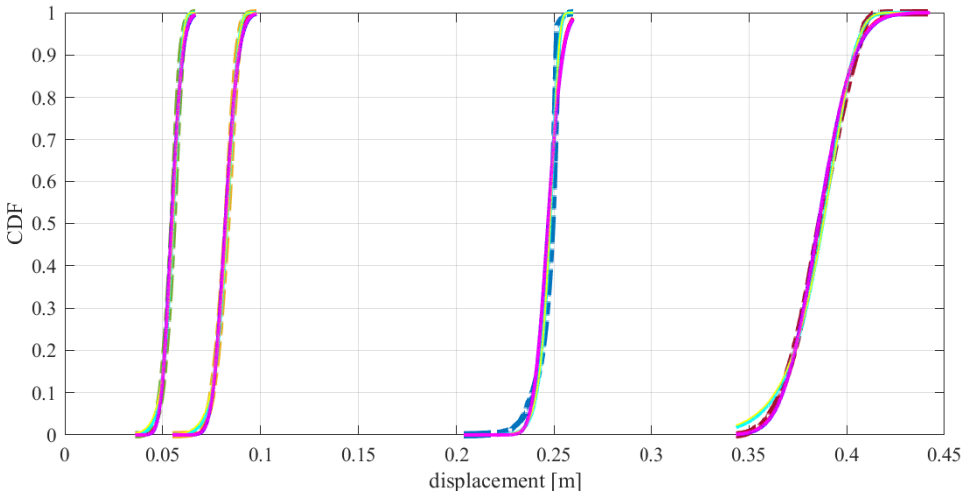

(b) Corresponding Cumulative Density Functions

Figure 19.3: Simulation results in longitudinal direction in terms of structural element displacements

Similarly, Figure 19.4 reports the results of the simulations in longitudinal direction (X) of the displacement of the isolator devices. They are reported in terms of relative frequency histograms of the displacements and their fitting with the five theoretical density functions, in terms of probability and cumulative ones.

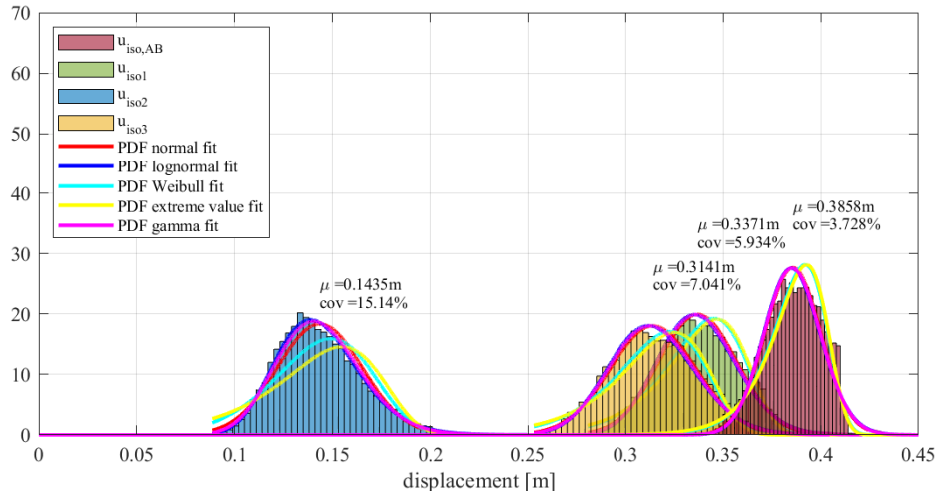

(a) Frequency histogram and theoretical Probability Density Functions

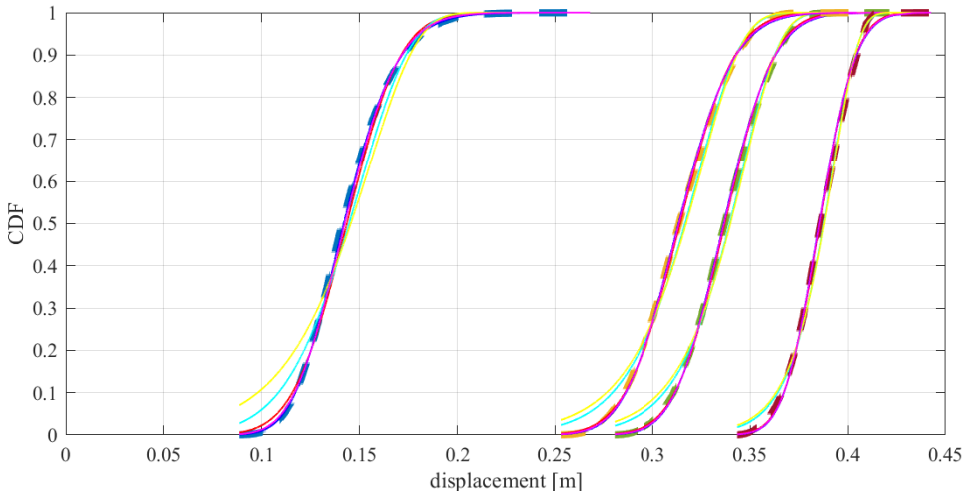

(b) Corresponding Cumulative Density Functions

Figure 19.4: Simulation results in longitudinal direction in terms of isolators displacements

It is worth noting that for each degree of freedoms (displacement of the deck and of the top of the piers, and displacement of the isolator devices) the mean value obtained during the simulations (10000), which take into account the variability of the shear modulus of the rubber in the isolators, is the same of that one obtained considering the mean value of the shear modulus ($G = 0.8MPa$ and $g = 1$).

19.4.2 Results along the transversal direction

Figure 19.5 reports the results of the simulations in transversal direction (Y) of the displacement of the structural elements (deck, and top of the piers). They are reported in

terms of relative frequency histograms of the displacements and their fitting with the five theoretical density functions, in terms of probability and cumulative ones.

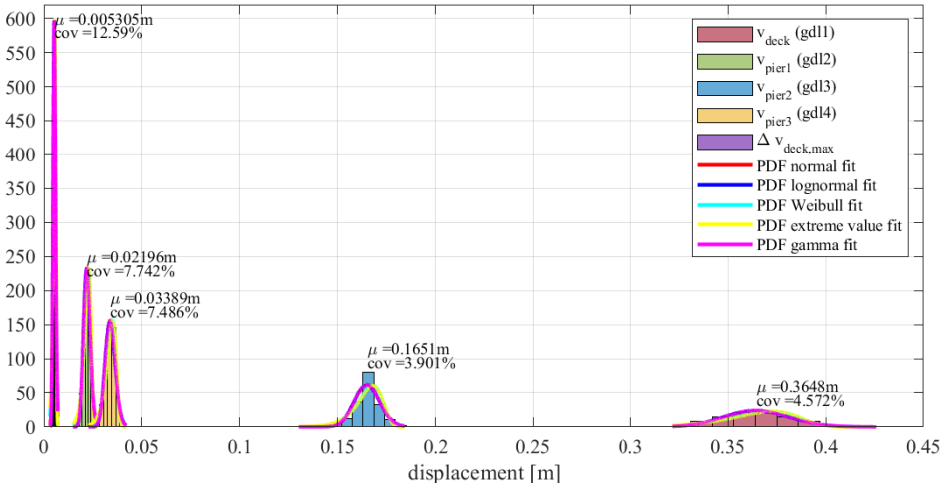

(a) Frequency histograms and theoretical Probability Density Functions

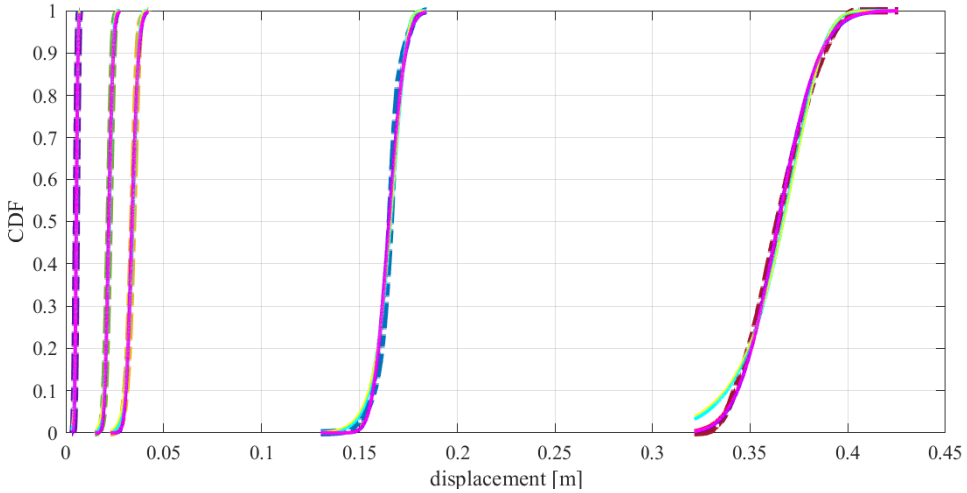

(b) Corresponding Cumulative Density Functions

Figure 19.5: Simulation results in transversal direction in terms of structural element displacements

Similarly, Figure 19.6 reports the results of the simulations in transversal direction (Y) of the displacement of the isolator devices. They are reported in terms of relative frequency histograms of the displacements and their fitting with the five theoretical density functions, in terms of probability and cumulative ones.

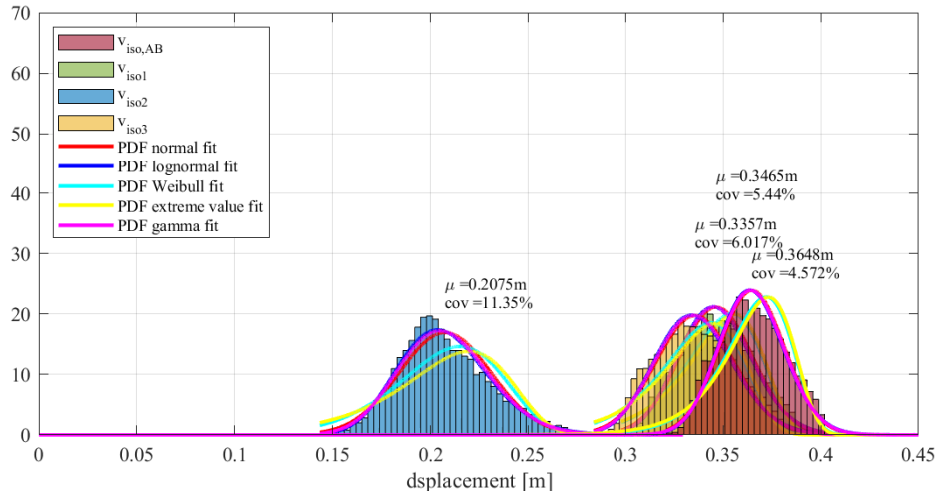

(a) Frequency histograms and theoretical Probability Density Functions

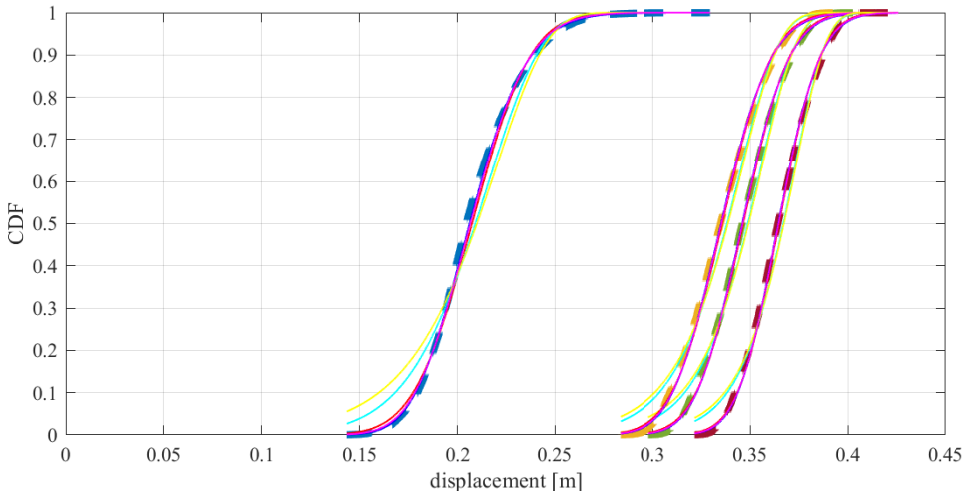

(b) Corresponding Cumulative Density Functions

Figure 19.6: Simulation results in transversal direction in terms of isolators displacements

It is worth noting that for each degree of freedoms (displacement of the deck and of the top of the piers, and displacement of the isolator devices) the mean value obtained during the simulations (10000), which take into account the variability of the shear modulus of the rubber in the isolators, is the same of that one obtained considering the mean value of the shear modulus ($G = 0.8MPa$ and $g = 1$).

19.4.3 Upper & Lower bounds

The best fit has been evaluated by means of two statistical tests: (i) the Chi-Square test and (ii) the Kolmogorov-Smirnov test [68]. In this respect, Table 19.2 reports the identified best PDFs for both the longitudinal direction (4 DOFs) and the transversal direction (5 DOFs). On the basis of the results of the numerical simulations, also the percentile val-

ues associated with selected percentages can be obtained. They can be either calculated directly from the results of the simulations (see Table 19.3) or estimated through the best fits of the relative frequency histograms (i.e., the identified PDFs) of the considered displacement response parameter (see Table 19.4). Then, from the values of the percentiles, it is possible to calculate the coefficients that allow to take into account the variability of the rubber shear modulus on the structural response of the bridge. These coefficients can be applied to the displacements of the isolators obtained considering the mean value of the rubber shear modulus. In fact, as it can be seen from the results in the previous sections, the coefficient of variation that characterizes the variability of the shear modulus does not keep unaltered in the variability of the response parameters, i.e. of the displacements of the deck, of the top of the piers, and of the isolator devices. Therefore, starting from the theoretical probability functions for each response parameter these coefficients can be calculated according to:

$$c_{x\%} = \frac{\delta_{x\%}}{\delta_{Gmean}} \tag{19.4}$$

Where $\delta_{x\%}$ indicates the percentile of the displacement response parameter characterized by a probability of non-exceedance equal to $x\%$, and therefore by a probability of being exceeded equal to $(1 - x\%)$, and δ_{Gmean} is the corresponding response parameter obtained considering the design mean value of the shear modulus G_{mean}. In this respect, Table 19.5 reports the coefficient calculated by Eq. 19.4 for all the response parameters in longitudinal and transversal directions.

Chi-Square test. The Chi-Square goodness-of-fit test allows to compare the observed/simulated frequencies n_1, n_2, ..., n_k of k values with the corresponding theoretical frequencies e_1, e_2, ..., e_k of k values calculated from the assumed theoretical distribution through the calculation of the ratio *C*. The goodness of this fit is then obtained by comparing the *C* value with the critical value $c_{1-\alpha}$ of the Chi-squared distribution χ^2_f at the cumulative probability of $(1-\alpha)$ (since C approaches the χ^2_f distribution with $f = k - 1$ degrees of freedom as $n \to \infty$).
α indicates the significance level at with the the theoretical distribution is assumed acceptable.

$$C = \sum_{i=1}^{k} \frac{(n_i - e_i)^2}{e_i} < c_{1-\alpha}$$

Values of $c_{1-\alpha}$ are available in tabulated form.

Kolmogorov-Smirnov test. The Kolmogorov-Smirnov goodness-of-fit test allows to compare the observed/simulated cumulative frequency $S_n(x)$ with the assumed theoretical Cumulative Density Function $F_X(x)$. The cumulative frequency function corresponding to the set of observed/simulated $x_1, x_2, ..., x_n$ values with size n, is evaluated as follows:

$$\begin{aligned} S_n(x) &= 0 \text{ for, } x < x_1 \\ &= \frac{k}{n} \text{ for } x_k \leq x \leq x_{k+1} \\ &= 1 \text{ for } x \geq x_k \end{aligned}$$

where $k = 1, 2, ..., n$ and the set of data is rearranged in increasing order. The goodness of this fit is then obtained by comparing the maximum difference between $F_X(x)$ and $S_n(x)$, which represents a random variable, with its critical value defined for significance level α at which the theoretical distribution is assumed acceptable. The latter is available in tabulated form.

Table 19.2: Parameters of the fitted statistical functions

	Element	PDF	Parameter 1	Parameter 2	Mode [m]	Mean [m]
Longitudinal direction	u_{deck}	Normal	$\mu = 0.3858$	$\sigma = 0.0144$	0.3858	0.3858
	u_{pier1}	Weibull	$a = 0.0565$	$b = 15.2919$	0.0562	0.0546
	u_{pier2}	Extreme values	$\mu = 0.2491$	$\sigma = 0.0036$	0.2491	0.2470
	u_{pier3}	Weibull	$a = 0.0844$	$b = 18.7585$	0.0841	0.0820
	$u_{iso,AB}$	Normal	$\mu = 0.3858$	$\sigma = 0.0144$	0.3858	0.3858
	u_{iso1}	Normal	$\mu = 0.3371$	$\sigma = 0.0200$	0.3371	0.3371
	u_{iso2}	LogNormal	$\mu = -1.9528$	$\sigma = 0.1492$	0.1387	0.1435
	u_{iso3}	Normal	$\mu = 0.3141$	$\sigma = 0.0221$	0.3141	0.3141
Transversal direction	v_{deck}	Normal	$\mu = 0.3648$	$\sigma = 0.0167$	0.3648	0.3648
	v_{pier1}	Weibull	$a = 0.0227$	$b = 14.4163$	0.0226	0.0219
	v_{pier2}	Normal	$\mu = 0.1651$	$\sigma = 0.0064$	0.1651	0.1651
	v_{pier3}	Weibull	$a = 0.0350$	$b = 14.9356$	0.0349	0.0338
	$\Delta v_{deck,max}$	Normal	$\mu = 0.0053$	$\sigma = 6.68e-4$	0.0053	0.0053
	$v_{iso,AB}$	Normal	$\mu = 0.3648$	$\sigma = 0.0167$	0.3648	0.3648
	v_{iso1}	Normal	$\mu = 0.3465$	$\sigma = 0.0188$	0.3465	0.3465
	v_{iso2}	LogNormal	$\mu = -1.5789$	$\sigma = 0.1120$	0.2036	0.2075
	v_{iso3}	LogNormal	$\mu = -1.0933$	$\sigma = 0.0601$	0.3339	0.3357

Table 19.3: Percentiles directly calculated from the simulations

		Displacement						
	Element	1%	5%	16%	median 50%	84%	95%	99%
Longitudinal direction	u_{deck}	0.3513	0.3608	0.3707	0.3863	0.4011	0.4080	0.4117
	u_{pier1}	0.0432	0.0472	0.0505	0.0551	0.0586	0.0608	0.0630
	u_{pier2}	0.2268	0.2349	0.2424	0.2488	0.2511	0.2517	0.2543
	u_{pier3}	0.0684	0.0730	0.0769	0.0827	0.0871	0.0895	0.0917
	$u_{iso,AB}$	0.3513	0.3608	0.3707	0.3863	0.4011	0.4080	0.4117
	u_{iso1}	0.2919	0.3035	0.3163	0.3370	0.3582	0.3696	0.3777
	u_{iso2}	0.1021	0.1119	0.1221	0.1411	0.1650	0.1828	0.2004
	u_{iso3}	0.2669	0.2779	0.2911	0.3136	0.3373	0.3508	0.3617
Transversal direction	v_{deck}	0.3318	0.3382	0.3469	0.3643	0.3828	0.3933	0.3994
	v_{pier1}	0.0177	0.0191	0.0202	0.0221	0.0237	0.0246	0.0255
	v_{pier2}	0.1462	0.1533	0.1598	0.1657	0.1703	0.1755	0.1800
	v_{pier3}	0.0271	0.0294	0.0314	0.0341	0.0363	0.0375	0.0395
	$\Delta v_{deck,max}$	0.0039	0.0042	0.0046	0.0053	0.0060	0.0064	0.0067
	$v_{iso,AB}$	0.3318	0.3382	0.3469	0.3643	0.3828	0.3933	0.3994
	v_{iso1}	0.3090	0.3161	0.3262	0.3460	0.3664	0.3786	0.3864
	v_{iso2}	0.1608	0.1729	0.1850	0.2045	0.2311	0.2506	0.2687
	v_{iso3}	0.2967	0.3042	0.3140	0.3349	0.3574	0.3704	0.3790

Table 19.4: Percentiles calculated from fitted statistical functions

		Displacement							
	Element	**PDF**	1%	5%	16%	median 50%	84%	95%	99%
Longitudinal direction	u_{deck}	Normal	0.3523	0.3621	0.3715	0.3858	0.4001	0.4094	0.4192
	u_{pier1}	Weibull	0.0419	0.0466	0.0504	0.0552	0.0588	0.0607	0.0625
	u_{pier2}	Extreme values	0.2325	0.2384	0.2428	0.2478	0.2513	0.2531	0.2547
	u_{pier3}	Weibull	0.0661	0.0721	0.0769	0.0828	0.0872	0.0895	0.0916
	$u_{iso,AB}$	Normal	0.3523	0.3621	0.3715	0.3858	0.4001	0.4094	0.4192
	u_{iso1}	Normal	0.2906	0.3042	0.3172	0.3371	0.3570	0.3700	0.3836
	u_{iso2}	LogNormal	0.1003	0.1110	0.1224	0.1419	0.1646	0.1814	0.2008
	u_{iso3}	Normal	0.2627	0.2777	0.2921	0.3141	0.3361	0.3505	0.3656
Transversal direction	v_{deck}	Normal	0.3260	0.3381	0.3486	0.3648	0.3817	0.3931	0.4036
	v_{pier1}	Weibull	0.0166	0.0186	0.0202	0.0222	0.0237	0.0246	0.0253
	v_{pier2}	Normal	0.1502	0.1545	0.1587	0.1651	0.1715	0.1757	0.1801
	v_{pier3}	Weibull	0.0258	0.0288	0.0312	0.0342	0.0365	0.0377	0.0388
	$\Delta v_{deck,max}$	Normal	0.0038	0.0043	0.0047	0.0053	0.0060	0.0065	0.0069
	$v_{iso,AB}$	Normal	0.3260	0.3381	0.3486	0.3650	0.3817	0.3931	0.4036
	v_{iso1}	Normal	0.3026	0.3155	0.3277	0.3465	0.3652	0.3755	0.3903
	v_{iso2}	LogNormal	0.1589	0.1715	0.1845	0.2062	0.2305	0.2479	0.2676
	v_{iso3}	LogNormal	0.2914	0.3036	0.3157	0.3351	0.3558	0.3699	0.3854

Table 19.5: Coefficients to take into account the variability shear modulus of the rubber isolator on the response parameter of the case-study bridge

		Deck	**Pier 1**		**Pier 2**		**Pier 3**		**Increment of displacement due to torsional rotation**
	$c_x\%$	Abutment/ Isolator	Top pier	Isolator	Top pier	Isolator	Top pier	Isolator	Abutment/Isolator
Longitudinal direction	$c_{1\%}$	0.9132	0.7674	0.8621	0.9413	0.6990	0.8061	0.8364	-
	$c_{5\%}$	0.9386	0.8535	0.9024	0.9652	0.7735	0.8793	0.8841	-
	$c_{16\%}$	0.9629	0.9231	0.9410	0.9830	0.8530	0.9378	0.9300	-
	$c_{50\%}$	1	1.0110	1	1.0032	0.9889	1.0098	1	-
	$c_{84\%}$	1.0371	1.0769	1.059	1.0174	1.1470	1.0634	1.0700	-
	$c_{95\%}$	1.0612	1.1117	1.0976	1.0247	1.2641	1.0915	1.1159	-
	$c_{99\%}$	1.0866	1.1447	1.1379	1.0312	1.3993	1.1171	1.1640	-
Transversal direction	$c_{1\%}$	0.8936	0.7580	0.8733	0.9098	0.7658	0.7633	0.8680	0.7170
	$c_{5\%}$	0.9268	0.8493	0.9105	0.9358	0.8265	0.8521	0.9044	0.8113
	$c_{16\%}$	0.9556	0.9224	0.9457	0.9612	0.8892	0.9231	0.9404	0.8868
	$c_{50\%}$	1	1.0137	1	1	0.9937	1.0118	0.9982	1
	$c_{84\%}$	1.0463	1.0822	1.054	1.0388	1.1108	1.0799	1.0599	1.1321
	$c_{95\%}$	1.0776	1.1233	1.0837	1.0642	1.1947	1.1154	1.1019	1.2264
	$c_{99\%}$	1.1064	1.1553	1.1264	1.0909	1.2896	1.1479	1.148	1.3019

Starting from the values of these percentiles, for each structural element and for each isolator, the multiplicative coefficients have been calculated which, once applied to the result (δ_{Gmean}) obtained assuming the mean design value of the rubber shear modulus, allow to immediately obtain the Upper Bound (here selected as the 99% percentile) and Lower Bound (1% percentile) values which take into account the variability of the rubber shear modulus:

$$\begin{aligned} \delta_{UppuerBuund} &= c_{UB} \cdot \delta_{Gmean} = c_{99\%} \cdot \delta_{Gmean} \\ \delta_{LowerBuund} &= c_{LB} \cdot \delta_{Gmean} = c_{1\%} \cdot \delta_{Gmean} \end{aligned} \tag{19.5}$$

Figure 19.7 and Figure 19.8 synthetically show the Upper and Lower bounds values obtained for all the response parameters in the two directions.

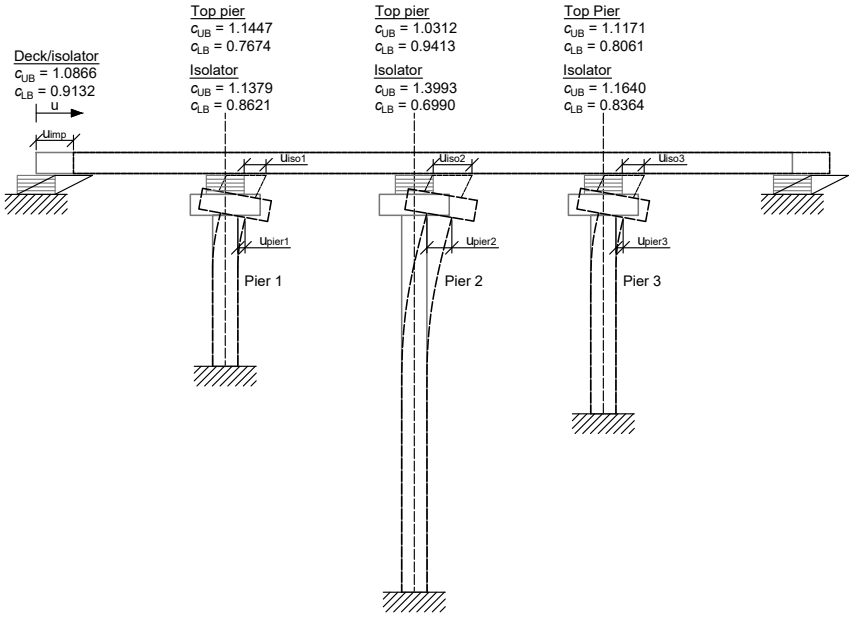

Figure 19.7: Upper and Lower bound values of the response parameters in longitudinal direction

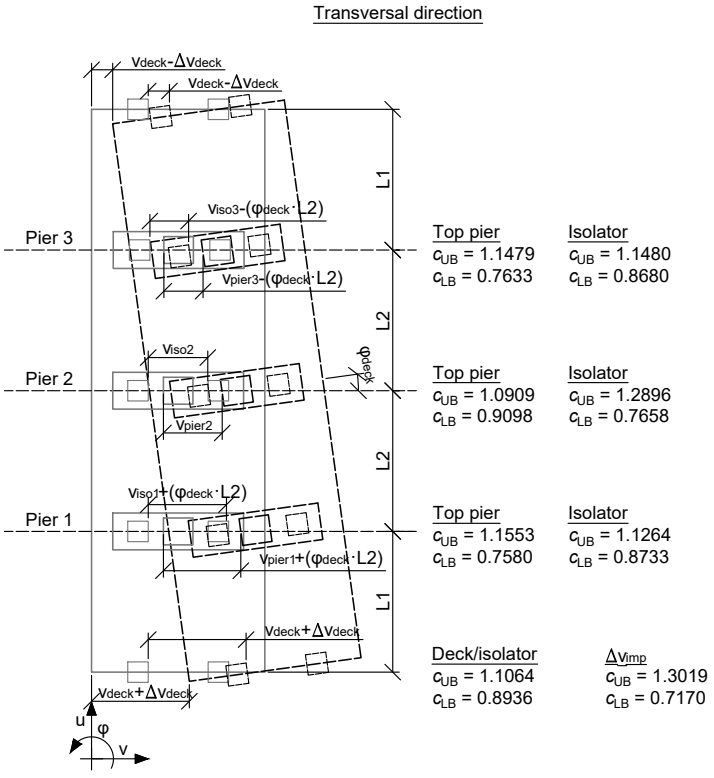

Figure 19.8: Upper and Lower bound values of the response parameters in transversal direction

Inspection of Table 19.5 allows the following observations. Regarding the isolators displacements:

- the Upper Bound coefficient increases as the flexibility of the underlying structural element (pile/abutment) increases;
- the Lower Bound coefficient decreases (and therefore deviates more and more from 1) as the flexibility of the structural element (pile/abutment) increases;

Regarding the top piers displacements:

- the Upper Bound coefficient decreases as the flexibility of the pile increases, with a trend qualitatively opposite to the coefficient for the displacement of the corresponding isolator;
- the Lower Bound coefficient increases (and therefore gets closer and closer to 1) as the flexibility of the pile increases, with a trend qualitatively opposite to the coefficient for the displacement of the corresponding isolator.

It has been verified that, by applying a typical variability (cov = 14.5%) to the mechanical properties of the elastomeric isolators (specifically: to the shear modulus of the rubber material), with linear dynamic analyses, a variability is obtained in the main displacement response parameters (underestimates/overestimations with respect to the results obtainable assuming the design mean values) no higher than 20% with reference to the 84th-percentile and no higher than 30% with reference to the 99th-percentile. This result is substantially in line with what is reported in the last sentence of paragraph 7.10.5.1 of the Italian code [11].

19.5 Concluding remarks of the chapter

In conclusion, a simplified procedure for the identification of HDRB isolators has been presented and applied to a RC bridge. The effects of the variability in the mechanical properties of the isolators (rubber shear modulus) on the structural behaviour of the isolated bridge emerged from several time-history analyses carried out on minimal models. They are characterized by few degrees of freedom, four in the longitudinal direction and five in the transversal one. The rubber shear modulus G is assumed as a random variable characterized by a normal distribution with mean value equal to 0.8 MPa and coefficient of variation equal to 14.5%. From 10000 sets of numerical simulations (each one carried out with seven natural accelerograms) which are representative of the realizations of the random variable G, the best fitting of the probability functions of the mean values of the displacements (for both isolators and piers) havs been performed. The analyses of

the associated percentiles allow the definition of coefficients for taking into account the variability of the rubber, i.e. Upper and Lower bounds values.

20

Conclusions

Sommario

Questo capitolo conclusivo riporta una sintesi delle analisi condotte e presentate in questa tesi, i principali risutati ottenuti e i possibili sviluppi futuri.

Il risultato fondamentale di questa tesi è il modello introdotto per la stima della resistenza di trefoli corrosi. Tale modello, che tiene conto della geometria di corrosione e dei parametri meccanici del materiale acciaio costituente i trefoli, può essere applicato secondo due approcci e secondo due procedure.

I parametri necessari a tali applicazioni, forniti in forma tabellare, sono stimati tramite delle simulazioni numeriche attraverso i modelli meccanici che descrivono il comportamento di fili e trefoli corrosi.

I domini di resistenza per trefoli corrosi rappresentano un importante risultato dell'applicazione del modello introdotto, che si pone come utile strumento ingegneristico per la stima della loro resistenza massima. Tale risultato, insieme ai domini di spostamento ultimo proposto, che forniscono indirettamente la duttilità ridotta di un trefolo corroso, consentono di stimare la legge costitutiva del materiale acciaio ridotta per effetto della corrosione.

Quest'ultimo, consente di valutare gli effetti della corrosione nei trefoli sulla risposta strutturale di travi post-tese attraverso il conseguente diagramma momento-curvatura ridotto.

La descrizione probabilistica del modello di resistenza ha permesso di definire i fattori di sicurezza per tenere conto della corrosione nelle verifiche di sicurezza di trefoli corrosi.

Summary

This concluding chapter reports a synthesis of the analyses conducted and presented in this thesis, the main results obtained and possible future developments.

The main result of this thesis is the model introduced for the estimation of the peak strength of corroded strands. This model, which takes into account the corrosion geometry and the mechanical parameters of the steel material constituting the strands, can be applied according to two approaches and two procedures.

The parameters necessary for these applications, provided in tabular form, are estimated by means of numerical simulations through the mechanical models that describe the behaviour of corroded wires and strands.

The important results of the application of the introduced model are the strength reduction curves for corroded strands, which represent useful engineering tools for estimating their maximum strength. These results, together with the proposed ultimate displacement reduction curves, which provide indirectly the reduced ductility of a corroded strand, allow to estimate the constitutive law of the steel material reduced by the effects of corrosion.

The latter allows to evaluate the effects of corrosion in the strands on the structural response of post-tensioned beams through the consequent reduced moment-curvature diagram.

The probabilistic description of the resistance model allowed to define safety factors to take into account corrosion in safety assessments of corroded strands.

20.1 Summary of the research

The thesis is composed of three parts.

Part I provides a general overview of the safety assessment of existing bridges.

Part II provides a series of studies and analyses that have been conducted in order to evaluate the effects of localized corrosion in corroded seven-wire strands.

Chapter 8 presents the methodological approach which is based on the following assumptions:

- the geometry of the corrosion has been modelled through two parameters that describe the transversal cross-section reduction and its longitudinal extension in corroded wires and strands;
- the steel material has been modelled by means of elastic-perfectly plastic and bilinear stress-strain relationships.

Chapter 8 provides analytical formulations for the mechanical behaviour of corroded single wires. A corroded wire is modelled as a series system between the corroded and not-corroded parts that are identified according to the geometry of the corrosion. Given the model, several parametric simulations have been conducted varying the parameters that describe the geometry of the corrosion and the steel material.

Chapter 9 provides analytical formulations for the mechanical behaviour of corroded strands. Two models have been presented: (i) the Darmawan-Stewart which is based on the brittle behaviour of the wires, and (ii) the parallel model which is based on the force-displacement relationships of the corroded wires. A parametric study has shown

the effects of the variability of the corrosion in the wires on the peak strength of corroded strands evaluated by means of the parallel model.

Chapter 10 presents the peak strength resistance model for corroded strands. The model introduces a new coefficient, which is defined as the group coefficient $\rho_G = \rho_{Gmin} \cdot \eta$, that takes into account the variability of the corrosion in the wires. This coefficient is described as made by two contributions representing: (i) the brittle behaviour of the wires through ρ_{Gmin}, and (ii) the ductile behaviour of the wires through the model coefficient η. The lower bound estimation of the group coefficient ρ_{Gmin} (brittle behaviour) has been achieved through the Darmawan-Stewart model, while the estimation of the model coefficient η has been obtained through several Monte Carlo simulations of corroded seven-wire strands. Finally, the application of the peak strength resistance model in deterministic and probabilist approaches allowed to define resistance curves and design-oriented results for corroded seven-wire strands.

Chapter 11 discusses the ductility through the the ultimate displacement reduction curves for corroded seven-wire strands.

Chapter 12 describes the reduced sigma-epsilon relationships that can be obtained starting from the strength reduction curves presented in Chapter 10 and the ultimate displacement reduction curves presented in Chapter 11.

Chapter 13 summarizes the results obtained in part II.

Part III regards the seismic upgrading through deck isolation. It provides a series of studies and analyses that have been conducted on a case-study RC bridge.

Chapter 15 describes the case-study bridge and its modelling by means of a finite element model and through the minimal systems. They describe the dynamic behaviour of the bridge in the longitudinal and transversal directions by means of a few degrees of freedom, four and five respectively.

Chapter 16 provides a simplified procedure for the identification of the high rubber bearing isolator devices (HDRBs) and their application to the case-study bridge.

Chapter 17 reports the results of dynamic analyses carried out for the evaluation of effects due to the force-displacement constitutive law of the isolators. Two laws have been considered: (i) bi-linear, and (ii) equivalent linear.

Chapter 18 reports the results of analyses carried out for the evaluation of the effects of the vertical component of the seismic input and the effectiveness of the rules for taking into account their effects through combination loads.

Chapter 19 reports the dynamic analyses carried out for the evaluation of the effects due to the variability in the shear modulus of the rubber of the isolators. These effects emerged from the analyses through the minimal systems of the case-study bridge. In addition, they allowed to calculate, for each response parameter, i.e. the displacements of

the deck, of the top of the piers, and of the isolator devices, the percentile values associated with selected percentages. Then, from the values of the percentiles, the coefficients that allow to take into account the variability of the rubber shear modulus on the structural response of the bridge have been calculated. These coefficients can be applied to the displacements of the isolators obtained considering the mean value of the rubber shear modulus since the coefficient of variation that characterizes the variability of the shear modulus does not keep unaltered in the variability of the response parameters. These coefficients include the Upper & Lower bound values, the 99% percentiles and the 1% percentile respectively.

20.2 Summary of the results obtained

The intense analyses conducted on the modelling of corroded wire and strands discussed in part II of this thesis highlighted the effects of the geometrical parameters (the cross-section reduction ρ_i and the adimensional corrosion extension λ_i) of the corrosion and of the steel material ones (ductility μ_ϵ and the hardening coefficient r) on the structural behaviour of corroded wires and strands.

In this regard, Chapter 8 reports the analytical mechanical model for corroded wires and a parametric study that has been conducted varying the parameters that describe the geometry of the corrosion and the steel material.

From the study emerged that:

- The effect of the coupling of ρ_i and λ_i can provide a post-yielding response exploitation of the not-corroded part leading to higher maximum force and ultimate displacement with respect to the ones of the corroded part, which can represent a first approximation of the mechanical behaviour of a corroded wire.
- For high values of ρ_i, the post-yielding response exploitation appears clear also for small values of hardening coefficient (i.e. $r = 0.5\%$), but it depends on the λ_i and μ_ϵ values.
- For small values of ρ_i, the same effect takes place only for higher values of r and λ_i. In other words, a particular coupling of ρ_i and λ_i might provide a post-yielding response exploitation of the not-corroded part leading to an increase in the performance of the corroded wire.

The results of the parametric study on corroded seven-wire strands presented in Chapter 9 highlighted the effects of the variability of the corrosion in the wires on the structural

behaviour of the strands. From this study, which has been conducted by varying the parameters that describe the geometry of the corrosion and the steel material, emerged that:

- The mechanical force-displacement response appears further depending on the corrosion variability in the wires.
- The reductions in the maximum force and ultimate displacement are provided both from the corrosion mean level and from the variability in the corrosion of the wires.
- For a fixed λ_i value, the higher the variability, the higher the reduction of the strand maximum force. This important aspect is currently under study and will be the object of future works.
- The further reduction in the peak force due to the variability in the wires decreases with an increasing of the adimensional corrosion extension λ_i.
- The hardening effect is limited for small material ductility (i.e. high strength steel with $\mu_\epsilon = 10$), whilst it leads to higher maximum force and higher ultimate displacement for large material ductility (i.e. mild steel with $\mu_\epsilon = 100$). In other words, the behaviour of corroded seven-wire strands made up of high-strength steel is well represented by an elastic perfectly plastic constitutive model.
- For elastic-perfectly plastic steel material with high values of material ductility μ_ϵ, the peak force depends only on the mean corrosion level ρ_M, in fact, the ductility content in the wires is enough to achieve the yielding stress. This is valid also if, in addition, high values of the adimensional corrosion length λ_i are considered

Consequently, Chapter 10 presents the peak strength resistance model for corroded strands introducing the group coefficient that takes into account the variability of the corrosion in the wires on the strength of corroded strands. Its lower bound estimation led to the following results:

- it assumes a minimum value that depends on the number of wires in the strands;
- it increases with an increasing of the variability of the corrosion in the wires;
- it has the minimum value, which means a maximum reduction of the peak force for a damage index equal to 0.5.

The model coefficient η has been estimated through Monte Carlo simulations of corroded strands following two procedures: for λ_i unknown and for λ_i known. The following results have been achieved:

- for the deterministic approach, which can be used for a direct estimation of the strength of corroded seven-wire strands by directly applying the Eq.10.1:

  - the mean corrosion level is reasonably estimated $\Rightarrow \rho_M$;
  - the peak force of the not-corroded strand is calculated $\Rightarrow F_0$;
  - the minimum group coefficient is calculated by applying Eq.10.3 $\Rightarrow \rho_{Gmin}$;
  - the model coefficient can be calculated thanks to its expressions that have been obtained by the fitting procedure of the Monte Carlo simulations results. These functions for all the damage index values are reported in Appendix A $\Rightarrow \eta$;

- for the probabilistic approach, which can be used for providing a statistical representation of the peak force:

  - the mean corrosion level ρ_M can be assumed as deterministic variable;
  - the peak force F_0 of the not-corroded strand is equal to $A_0 \cdot f_y$. The cross-section area A_0 of the not corroded strand can be assumed as a deterministic variable while the yielding stress of the steel material f_y is a random variable;
  - the minimum group coefficient ρ_{Gmin} can be assumed as deterministic variable;
  - the model coefficient η can be assumed as random variable. Its probability density functions have been obtained by the fitting procedure of the Monte Carlo simulations results. These functions for all the damage index values are reported in Appendix A.

All the results have been obtained with reference to a specific values for the cross-section of the strands (7 wires with 4 mm diameter) and for the steel material (steel stress and material ductility). However, the same approaches can be applied to other configurations of strands and materials.

Similarly, Chapter 11 presents ultimate displacement reduction curves estimated through the Monte Carlo simulations of corroded seven-wire strands. The strength and the ultimate displacement reduction curves allowed to estimate reduced sigma-epsilon relationships for the steel material that can be applied to evaluate the effect of corroded strands on the mechanical behaviour of post-tensioned beams, for instance by means the consequent reduced bending moment-curvature diagram.

As a part of the findings, Appendix A reports the expressions of the model coefficient η to be used in the application of the resistance model with two approaches and the two procedures, for all the damage index values.

Appendix B reports the mathematical demonstration for obtaining the analytical estimation of the lower bound of the group coefficient.

Appendix C reports the mathematical demonstration for obtaining the analytical expression for the elastic stiffness, yielding displacement, ultimate displacement and the ductility of a corroded wire.

Appendix D reports the mathematical demonstration for obtaining the integral expression of the probability and cumulative density function of the strength of corroded seven-wire strands.

20.3 Future developements

In this thesis, the problem of corrosion in wires and strands has been faced through simplified analytical models. Analogous results have been achieved in terms of strength and ductility of the corroded strands namely:

- modelling of the variability of the corrosion in the wires, that partially explain the dispersion that emerged in some experimental tests on corroded strands available in the literature;
- estimation of the capacity of corroded seven-wire strands in terms of strength and ultimate displacements;
- estimation of the safety factors associated with corroded seven-wire strands.
- estimation of the reduction of the flexural capacity of the post-tensioned beam through the reduced bending moment-curvature diagram.

All these results could play a role in the current management of post-tension bridges built in the 60/70s that today present problems of corrosion in the strands.

Clearly, this thesis represents a first step towards the complex solution for understanding the structural behaviour of corroded wires and strands. In this regard, the following activities could be implemented:

1. experimental validation of the results obtained by means of tensile test on corroded wires and strands;
2. numerical validation of the results obtained by means of sophisticated finite element models on corroded wires and strands;
3. updating of the presented models in terms of stress-strain relationships for the steel material;
4. identifying possible corrosion phenomena in post-tensioned beams through the variation of the bending moment-curvature diagram. This could be also implemented in monitoring systems.

References

[1] M Domaneschi et al. “Collapse analysis of the Polcevera viaduct by the applied element method”. In: *Engineering Structures* 214 (2020), p. 110659.

[2] Nicola Scattarreggia et al. “Collapse analysis of the multi-span reinforced concrete arch bridge of Caprigliola, Italy”. In: *Engineering Structures* 251 (2022), p. 113375.

[3] Chi-Ho Jeon, Cuong Duy Nguyen, and Chang-Su Shim. “Assessment of mechanical properties of corroded prestressing strands”. In: *Applied Sciences* 10.12 (2020), p. 4055.

[4] GholamReza Havaei and Seyyed Amirhossein Moayyedi. “Assessment of sliding-rubber isolator effect in progressive collapse of bridges under two scenarios”. In: *The Structural Design of Tall and Special Buildings* 27.3 (2018), e1418.

[5] Margherita Pauletta et al. “Tensile tests for the improvement of adhesion between rubber and steel layers in elastomeric isolators”. In: *Applied Sciences* 10.22 (2020), p. 8063.

[6] Mario Paolo Petrangeli. *Progettazione e costruzione di ponti*. Masson, 1997.

[7] U.S. Departement of Transportation (DOT) Federal Highway Administratione (FHWA). *National Bridge Inspection Standards*. Vol. 87. 2022.

[8] Harry AL Lindberg. “The Federal-Aid Highway Program: Present and Future”. In: (1978).

[9] US Congress. “Intermodal surface transportation efficiency act of 1991”. In: *Public Law* 1991 (1991), pp. 102–240.

[10] R Woodward et al. “Bridge management in Europe (BRIME)-Deliverable D14-Final Report”. In: (2001).

[11] Min. Infrastrutture e Trasporti. *Norme tecniche per le costruzioni (NTC 2018) D. Min. Infrastrutture e Trasporti 17 gennaio 2018*. 2018.

[12] Hartle et al. *Bridge Inspector’s Reference Manual: Volume 1 and Volume 2*. 2002-10-01. URL: https://rosap.ntl.bts.gov/view/dot/39863.

[13] American Association of State Highway and Transportation Officials. *Manual for Maintenance Inspection of Bridges 1983: Includes Revisions from Interim Specifications for Bridges 1984, 1985, 1986, 1987-1988, 1990*. AASHTO, 1990. URL: https://books.google.it/books?id=FsFjmgEACAAJ.

[14] United States. Federal Highway Administration. Bridge Division and United States. Federal Highway Administration. Bridge Division. Design & Inspection Branch. *Recording and Coding Guide for the Structure Inventory and Appraisal of the Nation's Bridges*. Department of Transportation, Federal Highway Administration, 1979. URL: https://books.google.it/books?id=aCnsRwakWDMC.

[15] J.D. Arnoult, MacDonald & Lewis Byrd Tallamy, and United States. Federal Highway Administration. Office of Implementation. *Culvert Inspection Manual: Supplement to the Bridge Inspector's Training Manual*. U.S. Department of Transportation, Federal Highway Administration, Research, Development, and Technology, 1986. URL: https://books.google.it/books?id=DqPlfOe%5C_8aIC.

[16] R.J. Conner et al. *Inspection and Management of Bridges with Fracture-critical Details*. National Cooperative Transit Research Program Synthesis Series. Transportation Research Board, 2005. ISBN: 9780309097611. URL: https://books.google.it/books?id=xJMLweRgufMC.

[17] F.H. Administration and U.S.D. Transportation. *Evaluating Scour at Bridges . Hydraulic Engineering Circular No. 18. Publication No. Fhwa-Hif-12-003*. Books Express Publishing, 2012. ISBN: 9781782661214. URL: https://books.google.it/books?id=94XhMgEACAAJ.

[18] American Association of State Highway, Transportation Officials. Subcommittee on Bridges, and Structures. *The Manual for Bridge Evaluation*. American Association of State Highway and Transportation Officials, 2011. ISBN: 9781560514961. URL: https://books.google.it/books?id=r2kR2FA0vQAC.

[19] U.S. Departement of Transportation (DOT) Federal Highway Administratione (FHWA). *Specifications for the National Bridge Inventory*. 2022. ISBN: 9781782661214. URL: https://www.fhwa.dot.gov/bridge/snbi.cfm.

[20] F Moses. "NCHRP Report 454: Calibration of load factors for LRFR bridge evaluation". In: *TRB, National Research Council, Wash* (2001).

[21] Ministero delle Infrastrutture e dei Trasporti and Consiglio Superiore dei Lavori Pubblici. "Linee guida per la classificazione e gestione del rischio, la valutazione della sicurezza ed il monitoraggio dei ponti esistenti". In: *Ministero delle Infrastrutture e dei Trasporti, Consiglio Superiore dei Lavori Pubblici: Roma, Italy* (2022).

[22] FIB-Féd Int du Béton. *Partial factor methods for existing concrete structures: Recommendation*. Vol. 80. FIB-Féd. Int. du Béton, 2016.

[23] Ministero delle Infrastrutture e dei Trasporti. “Circolare 21 gennaio 2019 n. 7 CS LL. PP. Istruzioni per l’applicazione dell’aggiornamento delle ‘Norme Tecniche per le Costruzioni’di cui al DM 17/01/2018 (in Italian)”. In: *Suppl. Ord. Alla GU n. 35 Del 11/2/19* (2019).

[24] George C Lee et al. *A study of US bridge failures (1980-2012)*. MCEER Buffalo, NY, 2013.

[25] Giuseppe Santarsiero, Angelo Masi, and Valentina Picciano. “Durability of Gerber Saddles in RC Bridges: Analyses and Applications (Musmeci Bridge, Italy)”. In: *Infrastructures* 6.2 (2021). ISSN: 2412-3811. DOI: 10.3390/infrastructures6020025. URL: https://www.mdpi.com/2412-3811/6/2/25.

[26] Marialaura Malena et al. “Arch bridges subject to pier settlements: Continuous vs. piecewise rigid displacement methods”. In: *Meccanica* 56.10 (2021), pp. 2487–2505.

[27] Keith Worden et al. “The fundamental axioms of structural health monitoring”. In: *Proceedings of the Royal Society A: Mathematical, Physical and Engineering Sciences* 463.2082 (2007), pp. 1639–1664.

[28] Daniel Balageas, Claus-Peter Fritzen, and Alfredo Güemes. *Structural health monitoring*. Vol. 90. John Wiley & Sons, 2010.

[29] Rune Brincker, Lingmi Zhang, Palle Andersen, et al. “Modal identification from ambient responses using frequency domain decomposition”. In: *Proceedings of the 18th international modal analysis conference (IMAC)*. Vol. 1. San Antonio, TX, USA. 2000, pp. 625–630.

[30] Carlo Rainieri and Giovanni Fabbrocino. “Operational modal analysis of civil engineering structures”. In: *Springer, New York* 142 (2014), p. 143.

[31] Rune Brincker and Carlos Ventura. *Introduction to operational modal analysis*. John Wiley & Sons, 2015.

[32] Peter Welch. “The use of fast Fourier transform for the estimation of power spectra: a method based on time averaging over short, modified periodograms”. In: *IEEE Transactions on audio and electroacoustics* 15.2 (1967), pp. 70–73.

[33] Rune Brincker, Lingmi Zhang, and Palle Andersen. “Modal identification of output-only systems using frequency domain decomposition”. In: *Smart materials and structures* 10.3 (2001), p. 441.

[34] Filipe Magalhães and Álvaro Cunha. “Explaining operational modal analysis with data from an arch bridge”. In: *Mechanical systems and signal processing* 25.5 (2011), pp. 1431–1450.

[35] Filipe Magalhães et al. “Damping estimation using free decays and ambient vibration tests”. In: *Mechanical Systems and Signal Processing* 24.5 (2010), pp. 1274–1290.

[36] Karl Pearson F.R.S. “LIII. On lines and planes of closest fit to systems of points in space”. In: *The London, Edinburgh, and Dublin Philosophical Magazine and Journal of Science* 2.11 (1901), pp. 559–572. DOI: 10.1080/14786440109462720. eprint: https://doi.org/10.1080/14786440109462720. URL: https://doi.org/10.1080/14786440109462720.

[37] Harold Hotelling. “Analysis of a complex of statistical variables into principal components.” In: *Journal of educational psychology* 24.6 (1933), p. 417.

[38] Laura Anania, Antonio Badalà, and Giuseppe D’Agata. “Damage and collapse mode of existing post tensioned precast concrete bridge: The case of Petrulla viaduct”. In: *Engineering Structures* 162 (2018), pp. 226–244.

[39] Fumin Li et al. “Numerical simulation method for fracture effect of corroded steel strand under tension”. In: (2014).

[40] Chi-Ho Jeon et al. “Equivalent material model of corroded prestressing steel strand”. In: *Journal of Materials Research and Technology* 8.2 (2019), pp. 2450–2460.

[41] Chul-Hwan Yoo, Yeun Chul Park, and Ho-Kyung Kim. “Section loss in naturally corroded 7-wire steel strands in external tendons”. In: *Structure and Infrastructure Engineering* 16.11 (2020), pp. 1593–1603.

[42] Changsu SHIM Chiho JEON Jaebin LEE. “Mechanical behaviour of corroded prestressing steel strand.” In: *Fifth Conference on Smart Monitoring, Assessment and Rehabilitation of Civil Structures* (2019).

[43] Jeon Chi-Ho, Lee Jae-Bin, and Shim Chang-Su. “Tensile Test of Corroded Strand and Maintenance of Corroded Prestressed Concrete Girders”. In: *International Journal of Urban and Civil Engineering* 11.10 (2017), pp. 1384–1388.

[44] Jun Xu and Weizhen Chen. “Behavior of wires in parallel wire stayed cable under general corrosion effects”. In: *Journal of Constructional Steel Research* 85 (2013), pp. 40–47.

[45] Richard Haskins et al. “Relating corroded seven-strand, posttensioned cable cross-sectional properties to load capacity”. In: *Journal of Engineering* 2016 (2016).

[46] Bang-Yeon Lee et al. “Corrosion and strength behaviors in prestressed tendon under various tensile stress and impressed current conditions”. In: *Advances in Materials Science and Engineering* 2017 (2017).

[47] Zhao-Hui Lu, Fan Li, and Yan-Gang Zhao. “An investigation of degradation of mechanical behaviour of prestressing strands subjected to chloride attacking”. In: (2016).

[48] Lorenzo Franceschini et al. “Mechanical behaviour of corroded strands under chloride attack: A new constitutive law”. In: *Construction and Building Materials* 316 (2022), p. 125872.

[49] Lorenzo Franceschini et al. “A simplified stress–strain relationship for the mechanical behavior of corroded prestressing strands: The SCPS-model”. In: *Structural Concrete* (2022).

[50] Lei Wang et al. “Corrosion morphology and mechanical behavior of corroded prestressing strands”. In: *Journal of Advanced Concrete Technology* 18.10 (2020), pp. 545–557.

[51] MS Darmawan and MG Stewart. “Effect of spatially variable pitting corrosion on structural reliability of prestressed concrete bridge girders”. In: *Australian Journal of Structural Engineering* 6.2 (2006), pp. 147–158.

[52] I Finozzi, A Saetta, and H Budelmann. “Structural response of reinforcing bars affected by pitting corrosion: experimental evaluation”. In: *Construction and Building Materials* 192 (2018), pp. 478–488.

[53] George A Costello. *Theory of wire rope*. Springer Science & Business Media, 1997.

[54] British Standard et al. “Eurocode—Basis of structural design”. In: *Eurocode 0* (2002).

[55] E Tubaldi, A Dall’Asta, and L Dezi. “Seismic response analysis of continuous multispan bridges with partial isolation”. In: *Shock and Vibration* 2015 (2015).

[56] S Silvestri et al. “Sistemi minimi per la progettazione sismica di ponti con diverse soluzioni per lo schema di vincolo”. In: *Atti del XVIII Convegno ANIDIS 2019 - L’Ingegneria sismica in Italia* (2019), pp. 18–28.

[57] Farzad Naeim and James M Kelly. *Design of seismic isolated structures: from theory to practice*. John Wiley & Sons, 1999.

[58] P Franchin, G Monti, and PE Pinto. “On the accuracy of simplified methods for the analysis of isolated bridges”. In: *Earthquake engineering & structural dynamics* 30.3 (2001), pp. 363–382.

[59] Marco Furinghetti. “Definition and Validation of Fast Design Procedures for Seismic Isolation Systems”. In: *Vibration* 5.2 (2022), pp. 290–305.

[60] Antonello De Luca and Laura Giovanna Guidi. “State of art in the worldwide evolution of base isolation design”. In: *Soil Dynamics and Earthquake Engineering* 125 (2019), p. 105722.

[61] Anil K. Chopra. *Dynamics of structures : theory and applications to earthquake engineering, 4/E*. 2012, p. 980. ISBN: 1292249188. URL: https://www.pearson.com/us/higher-education/product/Chopra-Dynamics-of-Structures-4th-Edition/9780132858038.html.

[62] Yi-Kwei Wen. "Method for random vibration of hysteretic systems". In: *Journal of the engineering mechanics division* 102.2 (1976), pp. 249–263.

[63] YJ Park, YK Wen, and A H-S Ang. "Random vibration of hysteretic systems under bi-directional ground motions". In: *Earthquake engineering & structural dynamics* 14.4 (1986), pp. 543–557.

[64] Satish Nagarajaiah, Andrei M Reinhorn, and Michalakis C Constantinou. "Nonlinear dynamic analysis of 3-D-base-isolated structures". In: *Journal of Structural Engineering* 117.7 (1991), pp. 2035–2054.

[65] Paolo Castaldo et al. "Resistance model uncertainty in non-linear finite element analyses of cyclically loaded reinforced concrete systems". In: *Engineering Structures* 211 (2020), p. 110496.

[66] Marco Furighetti and Alberto Pavese. "Numerical parametric study on property modification factors of isolation devices". In: *Atti del XVIII Convegno ANIDIS 2019 - L'Ingegneria sismica in Italia* (2019), pp. 2–10.

[67] European Committee for Standardization. *Eurocode 8: Design of structures for earthquake resistance*. 2004.

[68] Alfredo HS Ang and Wilson H Tang. *Probability Concepts in Engineering Planning: Emphasis on Applications to Civil and Environmental Engineering, John Wiley and Sons*. 2007.

Appendices

Appendix A

Summary of the results for deterministic and probabilistic approaches for fixed values of the damage index

This appendix reports the results of the fitting operations, of the Monte-Carlo simulations, applied with reference to the two procedures (λ unknown and λ known) and the two approaches (deterministic and probabilistic) presented in Chapter 10. The deterministic approach requires the expression of η and can be directly applied by Eq. 10.1, while the probabilistic one requires the expression of its statistic (here reported in terms of probability density function) according to Eq. 10.7.

In addition, the probabilistic approach is reported in terms of probability functions for for the resistance R of corroded strands (according to Eq. 10.8). According to the results shown in Chapter 10, η is defined in the range $[0, 1/\rho_{Gmin}]$.

The following results have been achieved for seven-wire strands ($n_w = 7$).

As explained in section 10.7.2, in order to determine the probability functions of the resistance model defined by Eq. 10.7 four hypotheses have been done:

1. the resistance R is a function of deterministic and random variables;
2. the yield stress of the steel material f_y, and the model coefficient η are considered random variables;
3. the not-corroded area of the wires A_0 (it is typically characterized by a small coefficient of variation, below 1%), the mean corrosion level ρ_M and the minimum group function ρ_{Gmin} are considered as deterministic variables;
4. the functions that define the resistance R can be assumed as independent variables.

In addition, the probability density function of the yield stress can be assumed as logNormal with a mean value equal to 1700 MPa and a coefficient of variation equal to 5%. Instead, the model coefficient η has a probability density function identified after the fitting of the Monte Carlo simulation results (and here reported for different λ_i values and different damage index scenarios), chosen according to the two procedures for λ_i unknown and for λ_i known.

The not-corroded strand area has been assumed equal to $87.96mm^2$ (seven wires with a diameter of $4mm$) and the minimum group function ρ_{Gmi} assumes values given by Eq. 10.3 according with the mean corrosion level (which means D).

A.1 Damage index $D = 0.01$

A.1.1 Deterministic approach

- **Procedure (a): λ is unknown** $\Rightarrow \eta = C$

Percentile	C
50^{th}	1.01
16^{th}	1.01
1^{th}	0.958

- **Procedure (b): λ is known** $\Rightarrow \eta(\lambda) = C_1\lambda^3 + C_2\lambda^2 + C_3\lambda + C_4$ for $\lambda \leq \lambda_{lim}$

Percentile	C_1	C_2	C_3	C_4	λ_{lim}	R^2
50^{th}	1	-1078.65	17.26	0.94	0.008	0.74
16^{th}	1	-1087.57	17.40	0.94	0.008	0.56
1^{th}	1	-1091.70	17.47	0.94	0.008	0.43

A.1.2 Probabilistic approach

For this level of damage index it was not possible to fit the statistic of η.

A.2 Damage index $D = 0.10$

A.2.1 Deterministic approach

- **Procedure (a): λ is unknown** $\Rightarrow \eta = C$

Percentile	C
50^{th}	1.07
16^{th}	1.04
1^{th}	0.891

- **Procedure (b): λ is known** $\Rightarrow \eta(\lambda) = C_1\lambda^3 + C_2\lambda^2 + C_3\lambda + C_4$ for $\lambda \leq \lambda_{lim}$

Percentile	C_1	C_2	C_3	C_4	λ_{lim}	R^2
50^{th}	26.22	-37.25	5.02	0.94	0.073	0.79
16^{th}	-650.29	50.5	3.02	0.89	0.073	0.87
1^{th}	-682.06	44.00	4.48	0.83	0.073	0.89

A.2.2 Probabilistic approach

- **Procedure (a): λ is unknown**

  For this level of damage index it was not possible to fit the statistic of η.

- **Procedure (b): λ is known**

λ	Probability function of η
0.001	$logN(\mu = -0.035, \sigma = 0.0858)$
0.01	$\beta(a = 14.71, b = 1.37)$
0.02	$\beta(a = 48.27, b = 4.24)$
0.03	$logN(\mu = 0.054, \sigma = 0.0222)$
0.04	$logN(\mu = 0.071, \sigma = 0.0253)$
0.05	$\beta(a = 7.83, b = 0.24)$
0.06	$\beta(a = 8.38, b = 0.17)$
0.07	-
0.08	-
0.09	-
0.10	-

Table A.6: Design-oriented results from the peak strength probability density function for the case of $D = 0.1$

Cumulative Curve	**Resistance characteristic value R_k [kN]**	**Resistance design value $R_{d,0.1\%}$ evaluated to CDF = 0.1 % [kN]**	**Resistance design value $R_{d,1\%}$ evaluated to CDF = 1 % [kN]**	**Resistance safety factor $\gamma = R_k/R_{d,0.1\%}$**	**Resistance safety factor $\gamma = R_k/R_{d,1\%}$**	**Corrosion characteristic coefficient $k_{corr} = R_k/(f_{y,k} \cdot A_0 \cdot \eta_k \cdot \rho_M \cdot \rho_{Gmin})$**
$\lambda_i = 0.001$	98.01	84.91	91.60	1.15	1.07	1.19
$\lambda_i = 0.01$	100.38	75.86	89.32	1.32	1.13	1.07
$\lambda_i = 0.02$	110.44	97.90	104.67	1.13	1.06	1.05
$\lambda_i = 0.03$	115.29	106.52	111.07	1.08	1.04	1.07
$\lambda_i = 0.04$	116.92	107.82	112.54	1.08	1.04	1.08
$\lambda_i = 0.05$	110.84	72.72	94.23	1.52	1.18	1.07
$\lambda_i = 0.06$	113.99	78.00	98.77	1.46	1.15	1.07

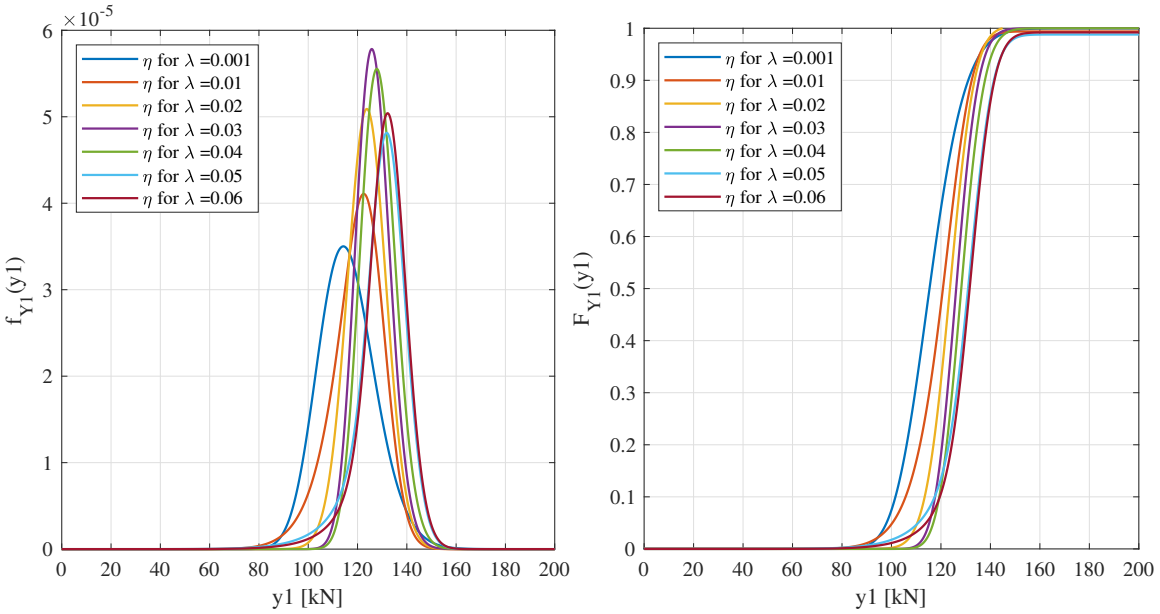

(a) Resistance probability density functions (b) Resistance cumulative density functions

Figure A.1: Probability functions of corroded seven-wire strands for different values of λ_i and $D = 0.1$

A.3 Damage index $D = 0.20$

A.3.1 Deterministic approach

- **Procedure (a): λ is unknown** $\Rightarrow \eta = C$

Percentile	C
50^{th}	1.28
16^{th}	1.15
1^{th}	0.95

- **Procedure (b): λ is known** $\Rightarrow \eta(\lambda) = C_1\lambda^3 + C_2\lambda^2 + C_3\lambda + C_4$ for $\lambda \leq \lambda_{lim}$

Percentile	C_1	C_2	C_3	C_4	λ_{lim}	R^2
50^{th}	121.72	-55.67	7.48	1.02	0.1	0.98
16^{th}	-141.85	-10.61	6.38	0.94	0.1	0.99
1^{th}	-331.14	19.13	6.11	0.86	0.1	0.99

A.3.2 Probabilistic approach

- **Procedure (a): λ is unknown**

  For this level of damage index it was not possible to fit the statistic of η.

- **Procedure (b): λ is known**

λ	Probability function of η
0.001	$logN(\mu = 0.036, \sigma = 0.0951)$
0.01	$\beta(a = 24.33, b = 4.58)$
0.02	$\beta(a = 35.80, b = 5.80)$
0.03	$logN(\mu = 0.172, \sigma = 0.0467)$
0.04	$logN(\mu = 0.205, \sigma = 0.0453)$
0.05	$\beta(a = 14.46, b = 0.76)$
0.06	$\beta(a = 13.44, b = 0.41)$
0.07	-
0.08	-
0.09	-
0.10	-

Table A.10: Design-oriented results from the peak strength probability density function for the case of $D = 0.2$

Cumulative Curve	**Resistance characteristic value R_k [kN]**	**Resistance design value $R_{d,0.1\%}$ evaluated to CDF = 0.1 % [kN]**	**Resistance design value $R_{d,1\%}$ evaluated to CDF = 1 % [kN]**	**Resistance safety factor $\gamma = R_k/R_{d,0.1\%}$**	**Resistance safety factor $\gamma = R_k/R_{d,1\%}$**	**Corrosion characteristic coefficient $k_{corr} = R_k/(f_{y,k} \cdot A_0 \cdot \eta_k \cdot \rho_M \cdot \rho_{Gmin})$**
$\lambda_i = 0.001$	77.83	66.61	72.32	1.17	1.08	1.21
$\lambda_i = 0.01$	82.40	66.29	74.94	1.24	1.10	1.07
$\lambda_i = 0.02$	89.18	75.72	82.96	1.18	1.08	1.06
$\lambda_i = 0.03$	94.99	85.93	90.6	1.11	1.05	1.13
$\lambda_i = 0.04$	98.45	89.29	94.02	1.10	1.05	1.12
$\lambda_i = 0.05$	98.21	75.80	88.41	1.30	1.11	1.06
$\lambda_i = 0.06$	102.130	79.24	92.49	1.29	1.10	1.06

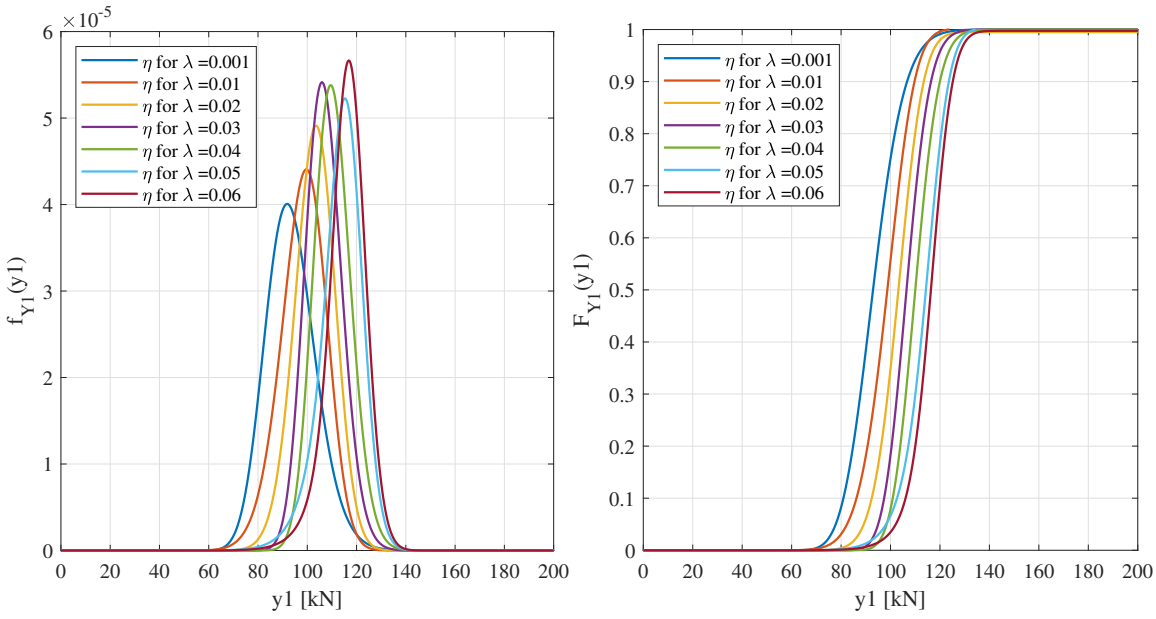

(a) Resistance probability density functions (b) Resistance cumulative density functions

Figure A.2: Probability functions of corroded seven-wire strands for different values of λ_i and $D = 0.2$

A.4 Damage index $D = 0.30$

A.4.1 Deterministic approach

- **Procedure (a): λ is unknown** $\Rightarrow \eta = C$

Percentile	C
50^{th}	1.53
16^{th}	1.31
1^{th}	1.05

- **Procedure (b): λ is known** $\Rightarrow \eta(\lambda) = C_1\lambda^3 + C_2\lambda^2 + C_3\lambda + C_4$ for $\lambda \leq \lambda_{lim}$

Percentile	C_1	C_2	C_3	C_4	λ_{lim}	R^2
50^{th}	6.51	-48.85	9.58	1.16	0.1	1
16^{th}	-226.52	-15.29	9.85	1.03	0.1	0.99
1^{th}	-719.85	76.54	6.29	0.96	0.1	0.98

A.4.2 Probabilistic approach

- **Procedure (a): λ is unknown**

  $\beta(a = 3.38, b = 0.322)$

- **Procedure (b): λ is known**

λ	**Probability function OF** η
0.001	$logN(\mu = 0.154, \sigma = 0.1007)$
0.01	$logN(\mu = 0.224, \sigma = 0.0847)$
0.02	$logN(\mu = 0.286, \sigma = 0.0716)$
0.03	$logN(\mu = 0.335, \sigma = 0.0667)$
0.04	$logN(\mu = 0.378, \sigma = 0.0575)$
0.05	$logN(\mu = 0.414, \sigma = 0.0449)$
0.06	$logN(\mu = 0.443, \sigma = 0.0322)$
0.07	$\beta(a = 14.64, b = 0.38)$
0.08	$\beta(a = 22.15, b = 0.25)$
0.09	$\beta(a = 65.63, b = 0.19)$
0.10	-

Table A.14: Design-oriented results from the peak strength probability density function for the case of $D = 0.3$

Cumulative Curve	**Resistance characteristic value R_k [kN]**	**Resistance design value $R_{d,0.1\%}$ evaluated to CDF = 0.1 % [kN]**	**Resistance design value $R_{d,1\%}$ evaluated to CDF = 1 % [kN]**	**Resistance safety factor $\gamma = R_k/R_{d,0.1\%}$**	**Resistance safety factor $\gamma = R_k/R_{d,1\%}$**	**Corrosion characteristic coefficient $k_{corr} = R_k/(f_{y,k} \cdot A_0 \cdot \eta_k \cdot \rho_M \cdot \rho_{Gmin})$**
λ_i unknown	63.61	22.06	41.90	2.88	1.52	1.08
$\lambda_i = 0.001$	62.11	52.82	57.54	1.18	1.08	1.21
$\lambda_i = 0.01$	68.21	59.22	63.82	1.15	1.07	1.19
$\lambda_i = 0.02$	73.68	64.88	69.39	1.14	1.06	1.17
$\lambda_i = 0.03$	77.97	69.09	73.65	1.13	1.06	1.16
$\lambda_i = 0.04$	82.44	73.88	78.29	1.12	1.05	1.15
$\lambda_i = 0.05$	86.75	78.76	82.89	1.10	1.05	1.12
$\lambda_i = 0.06$	90.38	82.95	86.80	1.09	1.04	1.09
$\lambda_i = 0.07$	90.56	72.08	82.92	1.26	1.09	1.06
$\lambda_i = 0.08$	93.83	81.96	89.12	1.14	1.05	1.04
$\lambda_i = 0.09$	95.74	88.83	92.44	1.08	1.04	1.01

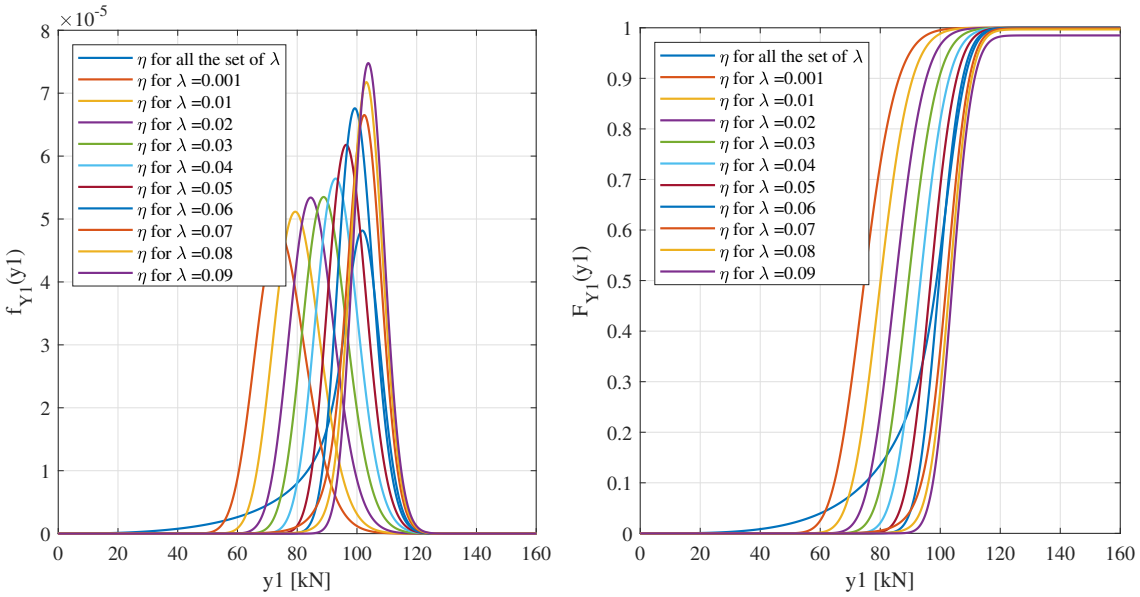

(a) Resistance probability density functions (b) Resistance cumulative density functions

Figure A.3: Probability functions of corroded seven-wire strands for different values of λ_i and $D = 0.3$

A.5 Damage index $D = 0.40$

A.5.1 Deterministic approach

- **Procedure (a): λ is unknown** $\Rightarrow \eta = C$

Percentile	C
50^{th}	1.62
16^{th}	1.33
1^{th}	1.08

- **Procedure (b): λ is known** $\Rightarrow \eta(\lambda) = C_1\lambda^3 + C_2\lambda^2 + C_3\lambda + C_4$ for $\lambda \leq \lambda_{lim}$

Percentile	C_1	C_2	C_3	C_4	λ_{lim}	R^2
50^{th}	7.68	-59.38	11.65	1.17	0.1	1
16^{th}	-423.69	15.08	9.69	1.05	0.1	1
1^{th}	-953.50	109.64	6.68	0.94	0.1	0.98

A.5.2 Probabilistic approach

- **Procedure (a): λ is unknown**

  $\beta(a = 3.00, b = 0.33)$

- **Procedure (b): λ is known**

λ	Probability function of η
0.01	$logN(\mu = 0.165, \sigma = 0.1007)$
0.01	$logN(\mu = 0.248, \sigma = 0.0919)$
0.02	$logN(\mu = 0.321, \sigma = 0.0868)$
0.03	$logN(\mu = 0.381, \sigma = 0.0788)$
0.04	$logN(\mu = 0.431, \sigma = 0.0653)$
0.05	$logN(\mu = 0.472, \sigma = 0.0518)$
0.06	$logN(\mu = 0.503, \sigma = 0.0397)$
0.07	$\beta(a = 13.07, b = 0.40)$
0.08	$\beta(a = 18.95, b = 0.25)$
0.09	$\beta(a = 57.64, b = 0.20)$
0.10	-

Table A.18: Design-oriented results from the peak strength probability density function for the case of $D = 0.4$

Cumulative Curve	**Resistance characteristic value R_k [kN]**	**Resistance design value $R_{d,0.1\%}$ evaluated to CDF = 0.1 % [kN]**	**Resistance design value $R_{d,1\%}$ evaluated to CDF = 1 % [kN]**	**Resistance safety factor $\gamma = R_k/R_{d,0.1\%}$**	**Resistance safety factor $\gamma = R_k/R_{d,1\%}$**	**Corrosion characteristic coefficient $k_{corr} = R_k/(f_{y,k} \cdot A_0 \cdot \eta_k \cdot \rho_M \cdot \rho_{Gmin})$**
λ_i unknown	50.73	15.23	31.53	3.33	1.61	1.08
$\lambda_i = 0.001$	50.14	42.60	46.43	1.18	1.08	1.21
$\lambda_i = 0.01$	55.17	47.35	51.33	1.17	1.07	1.20
$\lambda_i = 0.02$	59.83	51.74	55.87	1.16	1.07	1.20
$\lambda_i = 0.03$	64.38	56.30	60.44	1.14	1.07	1.18
$\lambda_i = 0.04$	68.92	61.25	65.19	1.13	1.06	1.16
$\lambda_i = 0.05$	72.94	65.76	69.46	1.11	1.05	1.14
$\lambda_i = 0.06$	76.31	69.61	73.07	1.10	1.04	1.11
$\lambda_i = 0.07$	76.55	59.03	69.17	1.30	1.11	1.06
$\lambda_i = 0.08$	79.90	68.03	75.26	1.17	1.06	1.04
$\lambda_i = 0.09$	81.94	75.94	79.09	1.08	1.04	1.02

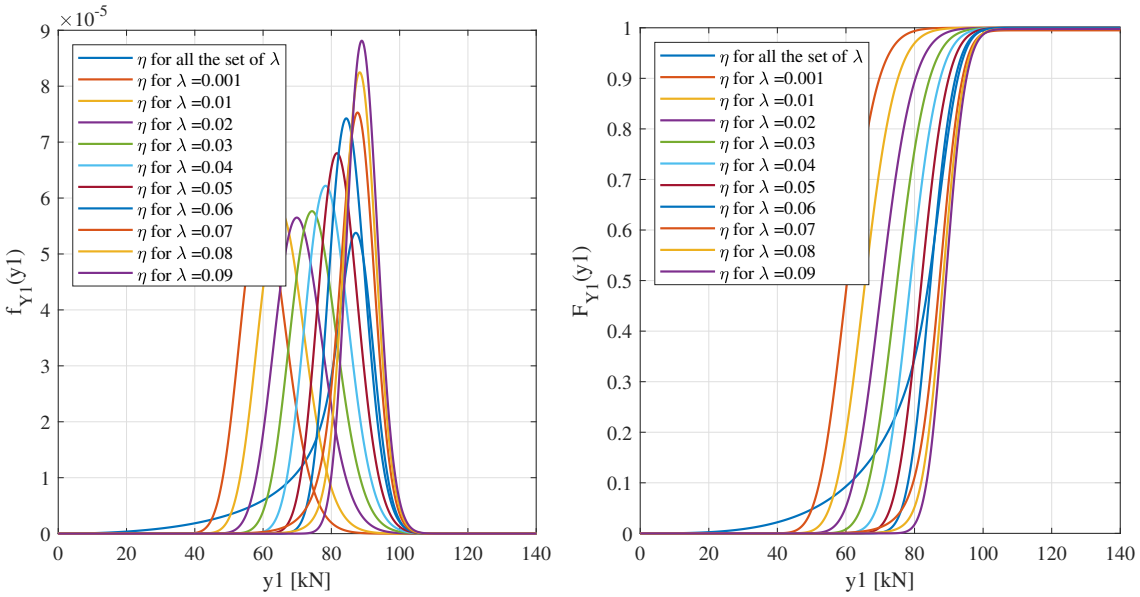

(a) Resistance probability density functions (b) Resistance cumulative density functions

Figure A.4: Probability functions of corroded seven-wire strands for different values of λ_i and $D = 0.4$

A.6 Damage index $D = 0.50$

A.6.1 Deterministic approach

- **Procedure (a): λ is unknown** $\Rightarrow \eta = C$

Percentile	C
50^{th}	1.64
16^{th}	1.33
1^{th}	1.02

- **Procedure (b): λ is known** $\Rightarrow \eta(\lambda) = C_1\lambda^3 + C_2\lambda^2 + C_3\lambda + C_4$ for $\lambda \leq \lambda_{lim}$

Percentile	C_1	C_2	C_3	C_4	λ_{lim}	R^2
50^{th}	-436.18	-27.25	12.73	1.13	0.08	1
16^{th}	-301.06	-15.10	12.05	1.00	0.1	1
1^{th}	-989.39	111.36	7.41	0.89	0.1	0.98

A.6.2 Probabilistic approach

- **Procedure (a): λ is unknown**

  $\beta(a = 2.48, b = 0.26)$

- **Procedure (b): λ is known**

λ	Probability function of η
0.001	$logN(\mu = 0.133, \sigma = 0.1152)$
0.01	$logN(\mu = 0.235, \sigma = 0.1098)$
0.02	$logN(\mu = 0.321, \sigma = 0.0977)$
0.03	$logN(\mu = 0.386, \sigma = 0.0851)$
0.04	$logN(\mu = 0.438, \sigma = 0.0730)$
0.05	$logN(\mu = 0.479, \sigma = 0.0593)$
0.06	$\beta(a = 8.33, b = 0.40)$
0.07	$\beta(a = 10.36, b = 0.26)$
0.08	$\beta(a = 18.16, b = 0.19)$
0.09	$\beta(a = 65.69, b = 0.16)$
0.10	-

Table A.22: Design-oriented results from the peak strength probability density function for the case of $D = 0.5$

Cumulative Curve	**Resistance characteristic value R_k [kN]**	**Resistance design value $R_{d,0.1\%}$ evaluated to CDF = 0.1 % [kN]**	**Resistance design value $R_{d,1\%}$ evaluated to CDF = 1 % [kN]**	**Resistance safety factor $\gamma = R_k/R_{d,0.1\%}$**	**Resistance safety factor $\gamma = R_k/R_{d,1\%}$**	**Corrosion characteristic coefficient $k_{corr} = R_k/(f_{y,k} \cdot A_0 \cdot \eta_k \cdot \rho_M \cdot \rho_{Gmin})$**
λ_i unknown	39.90	9.35	22.57	4.27	1.77	1.08
$\lambda_i = 0.001$	39.63	33.04	36.37	1.20	1.09	1.23
$\lambda_i = 0.01$	44.31	37.25	40.83	1.19	1.09	1.23
$\lambda_i = 0.02$	49.17	42.00	45.65	1.17	1.08	1.21
$\lambda_i = 0.03$	53.44	46.38	49.99	1.15	1.07	1.19
$\lambda_i = 0.04$	57.23	50.42	53.91	1.13	1.06	1.17
$\lambda_i = 0.05$	60.72	54.35	57.63	1.12	1.05	1.15
$\lambda_i = 0.06$	59.60	39.25	50.55	1.52	1.18	1.07
$\lambda_i = 0.07$	63.70	46.51	56.48	1.37	1.13	1.06
$\lambda_i = 0.08$	66.78	56.83	62.96	1.18	1.06	1.04
$\lambda_i = 0.09$	68.41	63.48	66.06	1.08	1.04	1.01

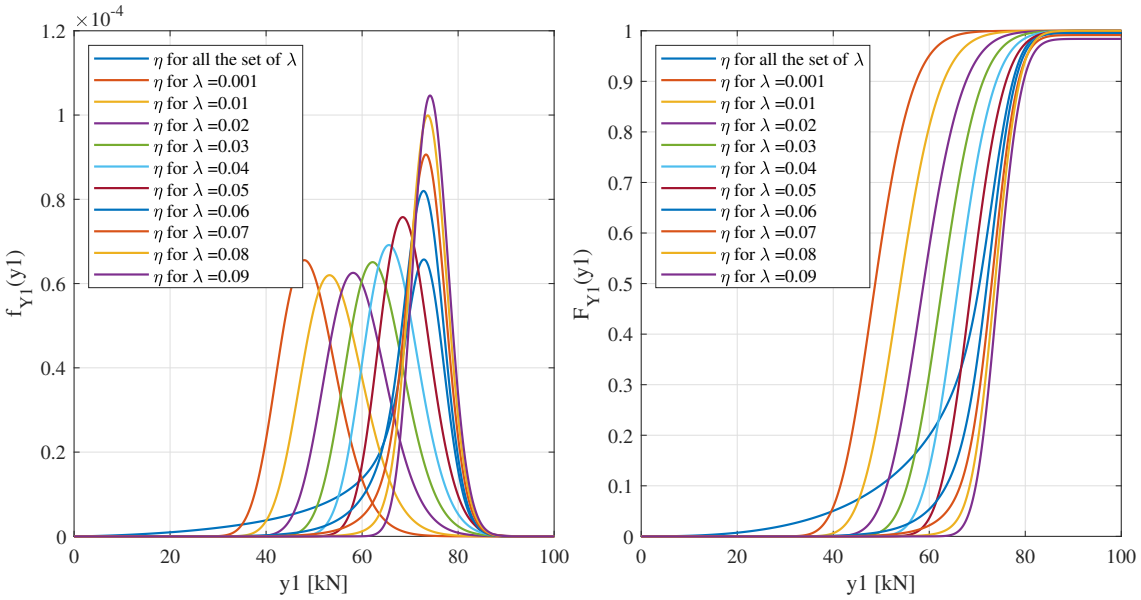

(a) Resistance probability density functions (b) Resistance cumulative density functions

Figure A.5: Probability functions of corroded seven-wire strands for different values of λ_i and $D = 0.5$

A.7 Damage index $D = 0.60$

A.7.1 Deterministic approach

- **Procedure (a): λ is unknown** $\Rightarrow \eta = C$

Percentile	C
50^{th}	1.69
16^{th}	1.35
1^{th}	1.02

- **Procedure (b): λ is known** $\Rightarrow \eta(\lambda) = C_1\lambda^3 + C_2\lambda^2 + C_3\lambda + C_4$ for $\lambda \leq \lambda_{lim}$

Percentile	C_1	C_2	C_3	C_4	λ_{lim}	R^2
50^{th}	688.55	-201.51	19.65	1.11	0.1	1
16^{th}	96.33	-95.86	16.28	0.98	0.1	1
1^{th}	-897.96	89.80	8.98	0.85	0.1	0.99

A.7.2 Probabilistic approach

- **Procedure (a): λ is unknown**

  $\beta(a = 2.25, b = 0.20)$

- **Procedure (b): λ is known**

λ	Probability function of η
0.001	$logN(\mu = 0.120, \sigma = 0.1172)$
0.01	$logN(\mu = 0.243, \sigma = 0.1116)$
0.02	$logN(\mu = 0.341, \sigma = 0.1017)$
0.03	$logN(\mu = 0.413, \sigma = 0.0883)$
0.04	$\beta(a = 7.44, b = 0.67)$
0.05	$\beta(a = 7.03, b = 0.36)$
0.06	$\beta(a = 8.56, b = 0.22)$
0.07	$\beta(a = 13.97, b = 0.16)$
0.08	$\beta(a = 34.49, b = 0.14)$
0.09	$\beta(a = 170.22, b = 0.16)$
0.10	-

Table A.26: Design-oriented results from the peak strength probability density function for the case of $D = 0.6$

Cumulative Curve	**Resistance characteristic value R_k [kN]**	**Resistance design value $R_{d,0.1\%}$ evaluated to CDF = 0.1 % [kN]**	**Resistance design value $R_{d,1\%}$ evaluated to CDF = 1 % [kN]**	**Resistance safety factor $\gamma = R_k/R_{d,0.1\%}$**	**Resistance safety factor $\gamma = R_k/R_{d,1\%}$**	**Corrosion characteristic coefficient $k_{corr} = R_k/(f_{y,k} \cdot A_0 \cdot \eta_k \cdot \rho_M \cdot \rho_{Gmin})$**
λ_i unknown	31.98	6.51	17.19	4.91 1.86	1.08	
$\lambda_i = 0.001$	31.24	26.00	28.65	1.20	1.09	1.24
$\lambda_i = 0.01$	35.66	29.91	32.82	1.19	1.09	1.23
$\lambda_i = 0.02$	39.94	33.98	37.01	1.18	1.08	1.21
$\lambda_i = 0.03$	43.83	37.96	40.95	1.15	1.07	1.19
$\lambda_i = 0.04$	43.00	26.07	35.12	1.65	1.22	1.07
$\lambda_i = 0.05$	46.48	28.40	38.29	1.64	1.21	1.07
$\lambda_i = 0.06$	50.17	34.32	43.39	1.46	1.16	1.07
$\lambda_i = 0.07$	52.94	42.80	49.04	1.24	1.08	1.05
$\lambda_i = 0.08$	54.40	49.82	52.35	1.09	1.04	1.02
$\lambda_i = 0.09$	54.92	51.08	53.07	1.08	1.03	1.01

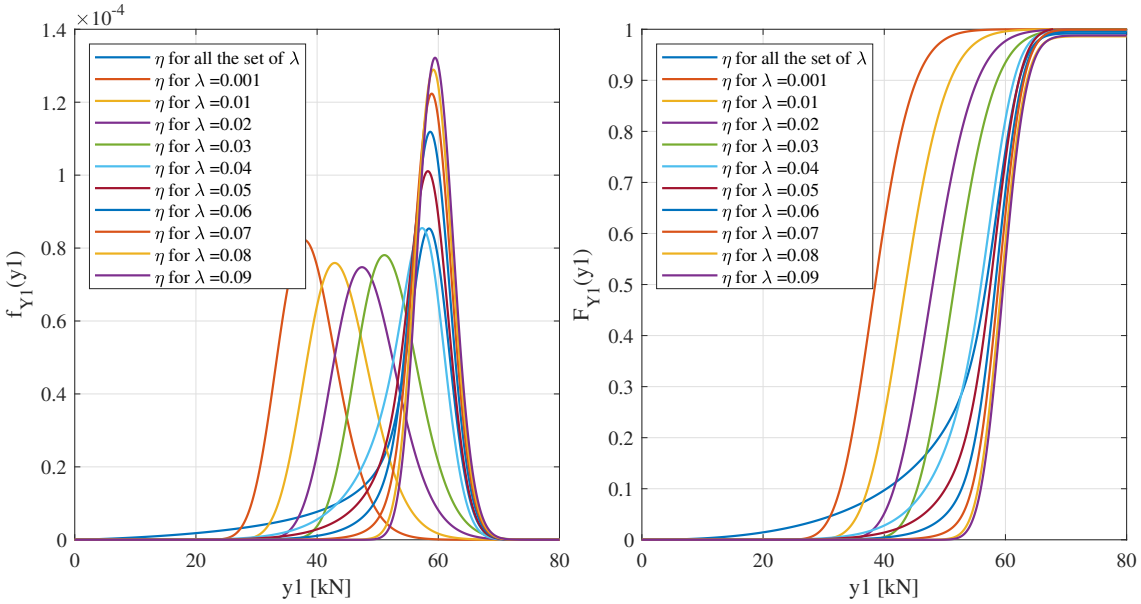

(a) Resistance probability density functions (b) Resistance cumulative density functions

Figure A.6: Probability functions of corroded seven-wire strands for different values of λ_i and $D = 0.6$

A.8 Damage index $D = 0.70$

A.8.1 Deterministic approach

- **Procedure (a): λ is unknown** $\Rightarrow \eta = C$

Percentile	C
50^{th}	1.75
16^{th}	1.42
1^{th}	1.03

- **Procedure (b): λ is known** $\Rightarrow \eta(\lambda) = C_1\lambda^3 + C_2\lambda^2 + C_3\lambda + C_4$ for $\lambda \leq \lambda_{lim}$

Percentile	C_1	C_2	C_3	C_4	λ_{lim}	R^2
50^{th}	-1743.79	-82.28	21.31	1.11	0.05	1
16^{th}	-1761.62	25.23	17.80	0.97	0.063	0.99
1^{th}	-476.45	-2.71	14.26	0.83	0.098	1

A.8.2 Probabilistic approach

- **Procedure (a): λ is unknown**

  $\beta(a = 2.33, b = 0.16)$

- **Procedure (b): λ is known**

λ	Probability function of η
0.001	$logN(\mu = 0.119, \sigma = 0.1223)$
0.01	$logN(\mu = 0.275, \sigma = 0.1148)$
0.02	$logN(\mu = 0.386, \sigma = 0.0992)$
0.03	$logN(\mu = 0.462, \sigma = 0.0785)$
0.04	$\beta(a = 6.93, b = 0.32)$
0.05	$\beta(a = 9.66, b = 0.18$
0.06	$\beta(a = 20.75, b = 0.14)$
0.07	$\beta(a = 62.00, b = 0.14)$
0.08	$\beta(a = 238.90, b = 0.17)$
0.09	-
0.10	-

Table A.30: Design-oriented results from the peak strength probability density function for the case of $D = 0.7$

Cumulative Curve	**Resistance characteristic value R_k [kN]**	**Resistance design value $R_{d,0.1\%}$ evaluated to CDF = 0.1 % [kN]**	**Resistance design value $R_{d,1\%}$ evaluated to CDF = 1 % [kN]**	**Resistance safety factor $\gamma = R_k/R_{d,0.1\%}$**	**Resistance safety factor $\gamma = R_k/R_{d,1\%}$**	**Corrosion characteristic coefficient $k_{corr} = R_k/(f_{y,k} \cdot A_0 \cdot \eta_k \cdot \rho_M \cdot \rho_{Gmin})$**
λ_i unknown	25.77	5.67	14.36	4.54	1.79	1.08
$\lambda_i = 0.001$	23.26	19.24	21.27	1.21	1.09	1.24
$\lambda_i = 0.01$	27.51	23.01	25.29	1.20	1.09	1.23
$\lambda_i = 0.02$	31.53	26.96	29.29	1.17	1.08	1.21
$\lambda_i = 0.03$	35.05	30.76	32.96	1.14	1.06	1.18
$\lambda_i = 0.04$	35.24	21.51	29.05	1.64	1.21	1.07
$\lambda_i = 0.05$	38.50	27.77	34.05	1.39	1.13	1.06
$\lambda_i = 0.06$	40.39	35.31	38.42	1.14	1.05	1.04
$\lambda_i = 0.07$	41.04	38.07	39.62	1.08	1.04	1.01
$\lambda_i = 0.08$	41.21	38.33	39.82	1.08	1.03	1.00

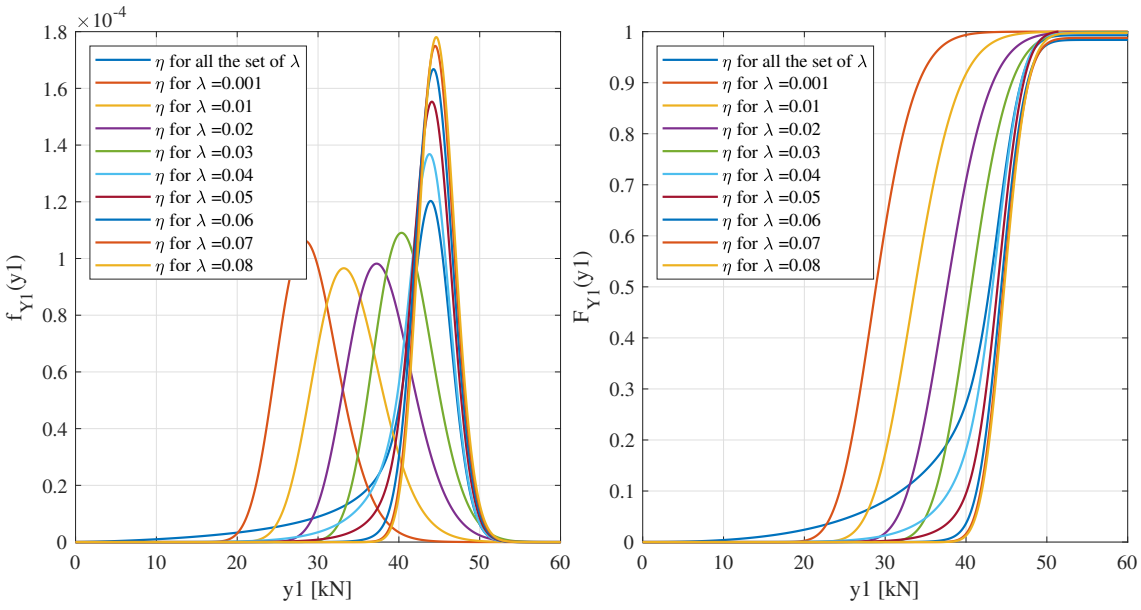

(a) Resistance probability density functions (b) Resistance cumulative density functions

Figure A.7: Probability functions of corroded seven-wire strands for different values of λ_i and $D = 0.7$

A.9 Damage index $D = 0.80$

A.9.1 Deterministic approach

- **Procedure (a): λ is unknown** $\Rightarrow \eta = C$

Percentile	C
50^{th}	1.75
16^{th}	1.53
1^{th}	1.06

- **Procedure (b): λ is known** $\Rightarrow \eta(\lambda) = C_1\lambda^3 + C_2\lambda^2 + C_3\lambda + C_4$ for $\lambda \leq \lambda_{lim}$

Percentile	C_1	C_2	C_3	C_4	λ_{lim}	R^2
50^{th}	-5109.00	-200.54	31.35	1.12	0.034	1
16^{th}	-7150.18	164.01	24.06	0.98	0.042	0.99
1^{th}	-4055.36	214.24	17.07	0.83	0.05	0.98

A.9.2 Probabilistic approach

- **Procedure (a): λ is unknown**

  $\beta(a = 2.91, b = 0.14)$

- **Procedure (b): λ is known**

λ	Probability function of η
0.001	$logN(\mu = 0.128, \sigma = 0.1331)$
0.01	$logN(\mu = 0.335, \sigma = 0.1078)$
0.02	$\beta(a = 7.31, b = 0.72)$
0.03	$\beta(a = 7.75, b = 0.26)$
0.04	$\beta(a = 18.52, b = 0.15)$
0.05	$\beta(a = 92.11, b = 0.16)$
0.06	$\beta(a = 722.02, b = 0.21)$
0.07	-
0.08	-
0.09	-
0.10	-

Table A.34: Design-oriented results from the peak strength probability density function for the case of $D = 0.8$

Cumulative Curve	**Resistance characteristic value R_k [kN]**	**Resistance design value $R_{d,0.1\%}$ evaluated to CDF = 0.1 % [kN]**	**Resistance design value $R_{d,1\%}$ evaluated to CDF = 1 % [kN]**	**Resistance safety factor $\gamma = R_k/R_{d,0.1\%}$**	**Resistance safety factor $\gamma = R_k/R_{d,1\%}$**	**Corrosion characteristic coefficient $k_{corr} = R_k/(f_{y,k} \cdot A_0 \cdot \eta_k \cdot \rho_M \cdot \rho_{Gmin})$**
λ_i unknown	19.73	6.10	12.60	3.23	1.57	1.08
$\lambda_i = 0.001$	15.61	12.90	14.27	1.21	1.09	1.24
$\lambda_i = 0.01$	19.70	16.65	18.20	1.18	1.08	1.22
$\lambda_i = 0.02$	21.08	12.61	17.11	1.67	1.23	1.07
$\lambda_i = 0.03$	24.47	15.94	20.73	1.54	1.18	1.07
$\lambda_i = 0.04$	26.80	22.98	25.35	1.17	1.06	1.04
$\lambda_i = 0.05$	27.41	25.47	26.48	1.08	1.04	1.01
$\lambda_i = 0.06$	27.50	25.59	26.58	1.07	1.03	1.00

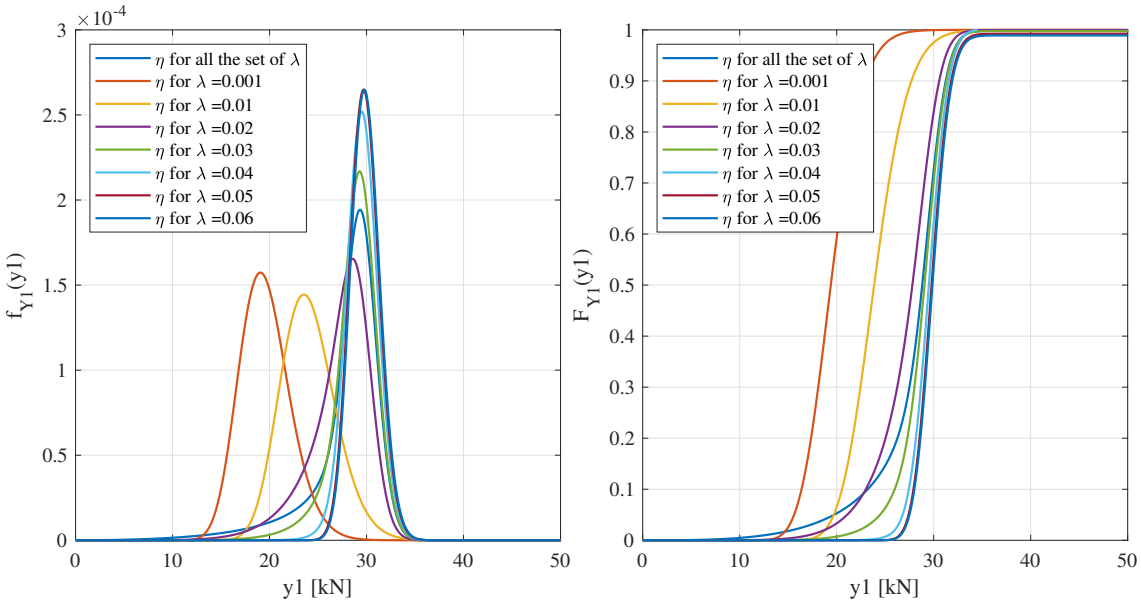

(a) Resistance probability density functions (b) Resistance cumulative density functions

Figure A.8: Probability functions of corroded seven-wire strands for different values of λ_i and $D = 0.8$

A.10 Damage index $D = 0.90$

A.10.1 Deterministic approach

- **Procedure (a): λ is unknown** $\Rightarrow \eta = C$

Percentile	C
50^{th}	1.75
16^{th}	1.73
1^{th}	1.11

- **Procedure (b): λ is known** $\Rightarrow \eta(\lambda) = C_1\lambda^3 + C_2\lambda^2 + C_3\lambda + C_4$ for $\lambda \leq \lambda_{lim}$

Percentile	C_1	C_2	C_3	C_4	λ_{lim}	R^2
50^{th}	1.00	-2228.15	80.21	1.03	0.018	1
16^{th}	1.00	-1523.25	70.07	0.94	0.023	0.98
1^{th}	-2674.02e1	688.54	34.04	0.82	0.031	0.99

A.10.2 Probabilistic approach

- **Procedure (a): λ is unknown**

  $\beta(a = 5.12, b = 0.13)$

- **Procedure (b): λ is known**

λ	Probability function of η
0.001	$logN(\mu = 0.137, \sigma = 0.1223)$
0.01	$\beta(a = 8.35, b = 0.90)$
0.02	$\beta(a = 18.12, b = 0.18)$
0.03	$\beta(a = 559.98, b = 0.23)$
0.04	-
0.05	-
0.06	-
0.07	-
0.08	-
0.09	-
0.10	-

Table A.38: Design-oriented results from the peak strength probability density function for the case of $D = 0.9$

Cumulative Curve	**Resistance characteristic value R_k [kN]**	**Resistance design value $R_{d,0.1\%}$ evaluated to CDF = 0.1 % [kN]**	**Resistance design value $R_{d,1\%}$ evaluated to CDF = 1 % [kN]**	**Resistance safety factor $\gamma = R_k/R_{d,0.1\%}$**	**Resistance safety factor $\gamma = R_k/R_{d,1\%}$**	**Corrosion characteristic coefficient $k_{corr} = R_k/(f_{y,k} \cdot A_0 \cdot \eta_k \cdot \rho_M \cdot \rho_{Gmin})$**
λ_i unknown	11.84	6.29	9.32	1.88	1.27	1.07
$\lambda_i = 0.001$	7.89	6.53	7.22	1.21	1.09	1.24
$\lambda_i = 0.01$	10.55	6.65	8.73	1.59	1.21	1.07
$\lambda_i = 0.02$	13.38	11.40	12.62	1.17	1.06	1.04
$\lambda_i = 0.03$	13.76	12.80	13.29	1.08	1.03	1.00

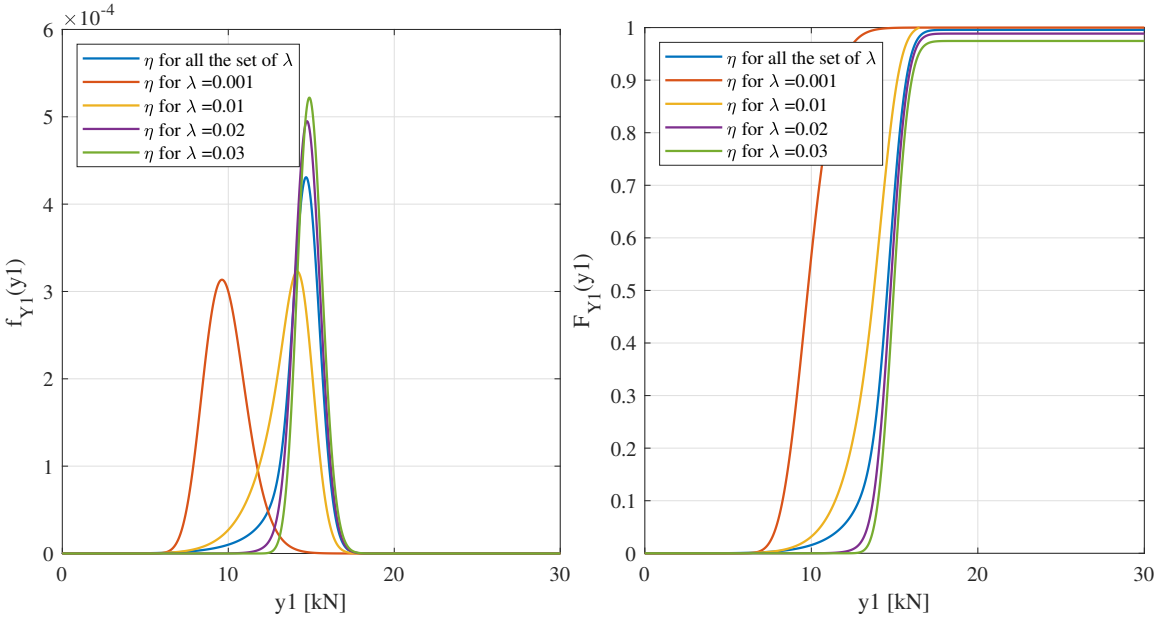

(a) Resistance probability density functions (b) Resistance cumulative density functions

Figure A.9: Probability functions of corroded seven-wire strands for different values of λ_i and $D = 0.9$

A.11 Damage index $D = 0.99$

A.11.1 Deterministic approach

- **Procedure (a): λ is unknown** $\Rightarrow \eta = C$

Percentile	C
50^{th}	1.75
16^{th}	1.75
1^{th}	1.58

- **Procedure (b): λ is known** $\Rightarrow \eta(\lambda) = C_1\lambda^3 + C_2\lambda^2 + C_3\lambda + C_4$ for $\lambda \leq \lambda_{lim}$

Percentile	C_1	C_2	C_3	C_4	λ_{lim}	R^2
50^{th}	1.00	-7287.70e1	436.26	1.09	0.003	0.99
16^{th}	1.00	-4769.21e1	381.54	0.99	0.004	0.98
1^{th}	1.00	-6891.36e1	558.51	0.633	0.004	0.92

A.11.2 Probabilistic approach

- **Procedure (a): λ is unknown**

  For this level of damage index it was not possible to fit the statistic of η.

- **Procedure (b): λ is known**

λ	Probability function of η
0.001	$logN(\mu = 0.369, \sigma = 0.0928)$
0.01	-
0.02	-
0.03	-
0.04	-
0.05	-
0.06	-
0.07	-
0.08	-
0.09	-
0.10	-

Table A.42: Design-oriented results from the peak strength probability density function for the case of $D = 0.99$

Cumulative Curve	**Resistance characteristic value R_k [kN]**	**Resistance design value $R_{d,0.1\%}$ evaluated to CDF = 0.1 % [kN]**	**Resistance design value $R_{d,1\%}$ evaluated to CDF = 1 % [kN]**	**Resistance safety factor $\gamma = R_k/R_{d,0.1\%}$**	**Resistance safety factor $\gamma = R_k/R_{d,1\%}$**	**Corrosion characteristic coefficient $k_{corr} = R_k/(f_{y,k} \cdot A_0 \cdot \eta_k \cdot \rho_M \cdot \rho_{Gmin})$**
$\lambda_i = 0.001$	1.05	0.90	0.97	1.16	1.08	1.21

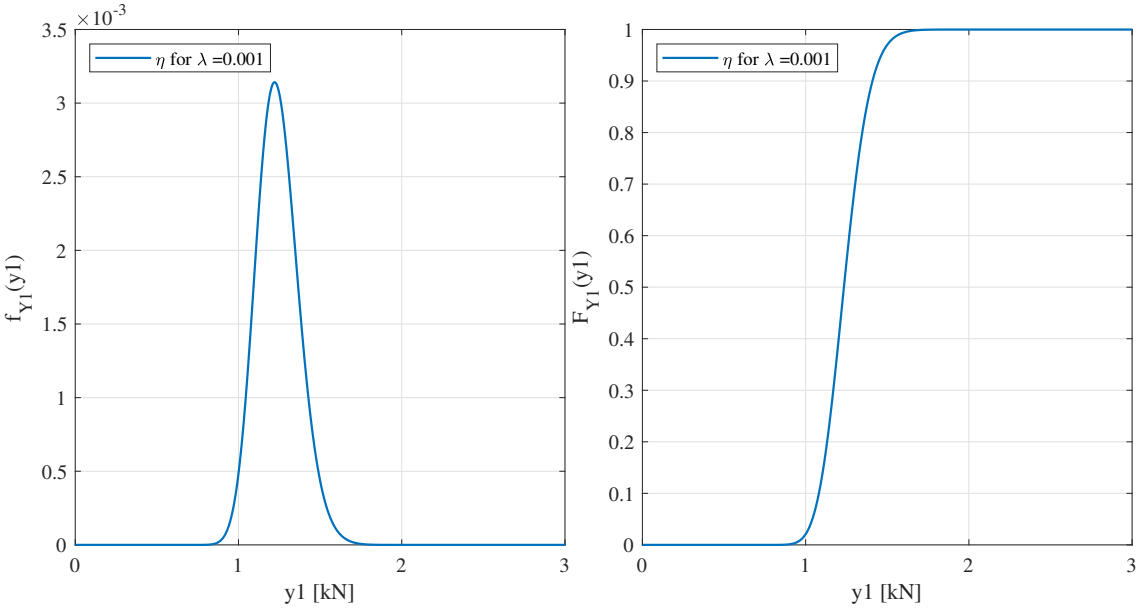

(a) Resistance probability density functions (b) Resistance cumulative density functions

Figure A.10: Probability functions of corroded seven-wire strands for different values of λ_i and $D = 0.99$

Appendix B

Demonstration of Eq. 10.3

In order to find an analytical formulation for the lower bound estimation of the group coefficient the following hypotheses have been done:

1. the adimensional reduction of cross-section area ρ_i is uniformly distributed in the domain $(m_{\rho_i} - p, m_{\rho_i} + p)$ which is described by Eq. B.1;

$$\rho_i = \frac{2p}{n_w - 1}(i-1) + (m_{\rho_i} - p) \tag{B.1}$$

   Where p and m_{ρ_i} represent the domain amplitude and the mean of the corrosion in the strand, respectively.

2. the adimensional reduction of cross-section area ρ_i in each wire of the strand is given by Eq. B.1;

3. the peak force is given by the Darmawan-Stewart model;

4. the relationship between the peak force, the adimensional reduction of cross-section area and the group function is given by Eq. 10.1.

Figure B.1 shows the trend taken by the adimensional reduction of cross-section areas ρ_i , according to Eq. B.1. As it can be seen from the figure, the maximum domain that is assumable by ρ_i (which means by the p value) depends on the mean of the corrosion m_{ρ_i}. In other words, the maximum domain amplitude is given when p assumes the following value.

$$p_{max} = min(m_{\rho_i}, 1 - m_{\rho_i}) \tag{B.2}$$

The peak force in a corroded strand, according to the Darmawan-Stewart model in Eq. 9.1 and the expression for the adimensional reduction of cross-section area in Eq. B.1, is given by Eq. B.3. This is obtained by substituting Eq. B.1 in Eq. 9.1.

$$\begin{aligned} F_{p,DS} &= max(F_{p,i}) \\ F_{p,i} &= (n_w - i + 1)\left[\frac{2p}{n_w - 1}(i-1)(m_{\rho_i} - p)\right] \cdot F_{0,i} \end{aligned} \tag{B.3}$$

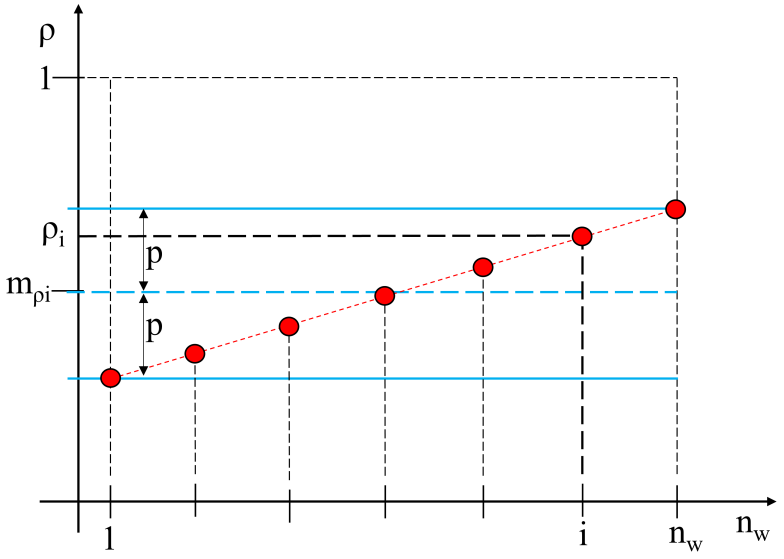

Figure B.1: Trend of the uniform reduction of cross-section area in the wires

Setting equal to zero the derivate of Eq. B.3 with respect to the i variable, which represents the generic wire in the strand, the expression of the index that gives the peak force in the corroded strand can be obtained as reported in Eq. B.4.

$$\begin{cases} i_{max} = round\left(1 + \dfrac{n_w}{2} - \dfrac{(m_{\rho_i} - p)(n_w - 1)}{4p}\right), \text{for } p > p_{min} \\ i_{max} = 1, \text{for } p \leq p_{min} \end{cases} \tag{B.4}$$

Where *round()* indicates the function for the nearest integer value and p_{min} is the minimum value that can be assumed by p, in fact, for $p \to 0$, which means uniform corrosion in the entire domain, the peak force is equal in all the corroded wires. Expression for p_{min} is reported in Eq. B.5.

$$p_{min} = m_{\rho_i} \frac{n_w - 1}{3n_w - 1} \tag{B.5}$$

Then, by inserting Eq. B.4 in Eq. B.3 the expression of maximum force can be obtained as reported in Eq. B.6.

$$\begin{cases} F_{p,DS} = (n_w - i_{max} + 1)\left[\dfrac{2p}{n_w - 1}(i-1)(m_{\rho_i} - p)\right] F_{0,i}, \text{for } p > p_{min} \\ F_{p,DS} = n_w(m_{\rho_i} - p)F_{0,i}, \text{for } p \leq p_{min} \end{cases} \tag{B.6}$$

The lower bound of the group coefficient, according to Eq. 10.1 and Eq. B.6, assumes

the following expressions:

$$\begin{cases} \rho_{Gmin} & = (n_w - i_{max} + 1)\left[\dfrac{2p_{max}}{n_w - 1}(i_{max} - 1) + (m_{\rho_i} - p)\right]\dfrac{1}{m_{\rho_i} n_w}\Big|_{p=p_{max}} & p > p_{min} \\ \rho_{Gmin} & = \dfrac{(m_{\rho_i} - p)}{m_{\rho_i}}\Big|_{p=p_{max}} & p \leq p_{min} \end{cases} \tag{B.7}$$

$$\Downarrow$$

$$\begin{cases} \rho_{Gmin} & = (n_w - i_{max} + 1)\left[\dfrac{2p_{max}}{n_w - 1}(i_{max} - 1) + (m_{\rho_i} - p_{max})\right]\dfrac{1}{m_{\rho_i} n_w} & p_{max} > p_{min} \\ \rho_{Gmin} & = \dfrac{(m_{\rho_i} - p_{max})}{m_{\rho_i}} & p_{max} \leq p_{min} \end{cases} \tag{B.8}$$

Appendix C

Demonstration of Eqs.: 8.1, 8.3, 8.4, 8.5

A corroded wire is modelled as series system between the corroded and not corroded parts that can be identified according the geometry of the corrosion in Figure 7.2. If we consider the presence of one corroded part (represented by the parameter $\rho_i = \frac{Ai}{A_{0i}}$ and $\lambda_i = \frac{L_c}{L_0}$) the system can be expressed by two springs representing the corroded part (length L_c) and the not-corroded one (length $L_0 - L_c$), as follows:

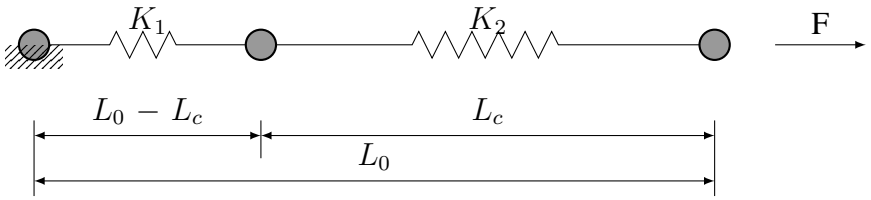

The displacement of a series system subjected to a force is the sum of the displacements in each spring. Then the elastic stiffness of the system K_i can be obtained by

applying the yielding force F_y:

$$
\begin{aligned}
K_i &= \frac{F_{yi}}{\delta_{yi}} = \\
\delta_{yi} &= \delta_{y,1} + \delta_{y,2} = \\
&= \frac{F_{yi}}{K_1} + \frac{F_{yi}}{K_2} = \\
&= \frac{F_{yi} \cdot (L_0 - L_c)}{E \cdot A_{0i}} + \frac{F_{yi} \cdot L_c}{E \cdot \rho_i \cdot A_{0i}} \\
\Rightarrow K_i &= \frac{F_{yi}}{u_{yi}} = \frac{1}{\dfrac{L_0 - L_c}{E \cdot A_{0i}} + \dfrac{L_c}{E \cdot \rho_i \cdot A_{0i}}} = \\
&= \frac{E \cdot \rho_i \cdot A_{0i}}{\rho_i (L_0 - L_c) + L_c} = \\
&= \frac{E \cdot A_{0i}}{L_0} \left[\frac{\rho_i}{\dfrac{\rho_i \cdot (L_0 - L_c)}{L_0} + \dfrac{L_c}{L_0}} \right] = \\
&= \frac{E \cdot A_{0i}}{L_0} \left[\frac{1}{\dfrac{(L_0 - L_c)}{L_0} + \dfrac{\lambda_i}{\rho_i}} \right] = \frac{E \cdot A_{0i}}{L_0} \left[\frac{1}{1 - \lambda_i + \dfrac{\lambda_i}{\rho_i}} \right] \\
K_i &= \frac{E \cdot A_{0i}}{L_0} \left[\frac{1}{1 + \lambda \left(\dfrac{1}{\rho_i} - 1 \right)} \right]
\end{aligned}
\tag{C.1}
$$

Then the yielding displacement of the system is:

$$
\delta yi = \frac{F_{yi}}{K_i} \tag{C.2}
$$

The ultimate displacement can be obtained considering that the plastic deformation occurs in the corroded part only (elasto-perfectly plastic steel material):

$$
\begin{aligned}
\delta_{ui} &= \delta_{yi} + \Delta_u = \\
&= \delta_{yi} + (\epsilon_u - \epsilon_y) \cdot L_c
\end{aligned}
\tag{C.3}
$$

The ductility can then be expressed as:

$$\begin{aligned}
\mu_{\delta_{ui}} &= \frac{\delta_{ui}}{\delta_{yi}} = \\
&= \frac{\delta_{yi} + (\epsilon_u - \epsilon_y) \cdot L_c}{\delta_{yi}} = \\
&= 1 + \frac{(\epsilon_u - \epsilon_y) \cdot L_c}{\frac{F_{yi} \cdot L_0}{E \cdot A_{0i}} \cdot \left(1 + \lambda_i \cdot \left(\frac{1}{\rho_i} - 1\right)\right)} \\
\mu_{\delta_{ui}} &= 1 + \frac{(\epsilon_u - \epsilon_y)}{\epsilon_y} \cdot \left[\frac{\lambda_i}{1 + \lambda_i \cdot \left(\frac{1}{\rho_i} - 1\right)}\right]
\end{aligned} \tag{C.4}$$

Appendix D

Demostration of Eq. 10.8

According to the resistance model, the peak force of corroded seven-wire strand can be written as:

$$F_{p,p} = F_0 \cdot \rho_M \cdot \rho_G = A_0 \cdot f_y \cdot \rho_M \cdot \rho_{Gmin} \cdot \eta \tag{D.1}$$

The objective is to estimate the functions that describes the statistic, in terms of probability and cumulative density functions, of the peak force $F_{p,p}$.

Assuming as deterministic variables the cross-section area of the not-corroded seven-wire strands A_0, the mean corrosion level ρ_M and the lower bound of the group coefficient ρ_{Gmin}, the statistic of the peak force is:

$$R(F_{p,p}) = A_0 \cdot \rho_M \cdot \rho_{Gmin} \cdot g(f_y, \eta) \tag{D.2}$$

where R and g are the functions that describe the statistic of the random variables in the model, the peak force and the yielding stress f_y and model coefficient η, respectively.

Assuming that the random variables are independent:

$$R = Y_1 = A_0 \cdot \rho_M \cdot \rho_{Gmin} \cdot X_2 \cdot X_3 \tag{D.3}$$

Where, for sake of clarity, it is done a change of notation for which $f_y = X_2$ and $\eta = X_3$.

- X_2 can be assumed as represent by a logNormal probability density function with a certain mean value and coefficient of variation. In the present case they assume values equal to 1700 MPa and 5%, respectively;
- X_3 assumes the probability density functions estimated through the Monte Carlo simulations (probability approach) of corroded strands according to the damage index level D and the knowledge of the corrosion in terms of adimensional corrosion extension: λ_i unknown and λ_i known. All the results are reported in Appendix A.

Thus, the following equality can be written:

$$\begin{aligned} f_{Y_1}(y_1) \cdot dy_1 &= A_0 \cdot \rho_M \cdot \rho_{Gmin} \cdot f_{X_2,X_3}(x_2, x_3) dx_2 \cdot dx_3 = \\ &= A_0 \cdot \rho_M \cdot \rho_{Gmin} \cdot f_{X_2}(x_2) \cdot f_{X_3}(x_3) \cdot |J_{x,y}| \cdot dy_2 \cdot dy_3 \end{aligned} \tag{D.4}$$

where $|J_{x,y}|$ is the determinant of the Jacobian matrix of the transformation: $dx_2 \cdot dx_3 = |J_{x,y}| \cdot dy_2 \cdot dy_3$.

The Jacobian Matrix can be obtained starting from Eq. D.3 and the change of variable $x_3 = y_2$:

$$\begin{cases} x_2 = \dfrac{y_1}{A_0 \cdot \rho_M \cdot \rho_{Gmin} \cdot x_3} \\ x_3 = y_2 \end{cases} \Rightarrow J_{x,y} = \begin{bmatrix} \frac{\partial x_2}{\partial y_1} & \frac{\partial x_2}{\partial y_3} \\ \frac{\partial x_3}{\partial y_1} & \frac{\partial x_3}{\partial y_3} \end{bmatrix}$$

$$J_{x,y} = \begin{bmatrix} \dfrac{1}{A_0 \cdot \rho_M \cdot \rho_{Gmin} \cdot y_3} & \dfrac{y_1}{A_0 \cdot \rho_M \cdot \rho_{Gmin} \cdot x_3^2} \\ 0 & 1 \end{bmatrix} \Rightarrow |J_{x,y}| = \frac{1}{A_0 \cdot \rho_M \cdot \rho_{Gmin} \cdot y_3} \tag{D.5}$$

Thus, Eq. D.4, taking into account that $dx_2 = \dfrac{dy_1}{A_0 \cdot \rho_M \cdot \rho_{Gmin} \cdot y_2}$ and $dx_3 = dy_2$, can be written as:

$$f_{Y_1}(y_1) \cdot dy_1 = f_{X_2}\left(\frac{y_1}{A_0 \cdot \rho_M \cdot \rho_{Gmin}}\right) \cdot f_{X_3}(y_2) \cdot \frac{dy_1}{A_0 \cdot \rho_M \cdot \rho_{Gmin} \cdot y_2} \cdot dy_2 \tag{D.6}$$

That leads to:

$$f_{Y_1}(y_1) = \frac{1}{A_0 \cdot \rho_M \cdot \rho_{Gmin}} \int_{y_2} f_{X_2}\left(\frac{1}{A_0 \cdot \rho_M \cdot \rho_{Gmin}}\right) \cdot f_{X_3}(y_2) \cdot dy_2 \tag{D.7}$$

Since the model coefficient η is defined in the range (1,$1/\rho_{Gmin}$), the probability density function of the resistance can be obtained by the following integral formula:

$$f_{Y_1}(y_1) = \frac{1}{A_0 \cdot \rho_M \cdot \rho_{Gmin}} \int_1^{1/\rho_{Gmin}} f_{X_2}\left(\frac{1}{A_0 \cdot \rho_M \cdot \rho_{Gmin}}\right) \cdot f_{X_3}(y_2) \cdot dy_2 \tag{D.8}$$

Consequently, the cumulative density function of the resistance can be obtained by the integral its probability density function:

$$F_{Y_1}(y_1) = \int f_{Y_1}(y_1) \cdot dy_1 \tag{D.9}$$

Acknowledgements

The choice of a young man depends on his inclination, but also in being lucky to meet a great master.

Rita Levi-Montalcini

During my Ph.D, I have met several of them, thanks to whom I have grown both professionally and personally.

I would like to express my deepest gratitude to my supervisor, professor Stefano Silvestri, for his invaluable guidance, support and encouragement throughout the duration of this research. I would also like to extend my gratitude to professor Tomaso Trombetti, professor Giada Gasparini and professor Michele Palermo for their valuable feedback and suggestions.

Their expertise and insights have been instrumental in shaping the direction and quality of this work.

I would like to express my sincere gratitude to professor Filipe Magalhães and to assistant professor Sérgio Pereira for their warm hospitality and generosity during my stay at University of Porto. Their kindness, support and guide have made my experience truly enjoyable and productive.

I would also like to thank my friends and my colleagues, in particular Vittoria and Said, for their support and good times spent together.

A particular thank to Cleme for her special support.

Ringraziamenti

La scelta di un giovane dipende dalla sua inclinazione, ma anche dalla fortuna di incontrare un grande maestro.

Rita Levi-Montalcini

Durante il mio percorso ne ho incontrati diversi, grazie ai quali sono cresciuto sia dal punto di vista professionale che personale.

Vorrei esprimere la mia più profonda gratitudine al mio relatore, il professor Stefano Silvestri, per la sua preziosa guida, supporto e incoraggiamento durante tutta la durata di questo percorso. Vorrei anche estendere la mia gratitudine al professor Tomaso Trombetti, alla professoressa Giada Gasparini e al professor Michele Palermo per i loro preziosi feedback e suggerimenti.

La loro esperienza e le loro intuizioni sono state determinanti nel plasmare la direzione e la qualità di questo lavoro.

Vorrei esprimere la mia sincera gratitudine al professor Filipe Magalhães e a Sérgio Pereira per la loro calorosa ospitalità e generosità durante il mio soggiorno all'Università di Porto. La loro gentilezza, il loro supporto e la loro guida hanno reso la mia esperienza davvero piacevole e produttiva.

Vorrei anche ringraziare gli amici e i colleghi, in particolare Vittoria e Said, per il loro sostegno e per i bei momenti trascorsi insieme.

Un ringraziamento particolare a Cleme per il suo speciale supporto.